Inter-model Comparative Testing and Empirical Validation of Annex 42 Models for Residential Cogeneration Devices

A Report of Subtask B of
FC+COGEN-SIM
The Simulation of Building-Integrated
Fuel Cell and Other Cogeneration Systems

Annex 42 of the
International Energy Agency
Energy Conservation in Buildings and Community Systems Programme
First published: December 2007

REPORT EDITORS:
Ian Beausoleil-Morrison (Natural Resources Canada)
Alex Ferguson (Natural Resources Canada)

ANNEX 42 OPERATING AGENT:
Ian Beausoleil-Morrison (Natural Resources Canada)

ANNEX 42 SUBTASK B LEADER:
Nick Kelly (University of Strathclyde)

CITATION

Ian Beausoleil-Morrison (Natural Resources Canada) and Alex Ferguson (Natural Resources Canada). Inter-model Comparative Testing and Empirical Validation of Annex 42 Models for Residential Cogeneration Devices. A Report of Subtask B of FC+COGEN-SIM The Simulation of Building-Integrated Fuel Cell and Other Cogeneration Systems. Annex 42 of the International Energy Agency Energy Conservation in Buildings and Community Systems Programme. (344 pages).

Copies of this report may be obtained from the Annex 42 web site at: www.cogen-sim.net or from the IEA/ECBCS Bookshop at: www.ecbcs.org.

DISCLAIMER

Participating countries in ECBCS:

Australia, Belgium, CEC, Canada, Czech Republic, Denmark, Finland, France, Germany, Greece, Israel, Italy, Japan, the Netherlands, New Zealand, Norway, Poland, Portugal, Sweden, Switzerland, Turkey, United Kingdom and the United States of America.

ISBN No. 978-0-662-47562-0
Catalogue No.: M154-14/5-2007E-PDF

Preface

International Energy Agency

The International Energy Agency (IEA) was established in 1974 within the framework of the Organisation for Economic Co-operation and Development (OECD) to implement an international energy programme. A basic aim of the IEA is to foster co-operation among the twenty-four IEA participating countries and to increase energy security through energy conservation, development of alternative energy sources and energy research, development and demonstration (RD&D).

Energy Conservation in Buildings and Community Systems

The IEA sponsors research and development in a number of areas related to energy. The mission of one of those areas, the ECBCS - Energy Conservation for Building and Community Systems Programme, is to facilitate and accelerate the introduction of energy conservation, and environmentally sustainable technologies into healthy buildings and community systems, through innovation and research in decision-making, building assemblies and systems, and commercialisation. The objectives of collaborative work within the ECBCS R&D programme are directly derived from the on-going energy and environmental challenges facing IEA countries in the area of construction, energy market and research. ECBCS addresses major challenges and takes advantage of opportunities in the following areas:

- exploitation of innovation and information technology;
- impact of energy measures on indoor health and usability;
- integration of building energy measures and tools to changes in lifestyles, work environment alternatives, and business environment.

The Executive Committee

Overall control of the programme is maintained by an Executive Committee, which not only monitors existing projects but also identifies new areas where collaborative effort may be beneficial. To date the following projects have been initiated by the executive committee on Energy Conservation in Buildings and Community Systems (completed projects are identified by (*)):

Annex 1: Load Energy Determination of Buildings (*)
Annex 2: Ekistics and Advanced Community Energy Systems (*)
Annex 3: Energy Conservation in Residential Buildings (*)
Annex 4: Glasgow Commercial Building Monitoring (*)
Annex 5: Air Infiltration and Ventilation Centre
Annex 6: Energy Systems and Design of Communities (*)
Annex 7: Local Government Energy Planning (*)
Annex 8: Inhabitants Behaviour with Regard to Ventilation (*)
Annex 9: Minimum Ventilation Rates (*)
Annex 10: Building HVAC System Simulation (*)
Annex 11: Energy Auditing (*)
Annex 12: Windows and Fenestration (*)

Annex 13: Energy Management in Hospitals (*)
Annex 14: Condensation and Energy (*)
Annex 15: Energy Efficiency in Schools (*)
Annex 16: BEMS 1- User Interfaces and System Integration (*)
Annex 17: BEMS 2- Evaluation and Emulation Techniques (*)
Annex 18: Demand Controlled Ventilation Systems (*)
Annex 19: Low Slope Roof Systems (*)
Annex 20: Air Flow Patterns within Buildings (*)
Annex 21: Thermal Modelling (*)
Annex 22: Energy Efficient Communities (*)
Annex 23: Multi Zone Air Flow Modelling (COMIS) (*)
Annex 24: Heat, Air and Moisture Transfer in Envelopes (*)
Annex 25: Real time HEVAC Simulation (*)
Annex 26: Energy Efficient Ventilation of Large Enclosures (*)
Annex 27: Evaluation and Demonstration of Domestic Ventilation Systems (*)
Annex 28: Low Energy Cooling Systems (*)
Annex 29: Daylight in Buildings (*)
Annex 30: Bringing Simulation to Application (*)
Annex 31: Energy-Related Environmental Impact of Buildings (*)
Annex 32: Integral Building Envelope Performance Assessment (*)
Annex 33: Advanced Local Energy Planning (*)
Annex 34: Computer-Aided Evaluation of HVAC System Performance (*)
Annex 35: Design of Energy Efficient Hybrid Ventilation (HYBVENT) (*)
Annex 36: Retrofitting of Educational Buildings (*)
Annex 37: Low Exergy Systems for Heating and Cooling of Buildings (LowEx) (*)
Annex 38: Solar Sustainable Housing
Annex 39: High Performance Insulation Systems
Annex 40: Building Commissioning to Improve Energy Performance
Annex 41: Whole Building Heat, Air and Moisture Response (MOIST-ENG)
Annex 42: The Simulation of Building-Integrated Fuel Cell and Other Cogeneration Systems (FC+COGEN-SIM)
Annex 43: Testing and Validation of Building Energy Simulation Tools
Annex 44: Integrating Environmentally Responsive Elements in Buildings
Annex 45: Energy Efficient Electric Lighting for Buildings
Annex 46: Holistic Assessment Tool-kit on Energy Efficient Retrofit Measures for Government Buildings (EnERGo)
Annex 47: Cost-Effective Commissioning for Existing and Low Energy Buildings
Annex 48: Heat Pumping and Reversible Air Conditioning
Annex 49: Low Exergy Systems for High Performance Buildings and Communities
Annex 50: Prefabricated Systems for Low Energy Renovation of Residential Buildings

Working Group - Energy Efficiency in Educational Buildings (*)
Working Group - Indicators of Energy Efficiency in Cold Climate Buildings (*)
Working Group - Annex 36 Extension: The Energy Concept Adviser (*)

(*) - Completed

Annex 42

The objectives of Annex 42 were to develop simulation models that advance the design, operation, and analysis of residential cogeneration systems, and to apply these models to assess the technical, environmental, and economic performance of the technologies. This was accomplished by developing and incorporating models of cogeneration devices and associated plant components within existing whole-building simulation programs. Emphasis was placed upon fuel cell cogeneration systems and the Annex considered technologies suitable for use in new and existing single and low-rise-multi-family residential buildings. The models were developed at a time resolution that is appropriate for whole-building simulation.

To accomplish these objectives Annex 42 conducted research and development in the framework of the following three Subtasks:

- Subtask A : Cogeneration system characterization and characterization of occupant-driven electrical and domestic hot water usage patterns.
- Subtask B : Development, implementation, and validation of cogeneration system models.
- Subtask C : Technical, environmental, and economic assessment of selected cogeneration applications, recommendations for cogeneration application.

Annex 42 was an international joint effort conducted by 26 organizations in 10 countries:

Belgium	▪ University of Liège / Department of Electrical Engineering and Computer Science ▪ COGEN Europe ▪ Catholic University of Leuven
Canada	▪ Natural Resources Canada / CANMET Energy Technology Centre ▪ University of Victoria / Department of Mechanical Engineering ▪ National Research Council / Institute for Research in Construction ▪ Hydro-Québec / Energy Technology Laboratory (LTE)
Finland	▪ Technical Research Centre of Finland (VTT) / Building and Transport
Germany	▪ Research Institute for Energy Economy (FfE)
Italy	▪ National Agency for New Technology, Energy and the Environment (ENEA) ▪ University of Sannio ▪ Second University of Napoli
Netherlands	▪ Energy Research Centre Netherlands (ECN) / Renewable Energy in the Built Environment
Norway	▪ Norwegian Building Research Institute (NBRI) ▪ Telemark University College
United Kingdom	▪ University of Strathclyde / Energy Systems Research Unit (ESRU) ▪ Cardiff University / Welsh School of Architecture
United States of America	▪ Penn State University / Energy Institute ▪ Texas A&M University / Department of Architecture ▪ National Institute of Standards and Technology ▪ National Renewable Energy Laboratory

	▪ National Fuel Cell Research Center of the University of California-Irvine
Switzerland	▪ Swiss Federal Laboratories for Materials Testing and Research (EMPA) / Building Technologies Laboratory ▪ Swiss Federal Institute of Technology (EPFL)/ Laboratory for Industrial Energy Systems ▪ Hexis AG (Hexis) ▪ Siemens Switzerland AG (Siemens)

Table of Contents

I. Introduction

The Need for Validation

Annex 42 has developed two models for simulating the performance of residential-scale cogeneration devices (Kelly and Beausoleil-Morrison, 2007). One of these models treats fuel cell systems while the other treats combustion-based systems. These models have been implemented into several simulation platforms some of which will be distributed widely to the building simulation community. This will enable the simulation of residential-scale cogeneration devices in widely available tools such as ESP-r (ESRU, 2005), TRNSYS (Klein, 2004), and EnergyPlus (Crawley et al., 2001).

The validity of these models and the accuracy of their calibration to represent specific cogeneration devices is critical given that these models will be widely distributed. Consequently, Annex 42 has invested considerable effort on validation. This report details these efforts. Following a brief overview of accepted validation methodologies in the building simulation field, this section outlines the approaches used within Annex 42 and provides an outline for the remainder of the report.

Accepted Validation Methodology

The validation of building simulation programs is a complex and challenging field that has existed almost as long as building simulation itself. Extensive efforts have been conducted under the auspices of the International Energy Agency (IEA), the American Society for Heating Refrigeration and Air-Conditioning Engineers (ASHRAE), the European Committee for Standardization (CEN), and others to create methodologies, tests, and standards to verify the accuracy and reliability of building simulation programs. Notable examples include Jensen (1993); Lomas et al. (1994); Judkoff and Neymark (1995); ANSI/ASHRAE

(2004); and CEN (2004).

In addition to providing consistent methods for comparing predicted results by simulation programs, these initiatives have proven effective at diagnosing *internal sources of errors*. Judkoff et al. (1983) provided a useful classification for these errors:

- Differences between the actual thermal transfer mechanisms taking place in the reality and the simplified model of those physical processes.
- Errors or inaccuracies in the mathematical solution of the models.
- Coding errors.

Judkoff and Neymark (1995) proposed a pragmatic approach composed of three primary validation constructs to check for these internal errors. These are:

- Analytical verification
- Empirical validation
- Comparative testing

With analytical verification, the program output is compared to a well known analytical solution for a problem that isolates a single heat transfer mechanism. Typically this necessitates very simple boundary conditions. Although analytical verification is limited to simple cases for which analytic solutions are known, it provides an exact standard for comparison.

Program outputs are compared to monitored data with empirical validation. The measurements can be made in real buildings, controlled test cells, or in a laboratory. The design and operation of experiments leading to high-quality data sets is complex and expensive,

thus restricting this approach to a limited number of cases. The characterization of some of the more complex physical processes treated by building simulation programs (such as heat transfer with the ground, infiltration, indoor air motion, and convection) is often excluded due to measurement difficulties and uncertainty.

A program is compared to itself or other programs with comparative testing. This includes both sensitivity testing and inter-model comparisons. This approach enables inexpensive comparisons at many levels of complexity. However, in practice the difficulties in equivalencing program inputs and outputs can lead to significant uncertainty in performing inter-model comparisons.

A general principle applies to all three validation constructs. The simpler and more controlled the test case, the easier it is to identify and diagnose sources of error. Realistic cases are suitable for testing the interactions between algorithms, but are less useful for identifying and diagnosing errors. Although the comparison of the actual long-term energy usage of a building with simulation results is perhaps the most convincing evidence of validity from the building designer's perspective, this is actually the least conclusive approach. This is because the simultaneous operation of all possible error sources combined with the possibility of offsetting errors means that good or bad agreement cannot be attributed to program validity.

Annex 42's Validation Approach

A validation programme following the accepted methodology outlined above was designed and executed for the Annex 42 models.

Since each model was independently implemented into a number of building simulation programs, emphasis was first placed upon inter-model comparative testing to identify coding errors and errors or inaccuracies in the mathematical solution of the models. This was a

significant undertaking that involved drafting test case descriptions, conducting simulations with each simulation platform, contrasting simulation predictions, and diagnosing and repairing coding errors. Iteration was often required during this process: some revision and re-testing was necessary to actualize test case descriptions that could be interpreted unambiguously to guarantee the equivalencing of program inputs. In addition to revealing errors in the programs, the comparative testing also revealed deficiencies and ambiguities in the mathematical models. Some of the initial predictive disagreements between programs were a result of differing interpretations of aspects of the mathematical models, which were substantially clarified. Over the course of this comparative testing numerous errors in all of the implementations were remedied. Therefore, the participants are confident that all four simulation platforms correctly implement the Annex 42 models.

Empirical validation was then used to assess the validity of the mathematical models to simulate the performance of actual cogeneration devices through the comparison of simulation results with measurements taken in laboratory situations. This not only verified the mathematical model but also the accuracy of its calibration using the empirical data gathered from the validation experiments. Although this empirical validation builds confidence in the Annex 42 models, in the future it would be desirable to extend this work to consider other devices and operating scenarios.

The third validation construct, analytical validation, was not employed due to the complex nature of these devices and the lack of appropriate analytic solutions for the relevant thermodynamic processes.

Report Outline

Section II of this report documents the inter-model comparative testing programme that was devised for the fuel cell cogeneration model. A suite of 50 test cases, each carefully constructed to isolate a specific aspect of the model, was created. Collectively these test

cases examine every aspect of the model and exercise each line of its source code implementations. This section documents each of these test cases in an unambiguous fashion to allow other developers to conduct the tests in the future. It also presents the calculation results from the five building simulation programs that applied the test suite. In a similar manner, section III documents the 44 test cases that form the inter-model comparative test suite for the combustion-based cogeneration model and presents the calculation results from three building simulation programs.

Section IV treats the empirical validation of the fuel cell cogeneration model using data gathered on a prototype solid-oxide fuel cell cogeneration device. In a similar manner, section V treats the empirical validation of the combustion-based cogeneration model using data gathered on a production Stirling engine cogeneration device.

References

ANSI/ASHRAE (2004). *Standard Method of Test for the Evaluation of Building Energy Analysis Computer Programs*. Standard 140-2004, Atlanta USA.

CEN (2004). *prEN ISO 13791: Thermal Performance of Buildings Calculation of Internal Temperatures of a Room in Summer without Mechanical Cooling—General Criteria and Validation Procedures*. ISO/FDIS 13791:2004, Brussels Belgium.

Crawley, D., Lawrie, L., Winkelmann, F., Buhl, W., Huang, Y., Pedersen, C., Strand, R., Liesen, R., Fisher, D., Witte, M., and Glazer, J. (2001). Energyplus: Creating a new-generation building energy simulation program. *Energy and Buildings*, 33:319–331.

ESRU (2005). The ESP-r system for building energy simulations: User guide version 10 series. Technical Report U05/1, University of Strathclyde, Glasgow UK.

Jensen, S., editor (1993). *Validation of Building Energy Simulation Programs, Part I and II*. PASSYS Subgroup Model Validation and Development. EUR 15115 EN.

Judkoff, R. and Neymark, J. (1995). *International Energy Agency Building Energy Simulation Test (BESTEST) and Diagnostic Method*. IEA/ECBCS Annex 21 Subtask C and IEA/SHC Task 12 Subtask B Report.

Judkoff, R., Wortman, D., O'Doherty, B., and Burch, J. (1983). A methodology for validating building energy analysis simulations. Technical Report TR-254-1508, Solar Energy Research Institute, Golden USA.

Kelly, N. and Beausoleil-Morrison, I., editors (2007). *Specifications for Modelling Fuel Cell and Combustion-Based Residential Cogeneration Devices within Whole-Building Simulation Programs*. IEA/ECBCS Annex 42 Report. ISBN No. 978-0-662-47116-5.

Klein, S. (2004). Trnsys 16, a transient system simulation program. Technical report, Solar Energy Laboratory, University of Wisconsin, Madison USA.

Lomas, K., Eppel, H., Martin, C., and Bloomfield, D. (1994). *Empirical Validation of Thermal Building Simulation Programs Using Test Room Data, Volume 1: Final Report*. IEA ECBCS Annex 21 and IEA SHC Task 12.

Section II

Inter-program Comparative Tests for the Annex 42 Fuel Cell Cogeneration Model

AUTHORS:

Ian Beausoleil-Morrison (Natural Resources Canada)

Brent Griffith (National Renewable Energy Laboratory, USA)

WITH INPUT FROM:

Teemu Vesanen (Technical Research Centre of Finland)

Sébastien Lerson (Université de Liège, Belgium),

Andreas Weber (Swiss Federal Laboratories for Materials Testing and Research)

Kathleen Siemens (Natural Resources Canada)

Section II Table of Contents

Introduction to this Section

This section documents the inter-model comparative testing suite that was devised for the Annex 42 fuel cell cogeneration (FC-cogeneration) model. The suite is composed of 50 test cases, each carefully constructed to isolate a specific aspect of the model. Collectively these test cases examine every aspect of the model and exercise each line of a source code implementation of the model. By design, these test cases make no attempt to represent realistic situations or FC-cogeneration systems. Rather, they are designed to exercise specific aspects of the model and to exaggerate differences between programs for the purposes of diagnosing errors.

The Annex 42 FC-cogeneration model has been implemented into five simulation programs: ESP-r (ESRU, 2005), EnergyPlus (Crawley *et al.*, 2001), TRNSYS (Klein, 2004), EES (Klein, 2005), and IDA-ICE (Sahlin and Sowell, 1989). The ESP-r, EnergyPlus, EES, and IDA-ICE implementations were conducted independently by four different developers. The TRNSYS implementation was performed by a fifth developer, but in this case a *wrapper routine* was written to encapsulate the ESP-r FORTRAN source code.

Each comparative test case is described here in an unambiguous fashion which enables the equivalencing of inputs from one simulation program to another. These descriptions are the product of an iterative process in which the five developers simulated the test cases, compared results, and refined the test case descriptions to eliminate ambiguities. Since all programs have implemented the same mathematical model they should produce identical or near-identical results. Consequently, this test suite acted as an efficient diagnostic tool for isolating internal sources of error through the comparison of program-to-program predictions. The iterative process that led to the final form of the comparative test suite presented here resulted in the diagnosis and subsequent repair of numerous solution problems and coding errors (Beausoleil-Morrison *et al.*, 2006). Without this kind of rigorous testing some of these errors would have gone undetected, perhaps for a significant period of time.

Results from the five simulation programs are presented in graphical form following the description of each of the 50 test cases. These are the final results produced by these programs following the correction of any errors that were detected through the program-to-program comparisons. Despite these efforts there are a few unresolved issues in the

model implementations as evidenced in the graphs presented here. The specific unresolved issues are summarized as follows:

- Case 400 indicates that there is likely a bug in the EES implementation regarding the calculation of the air enthalpy,
- There are some slight disagreements between EnergyPlus and the other programs in a number of the 600 series of comparisons. This might indicate a difference in the methods used to calculate thermophysical properties or be attributable to an error.
- Both IDA-ICE and EES exhibit unexpected behaviour in some of the case 604 comparisons, indicating a likely error in the treatment of condensation in the gas-to-water heat exchanger.
- IDA-ICE demonstrates an unexplained anomalous behaviour in one of the case 803 comparisons.

This document acts as a valuable resource for developers who wish to implement the Annex 42 FC-cogeneration model into other simulation programs. The comparison of results from their programs to those presented here can help to diagnose errors to specific sections of source code.

ESP-r and TRNSYS implement the full functionality of the Annex 42 FC-cogeneration model and consequently results from these programs are presented for all 50 cases. The structure of the Annex 42 FC-cogeneration model permitted the omission of certain control volumes. Results from EnergyPlus, IDA-ICE, and EES are presented for the aspects of the model that they support. For example, the EnergyPlus implementation omits the auxiliary burner, dilution air system, stack cooling loop, and the start-up and cool-down cycles. while the IDA-ICE implementation omits the stack cooling loop. The EES implementation omits a number of aspects of the model as it was not completed but its results are retained here as it provided a useful comparison for the other programs.

The tests are grouped by into nine series, each of which exercises a certain grouping of models:

- The *100 series* cases exercise the portions of code that calculate the flow rates and enthalpies of the fuel and air streams entering the fuel cell power module (FCPM).

- The *200 series* cases exercise the portions of code that calculate the flow rates and enthalpies of the gas constituents exiting the FCPM. They also exercise the calculation of air supply rate to the FCPM, AC-powered ancillaries, and skin losses from the FCPM, and the impact these have upon the FCPM energy balance.
- The *300 series* cases exercise the portions of code that treat the start-up and cool-down cycles and its operational degredation.
- The *400 series* cases exercise the models that treat the air supply blower, fuel supply compressor, and water pump that supply air, fuel, and liquid water to the FCPM.
- The *500 series* cases exercise the portions of the code that model the auxiliary burner.
- The *600 series* cases exercise the portions of the code that model the exhaust-gas-to-water heat exchanger.
- The *700 series* cases exercise the portions of the code that model the dilution air system and heat recovery ventilator (HRV).
- The *800 series* cases exercise the portions of the code that treat the FCPM's transient response characteristics, the electrical system control behaviour, as well as the models for electrical storage (battery) and DC-AC power conditioning (PCU).
- The *900 series* cases exercise the portions of the code that treat the stack cooling system.

The reader is referred to Section II of the Annex 42 final report that describes the FC-cogeneration model for details on the model's formulation (Kelly and Beausoleil-Morrison, 2007), which is referred to here as the *model specifications*. Equation symbols used here correspond to those in the model specifications and frequent reference is made to section and equation numbers from that report.

100 Series Tests

The *100 series* cases exercise the evaluation of air and fuel properties, such as the lower heating value (LHV) and enthalpies. It examines the temperature dependence of these properties and also exercises the model's determinination of the temperature of the air and fuel entering the FCPM. The ability of the FC-cogeneration device to follow electrical loads and the calculation of the FCPM's electrical efficiency is also examined. Additionally, it provides a check on the determination of the air and fuel flow rates entering the FCPM.

The battery and power conditioning unit (PCU) control volumes are nullified in this series of tests.

Case 100

Case 100 is the base case model.

The simulation is conducted for a single day (January 9) with whatever start-up or conditioning period is appropriate for the simulation program. The simulation should be performed with a time-step no greater than 15 minutes. The weather file is inconsequential.

Air and fuel are supplied to the FC-cogeneration device at a constant 20°C. This can be accomplished by locating the FC-cogeneration device within a building thermal zone whose temperature is controlled at a constant 20°C. The blower draws air from the room containing the FC-cogeneration device (refer to section II-3 of the model specifications). Likewise, the fuel compressor draws fuel at the temperature of the containing room (refer to section II-4 of the model specifications). The blower and compressor "heat loss fractions" are set to unity so that the electrical consumption of these devices do not affect the air and fuel temperatures entering the FCPM. Consequently, the air and fuel will enter the FCPM control volume at 20°C. The other parameters for the blower and fuel compressor are inconsequential for this test case.

The electrical efficiency of the FCPM is for a hypothetical system. The efficiency varies over the range of the operating points simulated in this case. There is no degredation associated with stop-start cycles nor with operating time (refer to section II-2.2 of the model specifications).

The DC electrical output of the FCPM is made to follow an electrical demand which varies from 1 000 W to 3 300 W. The demand is 1 000 W from 0h00 to 1h00 and there is a 100 W step increment at the top of each hour. This electrical demand (and thus the FCPM DC output) is illustrated in Figure II-1. The maximum allowable time derivative of the FCPM's electrical output (refer to section II-2.4 of the model specifications) is set sufficiently high to enable this 100 W step-change over the time-step of the simulation.

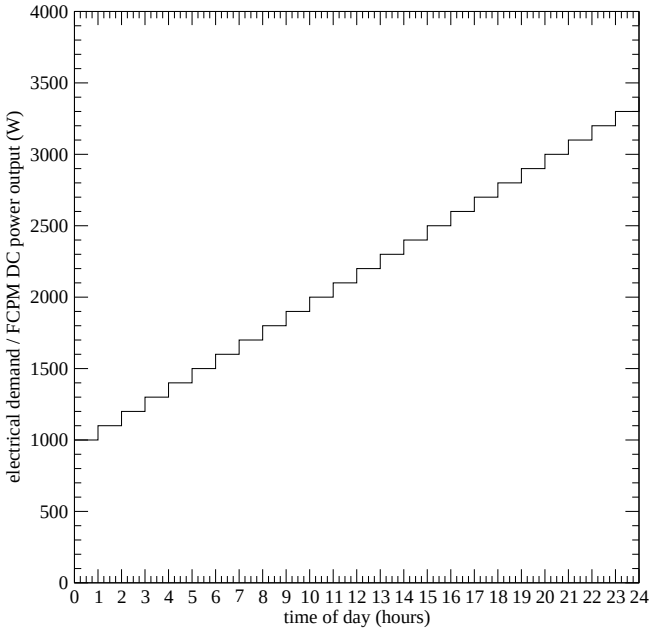

Figure II-1: Electrical demand upon FC-cogeneration unit for case 100

The fuel mixture provided to the FCPM is 100% methane and the air is of a typical composition. The air supply rate to the FCPM is determined using *method 2* (refer to section II-2.6 of the model specifications).

The pertinent input data to the FC-cogeneration model are listed in Table II-1.

The following simulation predictions are examined with this test case:

- The LHV of the fuel mixture, LHV_{fuel}. Refer to section II-2.5 of the model specifications.
- The electrical efficiency of the FCPM, ε_{el}. Refer to section II-2.2 of the model specifications.

FCPM electrical efficiency	$\varepsilon_0 = 0.3;\ \varepsilon_1 = 1.1 \cdot 10^{-4};\ \varepsilon_2 = -2 \cdot 10^{-8}$
	$D = 0$
	$L = 0$
FCPM transient response	$(dP_{el}/dt)_{\max}$ = 10 (W/s) for both increasing and decreasing power
fuel molar fractions	$\chi_{H_2} = 0;\ \chi_{CH_4} = 1.0;\ \chi_{C_2H_6} = 0;\ \chi_{C_3H_8} = 0;\ \chi_{C_4H_{10}} = 0;$ $\chi_{C_5H_{12}} = 0;\ \chi_{C_6H_{14}} = 0;\ \chi_{CH_3OH} = 0;\ \chi_{C_2H_5OH} = 0;\ \chi_{CO_2} = 0;$ $\chi_{N_2} = 0;\ \chi_{O_2} = 0$
air molar fractions	$\chi_{N_2} = 0.7728;\ \chi_{O_2} = 0.2073;\ \chi_{H_2O} = 0.0104;\ \chi_{Ar} = 0.0092;$ $\chi_{C_{O_2}} = 0.0003;$
air supply to FCPM	method 2 $a_0 = 5 \cdot 10^{-5};\ a_1 = 1.5 \cdot 10^{-7};\ a_2 = 1.1 \cdot 10^{-12};\ a_3 = 0$
air supply blower	$T_{blower-in} = 20^oC$ (air drawn at containing room's temperature)
	$\alpha_{blower-heat-loss} = 1.0$
fuel compressor	$T_{comp-in} = 20^oC$ (fuel drawn at containing room's temperature)
	$\alpha_{comp-heat-loss} = 1.0$

Table II-1: Input data for case 100

- The molar flow rate of the fuel supplied to the FCPM, $\dot{N}_{fuel}$. Refer to equation II-10 of the model specifications.
- The molar flow rate of the air supplied to the FCPM, $\dot{N}_{air}$. Refer to section II-2.6 of the model specifications.
- The total enthalpy flow rate relative to the standard state of the air stream entering the FCPM, $\sum_i (\dot{N}_i \cdot [\hat{h}_i - \Delta_f \hat{h}_i^o])_{air}$. Refer to sections II-2.1 and II-2.6 of the model specifications.
- The total enthalpy flow rate relative to the standard state of the fuel stream entering the FCPM, $\sum_i (\dot{N}_i \cdot [\hat{h}_i - \Delta_f \hat{h}_i^o])_{fuel}$. Refer to sections II-2.1 and II-2.5 of the model specifications.

These results are given in Figures II-2 through II-6.

100 Series

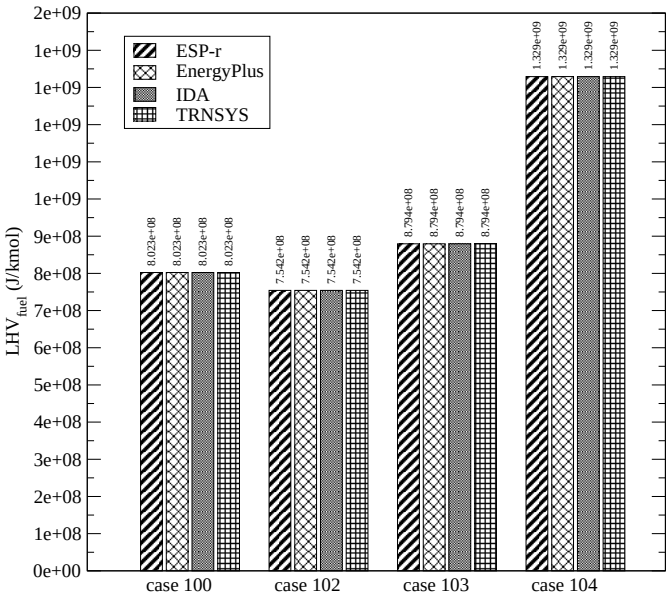

Figure II-2: 100 Series LHV_{fuel} results

Case 100

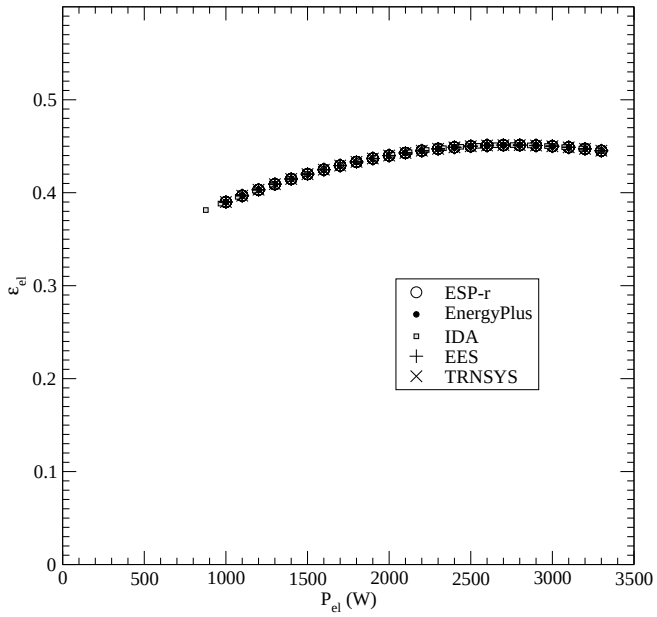

Figure II-3: Case 100 ε_{el} results

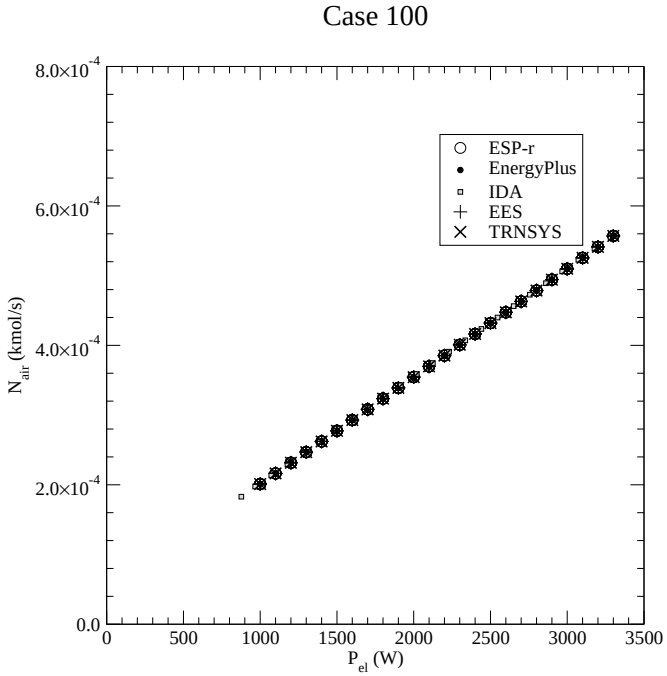

Figure II-4: Case 100 $\dot{N}_{air}$ results

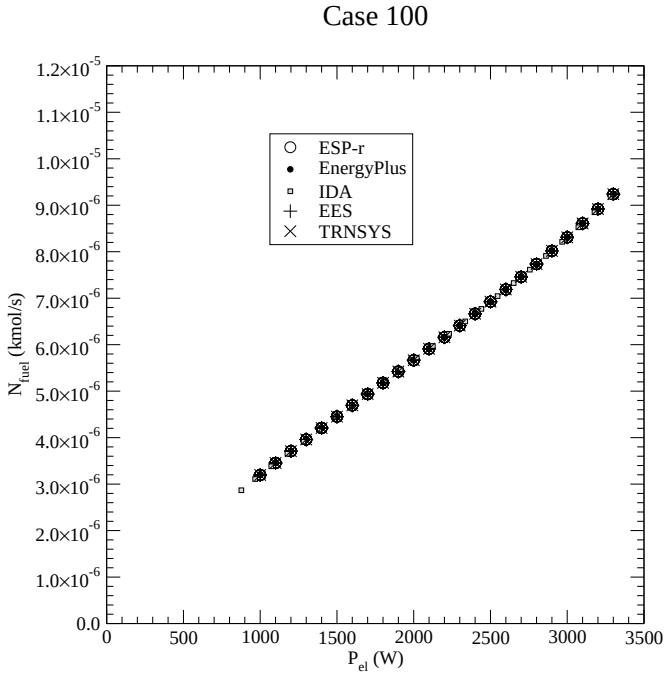

Figure II-5: Case 100 $\dot{N}_{fuel}$ results

Case 100

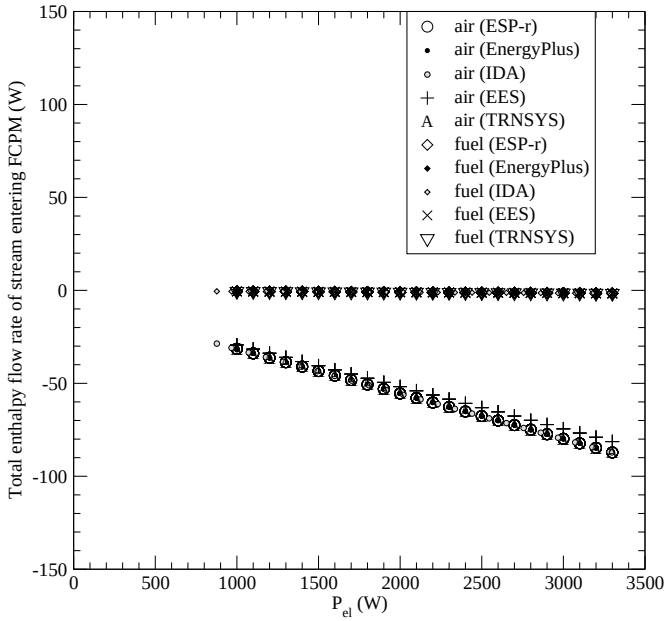

Figure II-6: Case 100 $\sum_i(\dot{N}_i \cdot [\hat{h}_i - \Delta_f \hat{h}_i^o])_{air}$ and $\sum_i(\dot{N}_i \cdot [\hat{h}_i - \Delta_f \hat{h}_i^o])_{fuel}$ results

Disagreement between programs in the prediction of LHV_{fuel} could be indicative of errors in the calculation of the enthalpy of methane, carbon dioxide, and/or water vapour.

Disagreement in the prediction of ε_{el} would be indicative of errors in the implementation of equation II-8 of the model specifications.

If LHV_{fuel} and ε_{el} predictions are in agreement then disagreement in the prediction of $\dot{N}_{fuel}$ would be indicative of errors in the implementation of equation II-10 of the model specifications.

Disagreement in the predictions of $\dot{N}_{air}$ would be indicative in the implementation of equation II-16 of the model specifications.

If $\dot{N}_{air}$ predictions are in agreement then disagreement in the predictions of $\sum_i(\dot{N}_i \cdot [\hat{h}_i - \Delta_f \hat{h}_i^o])_{air}$ could be indicative of errors in one or more of the following: the calculation of the enthalpies of the air constituents; the weighted sum by molar fraction of the enthalpies of the individual constituents of the air stream; or establishment of the temperature of the air at the FCPM inlet.

If $\dot{N}_{fuel}$ predictions are in agreement then disagreement in the predictions of $\sum_i (\dot{N}_i \cdot [\hat{h}_i - \Delta_f \hat{h}_i^o])_{fuel}$ could be indicative of errors in one or more of the following: the calculation of the enthalpies of methane; or the establishment of the temperature of the fuel at the FCPM inlet.

Case 101

Case 101 is identical to case 100 with the exception that the air and fuel are drawn into the FCPM at 50°C. The pertinent input data to the FC-cogeneration model are listed in Table II-1 with the changes noted in Table II-2.

air supply blower	$T_{blower-in} = 50^o C$ (air drawn at containing room's temperature)
fuel compressor	$T_{comp-in} = 50^o C$ (fuel drawn at containing room's temperature)

Table II-2: Input data for case 101 that override the data given in Table II-1

The following simulation predictions should be plotted against P_{el}:

- The difference in $\sum_i (\dot{N}_i \cdot [\hat{h}_i - \Delta_f \hat{h}_i^o])_{air}$ between case 101 and case 100 (case 101 result minus case 100 result).
- The difference in $\sum_i (\dot{N}_i \cdot [\hat{h}_i - \Delta_f \hat{h}_i^o])_{fuel}$ between case 101 and case 100.

These results are given in Figure II-7.

Case 101 Versus Case 100

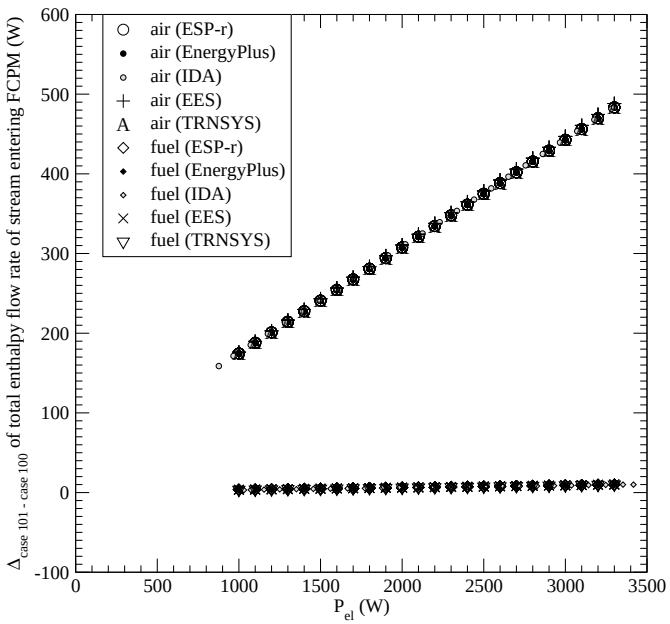

Figure II-7: $\Delta_{case\ 101\ -\ case\ 100} \sum_i (\dot{N}_i \cdot [\hat{h}_i - \Delta_f \hat{h}_i^o])_{air}$ **and** $\sum_i (\dot{N}_i \cdot [\hat{h}_i - \Delta_f \hat{h}_i^o])_{fuel}$ **results**

If case 100 predictions are in agreement then disagreement in the delta between cases 100 and 101 would be indicative of errors in the treatment of the temperature influence of the enthalpy of the air constituents and/or of methane.

Case 102

Case 102 is identical to case 100 with the exception that some inert gas is added to the fuel mixture. The pertinent input data to the FC-cogeneration model are listed in Table II-1 with the changes noted in Table II-3.

fuel molar fractions	$\chi_{H_2} = 0;\ \chi_{CH_4} = 0.94;\ \chi_{C_2H_6} = 0;\ \chi_{C_3H_8} = 0;\ \chi_{C_4H_{10}} = 0;$ $\chi_{C_5H_{12}} = 0;\ \chi_{C_6H_{14}} = 0;\ \chi_{CH_3OH} = 0;\ \chi_{C_2H_5OH} = 0;$ $\chi_{CO_2} = 0.02;\ \chi_{N_2} = 0.02;\ \chi_{O_2} = 0.02$

Table II-3: Input data for case 102 that override the data given in Table II-1

The following simulation predictions are examined with this test case:

- LHV_{fuel}.
- The difference in $\sum_i (\dot{N}_i \cdot [\hat{h}_i - \Delta_f \hat{h}_i^o])_{fuel}$ between case 102 and case 100 (case 102 result minus case 100 result).

These results are plotted in Figure II-8.

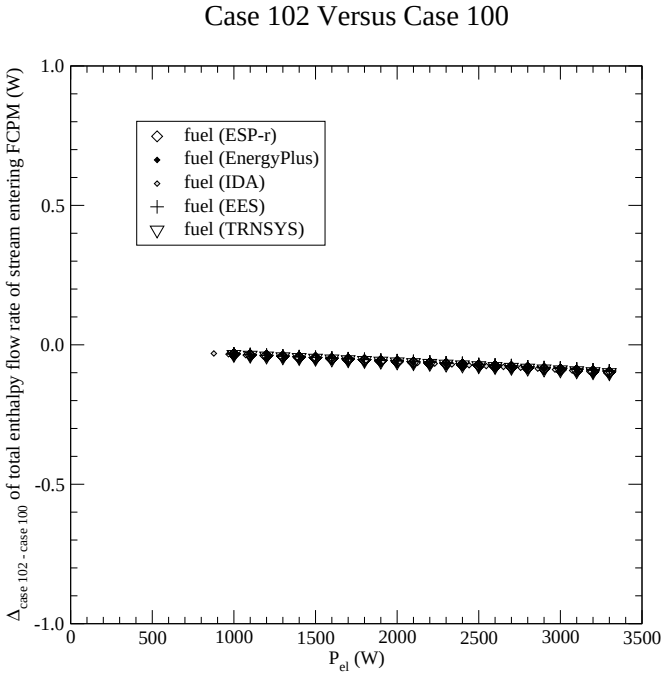

Figure II-8: $\Delta_{case\ 102\ -\ case\ 100} \sum_i (\dot{N}_i \cdot [\hat{h}_i - \Delta_f \hat{h}_i^o])_{fuel}$ **results**

Disagreement between programs in the prediction of LHV_{fuel} could be indicative of errors in the calculation of the enthalpies of the constituents of the fuel mixture and/or the determination of the quantity of carbon dioxide and water vapour produced by its complete reaction.

If case 100 and 101 predictions are in agreement then disagreement in the delta between cases 100 and 102 could be indicative of errors in one of more of the following: the calculation of $\dot{N}_{fuel}$; the weighted sum by molar fraction of the enthalpies of the fuel constituents.

Case 103

Case 103 is identical to case 102 with the exception that some ethane is added to the fuel mixture. The pertinent input data to the FC-cogeneration model are listed in Table II-1 with the changes noted in Table II-4.

fuel molar fractions	$\chi_{H_2} = 0;\ \chi_{CH_4} = 0.74;\ \chi_{C_2H_6} = 0.20;\ \chi_{C_3H_8} = 0;\ \chi_{C_4H_{10}} = 0;$ $\chi_{C_5H_{12}} = 0;\quad \chi_{C_6H_{14}} = 0;\quad \chi_{CH_3OH} = 0;\quad \chi_{C_2H_5OH} = 0;$ $\chi_{CO_2} = 0.02;\ \chi_{N_2} = 0.02;\ \chi_{O_2} = 0.02$

Table II-4: Input data for case 103 that override the data given in Table II-1

The following simulation predictions are examined with this test case:

- LHV_{fuel}.
- The difference in $\sum_i (\dot{N}_i \cdot [\hat{h}_i - \Delta_f \hat{h}_i^o])_{fuel}$ between case 103 and case 100 (case 103 result minus case 100 result).

These results are give in Figure II-9.

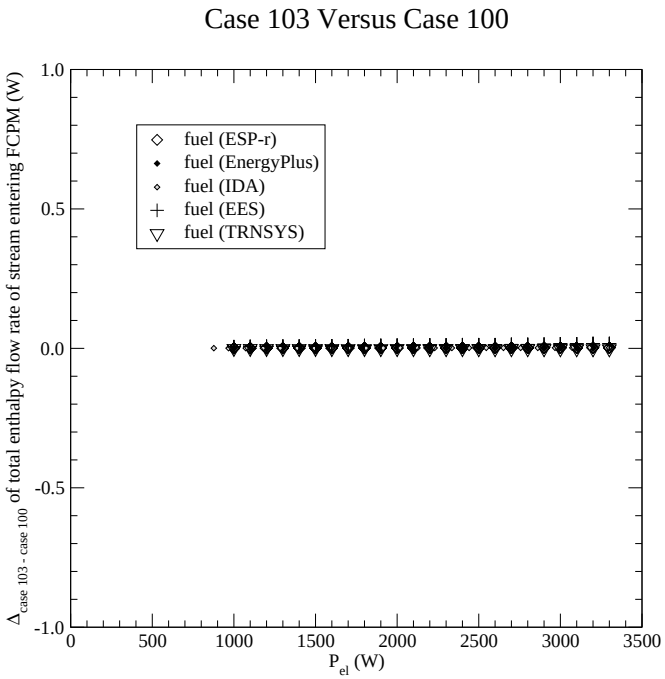

Figure II-9: $\Delta_{case\ 103\ -\ case\ 100} \sum_i (\dot{N}_i \cdot [\hat{h}_i - \Delta_f \hat{h}_i^o])_{fuel}$ **results**

Disagreement between programs in the prediction of LHV_{fuel} could be indicative of errors in the calculation of the enthalpies of the ethane constituent of the fuel mixture and/or the determination of the quantity of carbon dioxide and water vapour produced by its complete reaction.

If the predictions of the previous 100 series cases are in agreement then disagreement in the delta between cases 100 and 103 could be indicative of errors in one of more of the following: the calculation of $\dot{N}_{fuel}$; the weighted sum by molar fraction of the enthalpies of the fuel constituents.

Case 104

Case 104 is identical to case 103 with the exception that some higher hydrocarbons and alcohols are added to the fuel mixture. The pertinent input data to the FC-cogeneration model are listed in Table II-1 with the changes noted in Table II-5.

The following simulation predictions are examined with this test case:

fuel molar fractions	$\chi_{H_2} = 0$; $\chi_{CH_4} = 0.44$; $\chi_{C_2H_6} = 0.20$; $\chi_{C_3H_8} = 0.05$; $\chi_{C_4H_{10}} = 0.05$; $\chi_{C_5H_{12}} = 0.05$; $\chi_{C_6H_{14}} = 0.05$; $\chi_{CH_3OH} = 0.05$; $\chi_{C_2H_5OH} = 0.05$; $\chi_{CO_2} = 0.02$; $\chi_{N_2} = 0.02$; $\chi_{O_2} = 0.02$

Table II-5: Input data for case 104 that override the data given in Table II-1

- LHV_{fuel}.
- The difference in $\sum_i (\dot{N}_i \cdot [\hat{h}_i - \Delta_f \hat{h}_i^o])_{fuel}$ between case 104 and case 100 (case 104 result minus case 100 result).

These results are given in Figure II-10.

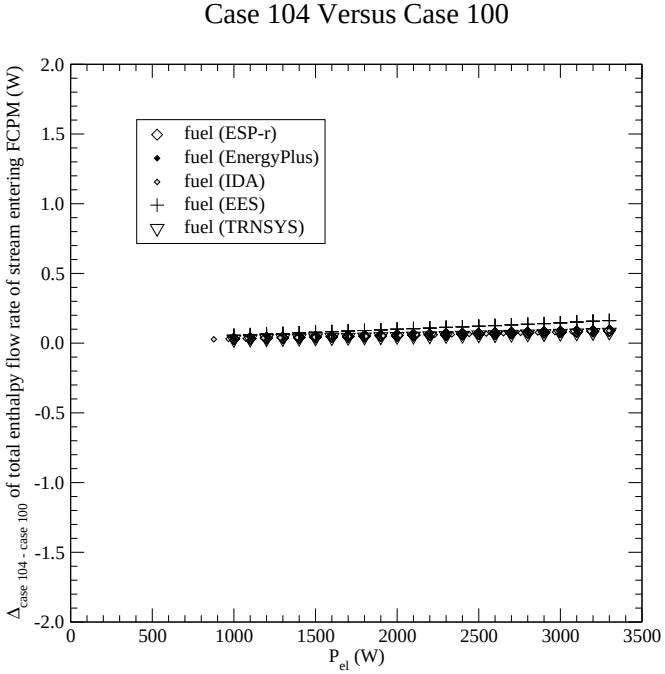

Figure II-10: $\Delta_{case\ 104 - case\ 100} \sum_i (\dot{N}_i \cdot [\hat{h}_i - \Delta_f \hat{h}_i^o])_{fuel}$ **results**

Disagreement between programs in the prediction of LHV_{fuel} could be indicative of errors in the calculation of the enthalpies of the higher hydrocarbon and alcohol constituents of the fuel mixture and/or the determination of the quantity of carbon dioxide

and water vapour produced by its complete reaction.

If the predictions of the previous 100 series cases are in agreement then disagreement in the delta between cases 100 and 104 could be indicative of errors in one of more of the following: the calculation of $\dot{N}_{fuel}$; the weighted sum by molar fraction of the enthalpies of the fuel constituents.

Case 105

Case 105 is identical to case 104 with the exception that the air and fuel are drawn into the FCPM at 50°C. The pertinent input data to the FC-cogeneration model are listed in Table II-1 with the changes noted in Table II-6.

fuel molar fractions	$\chi_{H_2} = 0;\quad \chi_{CH_4} = 0.44;\quad \chi_{C_2H_6} = 0.20;\quad \chi_{C_3H_8} = 0.05;$ $\chi_{C_4H_{10}} = 0.05;\ \chi_{C_5H_{12}} = 0.05;\ \chi_{C_6H_{14}} = 0.05;\ \chi_{CH_3OH} = 0.05;$ $\chi_{C_2H_5OH} = 0.05;\ \chi_{CO_2} = 0.02;\ \chi_{N_2} = 0.02;\ \chi_{O_2} = 0.02$
air supply blower	$T_{blower-in} = 50^oC$ (air drawn at containing room's temperature)
fuel compressor	$T_{comp-in} = 50^oC$ (fuel drawn at containing room's temperature)

Table II-6: Input data for case 105 that override the data given in Table II-1

The following simulation predictions should be plotted against P_{el}:

- The difference in $\sum_i (\dot{N}_i \cdot [\hat{h}_i - \Delta_f \hat{h}_i^o])_{air}$ between case 105 and case 104 (case 105 result minus case 104 result).
- The difference in $\sum_i (\dot{N}_i \cdot [\hat{h}_i - \Delta_f \hat{h}_i^o])_{fuel}$ between case 105 and case 104.

These results are given in Figure II-11.

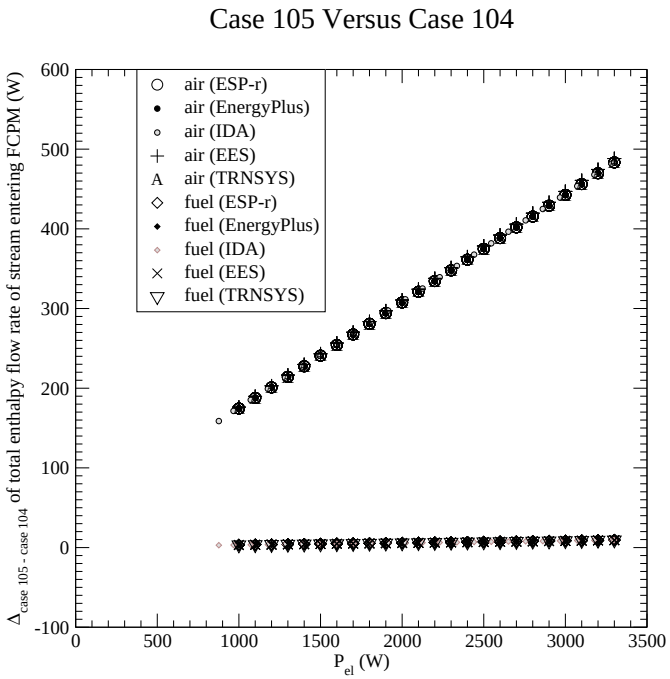

Figure II-11: $\Delta_{case\,105\,-\,case\,104}\ \sum_i(\dot{N}_i \cdot [\hat{h}_i - \Delta_f \hat{h}_i^o])_{air}$ **and** $\sum_i(\dot{N}_i \cdot [\hat{h}_i - \Delta_f \hat{h}_i^o])_{fuel}$ **results**

If case 104 predictions are in agreement then disagreement in the delta between cases 104 and 105 would be indicative of errors in the treatment of the temperature influence of the enthalpy of the air constituents and/or of the fuel constituents.

Case 106

Case 106 is identical to case 104 with the exception that the air and fuel are drawn into the FCPM at 100°C. The pertinent input data to the FC-cogeneration model are listed in Table II-1 with the changes noted in Table II-7.

The following simulation predictions should be plotted against P_{el}:

- The difference in $\sum_i(\dot{N}_i \cdot [\hat{h}_i - \Delta_f \hat{h}_i^o])_{air}$ between case 106 and case 104 (case 106 result minus case 104 result).
- The difference in $\sum_i(\dot{N}_i \cdot [\hat{h}_i - \Delta_f \hat{h}_i^o])_{fuel}$ between case 106 and case 104.

fuel molar fractions	$\chi_{H_2} = 0;\quad \chi_{CH_4} = 0.44;\quad \chi_{C_2H_6} = 0.20;\quad \chi_{C_3H_8} = 0.05;$ $\chi_{C_4H_{10}} = 0.05;\ \chi_{C_5H_{12}} = 0.05;\ \chi_{C_6H_{14}} = 0.05;\ \chi_{CH_3OH} = 0.05;$ $\chi_{C_2H_5OH} = 0.05;\ \chi_{CO_2} = 0.02;\ \chi_{N_2} = 0.02;\ \chi_{O_2} = 0.02$
air supply blower	$T_{blower-in} = 100^oC$ (air drawn at containing room's temperature)
fuel compressor	$T_{comp-in} = 100^oC$ (fuel drawn at containing room's temperature)

Table II-7: Input data for case 106 that override the data given in Table II-1

These results are given in Figure II-12.

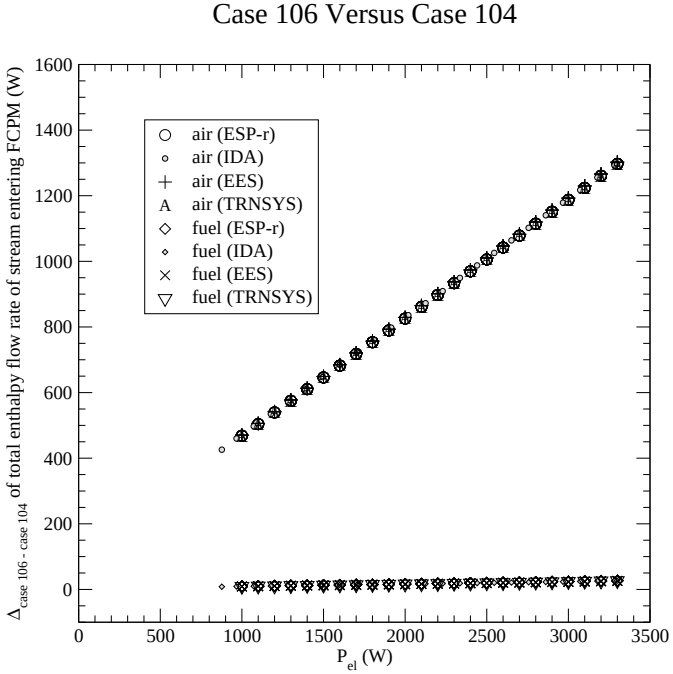

Figure II-12: $\Delta_{case\ 106\ -\ case\ 104}\ \sum_i(\dot{N}_i \cdot [\hat{h}_i - \Delta_f \hat{h}_i^o])_{air}$ **and** $\sum_i(\dot{N}_i \cdot [\hat{h}_i - \Delta_f \hat{h}_i^o])_{fuel}$ **results**

If case 104 predictions are in agreement then disagreement in the delta between cases 104 and 106 would be indicative of errors in the treatment of the temperature influence of the enthalpy of the air constituents and/or of the fuel constituents.

Case 107

Case 107 is identical to case 104 with the exception that the air and fuel are drawn into the FCPM at -30°C. The pertinent input data to the FC-cogeneration model are listed in

Table II-1 with the changes noted in Table II-8.

fuel molar fractions	$\chi_{H_2} = 0;\quad \chi_{CH_4} = 0.44;\quad \chi_{C_2H_6} = 0.20;\quad \chi_{C_3H_8} = 0.05;$ $\chi_{C_4H_{10}} = 0.05;\quad \chi_{C_5H_{12}} = 0.05;\quad \chi_{C_6H_{14}} = 0.05;\quad \chi_{CH_3OH} = 0.05;$ $\chi_{C_2H_5OH} = 0.05;\ \chi_{CO_2} = 0.02;\ \chi_{N_2} = 0.02;\ \chi_{O_2} = 0.02$
air supply blower	$T_{blower-in} = -30^oC$ (air drawn at containing room's temperature)
fuel compressor	$T_{comp-in} = -30^oC$ (fuel drawn at containing room's temperature)

Table II-8: Input data for case 107 that override the data given in Table II-1

The following simulation predictions should be plotted against P_{el}:

- The difference in $\sum_i (\dot{N}_i \cdot [\hat{h}_i - \Delta_f \hat{h}_i^o])_{air}$ between case 107 and case 104 (case 107 result minus case 104 result).
- The difference in $\sum_i (\dot{N}_i \cdot [\hat{h}_i - \Delta_f \hat{h}_i^o])_{fuel}$ between case 107 and case 104.

These results are given in Figure II-13.

Case 107 Versus Case 104

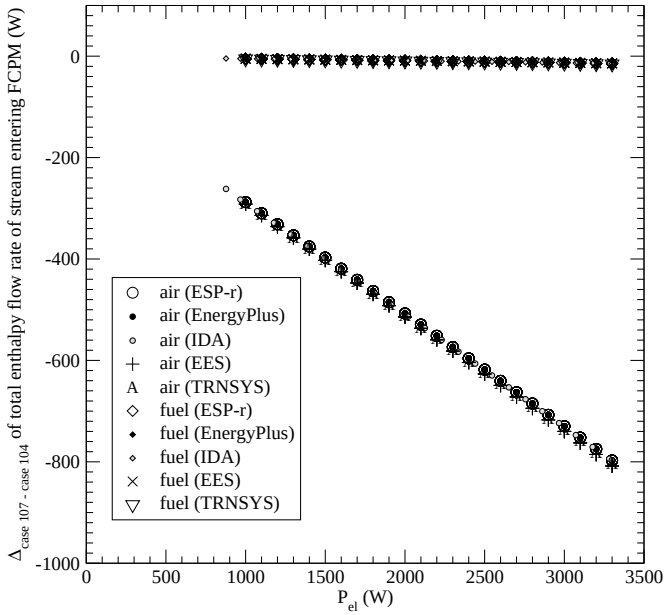

Figure II-13: $\Delta_{case\,107\,-\,case\,104}\ \sum_i(\dot{N}_i \cdot [\hat{h}_i - \Delta_f \hat{h}_i^o])_{air}$ **and** $\sum_i(\dot{N}_i \cdot [\hat{h}_i - \Delta_f \hat{h}_i^o])_{fuel}$ **results**

If case 104 predictions are in agreement then disagreement in the delta between cases 104 and 107 would be indicative of errors in the treatment of the temperature influence of the enthalpy of the air constituents and/or of the fuel constituents.

200 Series Tests

The *200 series* cases exercise the evaluation of the exhaust gases from the FCPM and the evaluation of the enthalpy of these exhaust gases. It also examines the temperature predictions of the FCPM exhaust gases and examines the integrity of the energy balance for the FCPM.

The battery and power conditioning unit (PCU) control volumes are nullified in this series of tests.

Case 200

The time period and time-step of the simulation and the weather conditions are identical to those used in case 100.

The treatment of the air supply blower and the fuel compressor is identical to that used in case 100. As with case 100, the air and fuel enter the FCPM at 20°C.

The electrical characteristics and electrical output of the FCPM are identical to case 100.

As with case 100, the fuel composition is 100% methane. The air supply rate is treated the same as case 100.

The following measures are taken to isolate terms in the FCPM energy balance (refer to equation II-7 of the model specifications). The AC-powered ancillaries which are included in the FCPM control volume (refer to section II-2.9 of the model specifications) draw no power. There are no skin losses from the FCPM (refer to section II-2.10 of the model specifications). There is no liquid water supplied to the FCPM (refer to section II-2.7 of the model specifications). There is no dilution air flow rate to the FCPM (refer to section II-9 of the model specifications). In this configuration, all of the enthalpy flowing into the FCPM control volume in the air and fuel streams is converted either to electricity or flows out of the control volume in the hot product gases.

The pertinent input data to the FC-cogeneration model are listed in Table II-1 with the changes noted in Table II-9.

The following simulation predictions should be plotted against P_{el}:

water supply to FCPM	$w_0 = 0.$; $w_1 = 0.$; $w_2 = 0.$
FCPM AC ancillaries	$anc_0 = 0.$; $anc_1 = 0.$
FCPM skin losses	method 1 $q_{skin-loss} = 0.$
dilution air	$\dot{N}_{dilution-air} = 0.$

Table II-9: Input data for case 200 that override the data given in Table II-1

- The flow rate of each product gas constituent, CO_2, H_2O, N_2, O_2, and Ar (refer to section II-2.8 of the model specifications).
- The total enthalpy flow rate relative to the standard state of the product gas stream exiting the FCPM, $\sum_i (\dot{N}_i \cdot [\hat{h}_i - \Delta_f \hat{h}_i^o])_{FCPM-cg}$ (refer to section II-2.8 of the model specifications).
- The temperature of the product gas stream exiting the FCPM, $T_{FCPM-cg}$.

These results are plotted in Figures II-14 through II-16.

Case 200

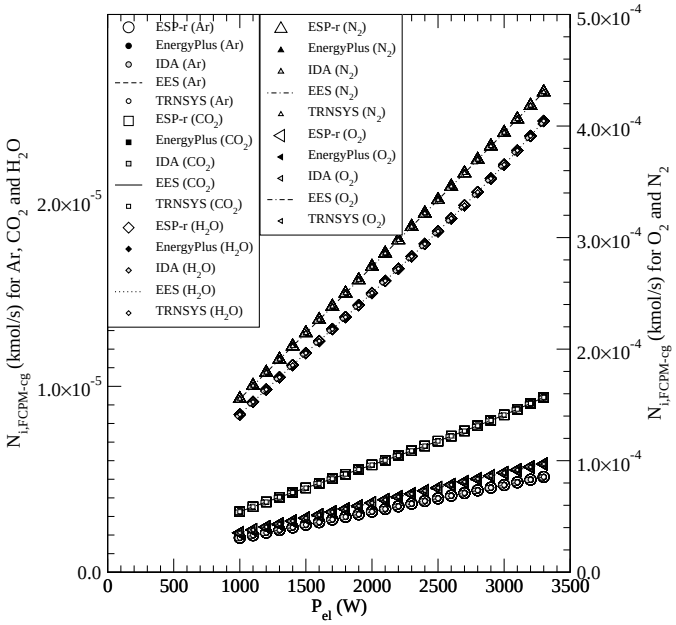

Figure II-14: Case 200 $\dot{N}_{i,FCPM-cg}$ results

Case 200

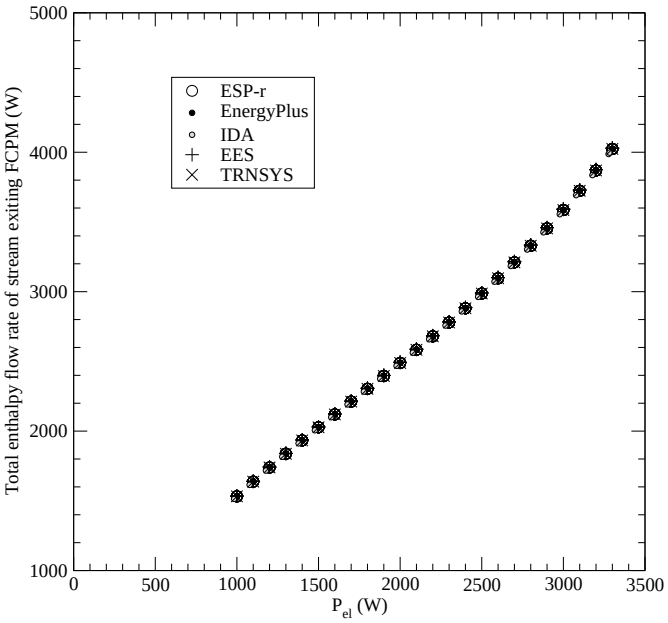

Figure II-15: Case 200 $\sum_i (\dot{N}_i \cdot [\hat{h}_i - \Delta_f \hat{h}_i^o])_{FCPM-cg}$ results

Case 200

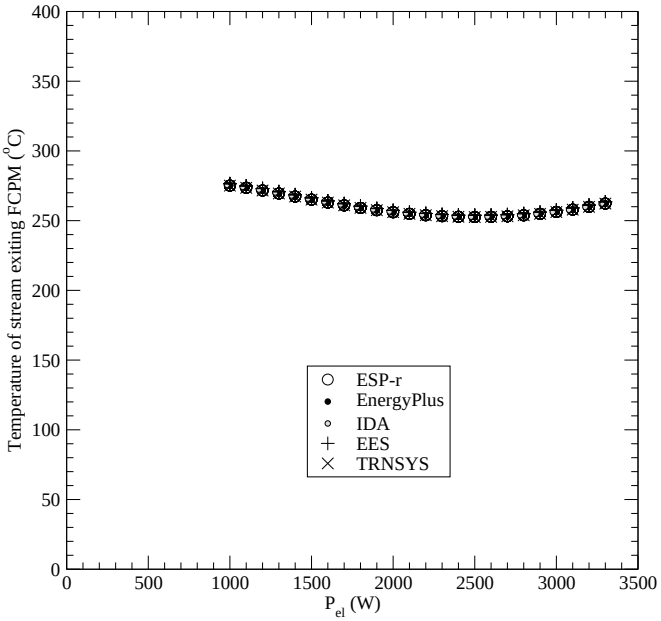

Figure II-16: Case 200 $T_{FCPM-cg}$ results

Disagreement between programs in the prediction of the flow rates of product gases would likely be indicative of an error in the modelling of the chemical reactions of the fuel constituents (equation II-15 of the model specifications) or an error in the treatment of the inert fuel and air constituents.

If the predictions of the 100 series cases were in agreement, then disagreement in the predictions of $\sum_i (\dot{N}_i \cdot [\hat{h}_i - \Delta_f \hat{h}_i^o])_{FCPM-cg}$ would be indicative of errors in the implementation or solution of the FCPM energy balance (equation II-7 of the model specifications). This case is configured to eliminate all terms of this energy balance except for those examined in the 100 series test cases and $\sum_i (\dot{N}_i \cdot [\hat{h}_i - \Delta_f \hat{h}_i^o])_{FCPM-cg}$. Additionally, the method used to evaluate the enthalpy relative to the standard state of each of the product gases as a function of temperature was examined in the 100 series tests. Consequently, hand calculations could be performed to isolate the errors in cases of disagreement.

Disagreement in the predictions of $T_{FCPM-cg}$ would be indicitive of the same problems as the above.

Case 201

Case 201 is identical to case 200 with the exception that some higher hydrocarbons and alcohols are added to the fuel mixture. The pertinent input data to the FC-cogeneration model are listed in Table II-1 with the changes noted in Table II-10.

fuel molar fractions	$\chi_{H_2} = 0;\quad \chi_{CH_4} = 0.44;\quad \chi_{C_2H_6} = 0.20;\quad \chi_{C_3H_8} = 0.05;$ $\chi_{C_4H_{10}} = 0.05;\quad \chi_{C_5H_{12}} = 0.05;\quad \chi_{C_6H_{14}} = 0.05;$ $\chi_{CH_3OH} = 0.05;\ \chi_{C_2H_5OH} = 0.05;\ \chi_{CO_2} = 0.02;\ \chi_{N_2} = 0.02;$ $\chi_{O_2} = 0.02$
water supply to FCPM	$w_0 = 0.;\ w_1 = 0.;\ w_2 = 0.$
FCPM AC ancillaries	$anc_0 = 0.;\ anc_1 = 0.$
FCPM skin losses	method 1 $q_{skin-loss} = 0.$
dilution air	$\dot{N}_{dilution-air} = 0.$

Table II-10: Input data for case 201 that override the data given in Table II-1

The following simulation predictions should be plotted against P_{el}:

- The flow rate of each product gas constituent, CO_2, H_2O, N_2, O_2, and Ar (refer to section II-2.8 of the model specifications).
- The total enthalpy flow rate relative to the standard state of the product gas stream exiting the FCPM, $\sum_i (\dot{N}_i \cdot [\hat{h}_i - \Delta_f \hat{h}_i^o])_{FCPM-cg}$ (refer to section II-2.8 of the model specifications).
- The temperature of the product gas stream exiting the FCPM, $T_{FCPM-cg}$.

These results are given in Figures II-17 through II-19.

Case 201

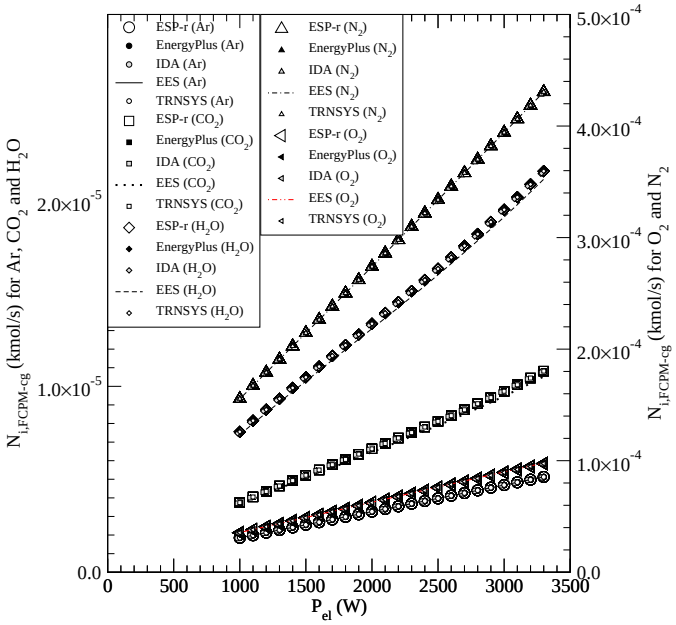

Figure II-17: Case 201 $\dot{N}_{i,FCPM-cg}$ results

Case 201

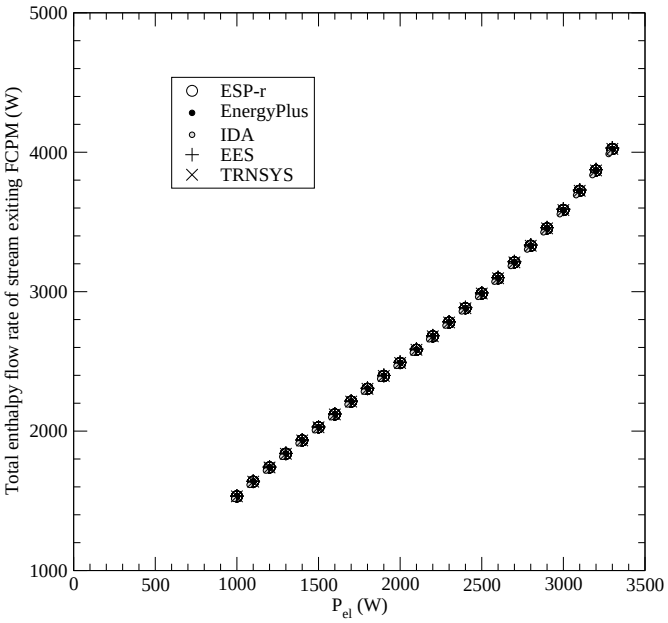

Figure II-18: Case 201 $\sum_i (\dot{N}_i \cdot [\hat{h}_i - \Delta_f \hat{h}_i^o])_{FCPM-cg}$ results

Case 201

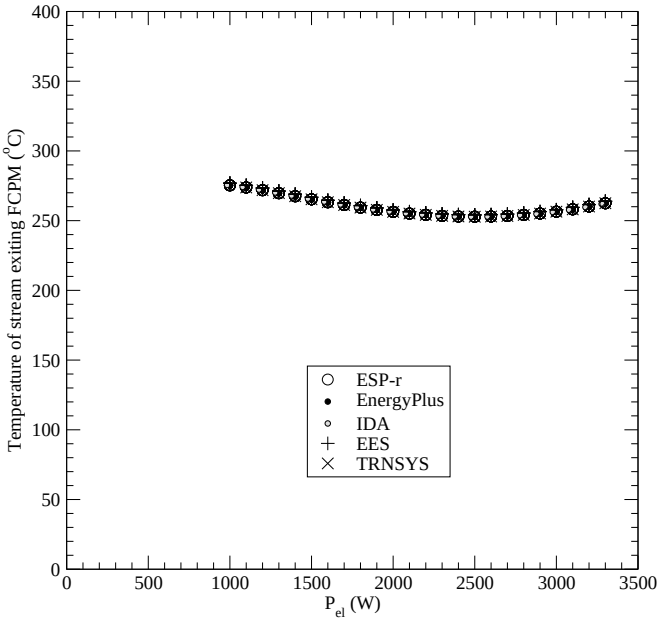

Figure II-19: Case 201 $T_{FCPM-cg}$ results

If case 200 predictions are in agreement then disagreement in case 201 predictions are most likely indicative of errors in the modelling of the chemical reactions of the higher hydrocarbon or alcohol fuel constituents (equation II-15 of the model specifications).

Case 202

Case 202 is identical to cases 200 and 201 with the exception that the fuel mixture is more typical for natural gas. The pertinent input data to the FC-cogeneration model are listed in Table II-1 with the changes noted in Table II-11.

The following simulation predictions should be plotted against P_{el}:

- The temperature of the product gas stream exiting the FCPM, $T_{FCPM-cg}$.

These results are given in Figure II-20.

fuel molar fractions	$\chi_{H_2} = 0$; $\chi_{CH_4} = 0.949$; $\chi_{C_2H_6} = 0.025$; $\chi_{C_3H_8} = 0.002$; $\chi_{C_4H_{10}} = 0.0006$; $\chi_{C_5H_{12}} = 0.0001$; $\chi_{C_6H_{14}} = 0.0001$; $\chi_{CH_3OH} = 0.$; $\chi_{C_2H_5OH} = 0.$; $\chi_{CO_2} = 0.007$; $\chi_{N_2} = 0.016$; $\chi_{O_2} = 0.0002$
water supply to FCPM	$w_0 = 0.$; $w_1 = 0.$; $w_2 = 0.$
FCPM AC ancillaries	$anc_0 = 0.$; $anc_1 = 0.$
FCPM skin losses	method 1 $q_{skin-loss} = 0.$
dilution air	$\dot{N}_{dilution-air} = 0.$

Table II-11: Input data for case 202 that override the data given in Table II-1

Case 202

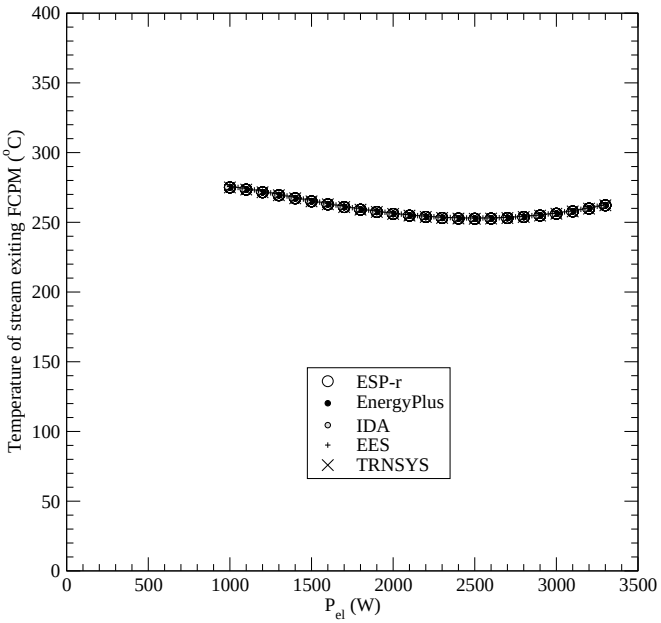

Figure II-20: Case 202 $T_{FCPM-cg}$ results

If case 200 and case 201 predictions are in agreement then it is highly unlikely that case 202 results will differ. This test is not diagnostic in itself, but rather provides a reference point for subsequent 200 series cases.

Case 203

Case 203 is identical to cases 202 with the exception of the calculation of the air supply rate. This is still calculated using *method 2* but now the air supply is made to vary with the temperature of the air supplied to the FCPM (refer to section II-2.6 of the model specifications). The pertinent input data to the FC-cogeneration model are listed in Table II-1 with the changes noted in Table II-12.

fuel molar fractions	$\chi_{H_2} = 0;\quad \chi_{CH_4} = 0.949;\quad \chi_{C_2H_6} = 0.025;\quad \chi_{C_3H_8} = 0.002;$ $\chi_{C_4H_{10}} = 0.0006;\quad \chi_{C_5H_{12}} = 0.0001;\quad \chi_{C_6H_{14}} = 0.0001;$ $\chi_{CH_3OH} = 0.;\quad \chi_{C_2H_5OH} = 0.;\quad \chi_{CO_2} = 0.007;\quad \chi_{N_2} = 0.016;$ $\chi_{O_2} = 0.0002$
water supply to FCPM	$w_0 = 0.;\ w_1 = 0.;\ w_2 = 0.$
air supply to FCPM	method 2 $a_0 = 5 \cdot 10^{-5};\ a_1 = 1.5 \cdot 10^{-7};\ a_2 = 1.1 \cdot 10^{-12};\ a_3 = 0.01$
FCPM AC ancillaries	$anc_0 = 0.;\ anc_1 = 0.$
FCPM skin losses	method 1 $q_{skin-loss} = 0.$
dilution air	$\dot{N}_{dilution-air} = 0.$

Table II-12: Input data for case 203 that override the data given in Table II-1

The following simulation predictions should be plotted against P_{el}:

- The difference in $T_{FCPM-cg}$ between case 203 and case 202 (case 203 result minus case 202 result).

These results are given in Figure II-21.

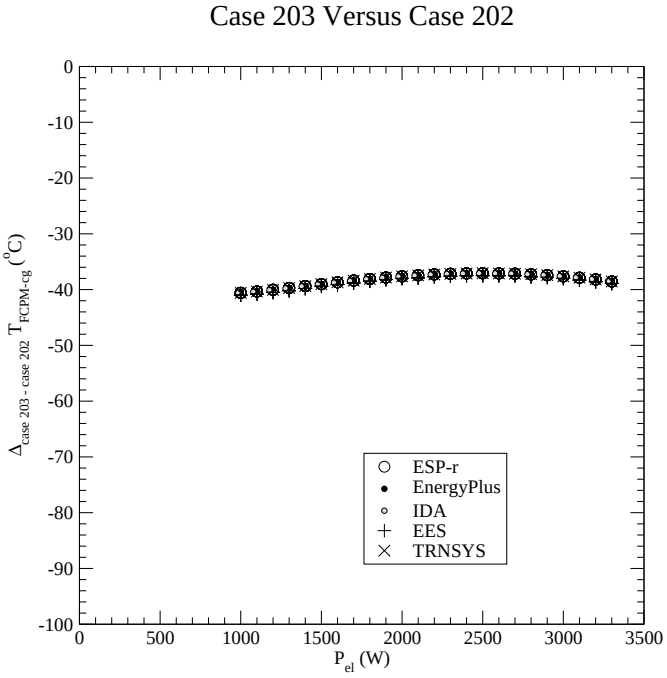

Figure II-21: $\Delta_{case\ 203\ -\ case\ 202}\ T_{FCPM-cg}$ **results**

If case 202 predictions are in agreement then disagreement in case 203 results would be indicative of errors in the implementation of the temperature-dependent term of the *method 2* air supply calculation (refer to equation II-16 of the model specifications).

Case 204

Case 204 is identical to cases 202 with the exception that the air supply rate is calculated using *method 1* (refer to section II-2.6 of the model specifications). The pertinent input data to the FC-cogeneration model are listed in Table II-1 with the changes noted in Table II-13.

The following simulation predictions should be plotted against P_{el}:

- The difference in $T_{FCPM-cg}$ between case 204 and case 202 (case 204 result minus case 202 result).

These results are given in Figure II-22.

fuel molar fractions	$\chi_{H_2} = 0$; $\chi_{CH_4} = 0.949$; $\chi_{C_2H_6} = 0.025$; $\chi_{C_3H_8} = 0.002$; $\chi_{C_4H_{10}} = 0.0006$; $\chi_{C_5H_{12}} = 0.0001$; $\chi_{C_6H_{14}} = 0.0001$; $\chi_{CH_3OH} = 0.$; $\chi_{C_2H_5OH} = 0.$; $\chi_{CO_2} = 0.007$; $\chi_{N_2} = 0.016$; $\chi_{O_2} = 0.0002$
water supply to FCPM	$w_0 = 0.$; $w_1 = 0.$; $w_2 = 0.$
air supply to FCPM	method 1 $\lambda = 2.5$
FCPM AC ancillaries	$anc_0 = 0.$; $anc_1 = 0.$
FCPM skin losses	method 1 $q_{skin-loss} = 0.$
dilution air	$\dot{N}_{dilution-air} = 0.$

Table II-13: Input data for case 204 that override the data given in Table II-1

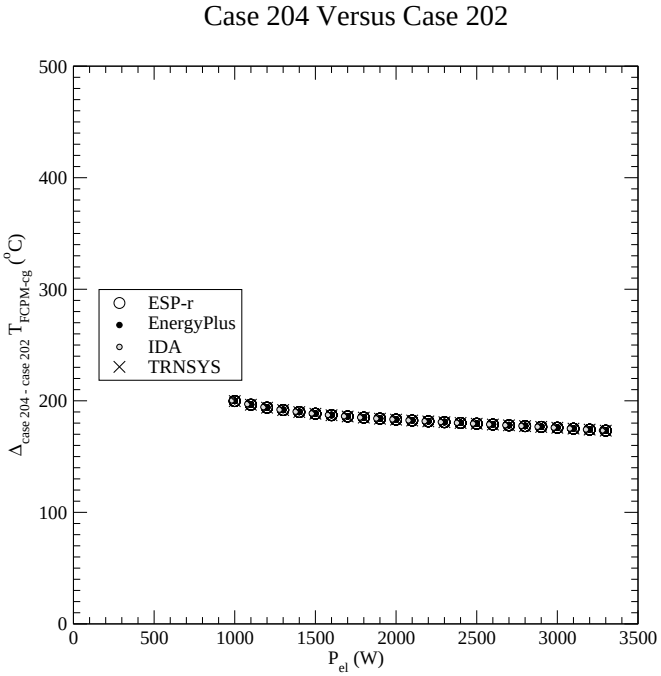

Figure II-22: $\Delta_{case\ 204\ -\ case\ 202}\ T_{FCPM-cg}$ **results**

If case 202 predictions are in agreement then disagreement in case 204 results would be indicative of errors in the implementation of the *method 1* air supply calculation (refer to section II-2.6 of the model specifications).

Case 205

Case 205 is identical to cases 202 with the exception that the air supply rate is calculated using *method 3* (refer to section II-2.6 of the model specifications). The pertinent input data to the FC-cogeneration model are listed in Table II-1 with the changes noted in Table II-14.

fuel molar fractions	$\chi_{H_2} = 0;\quad \chi_{CH_4} = 0.949;\quad \chi_{C_2H_6} = 0.025;\quad \chi_{C_3H_8} = 0.002;$ $\chi_{C_4H_{10}} = 0.0006;\quad \chi_{C_5H_{12}} = 0.0001;\quad \chi_{C_6H_{14}} = 0.0001;$ $\chi_{CH_3OH} = 0.;\quad \chi_{C_2H_5OH} = 0.;\quad \chi_{CO_2} = 0.007;\quad \chi_{N_2} = 0.016;$ $\chi_{O_2} = 0.0002$
water supply to FCPM	$w_0 = 0.;\ w_1 = 0.;\ w_2 = 0.$
air supply to FCPM	method 3 $a_0 = 1 \cdot 10^{-8};\ a_1 = 59.;\ a_2 = 2.0 \cdot 10^{6};\ a_3 = 0.01$
FCPM AC ancillaries	$anc_0 = 0.;\ anc_1 = 0.$
FCPM skin losses	method 1 $q_{skin-loss} = 0.$
dilution air	$\dot{N}_{dilution-air} = 0.$

Table II-14: Input data for case 205 that override the data given in Table II-1

The following simulation predictions should be plotted against P_{el}:

- The difference in $T_{FCPM-cg}$ between case 205 and case 202 (case 205 result minus case 202 result).

These results are given in Figure II-23.

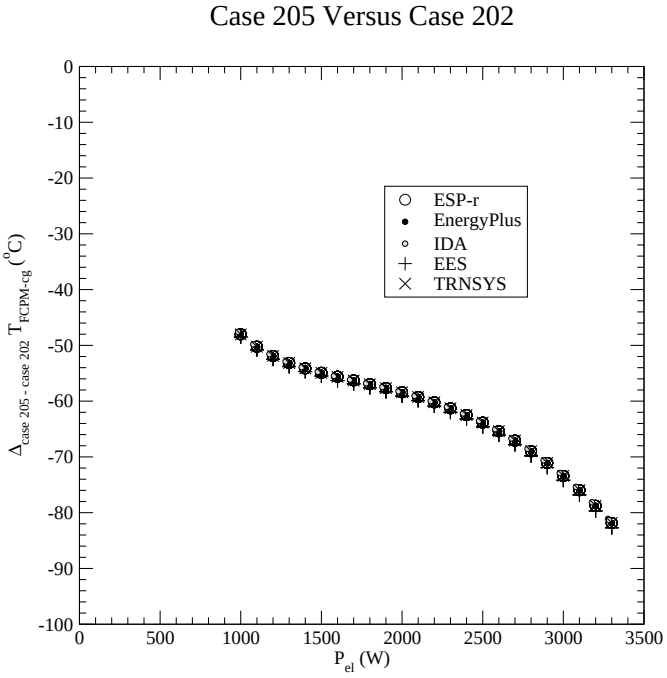

Figure II-23: $\Delta_{case\ 205\ -\ case\ 202}\ T_{FCPM-cg}$ **results**

If case 202 predictions are in agreement then disagreement in case 205 results would be indicative of errors in the implementation of the *method 3* air supply calculation (refer to equation II-17 of the model specifications).

Case 206

Case 206 is identical to cases 202 with the exception of the inclusion of AC-powered ancillaries within the FCPM control volume (refer to section II-2.9 of the model specifications). The pertinent input data to the FC-cogeneration model are listed in Table II-1 with the changes noted in Table II-15.

The following simulation predictions should be plotted against P_{el}:

- The difference in $T_{FCPM-cg}$ between case 206 and case 202 (case 206 result minus case 202 result).

These results are given in Figure II-24.

fuel molar fractions	$\chi_{H_2} = 0$; $\chi_{CH_4} = 0.949$; $\chi_{C_2H_6} = 0.025$; $\chi_{C_3H_8} = 0.002$; $\chi_{C_4H_{10}} = 0.0006$; $\chi_{C_5H_{12}} = 0.0001$; $\chi_{C_6H_{14}} = 0.0001$; $\chi_{CH_3OH} = 0.$; $\chi_{C_2H_5OH} = 0.$; $\chi_{CO_2} = 0.007$; $\chi_{N_2} = 0.016$; $\chi_{O_2} = 0.0002$
water supply to FCPM	$w_0 = 0.$; $w_1 = 0.$; $w_2 = 0.$
FCPM AC ancillaries	$anc_0 = 50.$; $anc_1 = 1.5 \cdot 10^7$
FCPM skin losses	method 1 $q_{skin-loss} = 0.$
dilution air	$\dot{N}_{dilution-air} = 0.$

Table II-15: Input data for case 206 that override the data given in Table II-1

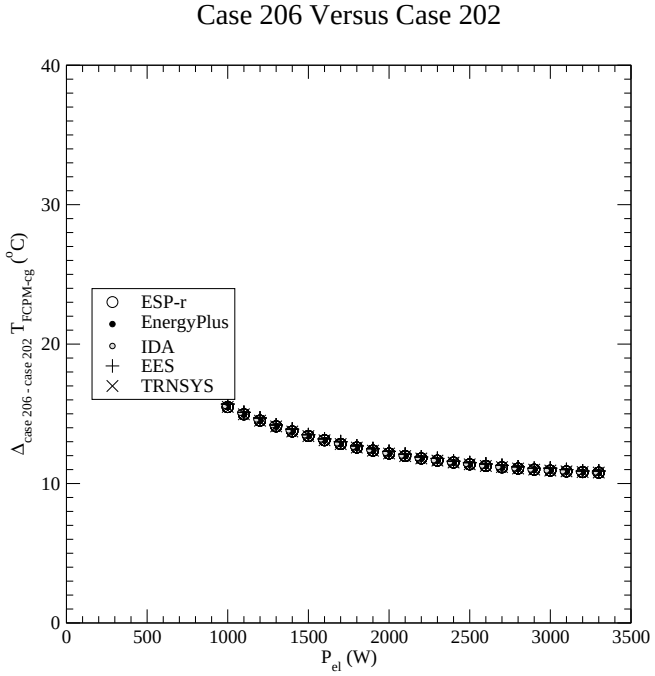

Figure II-24: $\Delta_{case\ 206\ -\ case\ 202}\ T_{FCPM-cg}$ **results**

If case 202 predictions are in agreement then disagreement in case 206 results would be indicative of errors in the calculation of the AC-powered ancillaries (equation II-19 of the model specifications) and/or their consideration in the FCPM energy balance (equation II-7 of the model specifications).

Case 207

Case 207 is identical to cases 202 with the exception that there are thermal losses from the skin of the FCPM (refer to section II-2.10 of the model specifications). The skin losses are determined using *method 1* and equal a constant 100 W. The pertinent input data to the FC-cogeneration model are listed in Table II-1 with the changes noted in Table II-16.

fuel molar fractions	$\chi_{H_2} = 0;\quad \chi_{CH_4} = 0.949;\quad \chi_{C_2H_6} = 0.025;\quad \chi_{C_3H_8} = 0.002;$ $\chi_{C_4H_{10}} = 0.0006;\qquad \chi_{C_5H_{12}} = 0.0001;\qquad \chi_{C_6H_{14}} = 0.0001;$ $\chi_{CH_3OH} = 0.;\quad \chi_{C_2H_5OH} = 0.;\quad \chi_{CO_2} = 0.007;\quad \chi_{N_2} = 0.016;$ $\chi_{O_2} = 0.0002$
water supply to FCPM	$w_0 = 0.;\ w_1 = 0.;\ w_2 = 0.$
FCPM AC ancillaries	$anc_0 = 0.;\ anc_1 = 0.$
FCPM skin losses	method 1 $q_{skin-loss} = 100.$
dilution air	$\dot{N}_{dilution-air} = 0.$

Table II-16: Input data for case 207 that override the data given in Table II-1

The following simulation predictions should be plotted against P_{el}:

- The difference in $T_{FCPM-cg}$ between case 207 and case 202 (case 207 result minus case 202 result).

These results are given in Figure II-25.

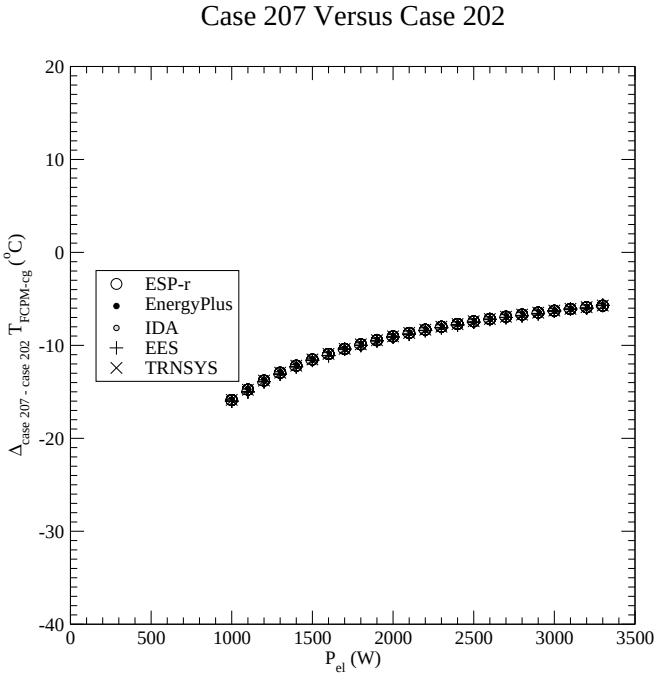

Figure II-25: $\Delta_{case\ 207\ -\ case\ 202}\ T_{FCPM-cg}$ **results**

If case 202 predictions are in agreement then disagreement in case 207 results would be indicative of errors in the consideration of skin losses in the FCPM energy balance (equation II-7 of the model specifications).

Case 208

Case 208 is identical to cases 202 with the exception that there are thermal losses from the skin of the FCPM (refer to section II-2.10 of the model specifications). The skin losses are determined using *method 2* and the room containing the FC-cogeneration device is conditioned to a constant 20°C. The pertinent input data to the FC-cogeneration model are listed in Table II-1 with the changes noted in Table II-17.

The following simulation predictions should be plotted against P_{el}:

- The difference in $T_{FCPM-cg}$ between case 208 and case 202 (case 208 result minus case 202 result).

fuel molar fractions	$\chi_{H_2} = 0$; $\chi_{CH_4} = 0.949$; $\chi_{C_2H_6} = 0.025$; $\chi_{C_3H_8} = 0.002$; $\chi_{C_4H_{10}} = 0.0006$; $\chi_{C_5H_{12}} = 0.0001$; $\chi_{C_6H_{14}} = 0.0001$; $\chi_{CH_3OH} = 0.$; $\chi_{C_2H_5OH} = 0.$; $\chi_{CO_2} = 0.007$; $\chi_{N_2} = 0.016$; $\chi_{O_2} = 0.0002$
water supply to FCPM	$w_0 = 0.$; $w_1 = 0.$; $w_2 = 0.$
FCPM AC ancillaries	$anc_0 = 0.$; $anc_1 = 0.$
FCPM skin losses	method 2 $(UA) = 0.4 W/K$; $T_{room} = 20^o C$
dilution air	$\dot{N}_{dilution-air} = 0.$

Table II-17: Input data for case 208 that override the data given in Table II-1

These results are given in Figure II-26.

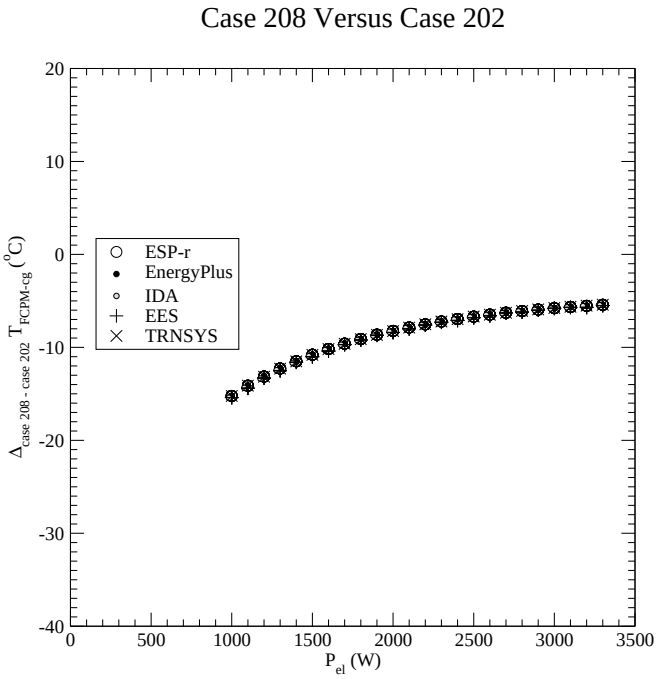

Figure II-26: $\Delta_{case\ 208\ -\ case\ 202}\ T_{FCPM-cg}$ **results**

If case 202 and case 207 predictions are in agreement then disagreement in case 208 results would be indicative of errors in the calculation of the skin losses using *method 2* (equation II-20 of the model specifications).

Case 209

Case 209 is identical to cases 202 with the exception that there are thermal losses from the skin of the FCPM (refer to section II-2.10 of the model specifications). The skin losses are determined using *method 3*. The pertinent input data to the FC-cogeneration model are listed in Table II-1 with the changes noted in Table II-18.

fuel molar fractions	$\chi_{H_2} = 0;\quad \chi_{CH_4} = 0.949;\quad \chi_{C_2H_6} = 0.025;\quad \chi_{C_3H_8} = 0.002;$ $\chi_{C_4H_{10}} = 0.0006;\qquad \chi_{C_5H_{12}} = 0.0001;\qquad \chi_{C_6H_{14}} = 0.0001;$ $\chi_{CH_3OH} = 0.;\quad \chi_{C_2H_5OH} = 0.;\quad \chi_{CO_2} = 0.007;\quad \chi_{N_2} = 0.016;$ $\chi_{O_2} = 0.0002$
water supply to FCPM	$w_0 = 0.;\ w_1 = 0.;\ w_2 = 0.$
FCPM AC ancillaries	$anc_0 = 0.;\ anc_1 = 0.$
FCPM skin losses	method 3 $s_0 = 10.;\ s_1 = 9.0 \cdot 10^6;\ s_2 = 2.0 \cdot 10^{11}$
dilution air	$\dot{N}_{dilution-air} = 0.$

Table II-18: Input data for case 209 that override the data given in Table II-1

The following simulation predictions should be plotted against P_{el}:

- The difference in $T_{FCPM-cg}$ between case 209 and case 202 (case 209 result minus case 202 result).

These results are given in Figure II-27.

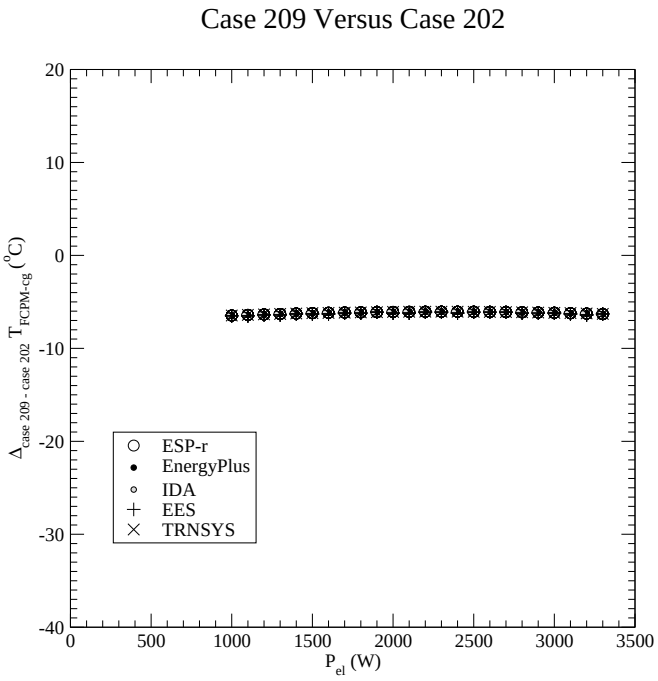

Figure II-27: $\Delta_{case\ 209\ -\ case\ 202}\ T_{FCPM-cg}$ **results**

If case 202 and case 207 predictions are in agreement then disagreement in case 209 results would be indicative of errors in the calculation of the skin losses using *method 3* (equation II-21 of the model specifications).

300 Series Tests

The *300 series* cases exercise the portions of code that treat the start-up and cool-down cycles and its operational degredation. All other test series examine performance only during "normal" operaion and when the electrical efficiency does not degrade with time.

Case 300

Case 300 is the base case for this series.

The simulation is conducted for a six-day period (January 9 to 14) with whatever start-up or conditioning period is appropriate for the simulation program. The simulation should be performed with a time-step no greater than 15 minutes. The weather file is inconsequential.

There is no degradation associated with stop-start cycling. Likewise, there is no operational degradation.

The net AC power demanded from the FC-cogeneration device (P_{demand}) is specified as the boundary condition as illustrated in Figure II-31. During the first 18 hours of the simulation the demand varies from 1 000 W to 3 000 W and the cogeneration device operates normally in response to this demand. At 18h00 a control signal is sent to shutdown the cogeneration device. Following a 36 hour shutdown sequence, the cogeneration device remains off another 24 hours. Then at 78 hours from the start of the simulation a control signal is sent to start the system up. Following a 24-hour controlled start-up the system then operates normally for the remaining 42 hours of the simulation.

The pertinent input data to the FC-cogeneration model are listed in Table II-19.

The following simulation predictions are examined with this case and should be plotted against time (in hours):

- The DC electrical power produced by the FCPM, P_{el}.
- The FC-cogeneration devices's net AC power production, P_{net-AC}.
- The molar flow rate of the fuel supplied to the FCPM, $\dot{N}_{fuel}$.

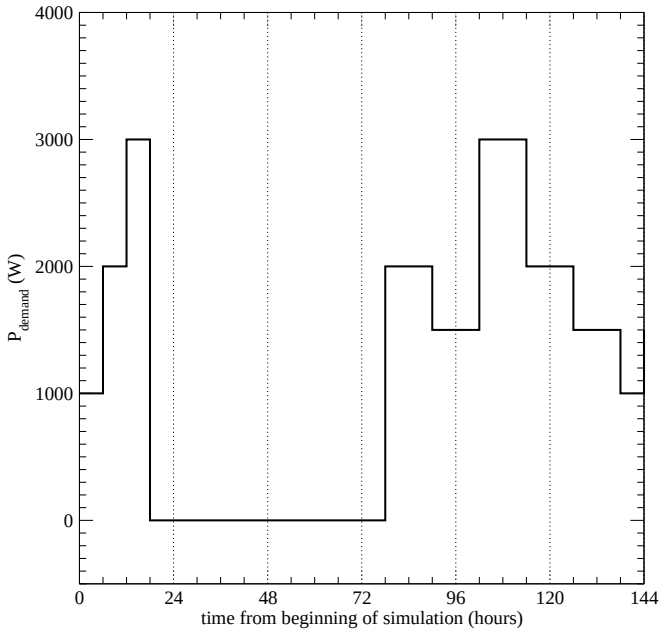

Figure II-31: Net AC electrical demand placed upon FC-cogeneration device for case 300

These results are given in Figures II-28 through II-30.

FCPM electrical efficiency	$\varepsilon_0 = 0.3;\ \varepsilon_1 = 1.1 \cdot 10^{-4};\ \varepsilon_2 = -2 \cdot 10^{-8}$
	$D = 0$
	$L = 0$
FCPM transient response	$(dP_{el}/dt)_{\max}$ = 10 (W/s) for both increasing and decreasing power
start-up period	$\delta t_{start-up}$ = 24 hours $kmol_{fuel,start-up}$ = 0.5 kmol $E_{heat+anc\_start-up}$ = 65 MJ $E_{el,start-up}$ = 40 MJ
cool-down period	$\delta t_{cool-down}$ = 36 hours $kmol_{fuel,start-up}$ = 0.1 kmol $E_{heat+anc\_start-up}$ = 50 MJ
FCPM operating range	$P_{el-min} = 1\ 000$ W $P_{el-max} = 5\ 000$ W
fuel molar fractions	$\chi_{H_2} = 0.0;\ \chi_{CH_4} = 0.949;\ \chi_{C_2H_6} = 0.025;\ \chi_{C_3H_8} = 0.002;$ $\chi_{C_4H_{10}} = 0.0006;\ \chi_{C_5H_{12}} = 0.0001;\ \chi_{C_6H_{14}} = 0.0001;\ \chi_{CH_3OH} = 0.0;$ $\chi_{C_2H_5OH} = 0.0;\ \chi_{CO_2} = 0.007;\ \chi_{N_2} = 0.016;\ \chi_{O_2} = 0.0002$
air molar fractions	$\chi_{N_2} = 0.7728;\ \chi_{O_2} = 0.2073;\ \chi_{H_2O} = 0.0104;\ \chi_{Ar} = 0.0092;$ $\chi_{C_{O_2}} = 0.0003;$
air supply to FCPM	method 2 $a_0 = 5 \cdot 10^{-5};\ a_1 = 1.5 \cdot 10^{-7};\ a_2 = 1.1 \cdot 10^{-12};\ a_3 = 0.0$
air supply blower	$T_{blower-in} = 20^oC$ (air drawn at containing room's temperature)
	$b_0 = 50.0;\ b_1 = 4.0 \cdot 10^5;\ b_2 = 0.0;\ b_3 = 0.0;$
	$\alpha_{blower-heat-loss} = 0.5$
fuel compressor	$T_{comp-in} = 20^oC$ (fuel drawn at containing room's temperature)
	$c_0 = 20.0;\ c_1 = 0.0;\ c_2 = 0.0;\ c_3 = 0.0;$
	$\alpha_{comp-heat-loss} = 0.5$
water supply to FCPM	$w_0 = 1.0 \cdot 10^{-7};\ w_1 = 2.0;\ w_2 = 5.0 \cdot 10^4$
water pump	$T_{pump-in} = 20^oC$ (water drawn at containing room's temperature)
	$p_0 = 10.0;\ p_1 = 0.0;\ p_2 = 0.0;\ p_3 = 0.0;$
	$\alpha_{pump-heat-loss} = 0.05$
FCPM AC ancillaries	$anc_0 = 50.;\ anc_1 = 1.5 \cdot 10^7$
FCPM skin losses	method 1 $q_{skin-loss} = 0.0$
dilution air	$\dot{N}_{dilution-air} = 0.0$

Table II-19: Input data for case 300

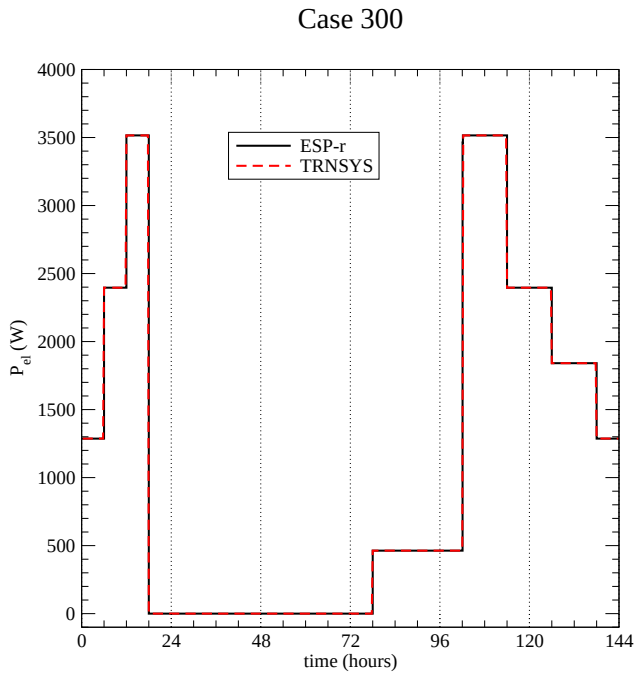

Figure II-28: Case 300 P_{el} results

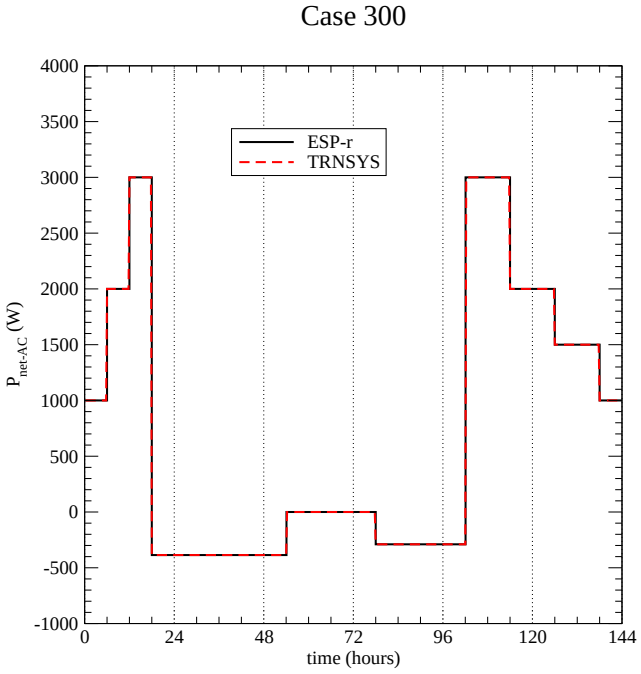

Figure II-29: Case 300 P_{net-AC} results

Case 300

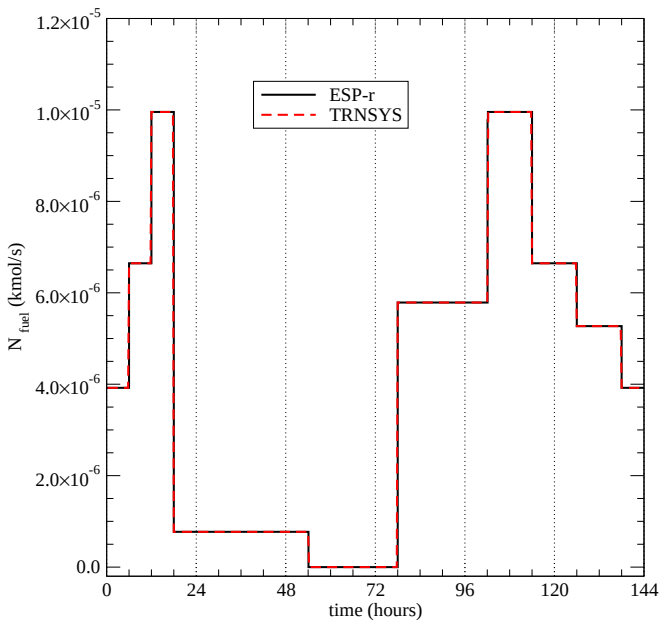

Figure II-30: Case 300 $\dot{N}_{fuel}$ results

Case 301

Case 301 is identical to case 300 with the exception that after only 12 hours of the 36-hour shutdown sequence has elapsed (i.e. at 30 hours from the start of the simulation), a control signal is sent to demand power. The net AC power demanded from the FC-cogeneration device (P_{demand}) is illustrated in Figure II-32.

The shutdown and start-up characteristics are identical to case 300. Consequently the device should complete its shutdown procedure prior to commening the start-up procedure to supply the requested power.

The following simulation predictions are examined with this case and should be plotted against time (in hours):

- The DC electrical power produced by the FCPM, P_{el}.
- The FC-cogeneration devices's net AC power production, P_{net-AC}.
- The molar flow rate of the fuel supplied to the FCPM, $\dot{N}_{fuel}$.

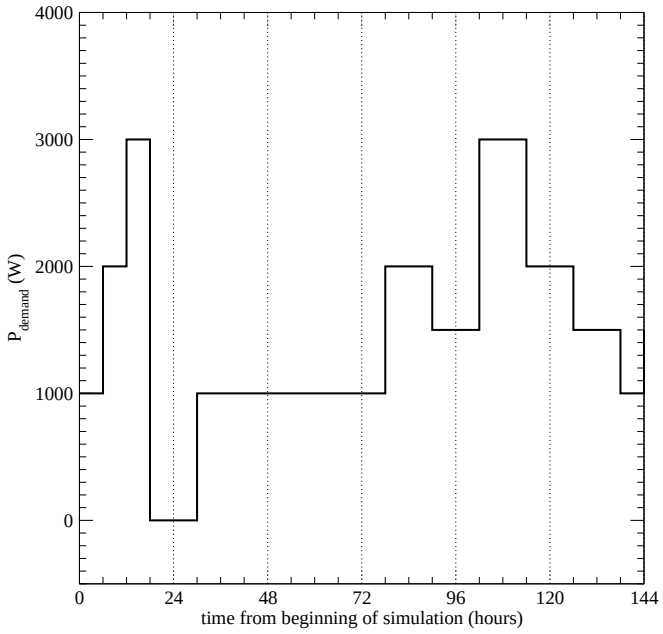

Figure II-32: Net AC electrical demand placed upon FC-cogeneration device for case 301

These results are given in Figures II-33 through II-35.

Case 301

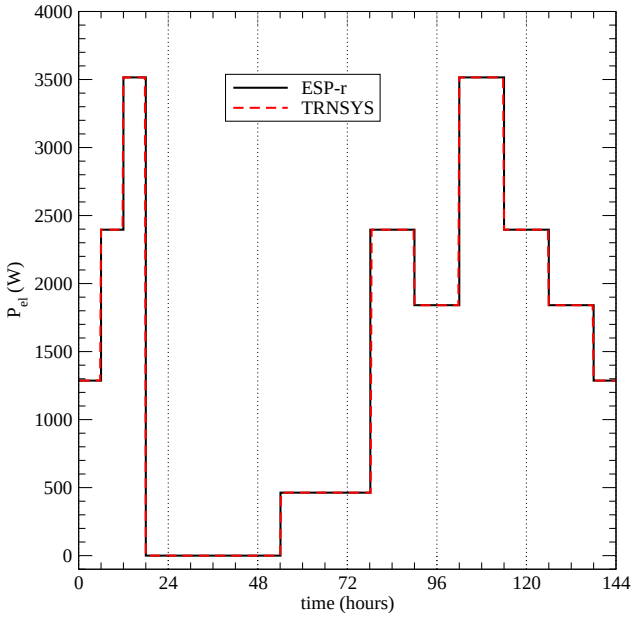

Figure II-33: Case 301 P_{el} results

Case 301

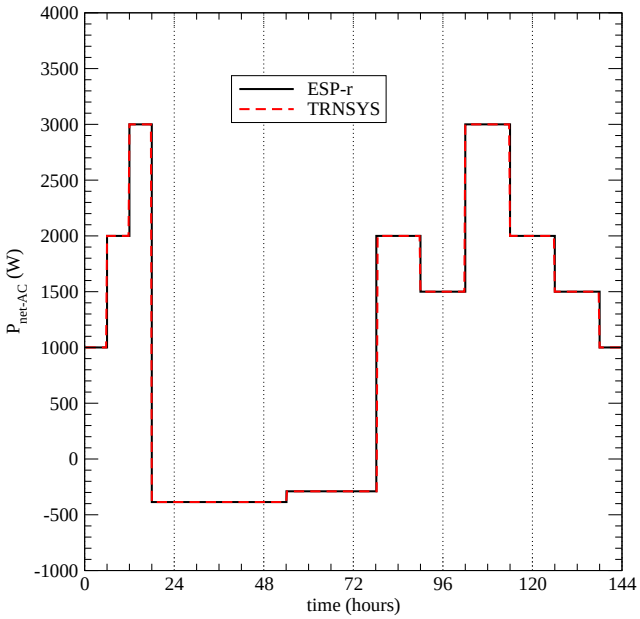

Figure II-34: Case 301 P_{net-AC} results

Case 301

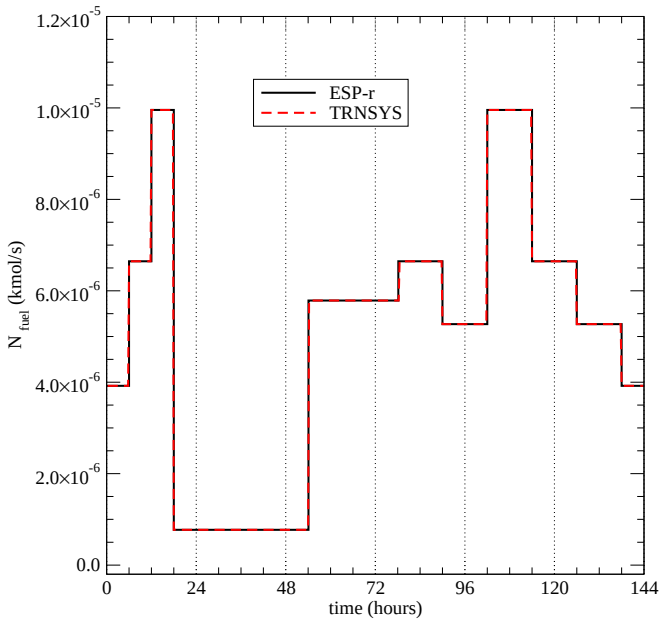

Figure II-35: Case 301 $\dot{N}_{fuel}$ results

Case 302

Case 302 is identical to case 300 with the exception that the performance of the FCPM degrades with stop-start cycling. The duration of the cool-down and start-up periods is also shorter. The pertinent input data to the FC-cogeneration model are listed in Table II-19 with the changes noted in Table II-20.

In addition, the net AC power demanded from the FC-cogeneration device (P_{demand}) follows the pattern illustrated in Figure II-36. The cogeneration device is shutdown twice (shutdown signals are sent at 24 and 84 hours) during the simulation.

The following simulation predictions are examined with this case and should be plotted against time (in hours):

- The electrical efficiency of the FCPM, ε_{el}. (This result is not pertinent when the cogeneration system is shutting down, starting up, or inoperative.)

FCPM electrical efficiency	$\varepsilon_0 = 0.3$; $\varepsilon_1 = 1.1 \cdot 10^{-4}$; $\varepsilon_2 = -2 \cdot 10^{-8}$
	$D = 0.1$
	$L = 0$
start-up period	$\delta t_{start-up}$ = 6 hours $kmol_{fuel,start-up}$ = 0.5 kmol $E_{heat+anc\_start-up}$ = 65 MJ $E_{el,start-up}$ = 40 MJ
cool-down period	$\delta t_{cool-down}$ = 6 hours $kmol_{fuel,start-up}$ = 0.1 kmol $E_{heat+anc\_start-up}$ = 50 MJ

Table II-20: Input data for case 302

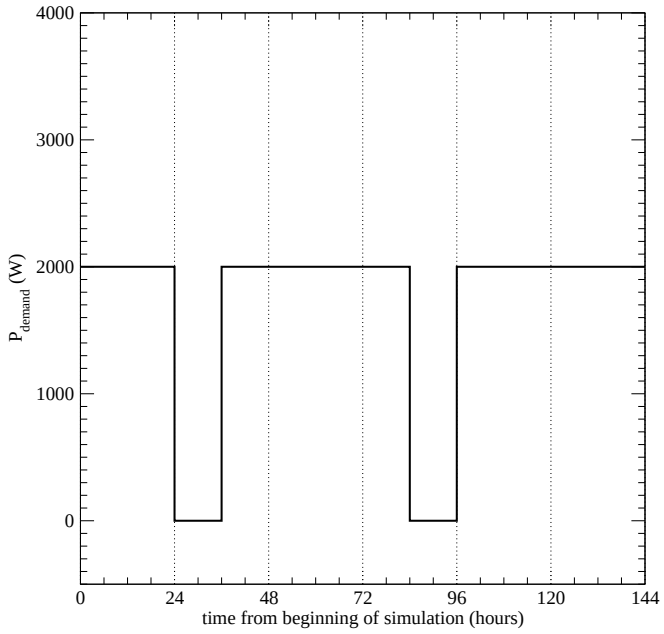

Figure II-36: Net AC electrical demand placed upon FC-cogeneration device for case 302

These results are given in Figure II-37.

Case 302

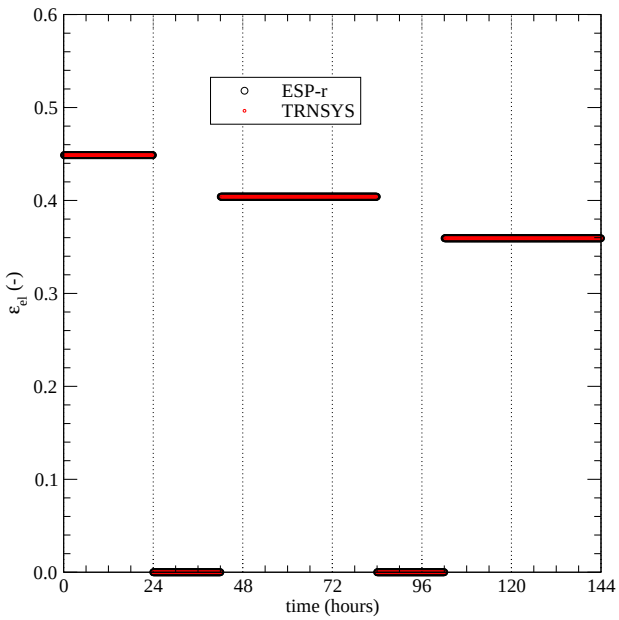

Figure II-37: Case 302 ε_{el} results

Case 303

Case 303 is identical to case 302 with the exception that the performance of the FCPM degrades with operational time.

The pertinent input data to the FC-cogeneration model are listed in Table II-19 with the changes noted in Table II-21. The net AC power demanded from the FC-cogeneration device (P_{demand}) follows the same pattern as for case 302, as illustrated in Figure II-36.

The following simulation predictions are examined with this case and should be plotted against time (in hours):

- The electrical efficiency of the FCPM, ε_{el}. (This result is not pertinent when the cogeneration system is shutting down, starting up, or inoperative.)

These results are given in Figure II-39.

FCPM electrical efficiency	$\varepsilon_0 = 0.3;\ \varepsilon_1 = 1.1 \cdot 10^{-4};\ \varepsilon_2 = -2 \cdot 10^{-8}$
	$D = 0.1$
	$L = 0.005/hr$ $t_{threshold}$ = 48 hours
start-up period	$\delta t_{start-up}$ = 6 hours $kmol_{fuel,start-up}$ = 0.5 kmol $E_{heat+anc\_start-up}$ = 65 MJ $E_{el,start-up}$ = 40 MJ
cool-down period	$\delta t_{cool-down}$ = 6 hours $kmol_{fuel,start-up}$ = 0.1 kmol $E_{heat+anc\_start-up}$ = 50 MJ

Table II-21: Input data for case 303

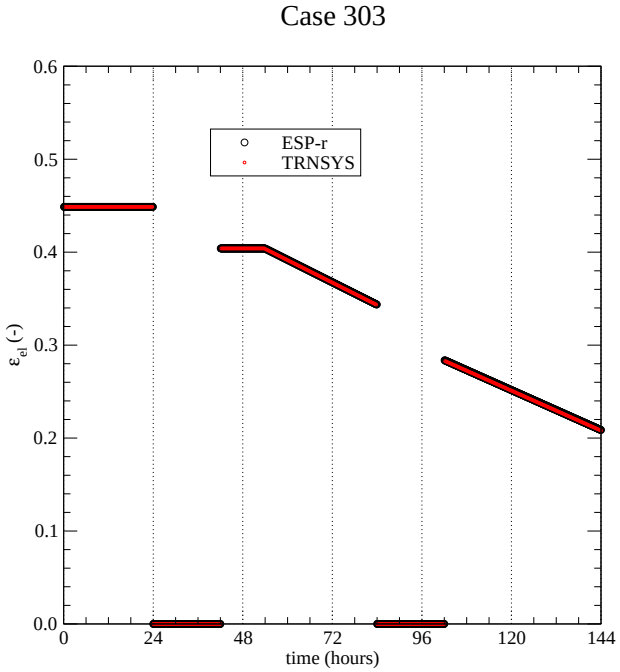

Figure II-39: Case 303 ε_{el} results

400 Series Tests

The *400 series* cases exercise the portion of the model that treats the FCPM inlet streams coming from the air supply blower, fuel supply compressor, and the water pump. Whereas previous test series set the heat loss coefficients for these components such that no heat was added to the air, fuel, and water streams, the *400 series* cases include heat additions to these streams and exercise this aspect of the model.

Case 400

Case 400 is the base case for this series.

Case 400 is derived from Case 202 except that:

- the air inlet blower heat loss factor is set to 0.5 instead of 1.0,
- the fuel inlet compressor heat loss factor is set to 0.5 instead of 1.0, and
- coefficients are prescribed for modelling the power used by these components.

The pertinent input data to the FC-cogeneration model are listed in Table II-22

The following simulation predictions are examined with this case and should be plotted against P_{el}:

- The temperatue of the inlet air stream entering the FCPM, $T_{blower-out}$.
- The air blower electrical power, $P_{blower-el}$
- The total enthalpy flow rate relative to the standard state of the air stream entering the FCPM, $\sum_i (\dot{N}_i \cdot [\hat{h}_i - \Delta_f \hat{h}_i^o])_{air}$
- The temperature of the fuel entering the FCPM, $T_{comp-out}$.
- The fuel compressor electrical power, $P_{comp-el}$
- The total enthalpy flow rate relative to the standard state of the fuel entering the FCPM, $\sum_i (\dot{N}_i \cdot [\hat{h}_i - \Delta_f \hat{h}_i^o])_{fuel}$

FCPM electrical efficiency	$\varepsilon_0 = 0.3;\ \varepsilon_1 = 1.1 \cdot 10^{-4};\ \varepsilon_2 = -2 \cdot 10^{-8}$
	$D = 0$
	$L = 0$
FCPM transient response	$(dP_{el}/dt)_{\max}$ = 10 (W/s) for both increasing and decreasing power
fuel molar fractions	$\chi_{H_2} = 0.0;\quad \chi_{CH_4} = 0.949;\quad \chi_{C_2H_6} = 0.025;\quad \chi_{C_3H_8} = 0.002;$ $\chi_{C_4H_{10}} = 0.0006;\quad \chi_{C_5H_{12}} = 0.0001;\quad \chi_{C_6H_{14}} = 0.0001;$ $\chi_{CH_3OH} = 0.0;\quad \chi_{C_2H_5OH} = 0.0;\quad \chi_{CO_2} = 0.007;\quad \chi_{N_2} = 0.016;$ $\chi_{O_2} = 0.0002$
air molar fractions	$\chi_{N_2} = 0.7728;\quad \chi_{O_2} = 0.2073;\quad \chi_{H_2O} = 0.0104;\quad \chi_{Ar} = 0.0092;$ $\chi_{C_{O_2}} = 0.0003;$
air supply to FCPM	method 2 $a_0 = 5 \cdot 10^{-5};\ a_1 = 1.5 \cdot 10^{-7};\ a_2 = 1.1 \cdot 10^{-12};\ a_3 = 0.0$
air supply blower	$T_{blower-in} = 20^oC$ (air drawn at containing room's temperature)
	$b_0 = 50.0;\ b_1 = 4.0 \cdot 10^5;\ b_2 = 0.0;\ b_3 = 0.0;$
	$\alpha_{blower-heat-loss} = 0.5$
fuel compressor	$T_{comp-in} = 20^oC$ (fuel drawn at containing room's temperature)
	$c_0 = 10.0;\ c_1 = 1.0 \cdot 10^6;\ c_2 = 0.0;\ c_3 = 0.0;$
	$\alpha_{comp-heat-loss} = 0.5$
water supply to FCPM	$w_0 = 0.0;\ w_1 = 0.0;\ w_2 = 0.0$
FCPM AC ancillaries	anc_0 = 0.0; $anc_1 = 0.0$
FCPM skin losses	method 1 $q_{skin-loss} = 0.0$
dilution air	$\dot{N}_{dilution-air} = 0.0$

Table II-22: Input data for case 400

- The temperature of the product gas stream exiting the FCPM, $T_{FCPM-cg}$.

These results are given in Figure II-40 through II-46.

Case 400

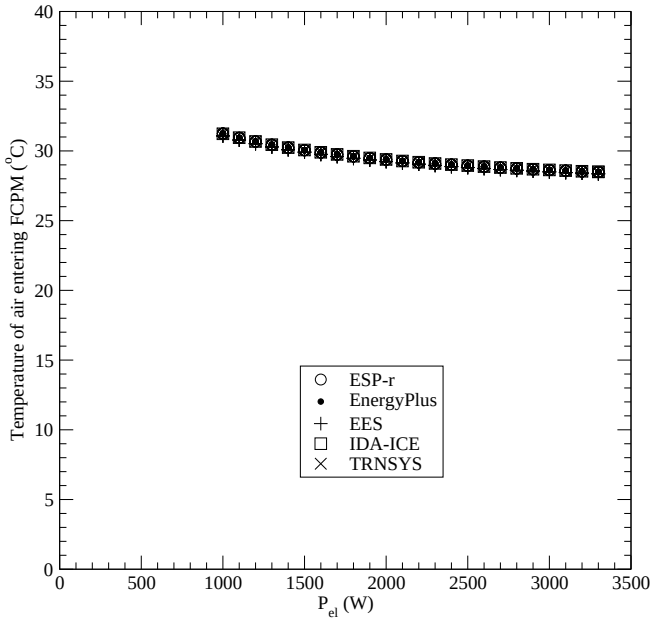

Figure II-40: Case 400 $T_{blower-out}$ results

Case 400

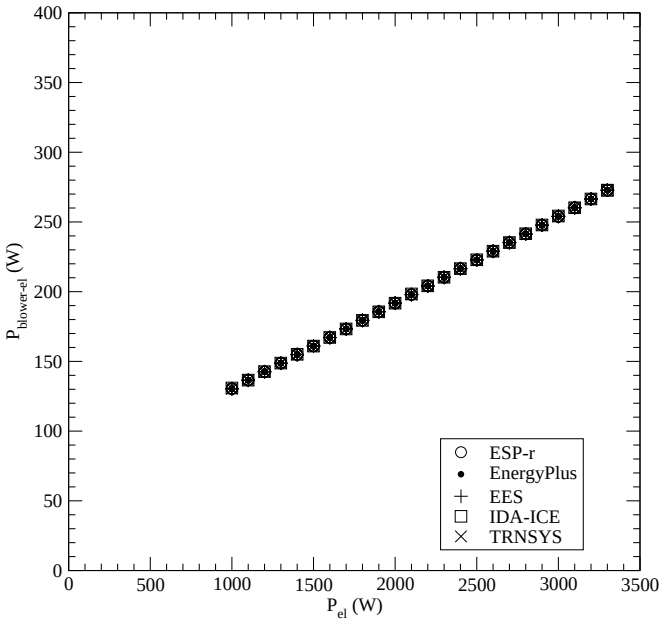

Figure II-41: Case 400 $P_{blower-el}$ results

Case 400

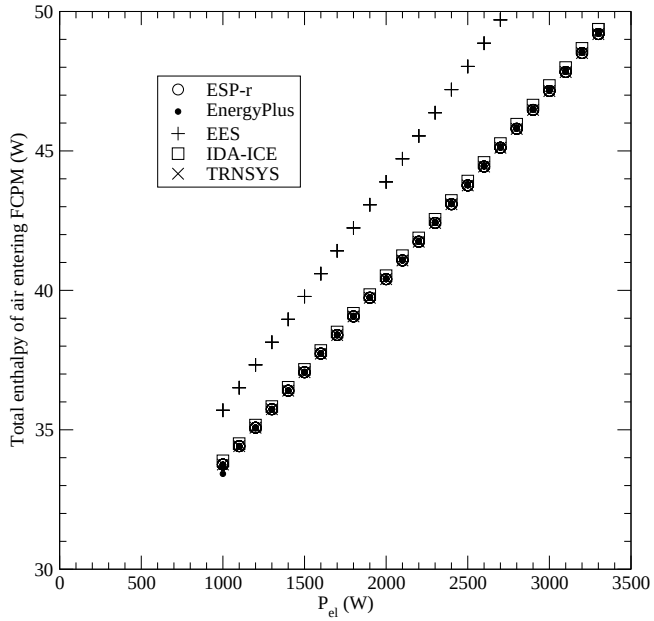

Figure II-42: Case 400 $\sum_i (\dot{N}_i \cdot [\hat{h}_i - \Delta_f \hat{h}_i^o])_{air}$ results

Case 400

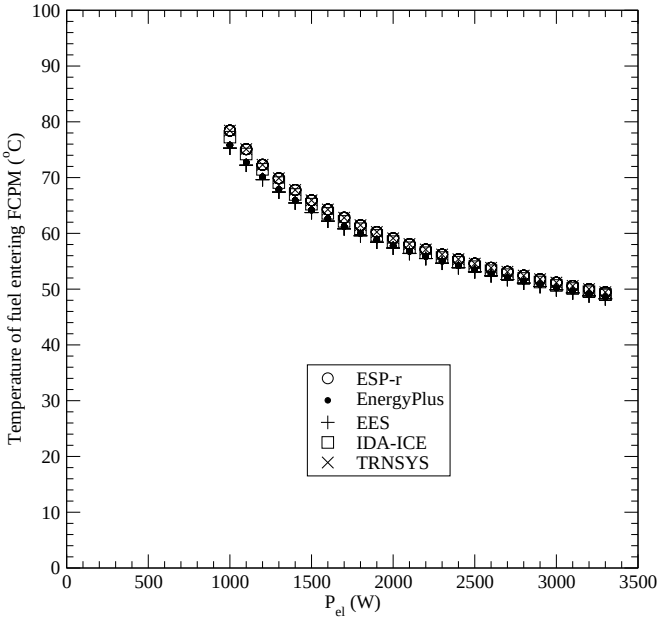

Figure II-43: Case 400 $T_{comp-out}$ results

Case 400

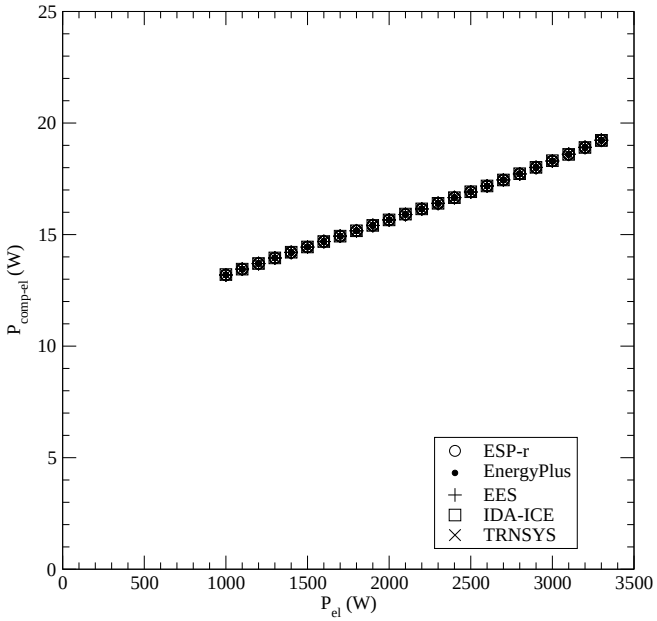

Figure II-44: Case 400 $P_{comp-el}$ results

Case 400

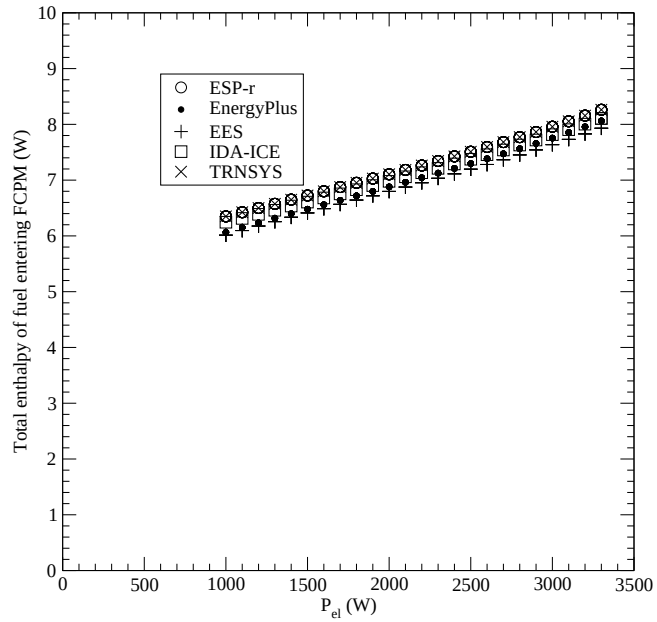

Figure II-45: Case 400 $\sum_i (\dot{N}_i \cdot [\hat{h}_i - \Delta_f \hat{h}_i^o])_{fuel}$ results

Case 400

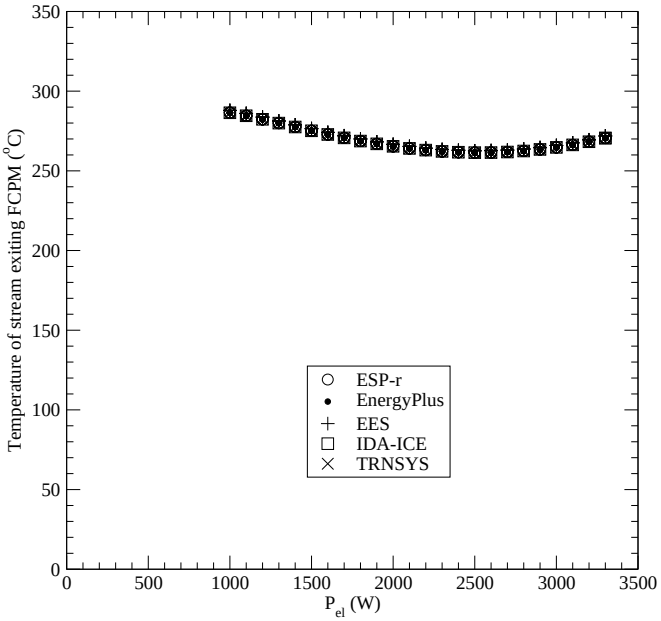

Figure II-46: Case 400 $T_{FCPM-cg}$ results

Disagreements in the prediction of $T_{blower-out}$ would indicate potential errors in implementing equation II-24 of the model specifications for calculating $P_{blower-el}$, property evaluations for the specific heat of the air stream, or the solution and implementation of equation II-26 of the model specifications.

Disagreements in the prediction of $P_{blower-el}$ indicate potential errors in implementing equation II-24 of the model specifications.

Disagreements in the prediction of $\sum_i (\dot{N}_i \cdot [\hat{h}_i - \Delta_f \hat{h}_i^o])_{air}$ would be expected if $T_{blower-out}$ results also disagree. But if $T_{blower-out}$ results are in agreement, then this would indicate implementation errors in property evaluations for the enthalpy of the air stream.

Disagreements in the prediction of $T_{comp-out}$ would indicate potential errors in implementing equation II-28 of the model specifications for calculating $P_{comp-el}$, property evaluations for the specific heat of the fuel stream, or the solution and implementation of equation II-27 of the model specifications.

Disagreements in the prediction of $P_{comp-el}$ indicate potential errors in implementing equation II-28 of the model specifications.

Disagreements in the prediction of $\sum_i (\dot{N}_i \cdot [\hat{h}_i - \Delta_f \hat{h}_i^o])_{fuel}$ would be expected if $T_{comp-out}$ results also disagree. But if $T_{comp-out}$ results are in agreement, then this would indicate implementation errors in property evaluations for the enthalpy of the fuel stream.

Case 401

Case 401 is identical to case 400 with the exception that a different air blower heat loss factor of 0.2 is used. The pertinent input data to the FC-cogeneration model are listed in Table II-22 with the changes noted in Table II-23.

air supply blower	$\alpha_{blower-heat-loss} = 0.2$

Table II-23: Input data for case 401 that override the data given in Table II-22

The following simulation predictions are examined with this case and should be plotted against P_{el}:

- The difference in $T_{blower-out}$ between case 401 and case 400 (case 401 result minus case 400 result).

These results are given in Figure II-47.

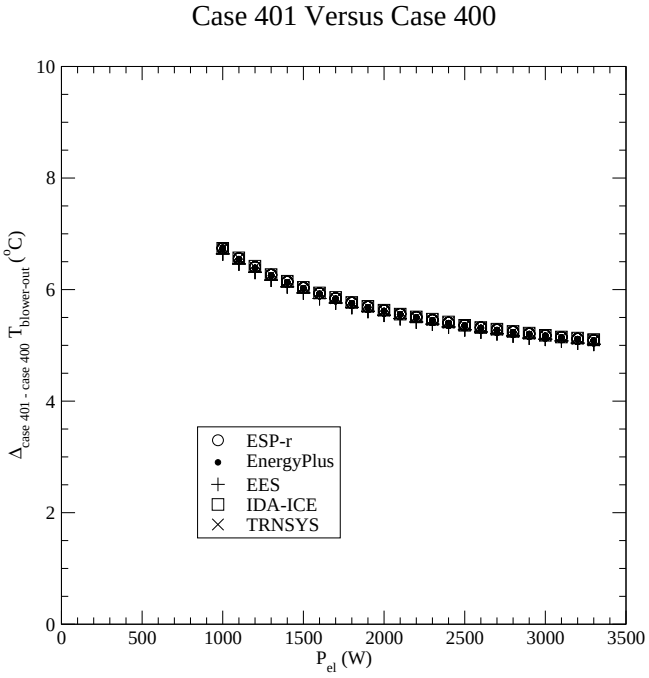

Figure II-47: $\Delta_{case\ 401\ -\ case\ 400}\ T_{blower-out}$ **results**

Disagreements in the difference between case 401 and case 400 prediction of $T_{blower-out}$ would indicate potential errors in implementing equation II-24 of the model specifications for calculating $P_{blower-el}$, property evaluations for the specific heat of the air stream, or the solution and implementation of equation II-26 of the model specifications.

Case 402

Case 402 is identical to case 400 with the exception that a different fuel compressor heat loss factor of 0.2 is used. The pertinent input data to the FC-cogeneration model are listed in Table II-22 with the changes noted in Table II-24.

fuel compressor	$\alpha_{comp-heat-loss} = 0.2$

Table II-24: Input data for case 402 that override the data given in Table II-22

The following simulation predictions are examined with this case and should be plotted against P_{el}:

- The difference in $T_{comp-out}$ between case 402 and case 400 (case 402 result minus case 400 result).

These results are given in Figure II-48.

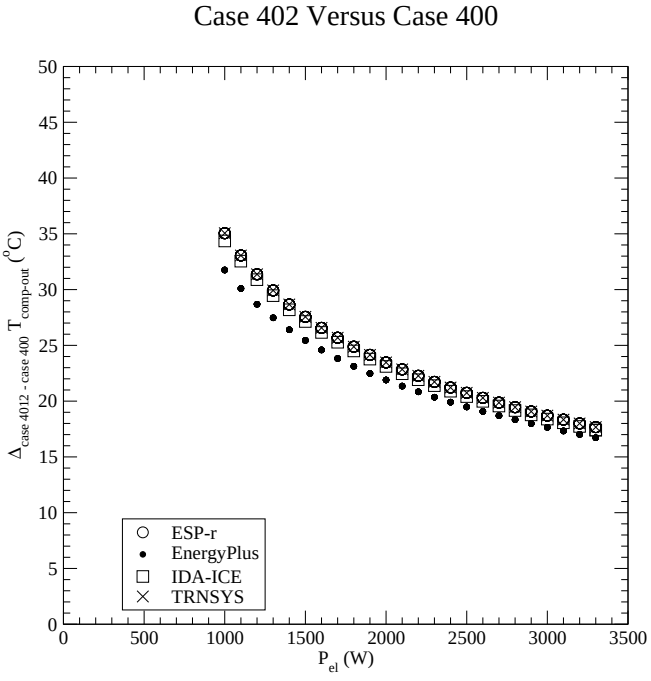

Figure : $\Delta_{case\ 402-\ case\ 400}\ T_{comp-out}$ **results**

Disagreements in the difference between case 402 and case 400 prediction of $T_{comp-out}$ would indicate potential errors in implementing equation II-28 of the model specifications for calculating $P_{comp-el}$, property evaluations for the specific heat of the air stream, or the solution and implementation of equation II-27 of the model specifications.

Case 403

Case 403 is identical to case 400 with the exception that a water supply pump is added. (This water is used for reforming and is not the same as water used for cogeneration heat recovery.) The pertinent input data to the FC-cogeneration model are listed in Table II-22

with the changes noted in Table II-25.

water supply to FCPM	$w_0 = 1.0 \cdot 10^{-7}$; $w_1 = 2.0$; $w_2 = 5.0 \cdot 10^{4}$
water pump	$T_{pump-in} = 20^{o}C$ (water drawn at containing room's temperature)
	$p_0 = 15.0$; $p_1 = 1.6 \cdot 10^{6}$; $p_2 = 4.3 \cdot 10^{10}$; $p_3 = 2.3 \cdot 10^{15}$;
	$\alpha_{pump-heat-loss} = 0.05$

Table II-25: Input data for case 403 that override and augment the data given in Table II-22

The following simulation predictions are examined with this case and should be plotted against P_{el}:

- The flow rate of reforming water, $\dot{N}_{liq-water}$
- The temperatue of the inlet water stream entering the FCPM, $T_{pump-out}$.
- The pump electrical power, $P_{pump-el}$
- The temperature of the product gas stream exiting the FCPM, $T_{FCPM-cg}$.

These results are given in Figure II-49 through II-52.

Case 403

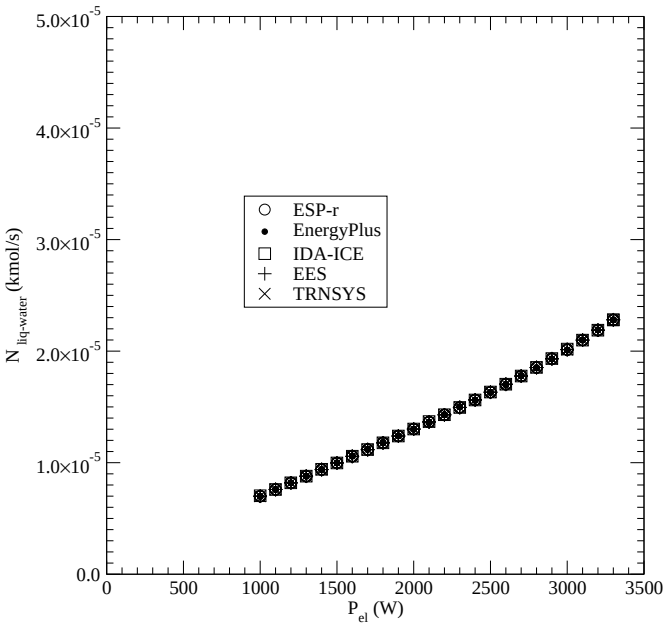

Figure II-49: Case 403 $\dot{N}_{liq-water}$ results

Case 403

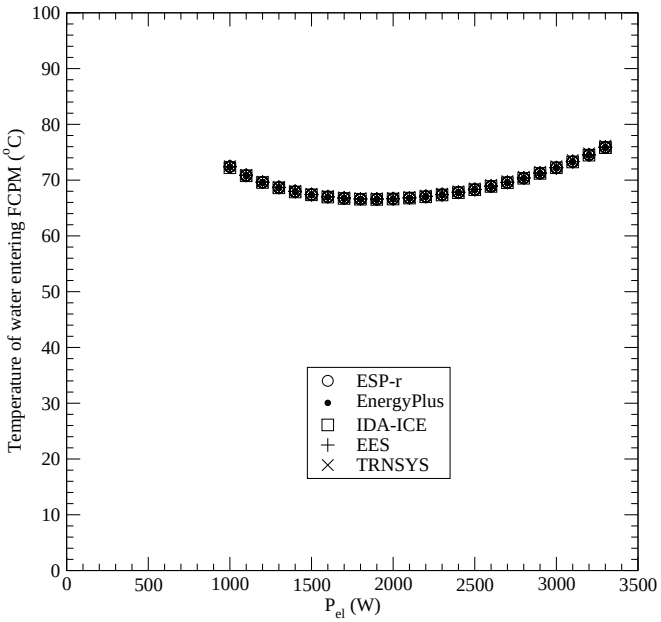

Figure II-50: Case 403 $T_{pump-out}$ results

Case 403

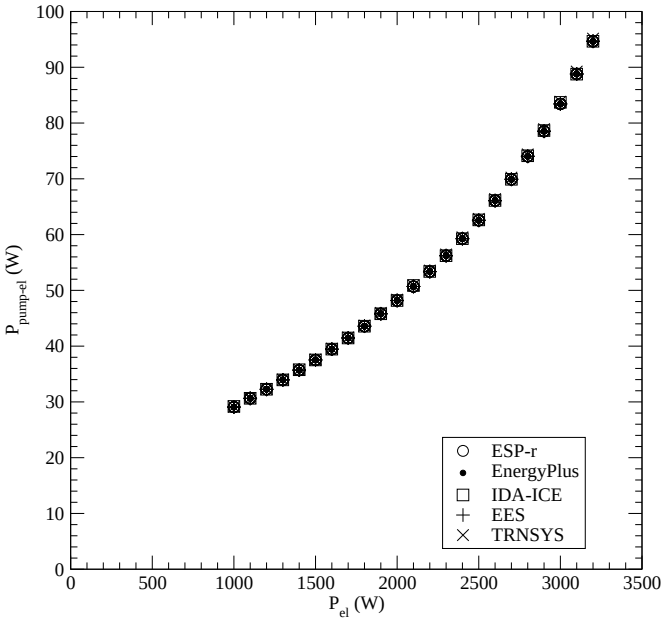

Figure II-51: Case 403 $P_{pump-el}$ results

Case 403

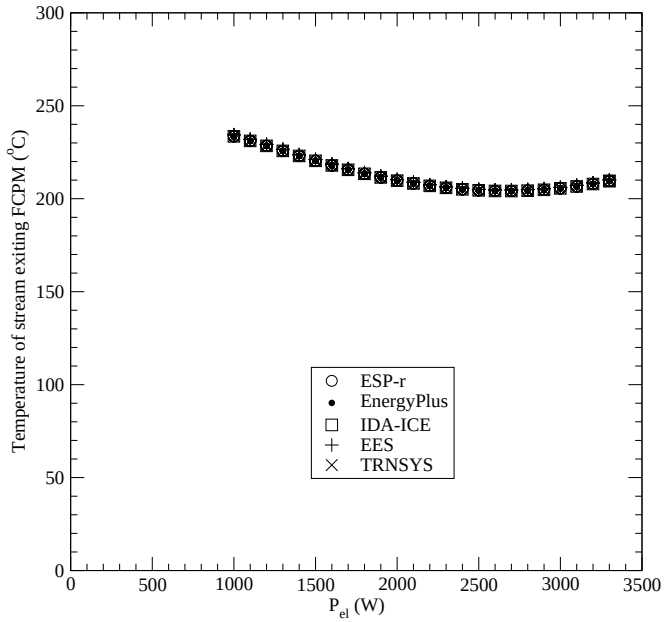

Figure II-52: Case 403 $T_{FCPM-cg}$ results

Disagreements in the prediction of $\dot{N}_{liq-water}$ would indicate potential erros in implementing equation II-18 of the model specifications.

Disagreements in the prediction of $T_{pump-out}$ would indicate potential errors in implementing equation II-30 of the model specifications for calculating $P_{pump-el}$, the determination of the heat capacity of water, or the solution and implementaton of equation II-29 of the model specifications.

Disagreements in the prediction of $P_{pump-el}$ would indicate potential errors in implementing equation II-30 of the model specifications.

Disagreements in the prediction of $\dot{H}_{liq-water}$ would be expected if $T_{pump-out}$ results also disagree. But if $T_{pump-out}$ results are in agreement, then this would indicate implementation errors in property evaluation for the enthalpy of the water stream.

Disagreements in the prediction of $T_{FCPM-cg}$ would indicate potential errors in implementing the FCPM heat balance with respect to the $\dot{H}_{liq-water}$ term.

Case 404

Case 404 is identical to Case 403 with the exception that a different heat loss factor is used for the water supply pump. The pertinent input data to the FC-cogeneration model are listed in Table II-22 with the changes noted in Table II-26.

water supply to FCPM	$w_0 = 1.0 \cdot 10^{-7};\ w_1 = 2.0;\ w_2 = 5.0 \cdot 10^4$
water pump	$T_{pump-in} = 20^o C$ (water drawn at containing room's temperature)
	$p_0 = 15.0;\ p_1 = 1.6 \cdot 10^6;\ p_2 = 4.3 \cdot 10^{10};\ p_3 = 2.3 \cdot 10^{15};$
	$\alpha_{pump-heat-loss} = 0.4$

Table II-26: Input data for case 404 that override and augment the data given in Table II-22

The following simulation predictions are examined with this case and should be plotted against P_{el}:

- The difference in $T_{pump-out}$ between case 404 and case 403 (case 404 result minus case 403 result).

These results are given in Figure II-53.

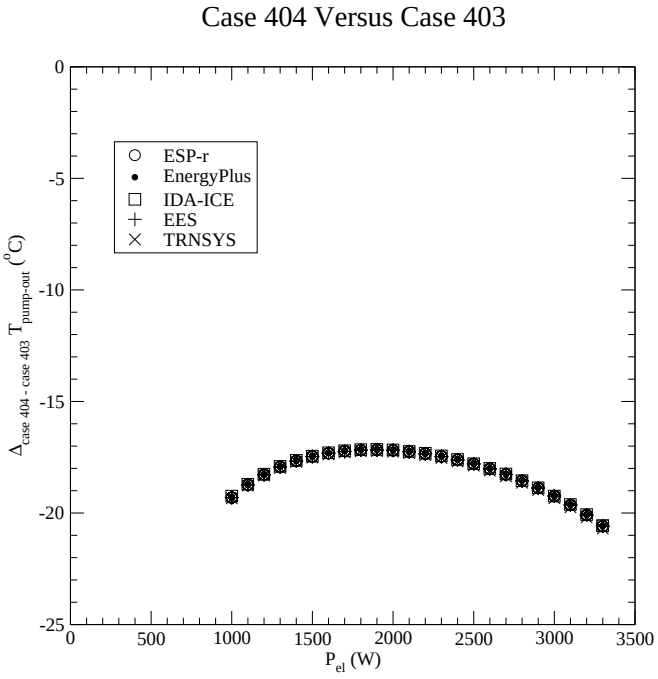

Figure II-53: $\Delta_{case\ 404 - case\ 403}\ T_{pump-out}$ **results**

Disagreements in the difference between case 404 and case 403 prediction of $T_{pump-out}$ would indicate potential errors in implementing property evaluations for the specific heat of the water stream or the solution and implementation of equation II-29 of the model specifications.

Case 405

Case 405 is identical to Case 404 with the exception that a warmer temperature is used for the containing room. This changes the inlet temperature of the air, fuel, and water and is generally implemented by changing the thermostat setting of the containing room. The pertinent input data to the FC-cogeneration model are listed in Table II-22 with the changes noted in Table II-27.

The following simulation predictions are examined with this case and should be plotted against P_{el}:

air supply blower	$T_{blower-in} = 50^{o}C$ (air drawn at containing room's temperature)
fuel compressor	$T_{comp-in} = 50^{o}C$ (fuel drawn at containing room's temperature)
water supply to FCPM	$w_0 = 1.0 \cdot 10^{-7}$; $w_1 = 2.0$; $w_2 = 5.0 \cdot 10^{4}$
water pump	$T_{pump-in} = 50^{o}C$ (water drawn at containing room's temperature)
	$p_0 = 15.0$; $p_1 = 1.6 \cdot 10^{6}$; $p_2 = 4.3 \cdot 10^{10}$; $p_3 = 2.3 \cdot 10^{15}$;
	$\varepsilon_{pump-heat-loss} = 0.4$

Table II-27: Input data for case 405 that override and augment the data given in Table II-22

- The difference in $T_{blower-out}$ between case 405 and case 400 (case 405 result minus case 400 result).
- The difference in $T_{comp-out}$ between case 405 and case 400 (case 405 result minus case 400 result).
- The difference in $T_{pump-out}$ between case 405 and case 404 (case 405 result minus case 404 result).
- The temperature of the product gas stream exiting the FCPM, $T_{FCPM-cg}$.

These results are given in Figure II-54 through II-57.

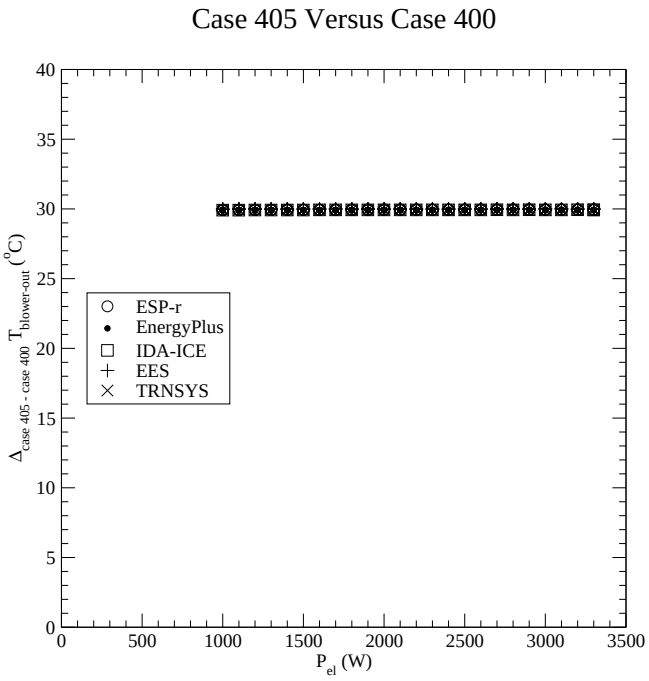

Figure II-54: $\Delta_{case\ 405-\ case\ 400}\ T_{blower-out}$ **results**

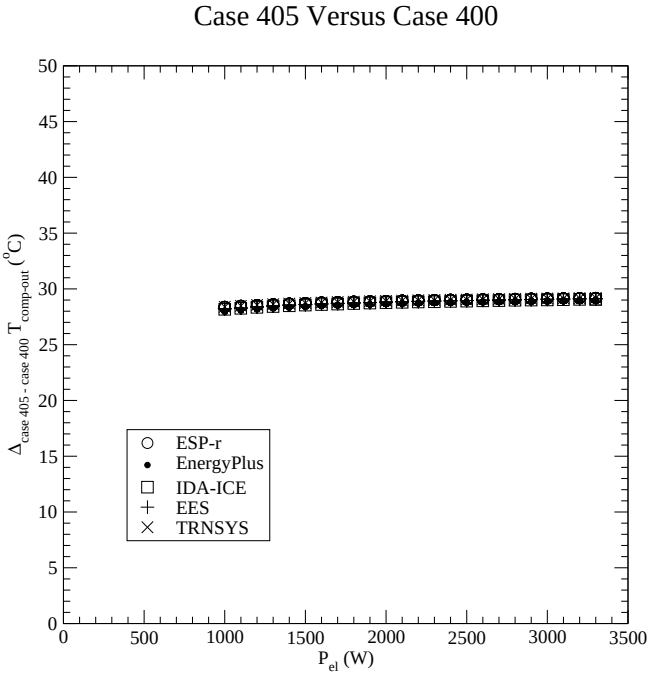

Figure II-55: $\Delta_{case\ 405-\ case\ 400}\ T_{comp-out}$ **results**

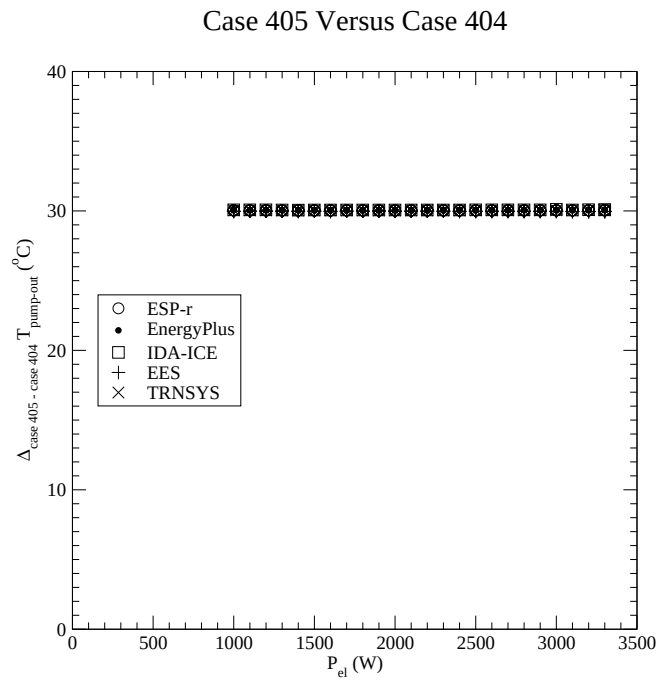

Figure II-56: $\Delta_{case\ 405 - case\ 404}\ T_{pump-out}$ **results**

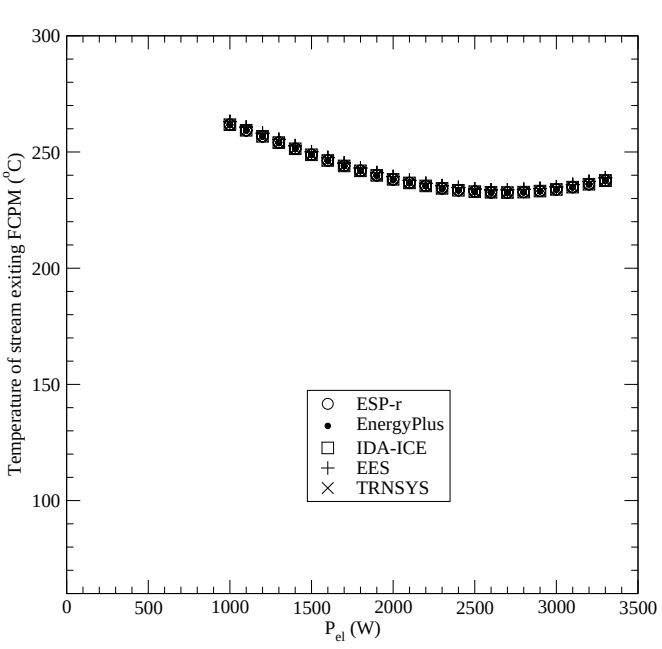

Figure II-57: Case 405 $T_{FCPM-cg}$ **results**

Disagreements in the difference between case 405 and case 400 predictions of $T_{blower-out}$ would indicate potential errors in implementing property evaluations for specific heat of the air stream or the solution and implementation of equation II-26 of the model specifications.

Disagreements in the difference between case 405 and case 400 predictions of $T_{comp-out}$ would indicate potential errors in implementing property evaluations for the specific heat of fuel stream, or the solution and implementation of equation II-27 of the model specifications.

Disagreements in the difference between case 405 and case 404 predictions of $T_{pump-out}$ would indicate potential errors in implementing property evaluations for the specific heat of the water stream, or the solution and implementation of equation II-29 of the model specifications.

500 Series Tests

The *500 series* cases exercise the portions of the code that model the auxiliary burner.

The battery and power conditioning unit (PCU) control volumes are nullified in this series of tests.

Case 500

Case 500 is the base case for this series. The model specifications allows the user to input the burner's capacity either in terms of heat output or fuel input. The former is used in this test case. As detailed in section II-6 of the model specifications, the heat loss from the burner can either be lost to the containing room or can be recovered to heat the FCPM's air intake. In this test case the heat is transferred to the containing room.

As before, the simulation is conducted for a single day (January 9) with whatever start-up or conditioning period is appropriate for the simulation program. The simulation should be performed with a time-step no greater than 15 minutes. The weather file is inconsequential.

The electrical demand placed upon the FC-cogeneration unit is identical to that used in the 100, 200, and 400 series tests and is illustrated in Figure II-1.

Multiple operating points are examined by varying the burner's output over the course of a day. The control signal sent to the burner is made to follow the pattern illustrated in Figure II-62. It is worth noting that the control signal from 18h00 to 24h00 attempts to operate the burner outside of its modulating range and thus constitutes a test on this aspect of the model.

The pertinent input data to the FC-cogeneration model are listed in Table II-28

The following simulation predictions are examined with this case and should be plotted against time (in hours):

- The fuel consumption of the auxiliary burner, $\dot{N}_{aux-fuel}$.
- The electrical draw of the auxiliary burner ancillaries, $P_{el,aux-ancillaries}$.

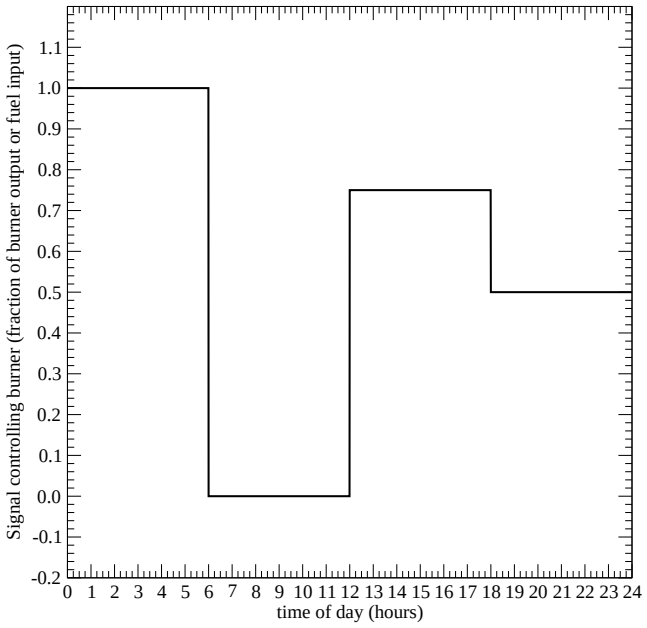

Figure II-62: Control signal sent to auxiliary burner for case 500

- The heat losses from the auxiliary burner, $q_{aux-skin-loss}$.
- The temperature of the product gases exiting the auxiliary burner, $T_{aux-mix}$.

These results are given in Figures II-58 through II-61.

FCPM electrical efficiency	$\varepsilon_0 = 0.3$; $\varepsilon_1 = 1.1 \cdot 10^{-4}$; $\varepsilon_2 = -2 \cdot 10^{-8}$
	$D = 0$
	$L = 0$
FCPM transient response	$(dP_{el}/dt)_{\max}$ = 10 (W/s) for both increasing and decreasing power
fuel molar fractions	$\chi_{H_2} = 0.0$; $\chi_{CH_4} = 0.949$; $\chi_{C_2H_6} = 0.025$; $\chi_{C_3H_8} = 0.002$; $\chi_{C_4H_{10}} = 0.0006$; $\chi_{C_5H_{12}} = 0.0001$; $\chi_{C_6H_{14}} = 0.0001$; $\chi_{CH_3OH} = 0.0$; $\chi_{C_2H_5OH} = 0.0$; $\chi_{CO_2} = 0.007$; $\chi_{N_2} = 0.016$; $\chi_{O_2} = 0.0002$
air molar fractions	$\chi_{N_2} = 0.7728$; $\chi_{O_2} = 0.2073$; $\chi_{H_2O} = 0.0104$; $\chi_{Ar} = 0.0092$; $\chi_{C_{O_2}} = 0.0003$;
air supply to FCPM	method 2 $a_0 = 5 \cdot 10^{-5}$; $a_1 = 1.5 \cdot 10^{-7}$; $a_2 = 1.1 \cdot 10^{-12}$; $a_3 = 0.0$
air supply blower	$T_{blower-in} = 20^oC$ (air drawn at containing room's temperature)
	$b_0 = 0.0$; $b_1 = 0.0$; $b_2 = 0.0$; $b_3 = 0.0$;
	$\alpha_{blower-heat-loss} = 1.0$
fuel compressor	$T_{comp-in} = 20^oC$ (fuel drawn at containing room's temperature)
	$c_0 = 0.0$; $c_1 = 0.0$; $c_2 = 0.0$; $c_3 = 0.0$;
	$\alpha_{comp-heat-loss} = 1.0$
water supply to FCPM	$w_0 = 0.0$; $w_1 = 0.0$; $w_2 = 0.0$
FCPM AC ancillaries	anc_0 = 0.0; $anc_1 = 0.0$
FCPM skin losses	method 1 $q_{skin-loss} = 0.0$
dilution air	$\dot{N}_{dilution-air} = 0.0$
auxiliary burner modulating range	5 000 W to 8 000 W
auxiliary burner excess air ratio	0.3
auxiliary burner heat losses	$(UA)_{aux}$ = 0.5 W/K lost to containing room
auxiliary burner ancillaries	$x_0 = 50$; $x_1 = 1 \cdot 10^8$

Table II-28: Input data for case 500

Case 500

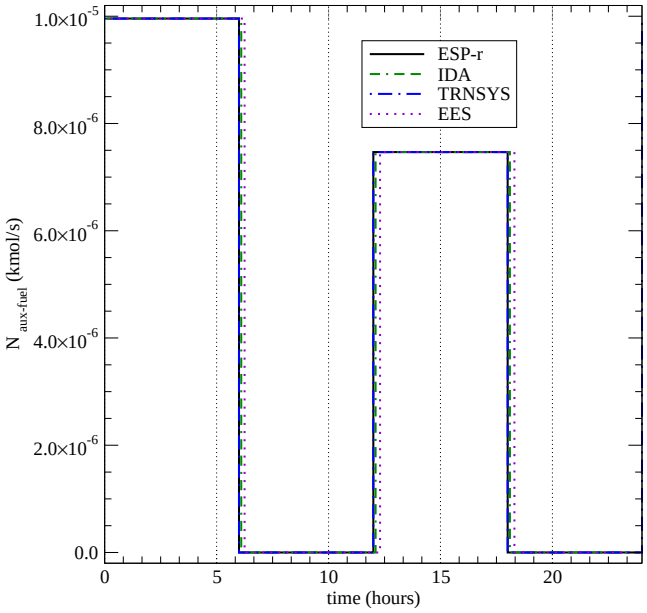

Figure II-58: Case 500 $\dot{N}_{aux-fuel}$ results

Case 500

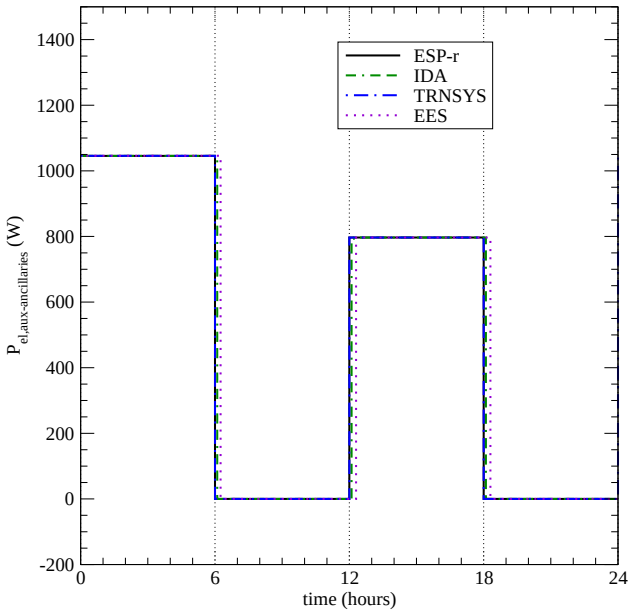

Figure II-59: Case 500 $P_{el,aux-ancillaries}$ results

Case 500

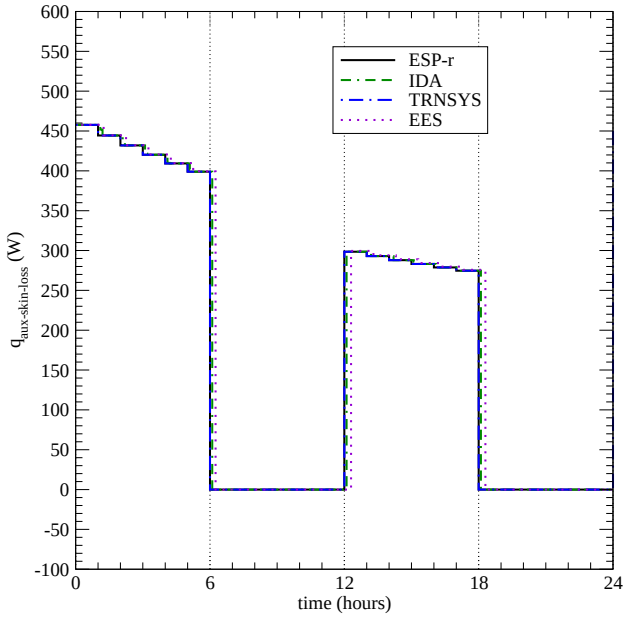

Figure II-60: Case 500 $q_{aux-skin-loss}$ results

Case 500

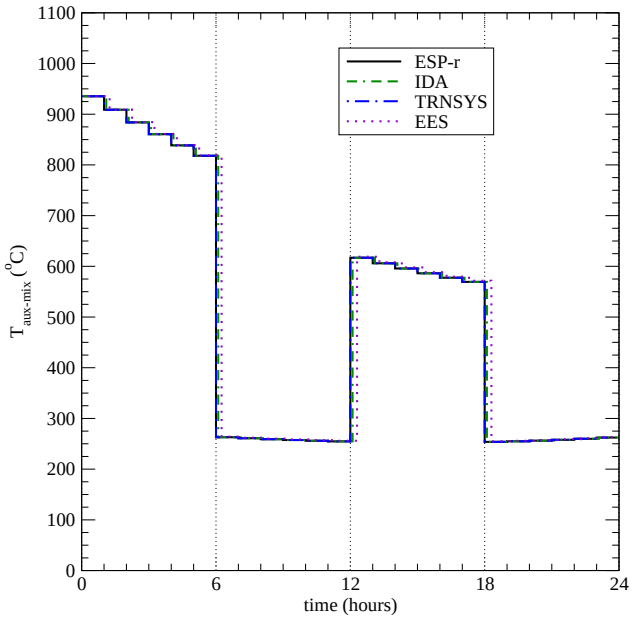

Figure II-61: Case 500 $T_{aux-mix}$ results

Case 501

Case 501 is identical to case 500 with the exception that the heat loss from the burner is recovered to heat the the FCPM's air intake. The pertinent input data to the FC-cogeneration model are listed in Table II-28 with the changes noted in Table II-29.

auxiliary burner heat losses	$(UA)_{aux}$ = 0.5 W/K recovered to heat FCPM's air intake

Table II-29: Input data for case 501 that override the data given in Table II-28

The following simulation predictions are examined with this case and should be plotted against time (in hours):

- The difference in $T_{aux-mix}$ between case 501 and case 500 (case 501 result minus case 500 result).

These results are given in Figure II-63.

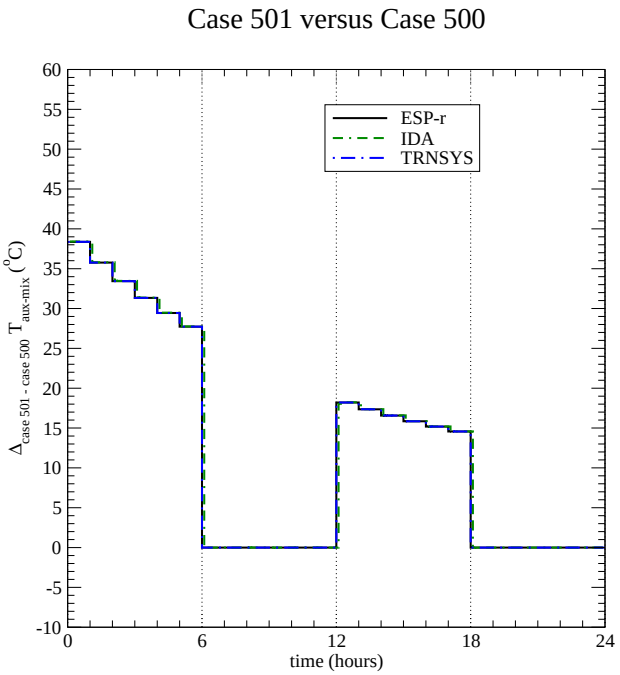

Figure II-63: $\Delta_{case\ 501\ -\ case\ 500}\ T_{aux-mix}$ **results**

Case 502

Case 502 is identical to case 500 with the exception that the burner's capacity is specified in terms of fuel input rather than heat output. The pertinent input data to the FC-cogeneration model are listed in Table II-28 with the changes noted in Table II-30.

auxiliary burner modulating range	$6.25 \cdot 10^{-6}$ kmol/s to $9.1 \cdot 10^{-6}$ kmol/s

Table II-30: Input data for case 502 that override the data given in Table II-28

The following simulation predictions are examined with this case and should be plotted against time (in hours):

- The difference in $T_{aux-mix}$ between case 502 and case 500 (case 502 result minus case 500 result).

These results are given in Figure II-64.

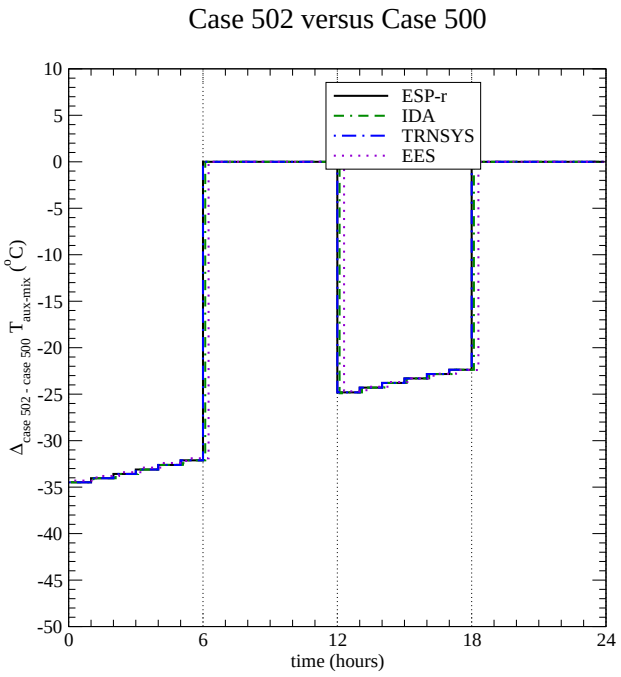

Figure II-64: $\Delta_{case\ 502\ -\ case\ 500}\ T_{aux-mix}$ **results**

600 Series Tests

The *600 series* cases exercise the portions of the code that model the exhaust-gas-to-water heat exchanger. The four heat exchanger methods described in section II-7 of the model specifications are exercised.

The battery and power conditioning unit (PCU) control volumes are nullified in this series of tests.

Case 600

Case 600 is the base case for this series. It examines the *method 1* heat exchanger approach wherein the user supplies a constant heat exchanger effectiveness.

This test is configured to span multiple operating points. For example, for the first half of case 600 the gas stream has a lower heat capacitance flow rate whereas the water has a lower rate in the latter half of the test. The heat exchanger effectiveness is set quite low in order to achieve this (otherwise the water outlet temperature would exceed 100 ^{o}C at some points).

As before, the simulation is conducted for a single day (January 9) with whatever start-up or conditioning period is appropriate for the simulation program. The simulation should be performed with a time-step no greater than 15 minutes. The weather file is inconsequential.

The examination of multiple operating points is achieved by controlling the electrical and thermal boundary conditions that are placed upon the FC-cogeneration device. These are:

- The electrical demand placed upon the FC-cogeneration unit is identical to that used in the 100, 200, and 400 series tests and is illustrated in Figure II-1.
- The temperature of the water flowing into the FC-cogeneration device's heat exchanger is equal to 50 ^{o}C from 0h00 to just before 8h00. At 8h00 this temperature drops to 30 ^{o}C and then at 16h00 it drops to 10 ^{o}C. This is illustrated in Figure II-65.
- The flow rate of the water through the FC-cogeneration device's heat exchanger is equal to 0.01 kg/s from 0h00 to just before 9h00. At 9h00 this flow rate drops to 0.0028 kg/s. This is illustrated in Figure II-66.

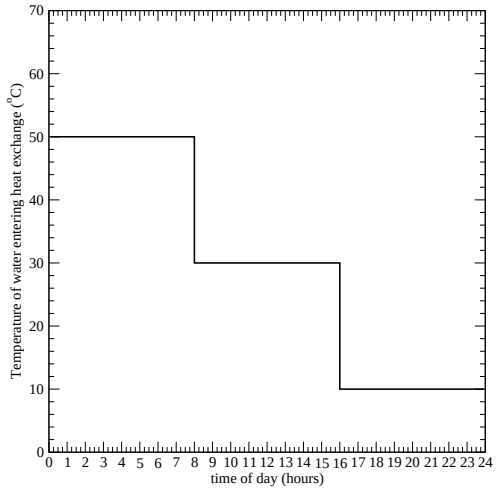

Figure II-65: Temperature of water flowing into heat exchanger for case 600

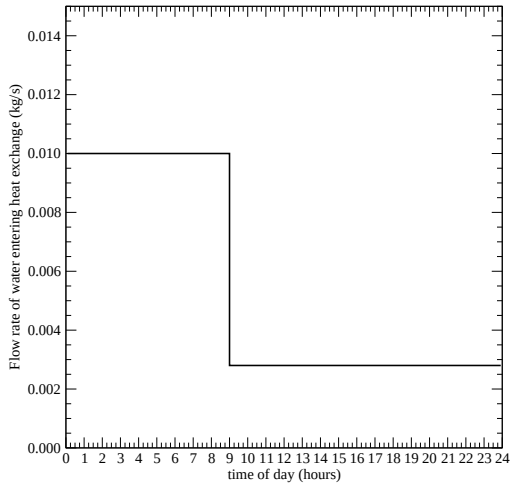

Figure II-66: Rate of water flowing into heat exchanger for case 600

The pertinent input data to the FC-cogeneration model are listed in Table II-31.

The following simulation predictions are examined with this case and should be plotted against time (in hours):

- The heat transfer rate to the water, q_{HX}.
- The temperature of the cooled gas exiting the heat exchanger, T_{HX-exh}.

FCPM electrical efficiency	$\varepsilon_0 = 0.3;\ \varepsilon_1 = 1.1 \cdot 10^{-4};\ \varepsilon_2 = -2 \cdot 10^{-8}$
	$D = 0$
	$L = 0$
FCPM transient response	$(dP_{el}/dt)_{\max}$ = 10 (W/s) for both increasing and decreasing power
fuel molar fractions	$\chi_{H_2} = 0.0;\quad \chi_{CH_4} = 0.949;\quad \chi_{C_2H_6} = 0.025;\quad \chi_{C_3H_8} = 0.002;$ $\chi_{C_4H_{10}} = 0.0006;\quad \chi_{C_5H_{12}} = 0.0001;\quad \chi_{C_6H_{14}} = 0.0001;$ $\chi_{CH_3OH} = 0.0;\quad \chi_{C_2H_5OH} = 0.0;\quad \chi_{CO_2} = 0.007;\quad \chi_{N_2} = 0.016;$ $\chi_{O_2} = 0.0002$
air molar fractions	$\chi_{N_2} = 0.7728;\quad \chi_{O_2} = 0.2073;\quad \chi_{H_2O} = 0.0104;\quad \chi_{Ar} = 0.0092;$ $\chi_{C_{O_2}} = 0.0003;$
air supply to FCPM	method 2 $a_0 = 5 \cdot 10^{-5};\ a_1 = 1.5 \cdot 10^{-7};\ a_2 = 1.1 \cdot 10^{-12};\ a_3 = 0.0$
air supply blower	$T_{blower-in} = 20^oC$ (air drawn at containing room's temperature)
	$b_0 = 0.0;\ b_1 = 0.0;\ b_2 = 0.0;\ b_3 = 0.0;$
	$\alpha_{blower-heat-loss} = 1.0$
fuel compressor	$T_{comp-in} = 20^oC$ (fuel drawn at containing room's temperature)
	$c_0 = 0.0;\ c_1 = 0.0;\ c_2 = 0.0;\ c_3 = 0.0;$
	$\alpha_{comp-heat-loss} = 1.0$
water supply to FCPM	$w_0 = 0.0;\ w_1 = 0.0;\ w_2 = 0.0$
FCPM AC ancillaries	anc_0 = 0.0; $anc_1 = 0.0$
FCPM skin losses	method 1 $q_{skin-loss} = 0.0$
dilution air	$\dot{N}_{dilution-air} = 0.0$
auxiliary burner	not present
heat exchanger	method 1 $\varepsilon_{HX} = 0.3$

Table II-31: Input data for case 600

- The temperature of the heated water exiting the heat exchanger, $T_{water,out}$.

These results are given in Figures II-67 through II-69.

Case 600

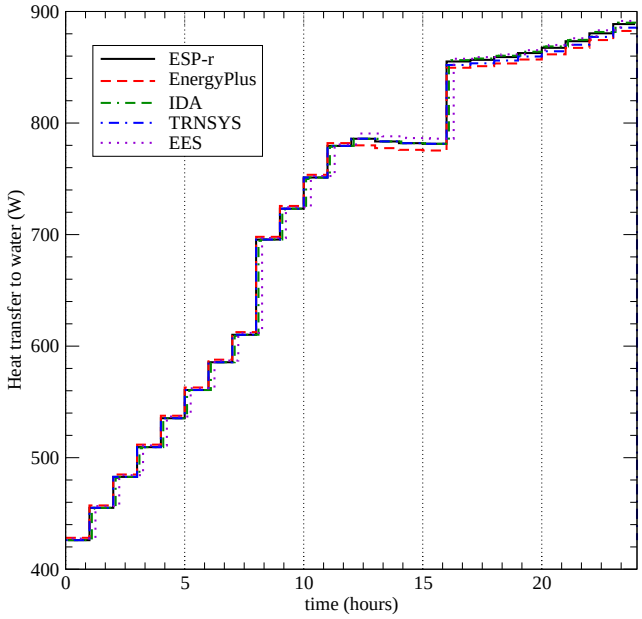

Figure II-67: Case 600 q_{HX} results

Case 600

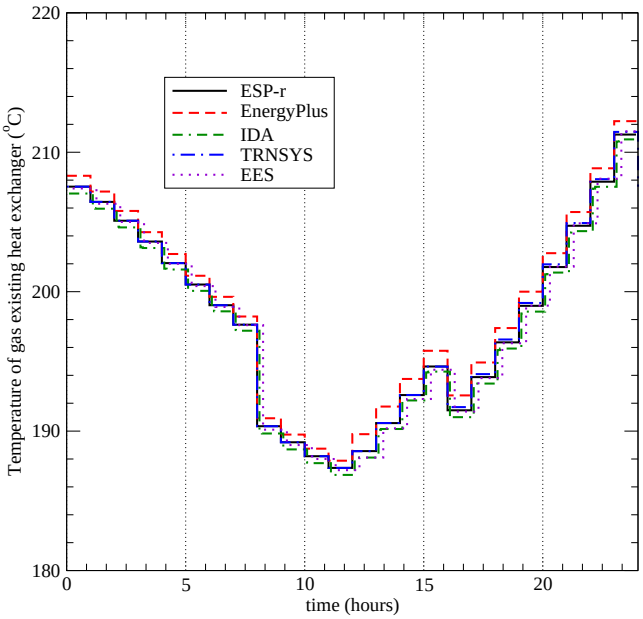

Figure II-68: Case 600 T_{HX-exh} results

Case 600

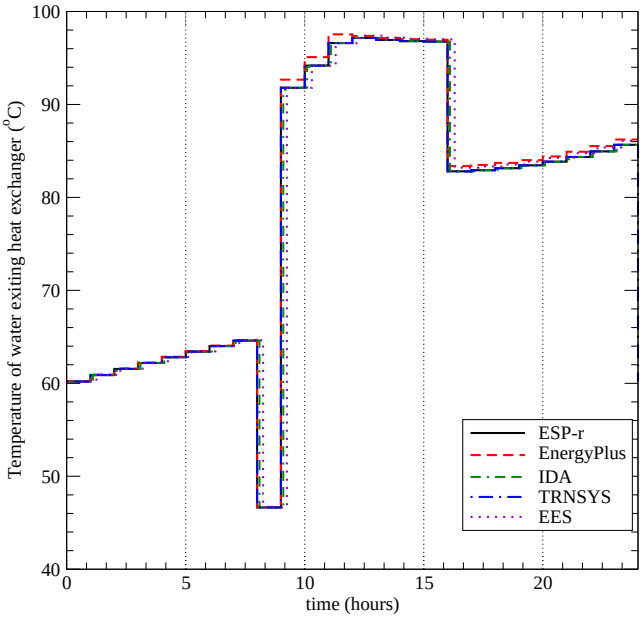

Figure II-69: Case 600 $T_{water,out}$ results

Case 601

Case 601 is identical to case 600 with the exception that the heat exchanger is modelled with *method 2*. The pertinent input data to the FC-cogeneration model are listed in Table II-31 with the changes noted in Table II-32.

heat exchanger	method 2 $hx_{s,0} = 0.5;$ $hx_{s,1} = 500.;$ $hx_{s,2} = 5000.;$ $hx_{s,3} = 5000.;$ $hx_{s,4} = 10^6$

Table II-32: Input data for case 601 that override the data given in Table II-31

The same results are plotted as with case 600. These results are given in Figures II-70 through II-72.

Case 601

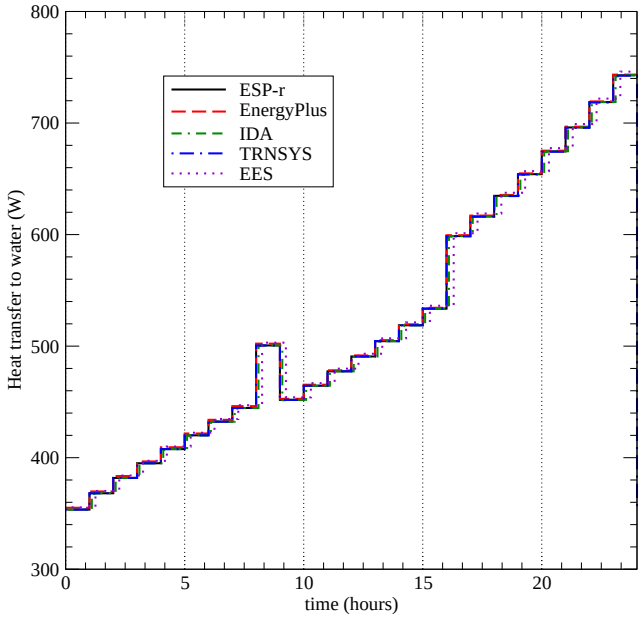

Figure II-70: Case 601 q_{HX} results

Case 601

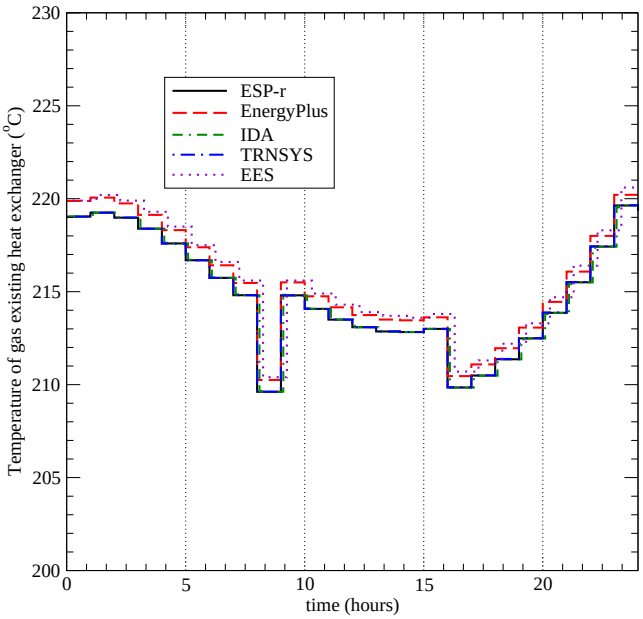

Figure II-71: Case 601 T_{HX-exh} results

Case 601

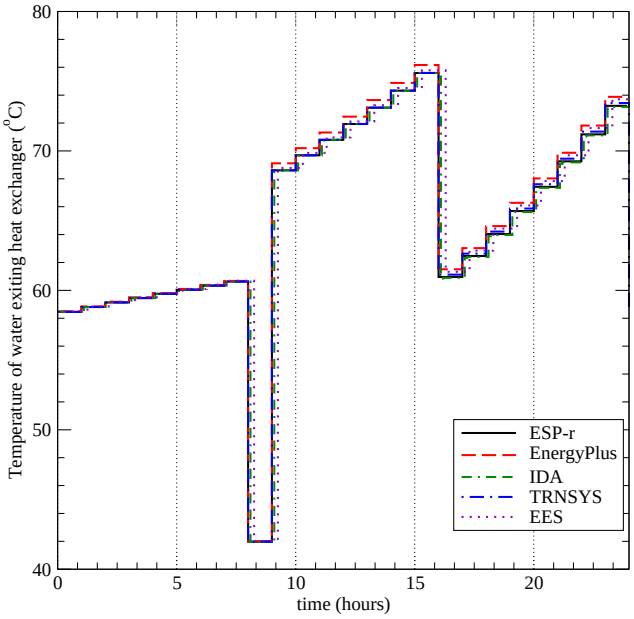

Figure II-72: Case 601 $T_{water,out}$ results

Case 602

Case 602 is identical to case 600 with the exception that the heat exchanger is modelled with *method 3*. The pertinent input data to the FC-cogeneration model are listed in Table II-31 with the changes noted in Table II-33.

heat exchanger	method 3 $h^0_{gas} = 100.;$ $\dot{N}^0_{gas} = 0.0003;$ $n = 0.5;$ $A_{gas} = 0.05;$ $h^0_{water} = 5000.;$ $\dot{N}^0_{water} = 0.0003;$ $m = 0.5;$ $A_{water} = 0.05;$ $F_{HX} = 0.2$

Table II-33: Input data for case 602 that override the data given in Table II-31

The same results are plotted as with case 600. These results are given in Figures II-73 through II-75.

Case 602

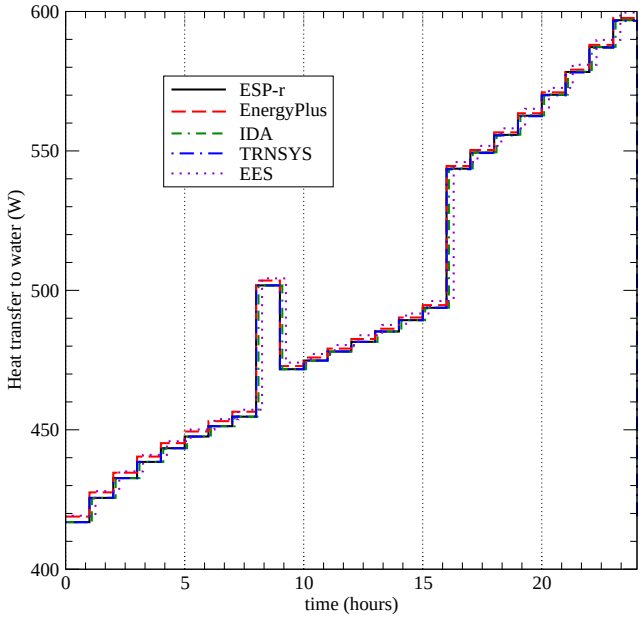

Figure II-73: Case 602 q_{HX} results

Case 602

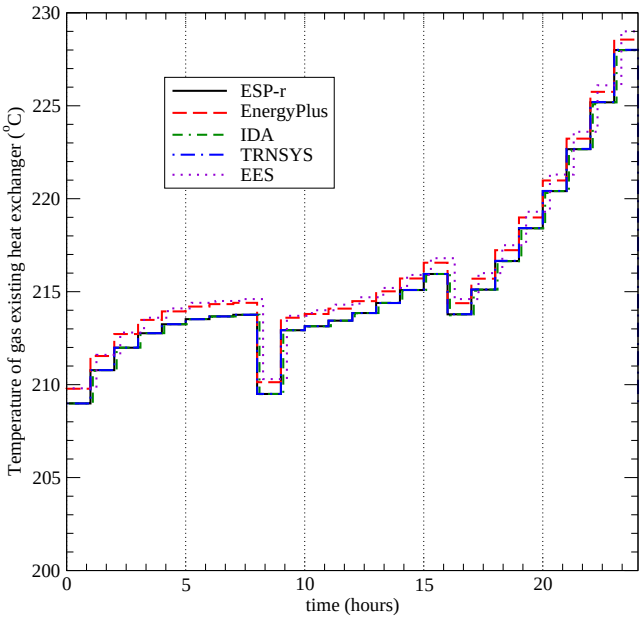

Figure II-74: Case 602 T_{HX-exh} results

Case 602

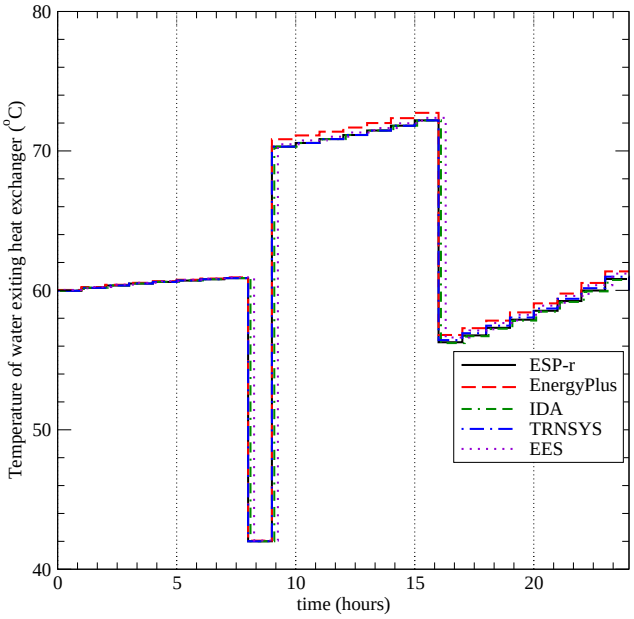

Figure II-75: Case 602 $T_{water,out}$ results

Case 603

Case 603 is identical to case 600 with the exception that the heat exchanger is modelled with *method 4*. The test is configured such that the condensation of water vapour from the exhaust gases occurs only during a portion of the test. The pertinent input data to the FC-cogeneration model are listed in Table II-31 with the changes noted in Table II-34.

heat exchanger	method 4 $hx_{s,0} = 0.5;$ $hx_{s,1} = 500.;$ $hx_{s,2} = 5000.;$ $hx_{s,3} = 5000.;$ $hx_{s,4} = 10^6;$ $hx_{l,1} = 5.0 \cdot 10^{-6};$ $hx_{l,2} = 6.0 \cdot 10^{-5};$ $T_{cond-threshold} = 25.0^o C$

Table II-34: Input data for case 603 that override the data given in Table II-31

The following simulation predictions are examined with this case and should be plotted against time (in hours):

- The fraction of water vapour in the exhaust gases flowing through the heat exchanger, $\dot{N}_{H_2O}/\dot{N}_{aux-mix}$.
- The rate of condensation of water from the gas stream, $\dot{N}_{H_2O-cond}$.
- The difference in q_{HX} between case 603 and case 601 (case 603 result minus case 601 result).
- The difference in T_{HX-exh} between case 603 and case 601 (case 603 result minus case 601 result).
- The difference in $T_{water,out}$ between case 603 and case 601 (case 603 result minus case 601 result).

These results are given in Figures II-76 through II-80.

Case 603

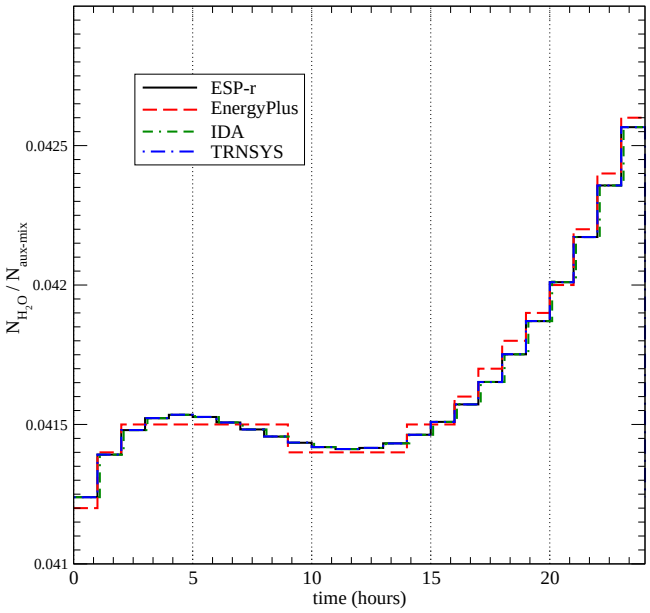

Figure II-76: Case 603 $\dot{N}_{H_2O}/\dot{N}_{aux-mix}$ results

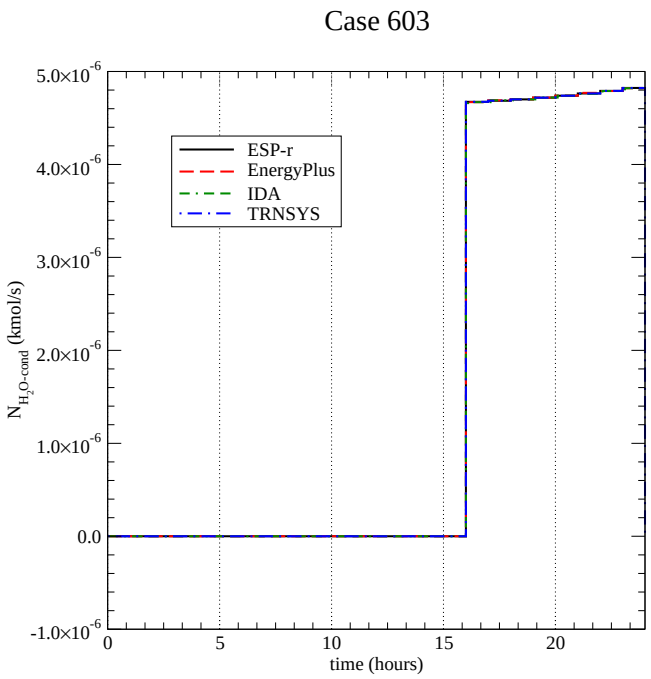

Figure II-77: Case 603 $\dot{N}_{H_2O-cond}$ results

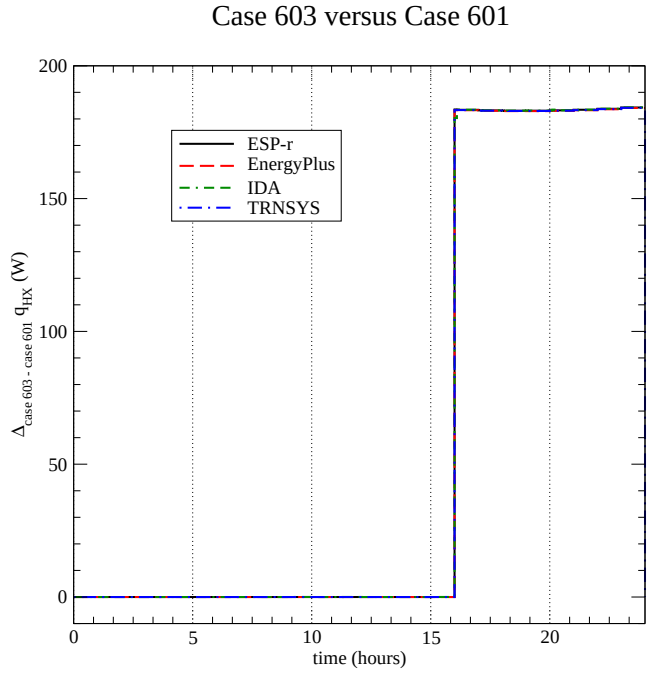

Figure II-78: $\Delta_{case\ 603\ -\ case\ 601}\ q_{HX}$ results

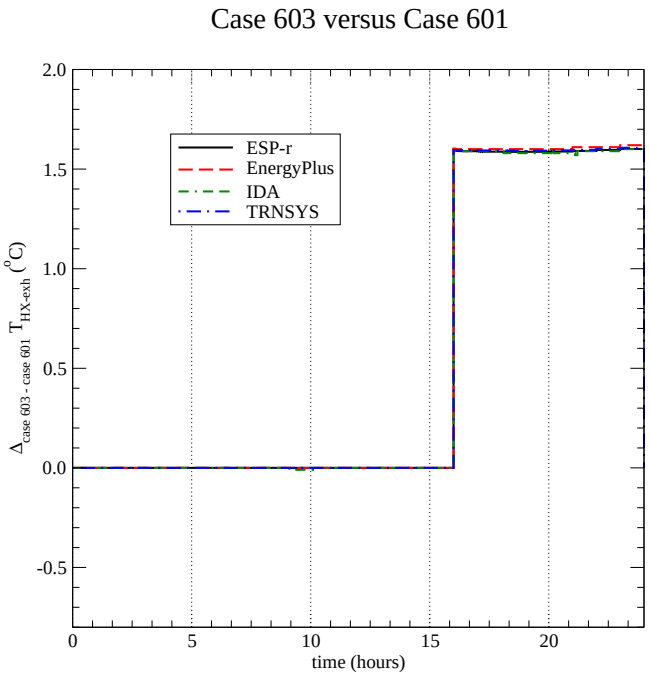

Figure II-79: $\Delta_{case\ 603\ -\ case\ 601}\ T_{HX-exh}$ **results**

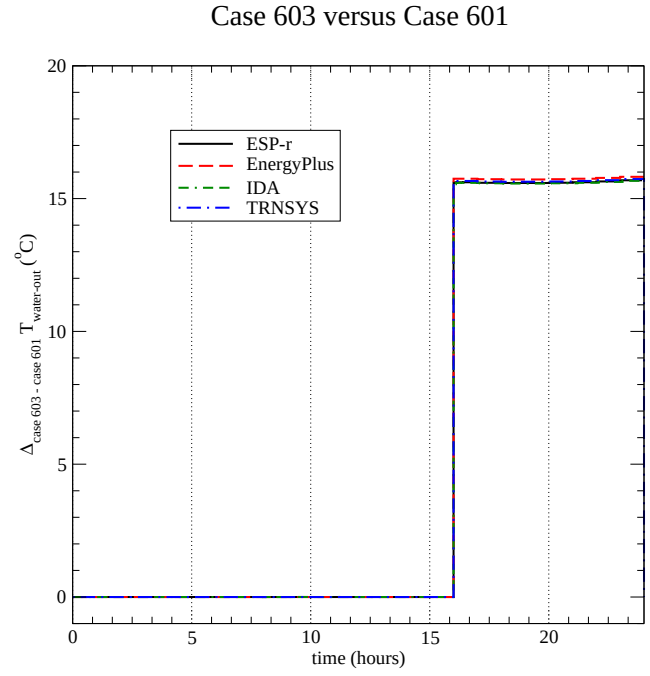

Figure II-80: $\Delta_{case\ 603\ -\ case\ 601}\ T_{water,out}$ **results**

Case 604

Case 604 is identical to case 600 with the exception that the auxiliary burner operates. This tests the situation whereby the heat exchanger recovers heat from both the FCPM product gases and the auxiliary burner product gases.

The control signal sent to the burner is made to follow the pattern illustrated in Figure II-62.

The pertinent input data to the FC-cogeneration model are listed in Table II-31 with the changes noted in Table II-35.

auxiliary burner modulating range	100 W to 500 W
auxiliary burner excess air ratio	0.3
auxiliary burner heat losses	$(UA)_{aux}$ = 0.5 W/K lost to containing room
auxiliary burner ancillaries	$x_0 = 50;\ x_1 = 1 \cdot 10^8$

Table II-35: Input data for case 604 that override the data given in Table II-31

The following simulation predictions are examined with this case and should be plotted against time (in hours):

- The difference in $T_{aux-mix}$ between case 604 and case 600 (case 604 result minus case 600 result).
- The difference in T_{HX-exh} between case 604 and case 600 (case 604 result minus case 600 result).
- The difference in $T_{water,out}$ between case 604 and case 600 (case 604 result minus case 600 result).
- The difference in q_{HX} between case 604 and case 600 (case 604 result minus case 600 result).

These results are given in Figures II-81 through II-84.

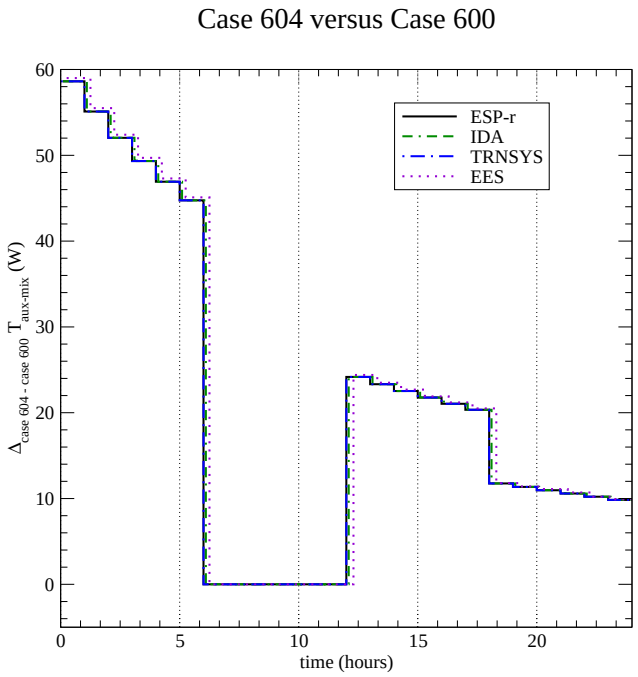

Figure II-81: $\Delta_{case\ 604\ -\ case\ 600}\ T_{aux-mix}$ **results**

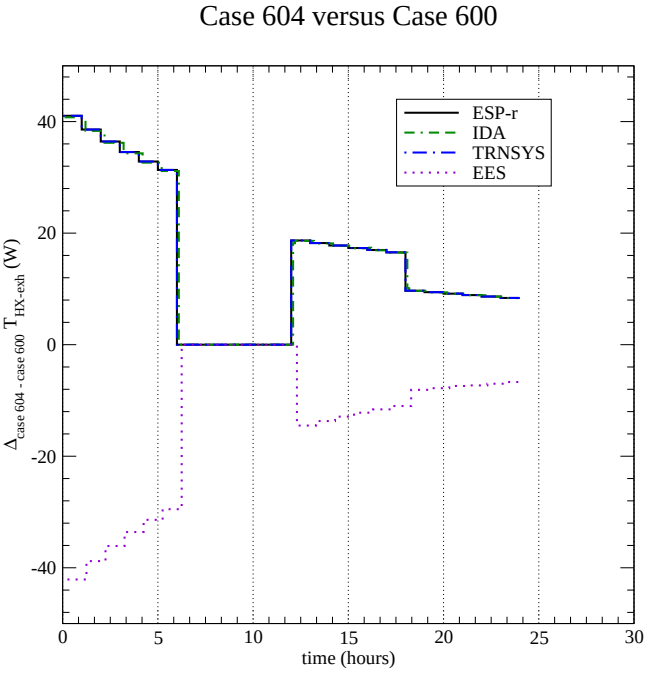

Figure II-82: $\Delta_{case\ 604\ -\ case\ 600}\ T_{HX-exh}$ **results**

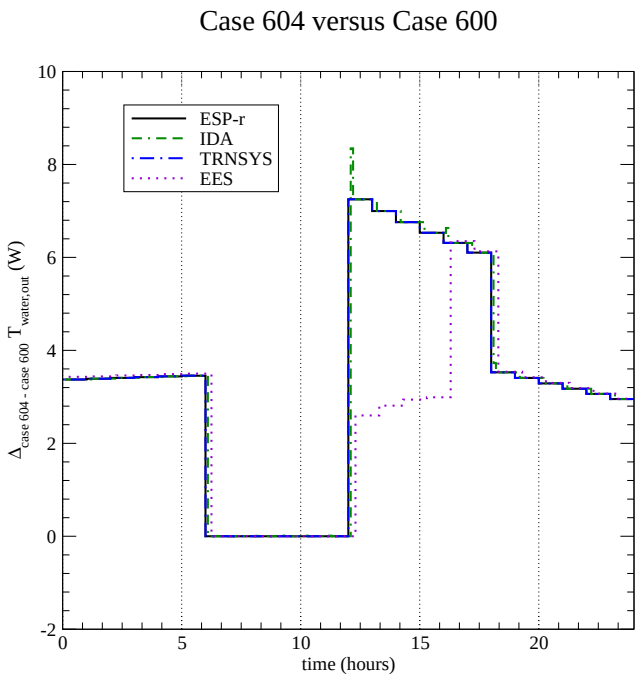

Figure II-83: $\Delta_{case\ 604\ -\ case\ 600}\ T_{water,out}$ **results**

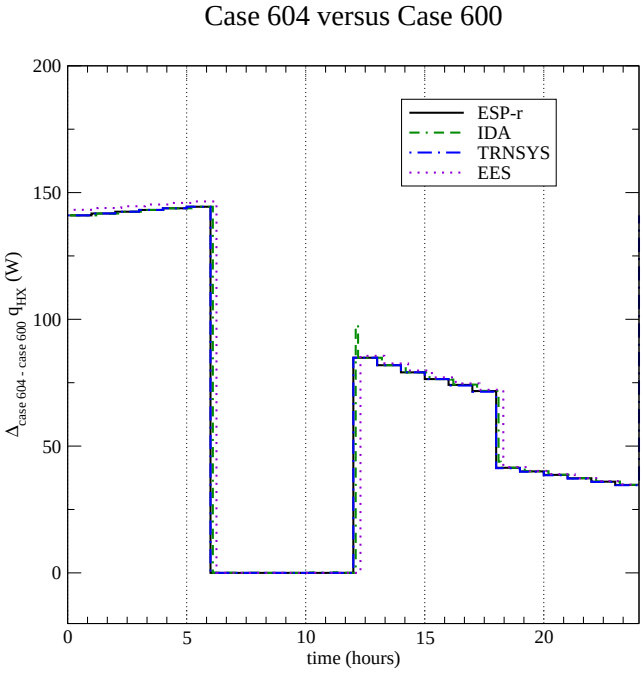

Figure II-84: $\Delta_{case\ 604\ -\ case\ 600}\ Q_{HX}$ **results**

700 Series Tests

The *700 series* cases exercise the portions of the code that model the dilution air system and heat recovery ventilator (HRV).

Case 700

Case 700 is the base case for this series and is based upon case 601. The dilution air system is active in this case but not the HRV.

The net AC power demanded from the FC-cogeneration device (P_{demand}) is specified as the boundary condition as illustrated in Figure II-1.

As before, the simulation is conducted for a single day (January 9) with whatever start-up or conditioning period is appropriate for the simulation program. The simulation should be performed with a time-step no greater than 15 minutes. The weather file is inconsequential.

The pertinent input data to the FC-cogeneration model are listed in Table II-36.

The following simulation predictions are examined with this case and should be plotted against time (in hours):

- The temperature of the product gas stream exiting the FCPM, $T_{FCPM-cg}$.
- The temperature of the cooled gas exiting the FC-cogeneration device, T_{exh}. (This is equal to the temperature of the gases exiting the dilution air system since the HRV is not present in this test case.)
- The temperature of the heated water exiting the heat exchanger, $T_{water,out}$.

These results are given in Figures II-85 through II-87.

FCPM electrical efficiency	$\varepsilon_0 = 0.3$; $\varepsilon_1 = 1.1 \cdot 10^{-4}$; $\varepsilon_2 = -2 \cdot 10^{-8}$
	$D = 0$
	$L = 0$
FCPM transient response	$(dP_{el}/dt)_{\max}$ = 10 (W/s) for both increasing and decreasing power
fuel molar fractions	$\chi_{H_2} = 0.0$; $\chi_{CH_4} = 0.949$; $\chi_{C_2H_6} = 0.025$; $\chi_{C_3H_8} = 0.002$; $\chi_{C_4H_{10}} = 0.0006$; $\chi_{C_5H_{12}} = 0.0001$; $\chi_{C_6H_{14}} = 0.0001$; $\chi_{CH_3OH} = 0.0$; $\chi_{C_2H_5OH} = 0.0$; $\chi_{CO_2} = 0.007$; $\chi_{N_2} = 0.016$; $\chi_{O_2} = 0.0002$
air molar fractions	$\chi_{N_2} = 0.7728$; $\chi_{O_2} = 0.2073$; $\chi_{H_2O} = 0.0104$; $\chi_{Ar} = 0.0092$; $\chi_{C_{O_2}} = 0.0003$;
air supply to FCPM	method 2 $a_0 = 5 \cdot 10^{-5}$; $a_1 = 1.5 \cdot 10^{-7}$; $a_2 = 1.1 \cdot 10^{-12}$; $a_3 = 0.0$
air supply blower	$T_{blower-in} = 20^oC$ (air drawn at containing room's temperature)
	$b_0 = 0.0$; $b_1 = 0.0$; $b_2 = 0.0$; $b_3 = 0.0$;
	$\alpha_{blower-heat-loss} = 1.0$
fuel compressor	$T_{comp-in} = 20^oC$ (fuel drawn at containing room's temperature)
	$c_0 = 0.0$; $c_1 = 0.0$; $c_2 = 0.0$; $c_3 = 0.0$;
	$\alpha_{comp-heat-loss} = 1.0$
water supply to FCPM	$w_0 = 0.0$; $w_1 = 0.0$; $w_2 = 0.0$
FCPM AC ancillaries	anc_0 = 0.0; $anc_1 = 0.0$
FCPM skin losses	method 1 $q_{skin-loss} = 0.0$
dilution air	$\dot{N}_{dilution-air} = 6.4 \cdot 10^{-3}$ kmol/s
	$P_{el,dilution-fan} = 0$ W
	$q_{FCPM-to-dilution} = 1\ 000$ W
HRV	not present
auxiliary burner	not present
heat exchanger	method 2 $hx_{s,0} = 0.5$; $hx_{s,1} = 500.$; $hx_{s,2} = 5000.$; $hx_{s,3} = 5000.$; $hx_{s,4} = 10^6$

Table II-36: Input data for case 700

Case 700

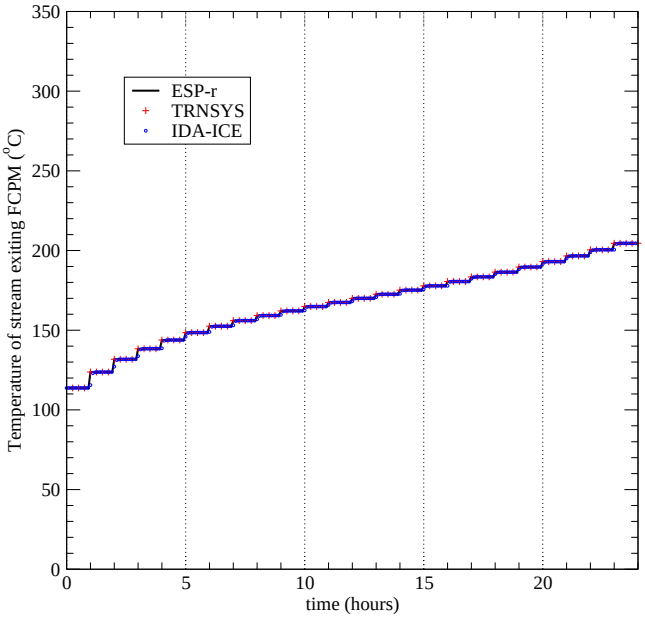

Figure II-85: Case 700 $T_{FCPM-cg}$ results

Case 700

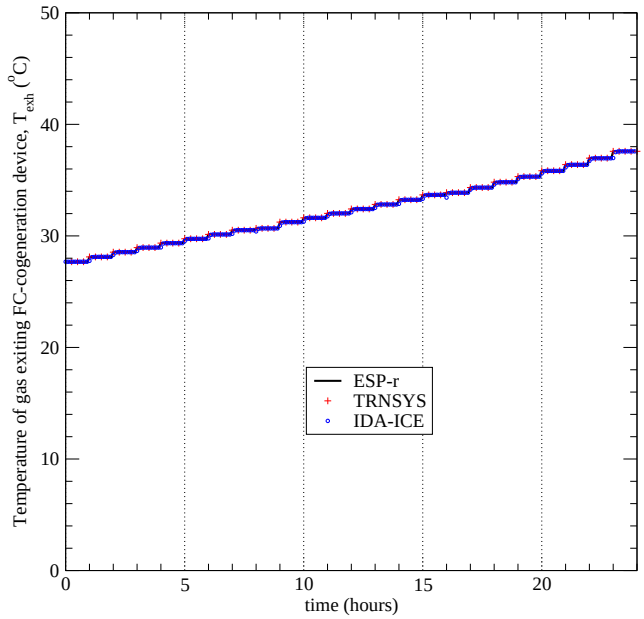

Figure II-86: Case 700 T_{exh} results

Case 700

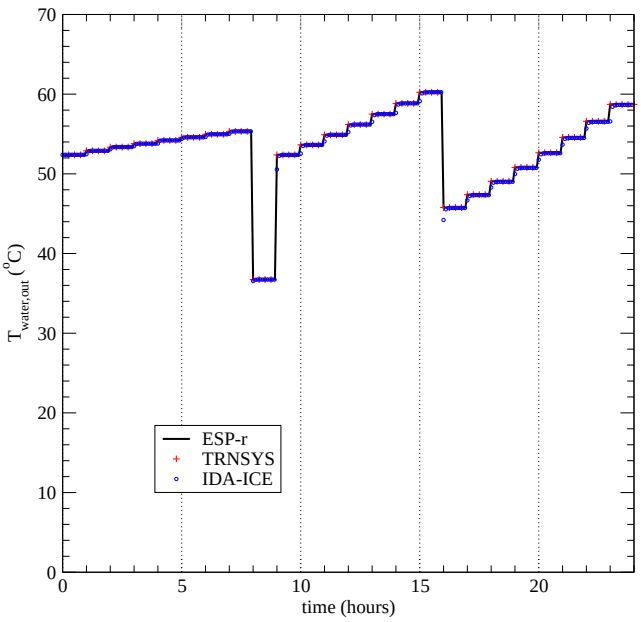

Figure II-87: Case 700 $T_{water,out}$ results

Case 701

Case 701 is identical to case 700 with the exception that the fan that draws dilution air from the room draws AC power. The pertinent input data to the FC-cogeneration model are listed in Table II-36 with the changes noted in Table II-37.

dilution air	$\dot{N}_{dilution-air} = 6.4 \cdot 10^{-3}$ kmol/s
	$P_{el,dilution-fan} = 300$ W
	$q_{FCPM-to-dilution} = 1\ 000$ W

Table II-37: Input data for case 701 that override the data given in Table II-36

The following simulation predictions are examined with this case and should be plotted against time (in hours):

- The temperature of the product gas stream exiting the FCPM, $T_{FCPM-cg}$.

- The temperature of the cooled gas exiting the FC-cogeneration device, T_{exh}. (This is equal to the temperature of the gases exiting the dilution air system since the HRV is not present in this test case.)
- The temperature of the heated water exiting the heat exchanger, $T_{water,out}$.

These results are given in Figures II-88 through II-90.

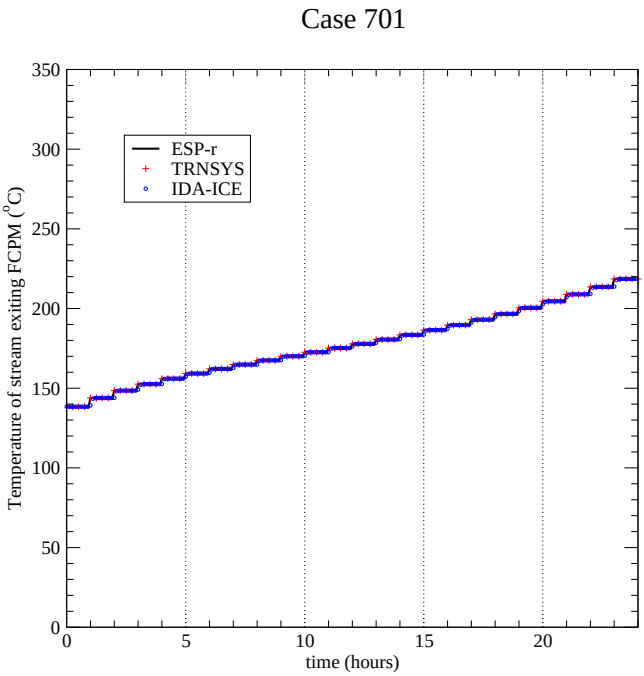

Figure II-88: Case 701 $T_{FCPM-cg}$ results

Case 701

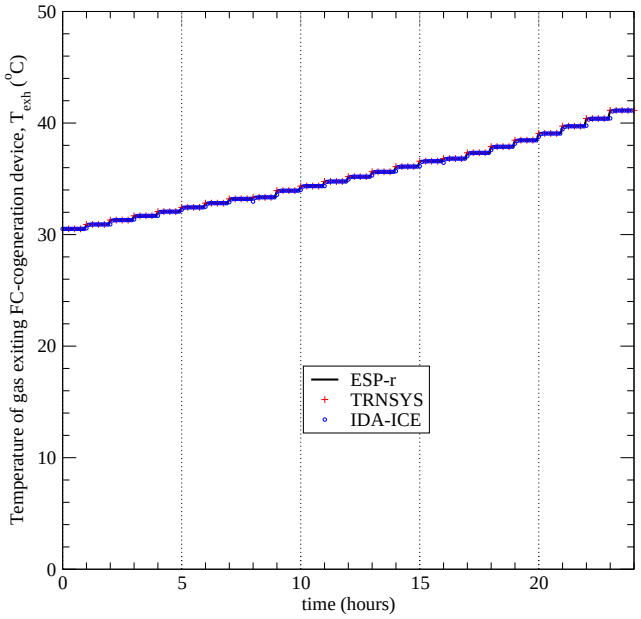

Figure II-89: Case 701 T_{exh} results

Case 701

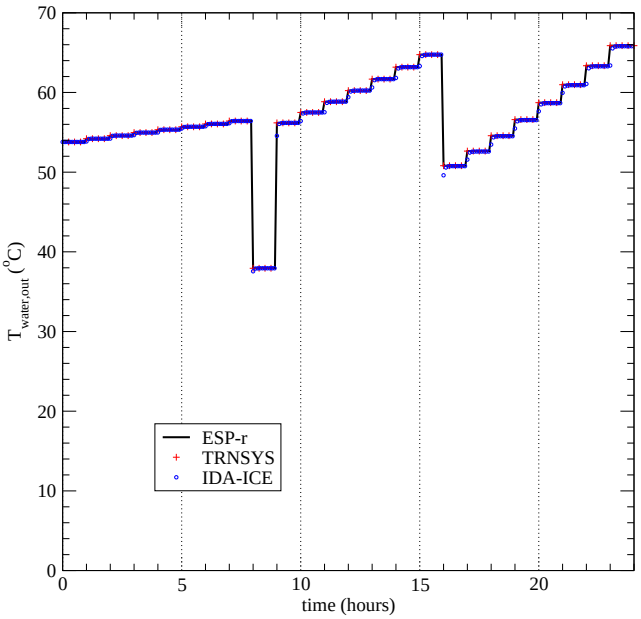

Figure II-90: Case 701 $T_{water,out}$ results

Case 702

Case 702 is identical to case 700 with the exception that an HRV is also present. The HRV draws its fresh air from the outdoors which has a constant ambient temperature of -10°C. The pertinent input data to the FC-cogeneration model are listed in Table II-36 with the changes noted in Table II-38.

HRV	$\dot{N}_{OA} = 2.7 \cdot 10^{-3}$ kmol/s
	$P_{el,\,fresh-air-fan} = 0$ W
	$\varepsilon_{HRV} = 0.75$

Table II-38: Input data for case 702 that override the data given in Table II-36

The following simulation predictions are examined with this case and should be plotted against time (in hours):

- The temperature of the cooled gas exiting the FC-cogeneration device, T_{exh}.
- The temperature of the warmed ventilation air that is delivered to the building, $T_{vent-air}$.
- The temperature of the heated water exiting the heat exchanger, $T_{water,out}$.

These results are given in Figures II-91 through II-93.

Case 702

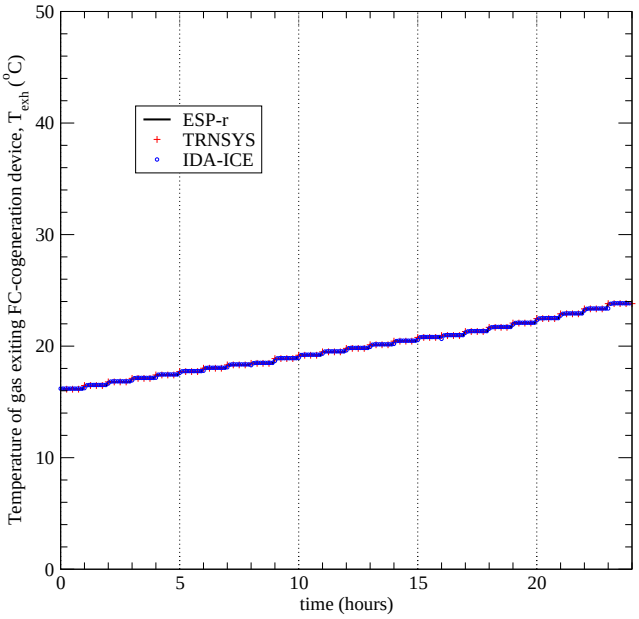

Figure II-91: Case 702 T_{exh} results

Case 702

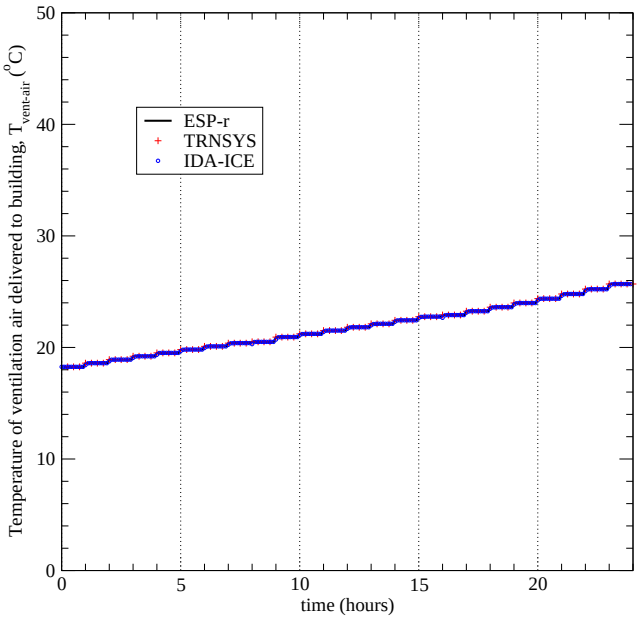

Figure II-92: Case 702 $T_{vent-air}$ results

Case 702

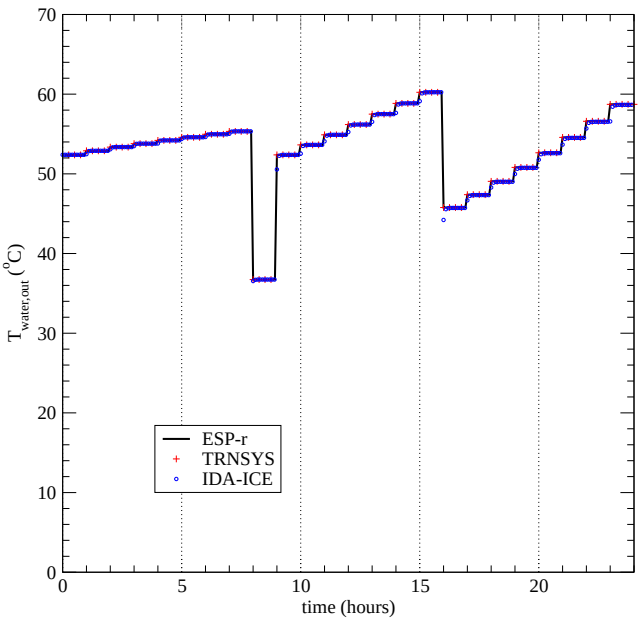

Figure II-93: Case 702 $T_{water,out}$ results

Case 703

In case 702 the fresh air side of the HRV had a lower heat capacitance rate than the exhaust gas side. Case 703 is identical to case 702 with the exception that the fresh air flow through the HRV is substantially higher. Consequently, in this test case the heat capacitance rate is higher on the fresh air side of the HRV. The pertinent input data to the FC-cogeneration model are listed in Table II-36 with the changes noted in Table II-39.

HRV	$\dot{N}_{OA} = 9.0 \cdot 10^{-3}$ kmol/s
	$P_{el,\,fresh-air-fan} = 0$ W
	$\varepsilon_{HRV} = 0.75$

Table II-39: Input data for case 703 that override the data given in Table II-36

The following simulation predictions are examined with this case and should be plotted against time (in hours):

- The temperature of the cooled gas exiting the FC-cogeneration device, T_{exh}.
- The temperature of the warmed ventilation air that is delivered to the building, $T_{vent-air}$.
- The temperature of the heated water exiting the heat exchanger, $T_{water,out}$.

These results are given in Figures II-94 through II-96.

Case 703

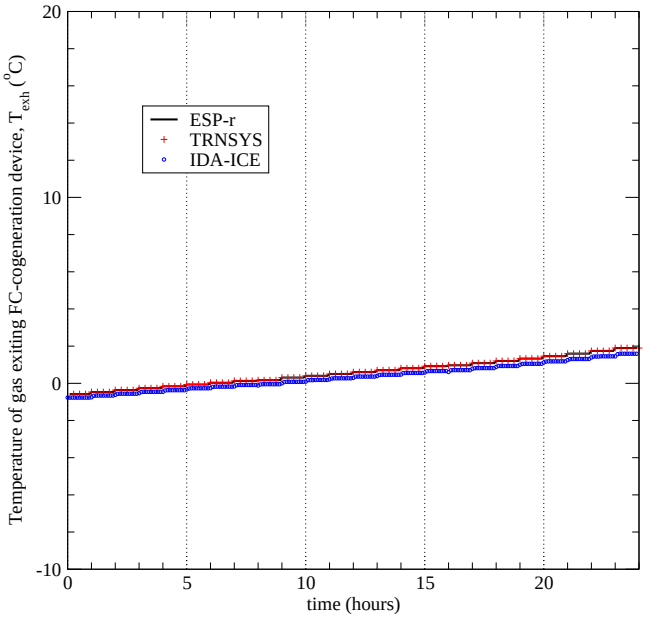

Figure II-94: Case 703 T_{exh} results

Case 703

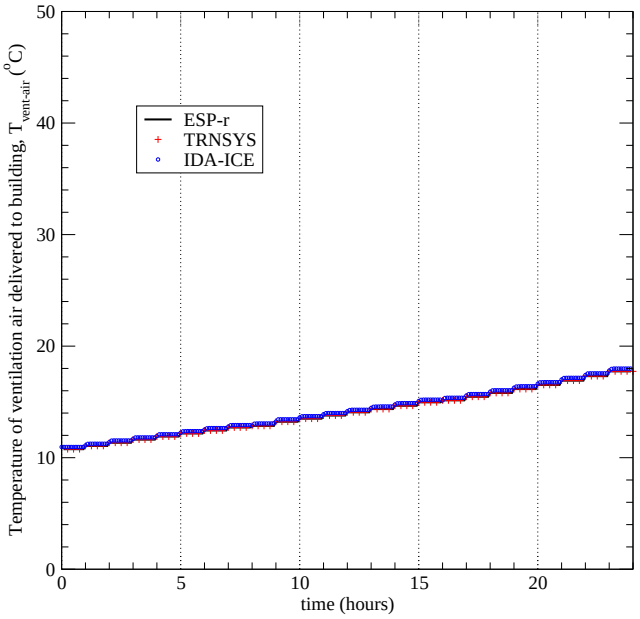

Figure II-95: Case 703 $T_{vent-air}$ results

Case 703

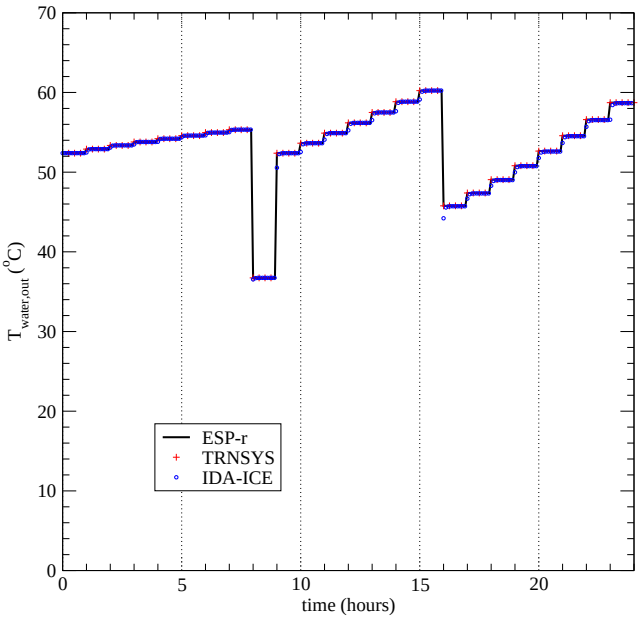

Figure II-96: Case 703 $T_{water,out}$ results

Case 704

Case 704 is identical to case 702 with the exception that fan drawing fresh air through the HRV draws AC power. The pertinent input data to the FC-cogeneration model are listed in Table II-36 with the changes noted in Table II-40.

HRV	$\dot{N}_{OA} = 2.7 \cdot 10^{-3}$ kmol/s
	$P_{el,\,fresh-air-fan} = 300$ W
	$\varepsilon_{HRV} = 0.75$

Table II-40: Input data for case 704 that override the data given in Table II-36

The following simulation predictions are examined with this case and should be plotted against time (in hours):

- The temperature of the warmed ventilation air that is delivered to the building, $T_{vent-air}$.
- The temperature of the heated water exiting the heat exchanger, $T_{water,out}$.

These results are given in Figures II-97 and II-98.

Case 704

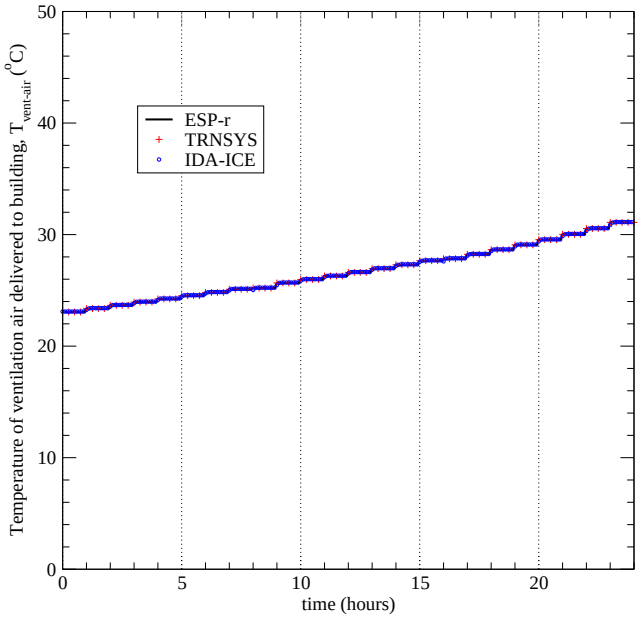

Figure II-97: Case 704 $T_{vent-air}$ results

Case 704

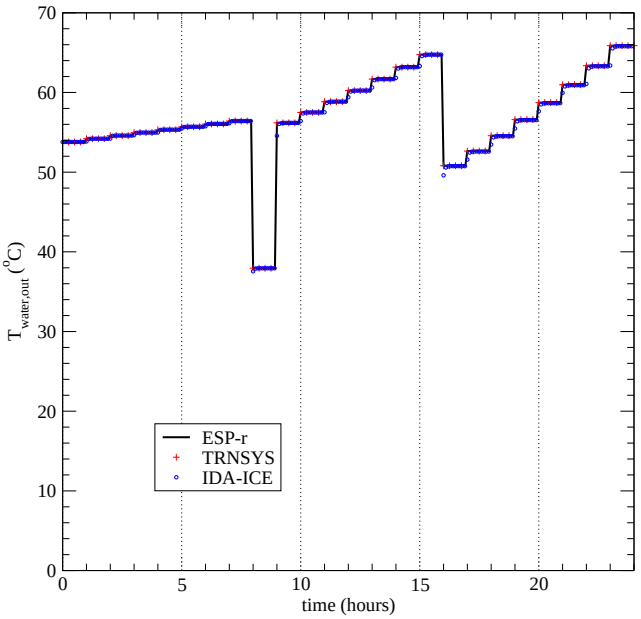

Figure II-98: Case 704 $T_{water,out}$ results

800 Series Tests

The *800 series* cases exercise the portions of the code that treat the FCPM's transient response characteristics, the electrical system control behaviour, as well as the models for electrical storage (battery) and DC-AC power conditioning (PCU).

Case 800

Case 800 is the base case for this series. As detailed in the model specifications, the heat loss from the battery and PCU can either be lost to the containing room or can be recovered to heat the FCPM's air intake. In this test case the heat is transferred to the containing room.

As before, the simulation is conducted for a single day (January 9) with whatever start-up or conditioning period is appropriate for the simulation program. The simulation should be performed with a time-step no greater than 15 minutes. The weather file is inconsequential.

In the previous series of test cases, the DC electrical output required by the FCPM was specified as a boundary condition. In this test case, the net AC power demanded from the FC-cogeneration device (P_{demand}) is specified as the boundary condition and the model must determine the DC electrical output required by the FCPM in order to supply this demand. P_{demand} varies from 1 000 W to 4 000 W over the day. It is 1 000 W from 0h00 to 6h00 and there is a 1 000 W step increment at 6h00. There are similar step increments at 12h00 and 18h00. This is illustrated in Figure II-105.

In this test case the transient response characteristics of the FCPM and its operating range are such that the battery will not be called upon to either help supply the load or to store excess power production. The air blower, fuel compressor, water pump, and FCPM ancillaries all draw AC power. There is no auxiliary burner, dilution air fan, or HRV fan.

The pertinent input data to the FC-cogeneration model are listed in Table II-41.

The followings imulation predictions are examined with this case and should be plotted against time (in hours):

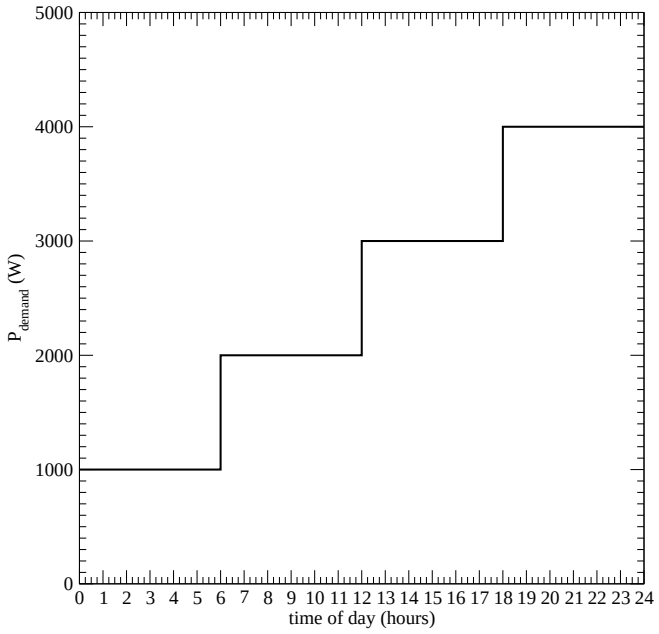

Figure II-105: Net AC electrical demand placed upon FC-cogeneration device for case 800

- The FC-cogeneration devices's net AC power production, P_{net-AC}.
- The PCU's gross AC power production, $P_{PCU-out}$.
- The FCPM's DC power production, P_{el}.
- The power conditioning losses, $P_{PCU-losses}$.
- The power flow from the battery: the power drawn from the battery ($P_{battery-discharge}$) is positive while the power added to the battery ($P_{battery-charge}$) is negative.
- The PCU's efficiency, η_{PCU}.

These results are given in Figures II-99 through II-104.

FCPM electrical efficiency	$\varepsilon_0 = 0.3;\ \varepsilon_1 = 1.1 \cdot 10^{-4};\ \varepsilon_2 = -2 \cdot 10^{-8}$
	$D = 0$
	$L = 0$
FCPM transient response	$(dP_{el}/dt)_{\max}$ = 10 (W/s) for both increasing and decreasing power
FCPM operating range	$P_{el-min} = 1\ 000$ W $P_{el-max} = 5\ 000$ W
fuel molar fractions	$\chi_{H_2} = 0.0;\quad \chi_{CH_4} = 0.949;\quad \chi_{C_2H_6} = 0.025;\quad \chi_{C_3H_8} = 0.002;$ $\chi_{C_4H_{10}} = 0.0006;\quad \chi_{C_5H_{12}} = 0.0001;\quad \chi_{C_6H_{14}} = 0.0001;$ $\chi_{CH_3OH} = 0.0;\quad \chi_{C_2H_5OH} = 0.0;\quad \chi_{CO_2} = 0.007;\quad \chi_{N_2} = 0.016;$ $\chi_{O_2} = 0.0002$
air molar fractions	$\chi_{N_2} = 0.7728;\quad \chi_{O_2} = 0.2073;\quad \chi_{H_2O} = 0.0104;\quad \chi_{Ar} = 0.0092;$ $\chi_{C_{O_2}} = 0.0003;$
air supply to FCPM	method 2 $a_0 = 5 \cdot 10^{-5};\ a_1 = 1.5 \cdot 10^{-7};\ a_2 = 1.1 \cdot 10^{-12};\ a_3 = 0.0$
air supply blower	$T_{blower-in} = 20^oC$ (air drawn at containing room's temperature)
	$b_0 = 50.0;\ b_1 = 4.0 \cdot 10^5;\ b_2 = 0.0;\ b_3 = 0.0;$
	$\alpha_{blower-heat-loss} = 0.5$
fuel compressor	$T_{comp-in} = 20^oC$ (fuel drawn at containing room's temperature)
	$c_0 = 20.0;\ c_1 = 0.0;\ c_2 = 0.0;\ c_3 = 0.0;$
	$\alpha_{comp-heat-loss} = 0.5$
water supply to FCPM	$w_0 = 1.0 \cdot 10^{-7};\ w_1 = 2.0;\ w_2 = 5.0 \cdot 10^4$
water pump	$T_{pump-in} = 20^oC$ (water drawn at containing room's temperature)
	$p_0 = 10.0;\ p_1 = 0.0;\ p_2 = 0.0;\ p_3 = 0.0;$
	$\alpha_{pump-heat-loss} = 0.05$
FCPM AC ancillaries	$anc_0 = 50.;\ anc_1 = 1.5 \cdot 10^7$
FCPM skin losses	method 1 $q_{skin-loss} = 0.0$
dilution air	$\dot{N}_{dilution-air} = 0.0$
battery	$Q_{battery-max} = 3.6 \cdot 10^7;\quad Q_{battery-initial} = 1.8 \cdot 10^7;$ $P_{battery-charge-max} = 10\ 000W;\quad \varepsilon_{charge} = 1.0;$ $P_{battery-discharge-max} = 10\ 000W;\ \varepsilon_{discharge} = 1.0$
PCU	$u_0 = 0.9;\ u_1 = 5.0 \cdot 10^{-6};\ u_2 = 1.25 \cdot 10^{-9}$

Table II-41: Input data for case 800

Case 800

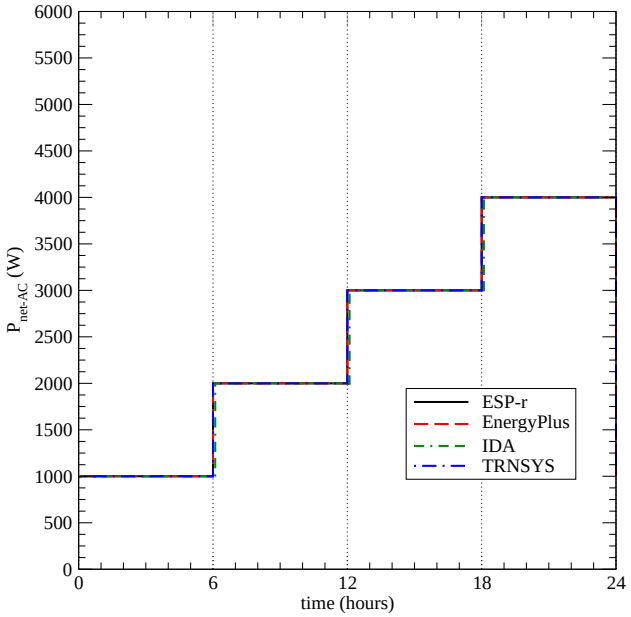

Figure II-99: Case 800 P_{net-AC} results

Case 800

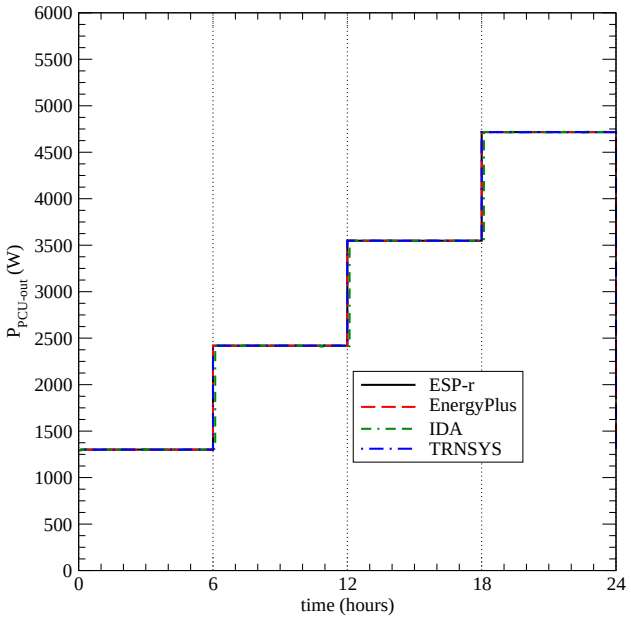

Figure II-100: Case 800 $P_{PCU-out}$ results

Case 800

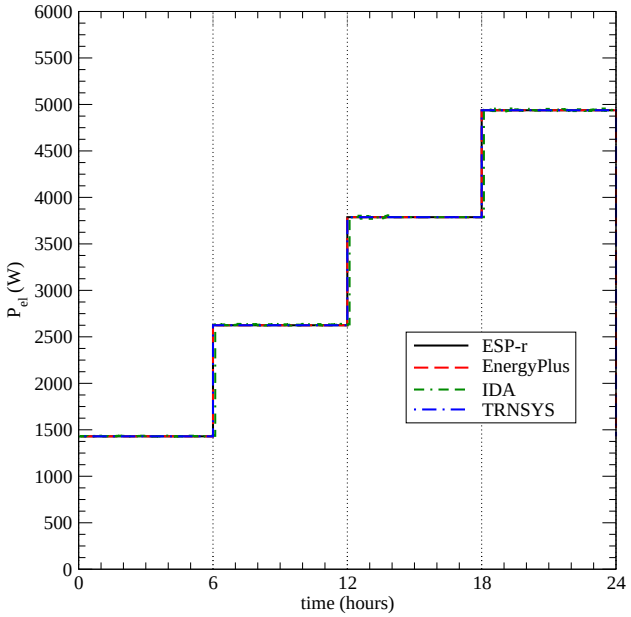

Figure II-101: Case 800 P_{el} results

Case 800

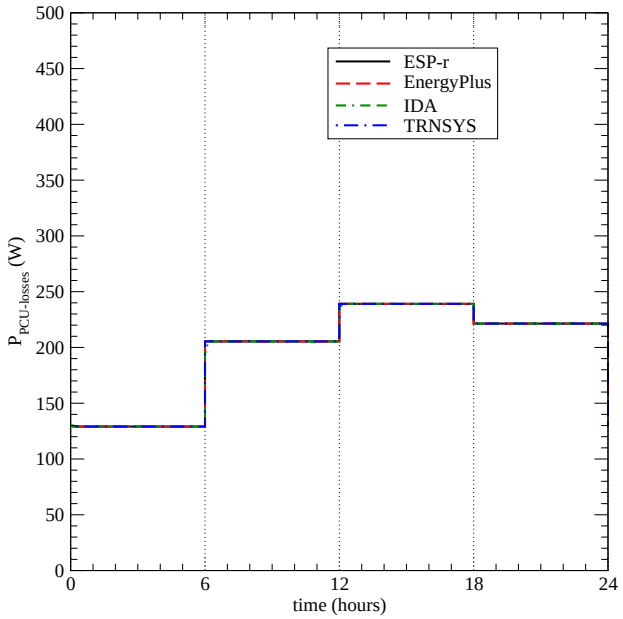

Figure II-102: Case 800 $P_{PCU-losses}$ results

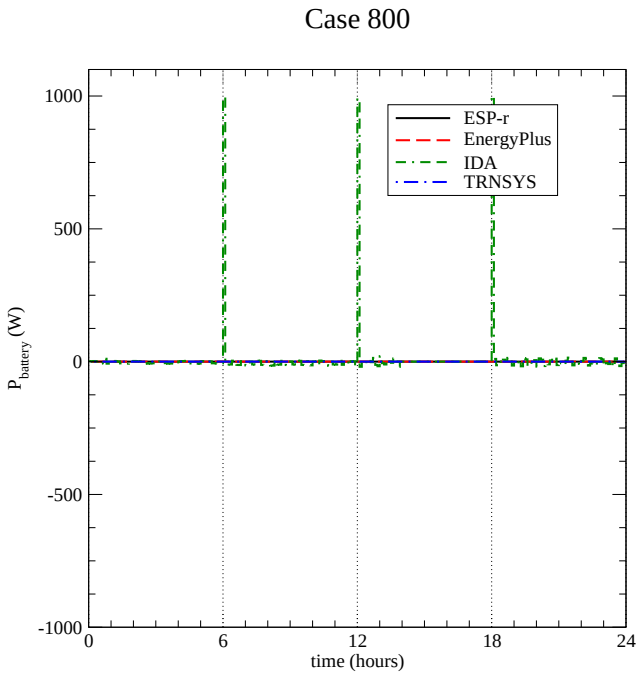

Figure II-103: Case 800 $P_{battery-discharge}$ and $P_{battery-charge}$ results

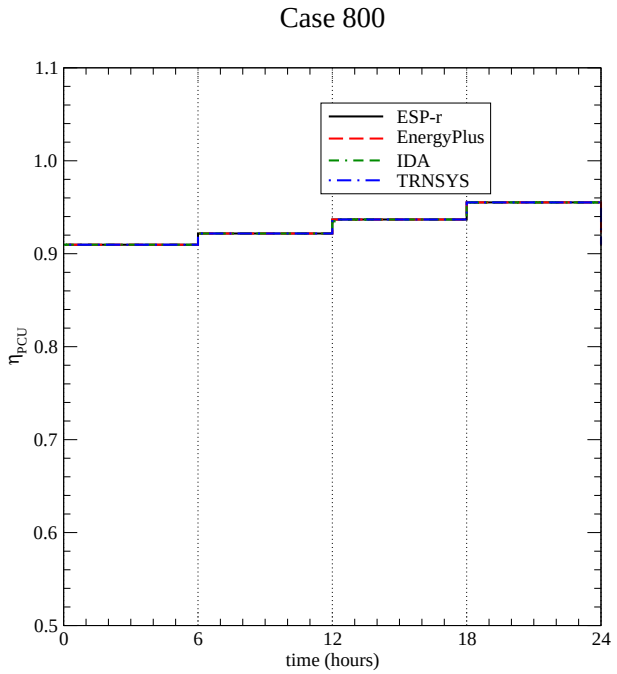

Figure II-104: Case 800 η_{PCU} results

Case 801

Case 801 is identical to case 800 with three exceptions:

- The FCPM has slower transient response characteristics.
- The step changes in the net AC power demanded from the FC-cogeneration device are greater.
- As before, the simulation is conducted for a single day (January 9). However, in this case the conditioning period is one day.

As a result these conditions battery will be used to help meet the demand at certain points in time and will be used to store excess power production at other points in time. The duration of the conditioning period and the duration of the simulation period are critical (as is the initial SOC of the battery) as the battery's SOC will not have achieved steady-state.

The net AC power demanded from the FC-cogeneration device varies from 500 W to 5 000 W over the day. It is 500 W from 0h00 to 6h00. There are step increases to 3 000 W at 6h00 and to 5 000 W at 12h00, and then a step decrease to 500 W at 18h00. This is illustrated in Figure II-106.

The battery's capacity is sufficiently high, as are its maximum permissible charging and discharging rates, such that the FC-cogeneration device can respond to the demand profile without necessitating grid interaction. There are no energetic losses associated with charging or discharging the battery.

The pertinent input data to the FC-cogeneration model are listed in Table II-41 with the changes noted in Table II-42.

FCPM transient response	$(dP_{el}/dt)_{\max}$ = 0.5 (W/s) for increasing power $(dP_{el}/dt)_{\max}$ = 0.3 (W/s) for decreasing power

Table II-42: Input data for case 801 that override the data given in Table II-41

The following simulation predictions are examined with this case and should be plotted against time (in hours):

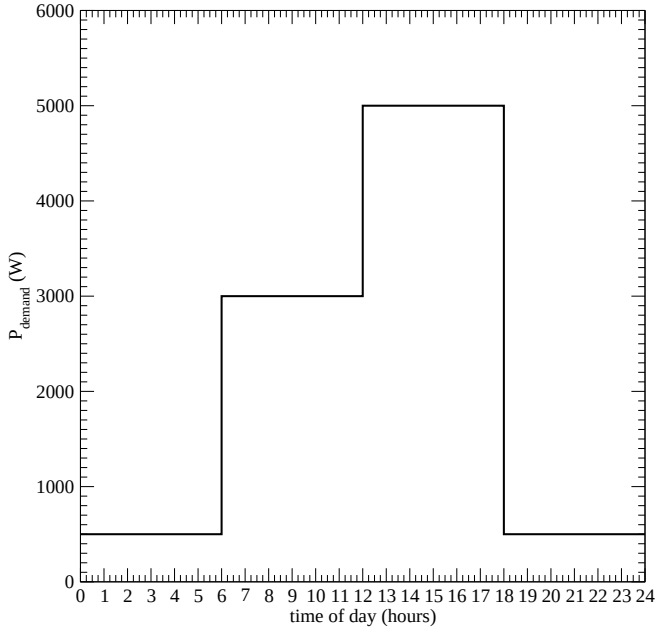

Figure II-106: Net AC electrical demand placed upon FC-cogeneration device for case 801

- The FC-cogeneration devices's net AC power production, P_{net-AC}.
- The FCPM's DC power production, P_{el}.
- The power flow from the battery: the power drawn from the battery ($P_{battery-discharge}$) is positive while the power added to the battery ($P_{battery-charge}$) is negative.
- The ratio of the battery's SOC to its maxiumum SOC, $Q_{battery}^{t+\Delta t}/Q_{battery-max}$.

These results are given in Figures II-107 through II-110.

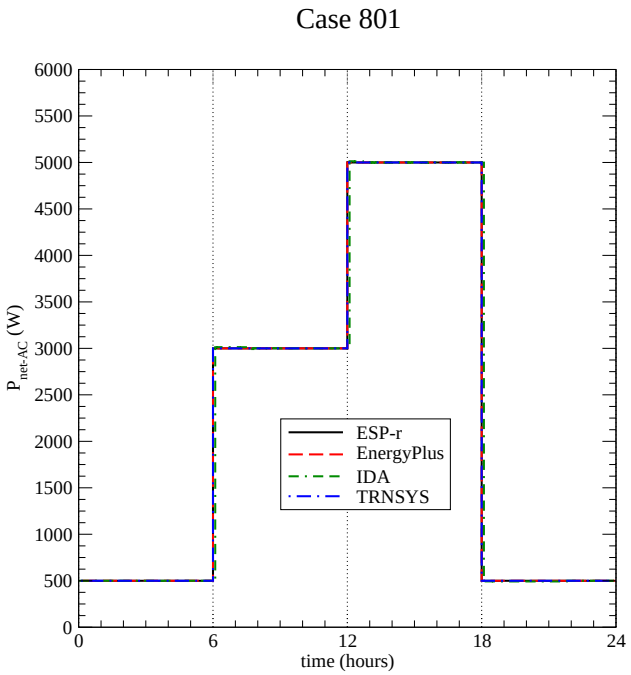

Figure II-107: Case 801 P_{net-AC} results

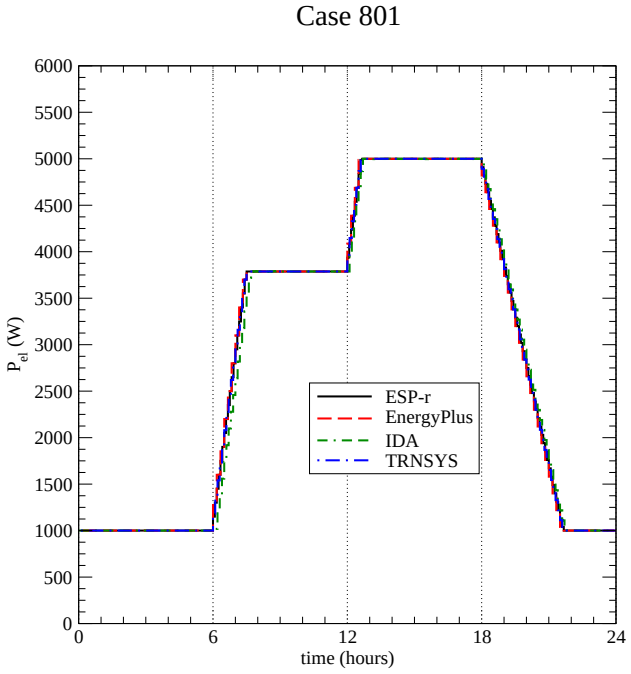

Figure II-108: Case 801 P_{el} results

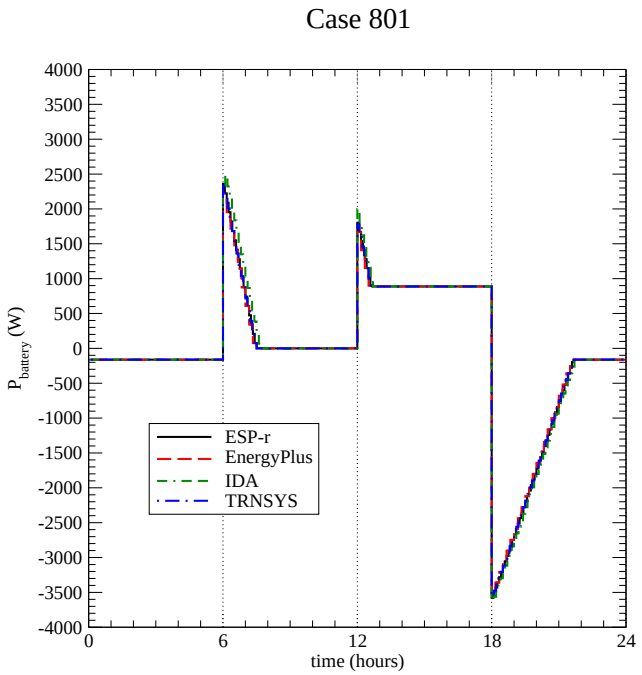

Figure II-109: Case 801 $P_{battery-discharge}$ and $P_{battery-charge}$ results

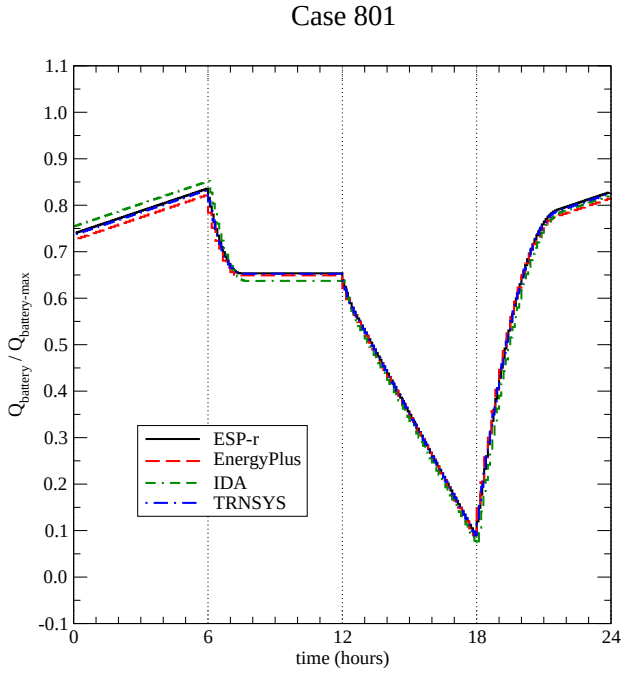

Figure II-110: Case 801 $Q^{t+\Delta t}_{battery}/Q_{battery-max}$ results

Case 802

Case 802 is identical to case 801 except that there are energetic losses associated with the charging and discharging of the battery.

The pertinent input data to the FC-cogeneration model are listed in Table II-41 with the changes noted in Table II-43.

battery	$Q_{battery-max} = 3.6 \cdot 10^7$; $Q_{battery-initial} = 1.8 \cdot 10^7$; $P_{battery-charge-max} = 10\ 000W$; $\varepsilon_{charge} = 0.97$; $P_{battery-discharge-max} = 10\ 000W$; $\varepsilon_{discharge} = 0.95$

Table II-43: Input data for case 802 that override the data given in Table II-41

The following simulation predictions are examined with this case and should be plotted against time (in hours):

- The difference in the ratio of the battery's SOC to its maxiumum SOC ($Q_{battery}^{t+\Delta t}/Q_{battery-max}$) between case 802 and case 801 (case 802 result minus case 801 result).

These results are given in Figure II-111.

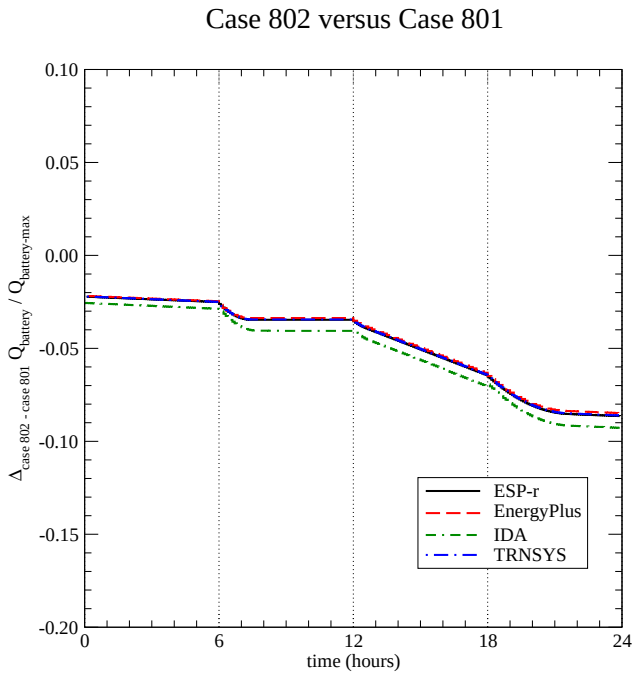

Figure II-111: $\Delta_{case\ 802\ -\ case\ 801}\ Q^{t+\Delta t}_{battery}/Q_{battery-max}$ **results**

Case 803

Case 803 is identical to case 801 except that the battery has a lower storage capacity and lower maximum charge and discharge rates. As a consequence, the FCPM and battery are unable to follow the demand pattern and importation from the grid is used to meet deficits and exportation to the gid is used to absorb surpluses.

The pertinent input data to the FC-cogeneration model are listed in Table II-41 with the changes noted in Table II-44.

battery	$Q_{battery-max} = 1.0 \cdot 10^7$; $Q_{battery-initial} = 2.5 \cdot 10^6$; $P_{battery-charge-max} = 2\ 000W$; $\varepsilon_{charge} = 1.0$; $P_{battery-discharge-max} = 1\ 000W$; $\varepsilon_{discharge} = 1.0$

Table II-44: Input data for case 803 that override the data given in Table II-41

The following simulation predictions are examined with this case and should be plotted against time (in hours):

- The power flow from the battery: the power drawn from the battery ($P_{battery-discharge}$) is positive while the power added to the battery ($P_{battery-charge}$) is negative.
- The ratio of the battery's SOC to its maxiumum SOC, $Q_{battery}^{t+\Delta t}/Q_{battery-max}$.
- The grid interaction required to meet the net AC electrical demand placed upon the FC-cogeneration device: power exported to the grid is positive while power imported from the grid is negative.

These results are given in Figures II-112 through II-114.

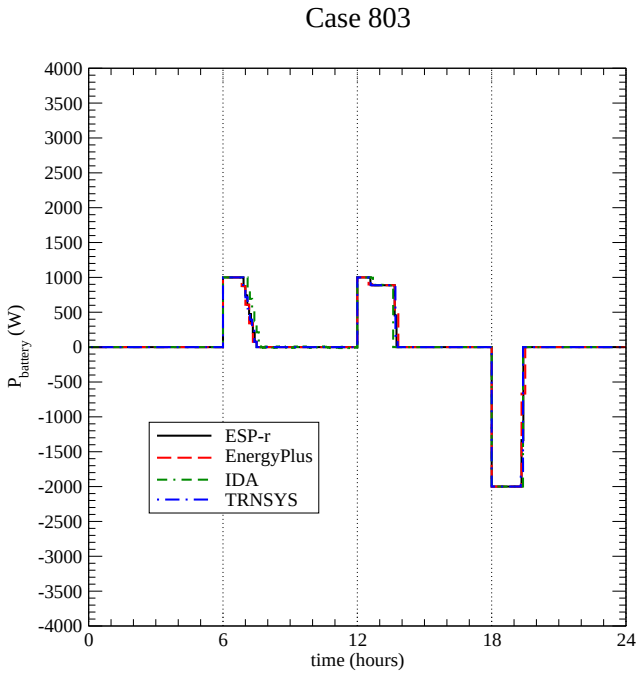

Figure II-112: Case 803 $P_{battery-discharge}$ and $P_{battery-charge}$ results

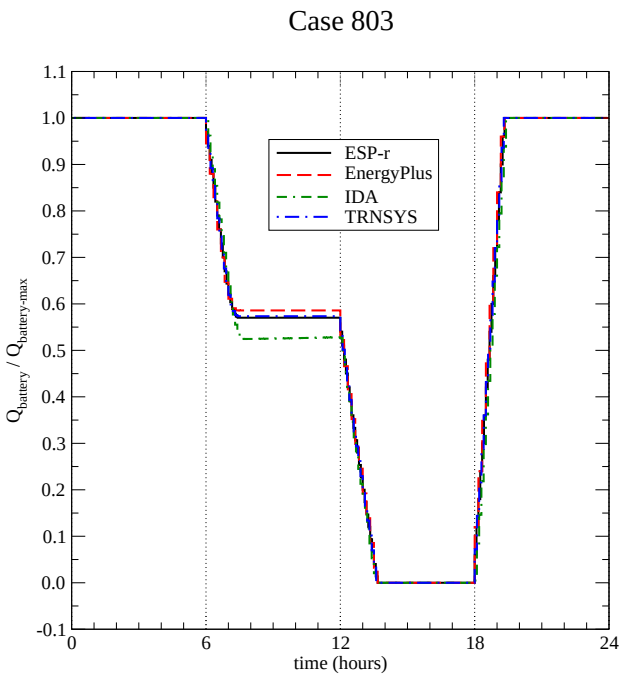

Figure II-113: Case 803 $Q^{t+\Delta t}_{battery}/Q_{battery-max}$ results

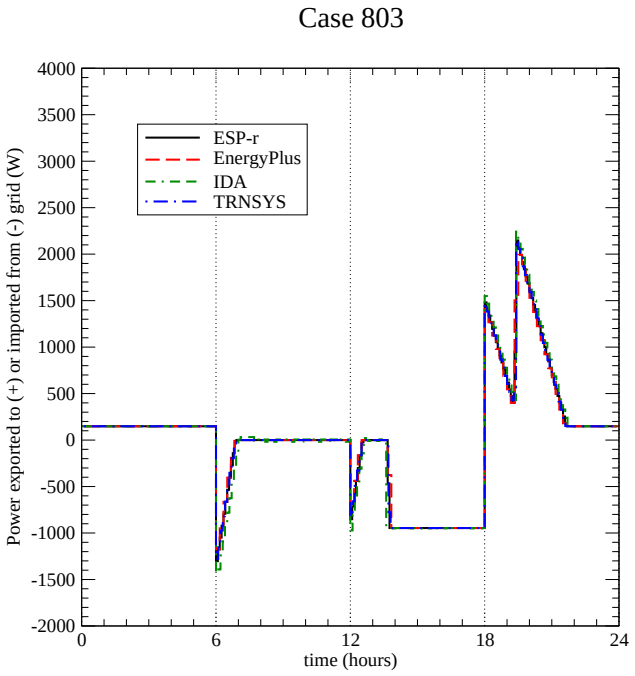

Figure II-114: Case 803 grid interaction results

Case 804

Case 804 is identical to case 802 except that the heat losses from the battery and PCU are recovered to heat the the FCPM's air intake.

The following simulation predictions are examined with this case and should be plotted against time (in hours):

- The difference in $T_{FCPM-cg}$ between case 804 and case 802 (case 804 result minus case 802 result).

These results are given in Figure II-115.

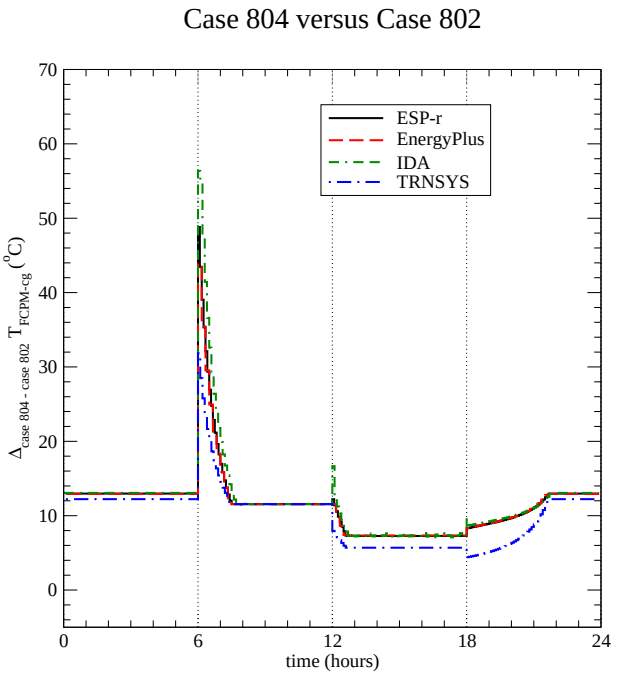

Figure II-115: $\Delta_{case\ 804\ -\ case\ 802}\ T_{FCPM-cg}$ **results**

900 Series Tests

The *900 series* cases exercise the portions of the code that treat the PEM stack cooling system.

Case 900

Case 900 is the base case for this series and is based upon case 601.

The net AC power demanded from the FC-cogeneration device (P_{demand}) is specified as the boundary condition as illustrated in Figure II-1.

The water on the heat recovery loop side of the external heat exchanger enters the heat exchanger at a constant temperature of 30 °C ($T_{s-cogen-in}$) and a constant flow of 0.1 kg/s ($\dot{m}_{s-cogen}$).

As before, the simulation is conducted for a single day (January 9) with whatever start-up or conditioning period is appropriate for the simulation program. The simulation should be performed with a time-step no greater than 15 minutes. The weather file is inconsequential.

The pertinent input data to the FC-cogeneration model are listed in Table II-31 with the changes and additions given in Table II-45.

The following simulation predictions are examined with this case and should be plotted against time (in hours):

- The temperature of the product gas stream exiting the FCPM, $T_{FCPM-cg}$.
- The temperature of the water flowing into ($T_{s-cool,in}$) and out of ($T_{s-cool,out}$) the stack's internal heat exchanger.
- The temperature rise through the external heat exchanger of the water on the heat recovery loop side, $T_{s-cogen,out} - T_{s-cogen,in}$.
- The electric power consumption of the air-cooler's fan, $P_{s-air-el}$.

These results are given in Figures II-116 through II-119.

heat exchanger	method 2 $hx_{s,0} = 0.5;\quad hx_{s,1} = 500.;\quad hx_{s,2} = 5000.;\quad hx_{s,3} = 5000.;$ $hx_{s,4} = 10^6$
PEM stack temperature	$T_{stack} = 80^o C$
	$T^0_{stack} = 78^o C$
PEM stack cooling	$r_0 = 0.2;\ r_1 = 0.035;\ r_2 = 1 \cdot 10^{-4};\ r_3 = 4 \cdot 10^{-8}$
PEM internal heat exchanger	$(UA)_{s-cool} = 50 W/K$
PEM stack cooling loop water flow rate	$\dot{N}_{s-cool} = 7.214 \cdot 10^{-3} kmol/s$
PEM external heat exchanger	$h^0_{s-cogen} = 100 W/m^2 K;\qquad A_{s-cogen} = 1 m^2;$ $N^0_{s-cogen} = 5.549 \cdot 10^{-3} kmol/s;\ n_s = 0.6;\ F_{s-cogen} = 0 K/W$
PEM air cooler	$f_0 = 0;\ f_1 = 0.1;\ f_2 = 2 \cdot 10^{-5}$
PEM pump	$P_{stack-pump-el} = 0 W$
	$\alpha_{stack-pump-heat-loss} = 0$

Table II-45: Input data for case 900 that override the data given in Table II-31

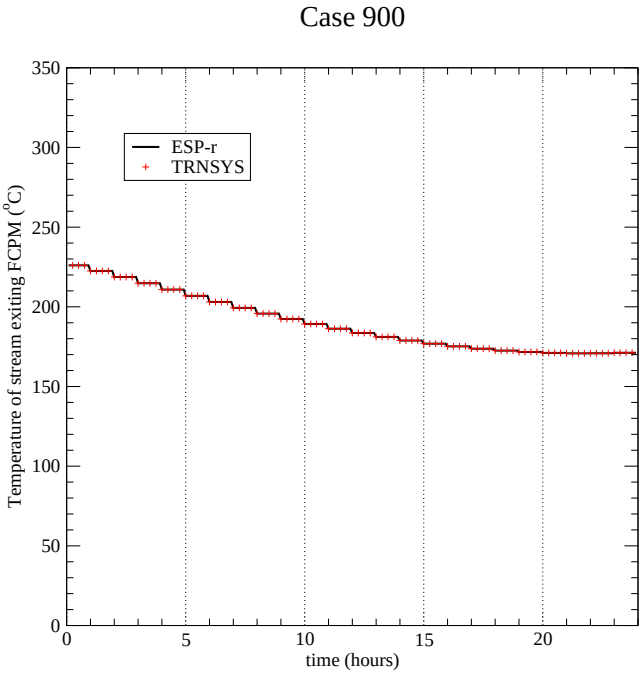

Figure II-116: Case 900 $T_{FCPM-cg}$ results

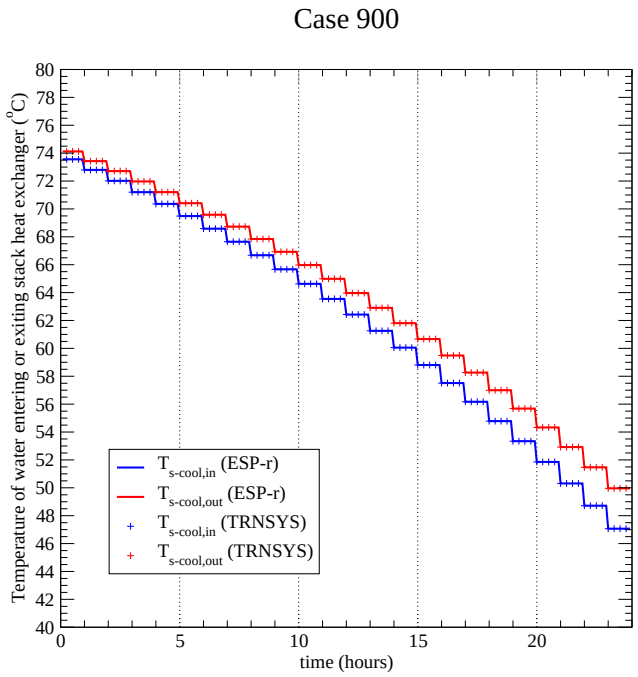

Figure II-117: Case 900 $T_{s-cool,in}$ and $T_{s-cool,out}$ results

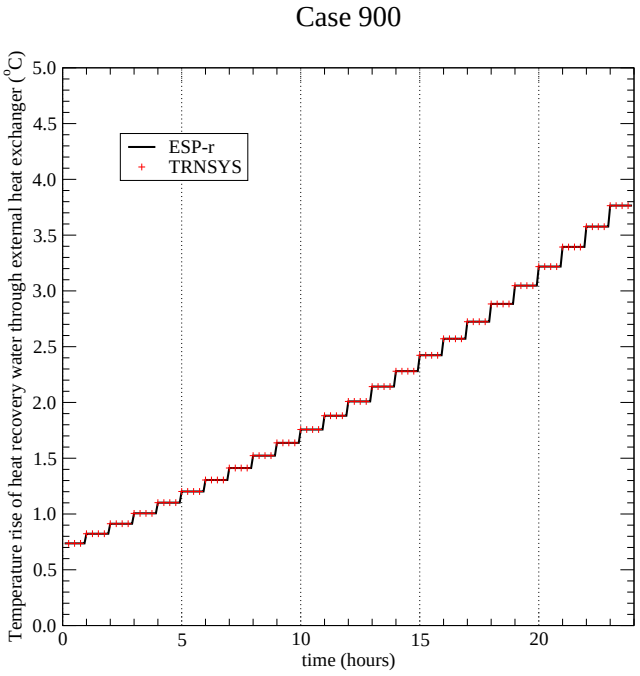

Figure II-118: Case 900 $T_{s-cogen,out} - T_{s-cogen,in}$ results

Case 900

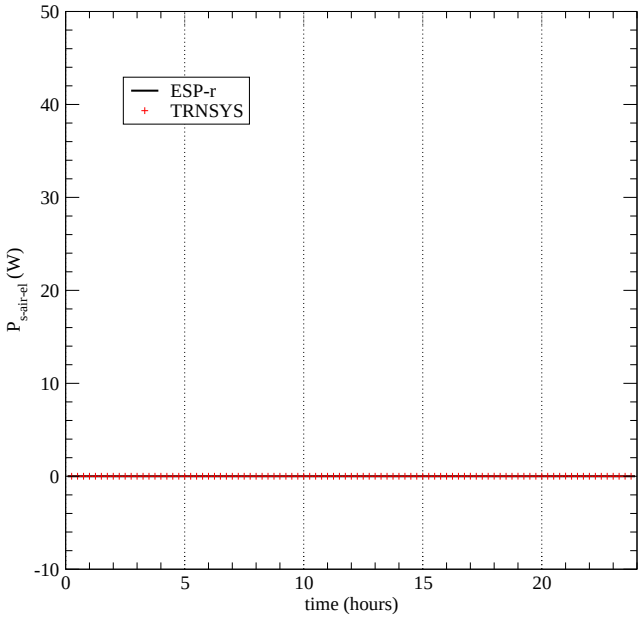

Figure II-119: Case 900 $P_{s-air-el}$ results

Case 901

Case 901 is identical to case 900 with the exception that the water flow rate on the heat recovery loop side of the external heat exchanger varies in time. This flow rate is equal to 0.01 kg/s from 0h00 to just before 9h00. At 9h00 this flow rate increases to 0.1 kg/s and then increases to 0.2 at 16h00. This is illustrated in Figure II-120.

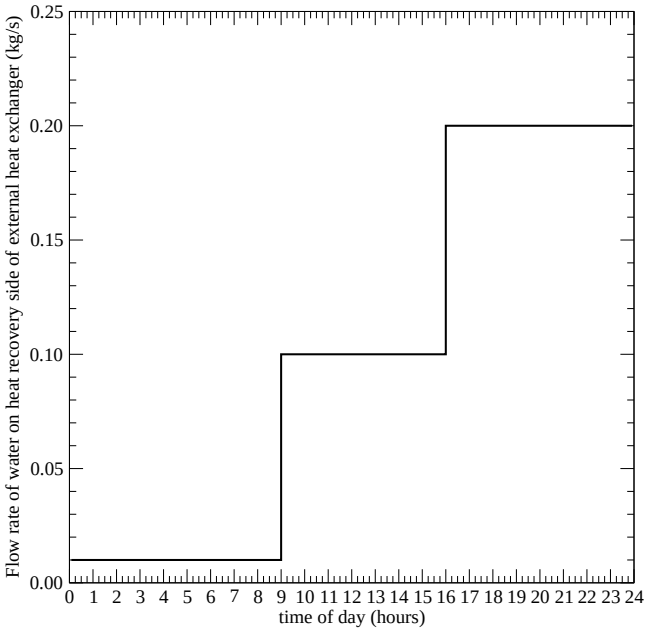

Figure II-120: Flow rate of water on heat recovery side of external heat exchanger for case 901

There are no changes to the inputs of the FC-cogeneration model. Consequently, the pertinent input data to the FC-cogeneration model are listed in Table II-31 with the changes and additions given in Table II-45.

The following simulation predictions are examined with this case and should be plotted against time (in hours):

- The temperature rise through the external heat exchanger of the water on the heat recovery loop side, $T_{s-cogen,out} - T_{s-cogen,in}$.

These results are given in Figure II-121.

Case 901

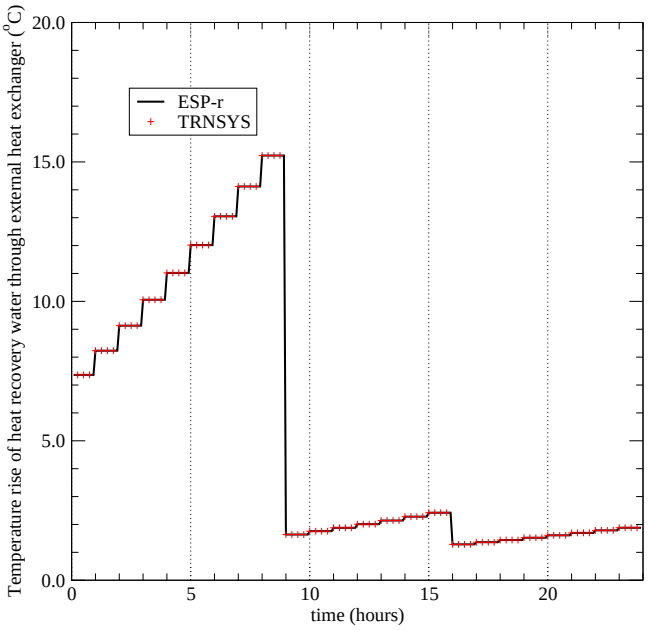

Figure II-121: Case 901 $T_{s-cogen,out} - T_{s-cogen,in}$ results

Case 902

Case 902 is identical to case 900 with the excection that the pump that circulates water in the stack cooling loop draws power. The pertinent input data to the FC-cogeneration model are listed in Table II-31 with the changes and additions given in Table II-45 and the changes given in Table II-46.

PEM pump	$P_{stack-pump-el} = 500W$
	$\alpha_{stack-pump-heat-loss} = 0.05$

Table II-46: Input data for case 902 that override the data given in Table II-45

The following simulation predictions are examined with this case and should be plotted against time (in hours):

- The temperature of the water flowing into ($T_{s-cool,in}$) the stack's internal heat exchanger.

- The temperature rise through the external heat exchanger of the water on the heat recovery loop side, $T_{s-cogen,out} - T_{s-cogen,in}$.

These results are given in Figures II-122 and II-123.

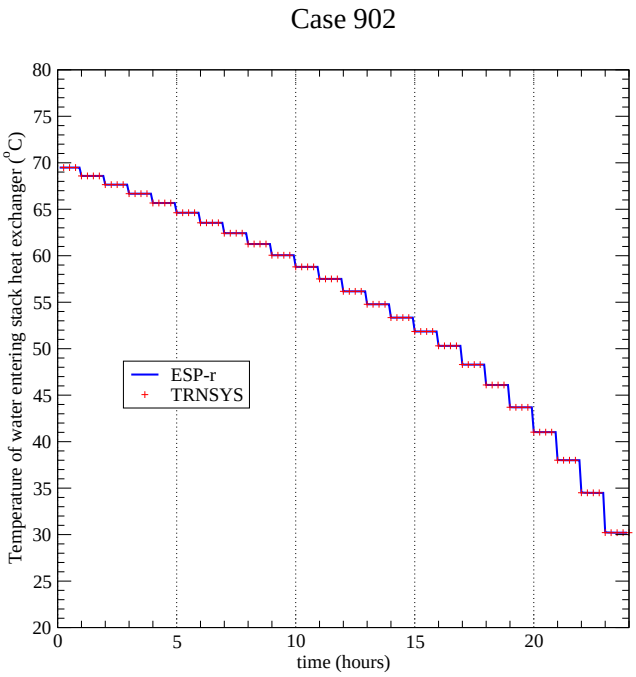

Figure II-122: Case 902 $T_{s-cool,in}$ results

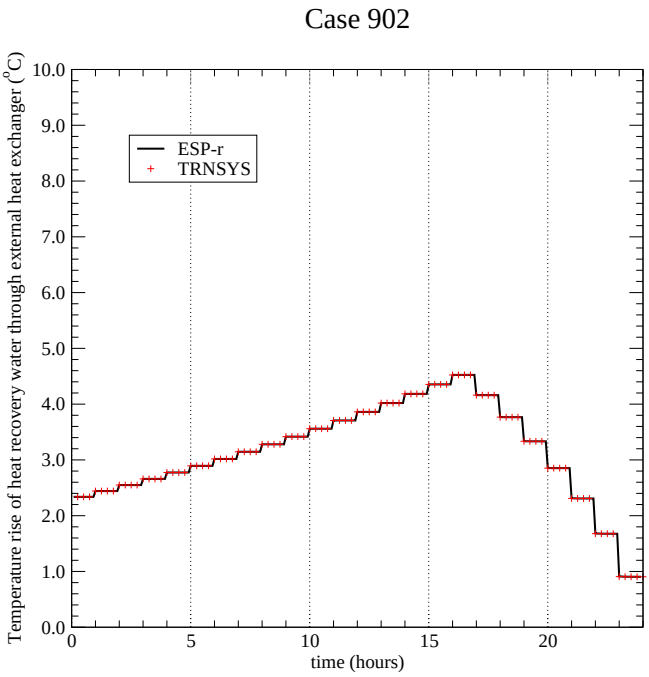

Figure II-123: Case 902 $T_{s-cogen,out} - T_{s-cogen,in}$ results

Case 903

Case 903 is identical to case 900 with the excection that the water on the heat recovery loop side of the external heat exchanger enters the heat exchanger at a constant temperature of 70 °C ($T_{s-cogen-in}$). In the previous test cases in this series the external heat exchanger was able to extract all of the heat that was rejected from the stack. In this case, however, the air cooler is required to reject some of the heat.

There are no changes to the inputs of the FC-cogeneration model. Consequently, the pertinent input data to the FC-cogeneration model are listed in Table II-31 with the changes and additions given in Table II-45.

The following simulation predictions are examined with this case and should be plotted against time (in hours):

- The heat released by the air cooler to the ambient, $q_{air-cooler}$.
- The AC power consumption of the air cooler's fan, $P_{s-air-el}$.

- The temperature rise through the external heat exchanger of the water on the heat recovery loop side, $T_{s-cogen,out} - T_{s-cogen,in}$.

These results are given in Figures II-124 through II-126.

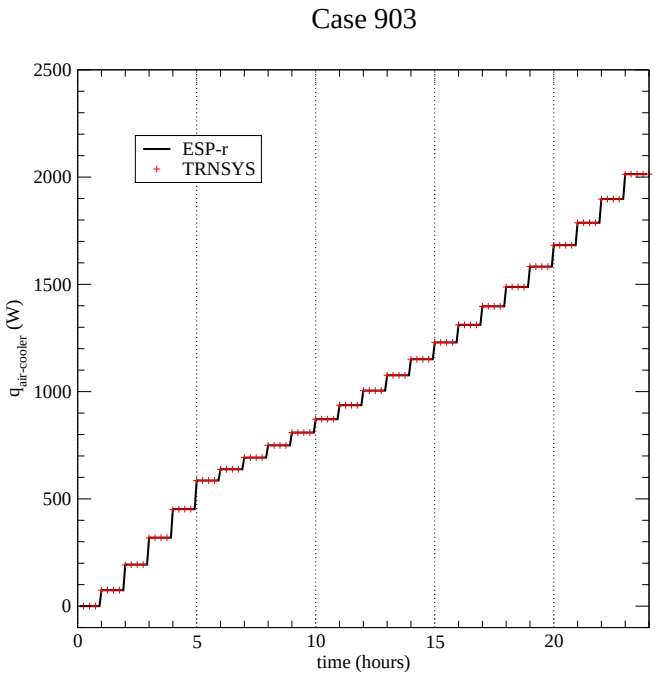

Figure II-124: Case 903 $q_{air-cooler}$ results

Case 903

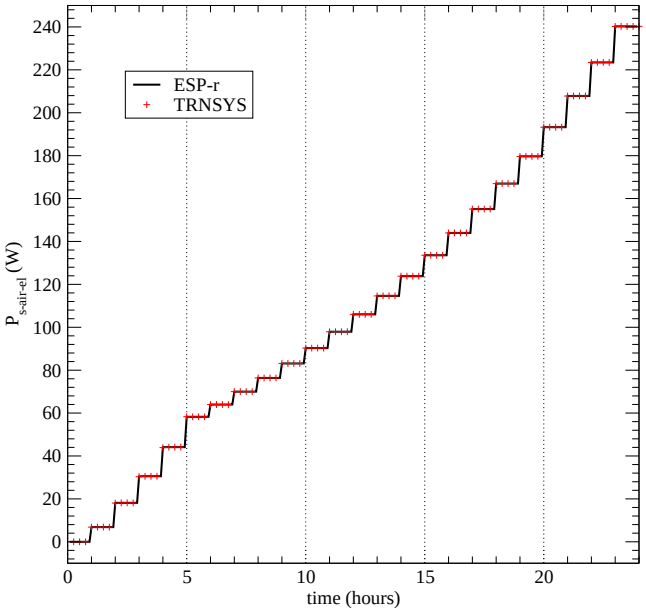

Figure II-125: Case 903 $P_{s-air-el}$ results

Case 903

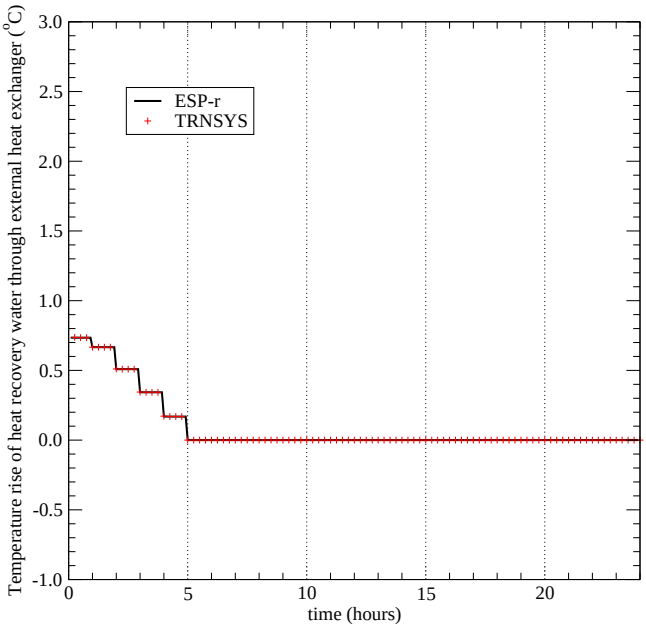

Figure II-126: Case 903 $T_{s-cogen,out} - T_{s-cogen,in}$ results

References

Beausoleil-Morrison, I., Griffith, B., Vesanen, T., Lerson, S., and Weber, A., "A Case Study Demonstrating the Utility of Inter-Program Comparative Testing for Diagnosing Errors in Building Simulation Programs," *Proc. eSim 2006,* pp. 181-188, Toronto Canada (2006).

Crawley, D.B., Lawrie, L.K., Winkelmann, F.C., Buhl, W.F., Huang, Y.J., Pedersen, C.O., Strand, R.K., Liesen, R.J., Fisher, D.E., Witte, M.J., and Glazer, J., "EnergyPlus: Creating a New-Generation Building Energy Simulation Program," *Energy and Buildings,* 33, pp. 319-331 (2001).

ESRU, "The ESP-r System for Building Energy Simulations: User Guide Version 10 Series," ESRU Manual U05/1, University of Strathclyde, Glasgow UK (2005).

Kelly, N. and Beausoleil-Morrison, I. (eds), "Specifications for Modelling Fuel Cell and Combustion-Based Residential Cogeneration Device within Whole-Building Simulation Programs," *IEA/ECBCS Annex 42 Report, ISBN No. 978-0-662-47116-5* (2007).

Klein, S.A., *TRNSYS 16, A Transient System Simulation Program,* Solar Energy Laboratory, University of Wisconsin, Madison USA (2004).

Klein, S.A., *Engineering Equation Solver Manual,* F-Chart Software, Madison USA (2005).

Sahlin, P. and Sowell, E.F., "A Neutral Model Format for Building Simulation Models," *Proc. Building Simulation 1989,* pp. 147-154, Vancouver Canada (1989).

Section III

Inter-program Comparative tests for the Annex 42 Combustion Cogeneration model

AUTHORS:

Alex Ferguson (Natural Resources Canada)

Brent Griffith (National Renewable Energy Laboratory, USA)

Andreas Weber (Swiss Federal Laboratories for Materials Testing and Research)

WITH INPUT FROM:

Ian Beausoleil-Morrison (Natural Resources Canada)

Section III

Section III Table of Contents

Introduction to this section

This section presents a suite of inter-program comparative tests to validate the implementation of the Annex 42 Combustion cogeneration model in building simulation programs. The test suite is loosely based on the suite developed for the Annex 42 fuel cell model (refer to Section II of this report), and aims to be syntactically similar to the fuel cell comparative testing specification.

This section frequently references the Annex 42 combustion-based cogeneration model specification described in Kelly and Beausoleil-Morrison (2007, Section III), and hereafter referred to as the *model specification*. Equation numbers and symbols correspond to those in that document.

Test series

The test suite comprises 44 separate cases aggregated into nine groups, each of which exercises distinct aspects of the model:

The 100 series tests exercise the evaluation of fuel compositions, and fuel heating value. To pass the 100 series tests, models must successfully compute the fuel heating value and molar mass for a variety of different fuel compositions.

The 200 series tests exercise the steady-state performance correlations. To pass the 200 series tests, the models must successfully calculate the steady-state electrical and thermal efficients, and fuel, air and cooling water flow rates. The models will be exercised over a range of boundary conditions and input configurations.

The 300 series tests exercise the dynamic thermal mass model. To pass these tests, the thermal mass model must correctly predict the engine control volume temperature, the cooling water control volume temperature, and the heat transfer between these

control volumes in response to varying cooling water temperatures, flow rates and operating points.

The 400 series tests exercise the model's treatment of standby, warm-up and cool-down operation. To pass these tests, the model must correctly predict the unit's progression through the four operating modes, as well as the fuel and energy flows in each mode.

The 500 series tests exercise the model's treatment of the warm-up period fuel flow and power generation correlations, which are specific to the Stirling engine configuration. To pass these tests, the model must correctly predict the Stirling engine's fuel flow, power and heat generation in response to the temperature of the engine control volume.

The 600 series tests exercise the model's facility for limiting the rate of change in the system fuel flow and electric output. To pass these tests, the model must correctly predict the rate-limited fuel flow and electrical output in response to varying electrical demand.

The 700 series tests exercise the model's low-level controls that protect the unit from overheating when the cooling water temperature is to high, or the flow of the cooling water is interrupted. To pass these tests, the model must correctly predict the unit's response when these conditions are encountered.

The 800 series tests exercise the model's dimensionless control signal interface. To pass these tests, the model must correctly determine the unit's operating point when regulated by a dimensionless control signal varying between zero and one.

The 900 series tests exercise the model's emissions calculations. To pass these tests, the model must correctly predict the carbon dioxide emissions produced by the unit in various states of operation.

Implementations

Within Annex 42, implementations of the combustion cogeneration model were undertaken in three programs listed in Table III-1. While the EnergyPlus model is a completely independent implementation, both the ESP-r and TRNSYS implementations share common source code. The TRNSYS implementation incorporates the original ESP-r implementation and adds a TRNSYS specific interface that:

- collects the data required by the combustion cogeneration model from the TRNSYS environment,
- invokes the ESP-r source code,
- solves the state equations produced by the ESP-r source code to determine the state variables required by TRNSYS

The common source code shared between ESP-r and TRNSYS has important implications for the comparative testing project. Logical errors in the common source code will manifest in both the ESP-r and TRNSYS implementations, and therefore may go undetected when results from the two implementations are compared. Nevertheless, comparisons between these implementations are useful for diagnosing errors in the TRNSYS-to-ESP-r interface, as well as the interactions between the ESP-r model and the ESP-r's plant domain solver.

Comparisons between the EnergyPlus and ESP-r/TRNSYS implementations provide more rigorous test of the combustion cogeneration source code.

Table III-1: Annex 42 Combustion cogeneration model implementations

Program	Author	Organization
EnergyPlus	Brent Griffith	NREL (USA)
ESP-r	Alex Ferguson	NRCan (Canada)
TRNSYS	Andreas Weber	EMPA (Switzerland)

Status

Presently, the ESP-r and TRNSYS implementations have been exercised over the 100–900 series tests, and EnergyPlus has been exercised over the 100-600 series tests. The EnergyPlus implementation does not completely implement the facilities exercised in the 700–900 series tests, which precludes exercising it over these test cases as well.

This comparative testing study identified and corrected numerous errors in all three implementations. It also identified aspects of the model that are sensitive to different implementing approaches. The 300 series tests showed that solution of the dynamic thermal model is very sensitive to the simulation time resolution, and the maximum appropriate time step duration may vary from one implementation to another.

In all but one of the test cases, the EnergyPlus, ESP-r and TRNSYS implementations have either achieved exact agreement, or satisfactory explanations for the observed differences between the models have been proposed. The exception is test case 305.

Results from test case 305 show that varying a particular model input yields an order-of-magnitude larger response in ESP-r and TRNSYS than in EnergyPlus. While the cause of this discrepancy remains undiagnosed, work to identify and remedy it continues.

Base case configuration

All test cases defined in this specification draw upon one of two basic configurations. In the *external pump configuration*, depicted in Figure III-1, an external pump draws cooling water from an upstream temperature source and circulates it through the combustion cogeneration model's cooling water control volume. In the *internal pump configuration*, depicted in Figure III-2, the cogeneration model imposes the flow rate on the cooling water loop.

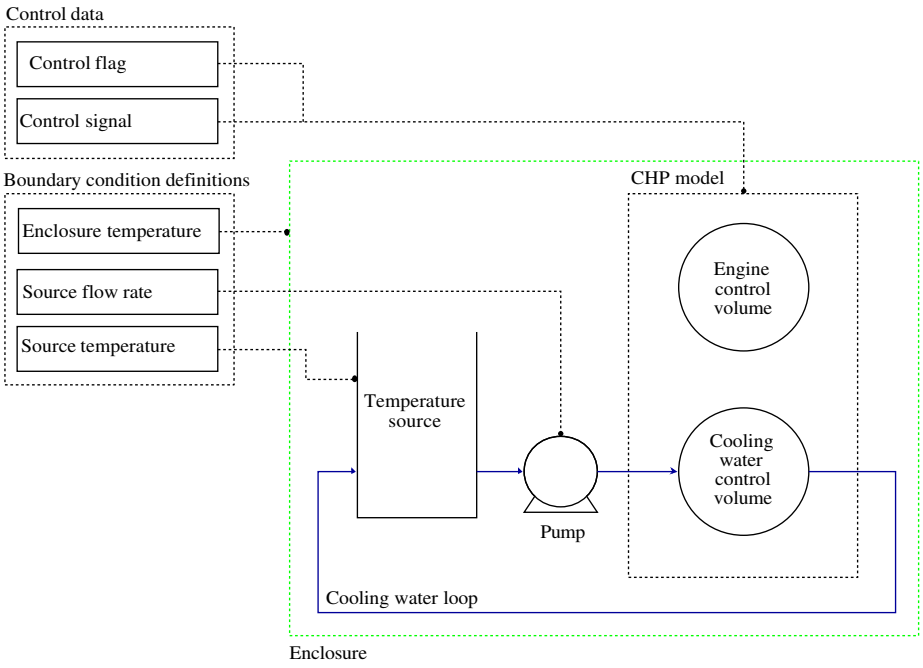

Figure III-1: Connections to cogeneration model in external pump configuration

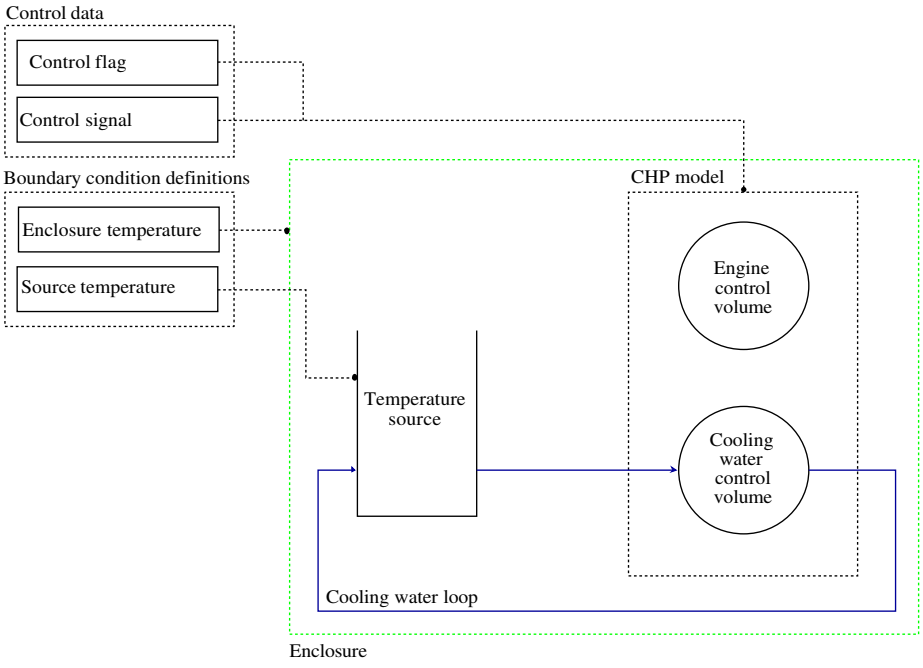

Figure III-2: Connections to cogeneration model in internal pump configuration

Boundary conditions

In both configurations, the comparative test suite requires specification of boundary condition and control data. In the external pump configuration, the enclosure temperature, cooling water temperature and cooling water flow rate must be specified. However, in the internal pump configuration, only the enclosure temperature and cooling water temperature must be specified—the cogeneration model will impose the flow rate on the cooling water loop.

Some of the test cases specify constant boundary conditions throughout the duration of the simulation, while others specify step changes in the cooling water temperature and flow rate boundary conditions between time steps. Constant and temporal boundary conditions may be defined using either a dedicated facility or a combination of hydronic plant equipment and control models regulating conditions upstream of the cogeneration model. The specification of such hydronic networks is beyond the scope of this document. Instead, it is assumed the developer has a suitable means for imposing both constant and temporal boundary within the simulation environment. However, developers using hydronic network models to manage temporal boundary conditions are cautioned that these networks must accomplish step changes in the boundary conditions as quickly as possible—time lags associated with the simulated effects of thermal mass will introduce uncertainty in the results.

In all test cases, the simulation's climatic conditions are inconsequential.

Controls

The combustion cogeneration model is also coupled to two controls:

- the unit's *control flag*, which i) activates and deactivates the unit, and ii) specifies the

control interface in use, and

- the unit's *control signal*, which represents either the electrical demand placed on the unit, or a dimensionless value describing the unit's operating point.

In many of the test cases, the values of these controls vary between time steps. Therefore, they must be implemented in a manner supporting specification of step changes.

Model parameters

The base case model parameters are presented in Table III-2, and the configuration of each test case is a a variation of this parameter set. In this test specification, the parameters differing from test case to test case are described, and all other parameters are assumed to be unchanged from the base case.

Simulation period and time resolution

All simulations commence at 00:00 h on January 9th and end at 23:59 h on the same day. A preconditioning startup period appropriate for the simulation environment should also be specified.

With the exception of the 400 series tests, this specification does not prescribe the time step duration used in the test cases. However, when the Annex 42 comparative testing work commenced, EnergyPlus only supported time steps as short as ten-minutes.[1] Therefore, a ten-minute time step was used for all tests to equivalence the implementations as much as possible.

In fact, the different strategies used by EnergyPlus, ESP-r and TRNSYS to implement the dynamic thermal model proved surprisingly sensitive to the time step duration. The

[1] Support for one-minute time steps has since been added.

Table III-2: Reference model parameters — Base case

Model parameter		Value	Units
Engine type		*ICE*[a]	–
Fuel type		*Gaseous mixture*	–
Liquid fuel heating value[b]	LHV_{fuel}	0.	J/kg
Liquid fuel carbon intensity[b]	e_{CO_2}	0.	kg CO_2 / kg fuel
Gaseous fuel composition	χ_{H_2}	0.0	mol/mol
	χ_{CH_4}	1.0	mol/mol
	$\chi_{C_2H_6}$	0.0	mol/mol
	$\chi_{C_3H_8}$	0.0	mol/mol
	$\chi_{C_4H_{10}}$	0.0	mol/mol
	$\chi_{C_5H_{12}}$	0.0	mol/mol
	$\chi_{C_6H_{14}}$	0.0	mol/mol
	χ_{CH_3OH}	0.0	mol/mol
	$\chi_{C_2H_5OH}$	0.0	mol/mol
	χ_{CO_2}	0.0	mol/mol
	χ_{N_2}	0.0	mol/mol
	χ_{O_2}	0.0	mol/mol
Operating bounds	P_{max}	1000.	W
	P_{min}	0.	W
Maximum outlet temperature	$T_{cw,o_{max}}$	100.	°C
Max rate of change in fuel flow	$(d\dot{m}_{fuel}/dt)_{max}$	∞[c]	kg/s^2
Max rate of change in power	$(d\dot{P}_{net}/dt)_{max}$	∞[c]	W/s
Thermal model characteristics	$[MC]_{eng}$	20.0 E03	J/K
	$[MC]_{HX}$	20.0 E03	J/K
	UA_{HX}	50.	W/K
	UA_{loss}	0.0	W/K

Notes:

[a] *ICE*: internal combustion engine, *SE*: Stirling engine.

[b] The liquid fuel parameters are inconsequential when the gaseous mixture configuration is specified.

[c] The model's rate limiting facilities should be disabled.

Continued on page III-11...

Table III-2: Reference model parameters — Base case, concluded

Model parameter		Value	Units
Standby mode power use	$P_{net,standby}$	0.	W
SE warm-up characteristics[d]	$T_{eng,nom}$	150.	°C
	k_f	1.0	–
	k_p	1.0	–
	$r_{fuel,warm-up}$	10.	kg/s
ICE warm-up period duration	$t_{warm-up}$	0.	s
Cool-down characteristics	$P_{net,cool-down}$	0.	W
	$t_{cool-down}$	0.	s
	Cool-down mode	MC[e]	–
Electrical efficiency coefficients	a_0	0.25	–
	a_1–a_{26}	0.	–
Thermal efficiency coefficients	b_0	0.50	–
	b_1–b_{26}	0.	–
Cooling water mass flow coefficients	c_0–c_8	0.	–
Combustion air coefficients	d_0–d_2	0.	–

Notes:

[d] The Stirling engine start-up characteristics are inconsequential when the engine is configured to represent an internal combustion engine.

[e] *MC*: mandatory cool-down period, *OC*: optional cool-down period. Refer to the model specification for more details.

300 Series tests section discusses these effects in detail, and bears reading before different time step durations are selected for future comparative testing work.

100 Series tests

The 100 series tests exercise the model's calculation of fuel heating value and molar mass. Each test case in the 100 series defines the composition of a fuel on a molar basis. To pass these cases, the model must correctly predict that fuel's molar mass and lower heating value.

Six 100 series test cases have been defined, and the variations between these test cases and the base configuration are presented in Table III-3. In each of these tests, the model is configured in the external cooling pump configuration. The boundary conditions are presented in Table III-4, and the control parameters are presented in Table III-5. In each of the 100 series tests, the engine is activated one hour into the test, and remains on for an hour. The cooling water temperature, flow rate and enclosure temperature remain constant throughout the simulation.

Test case 106 specifies a liquid fuel be used in the model. This feature is not yet implemented in EnergyPlus, and EnergyPlus results are not available for test case 106.

Test case 101

Test case 101 adopts the base configuration without any changes. The fuel comprises 100% methane.

The lower heating value of the fuel calculated during the simulation should be reported. Disagreements in this value may indicate errors in the fuel lower heating calculation facility or the specification of the heating value of methane. Developers should review the

Table III-3: Model parameter variations — Series 100 tests

		Test case						
Parameter	Units	Base	101	102	103	104	105	106
Fuel type	–	*gaseous mixture*	†	†	†	†	†	*liquid fuel*
LHV_{fuel}	J/kg	‡	‡	‡	‡	‡	‡	50.0 E06
χ_{H_2}	mol/mol	0.	†	†	†	†	0.1	*
χ_{CH_4}	mol/mol	1.	†	0.94	0.74	0.44	0.34	*
$\chi_{C_2H_6}$	mol/mol	0.	†	†	0.20	0.20	0.20	*
$\chi_{C_3H_8}$	mol/mol	0.	†	†	†	0.05	0.05	*
$\chi_{C_4H_{10}}$	mol/mol	0.	†	†	†	0.05	0.05	*
$\chi_{C_5H_{12}}$	mol/mol	0.	†	†	†	0.05	0.05	*
$\chi_{C_6H_{14}}$	mol/mol	0.	†	†	†	0.05	0.05	*
χ_{CH_3OH}	mol/mol	0.	†	†	†	0.05	0.05	*
$\chi_{C_2H_5OH}$	mol/mol	0.	†	†	†	0.05	0.05	*
χ_{CO_2}	mol/mol	0.	†	0.02	0.02	0.02	0.02	*
χ_{N_2}	mol/mol	0.	†	0.02	0.02	0.02	0.02	*
χ_{O_2}	mol/mol	0.	†	0.02	0.02	0.02	0.02	*

Notes:
† Value unchanged from base case.
‡ The fuel lower heating value is calculated by the model when a gaseous fuel mixture is specified
* The fuel composition is inconsequential when the liquid fuel configuration is specified.

Table III-4: Boundary conditions — Series 100 tests

				Test Case
Condition	Units	Start	End	101–105
Cooling water inlet temperature	°C	00:00	23:59	10.
Cooling water flow rate	kg/s	00:00	23:59	0.20
Enclosure temperature	°C	00:00	23:59	20.

Table III-5: Control parameters — Series 100 tests

				Test Case
Parameter	Units	Start	End	101–105
Control flag	–	00:00	01:00	*off*
		01:00	02:00	*ECI*
		02:00	23:59	*off*
Control signal	W	00:00	01:00	0.
		01:00	02:00	1000.
		02:00	23:59	0.

Notes:
ECI: Electric load following control interface

implementation of Equation III-5 in the model specification

Test case 102

Test case 102 is identical to test case 101, except some oxygen, nitrogen and carbon dioxide are introduced into the fuel mixture.

The difference between the lower heating values calculated in test cases 102 and 101 should be reported (ie. $LHV_{fuel,102} - LHV_{fuel,101}$). Disagreement in these results may indicate an error in the specification of the heating value oxygen, nitrogen or carbon dioxide.

Test case 103

Test case 103 is identical to test case 102, except that some ethane is introduced to the fuel mixture.

The difference between the lower heating values calculated in test cases 103 and 102 should be reported (ie. $LHV_{fuel,103} - LHV_{fuel,102}$). Disagreement in these results may indicate an

error in the specification of the heating value of ethane.

Test case 104

Test case 104 is identical to test case 103, except that some higher hydrocarbons and alcohols are introduced to the fuel mixture.

The difference between the lower heating values calculated in test cases 104 and 103 should be reported (ie. $LHV_{fuel,104} - LHV_{fuel,103}$). Disagreement in these results may indicate an error in the specification of the heating value of the higher hydrocarbons and alcohols.

Test case 105

Test case 105 is identical to test case 104, except that hydrogen is introduced to the fuel mixture.

The difference between the lower heating values calculated in test cases 105 and 104 should be reported (ie. $LHV_{fuel,105} - LHV_{fuel,104}$). Disagreement in these results may indicate an error in the specification of the heating value of hydrogen.

Test case 106

Test case 106 reconfigures the model in the *liquid fuel* configuration, and sets the fuel heating value to 50.0 E06 J/kg.

The lower heating value for test case 106 should be reported. Disagreement in this value may indicate an error in the treatment of the liquid fuel configuration.

Series 100 results

The fuel heating values calculated in the 100 series test cases are presented in Table III-6. The same values are plotted in Figure III-3, along with the difference between the values reported for each test case. EnergyPlus does not presently implement the liquid fuel configuration, and test case 106 results for EnergyPlus are not available.

Exact agreement was observed between the ESP-r and TRNSYS results, which is not surprising as ESP-r and TRNSYS both use the same parameters and library routines when calculating fuel heating values. The EnergyPlus results differed slightly from the ESP-r and TRNSYS values, and the relative differences between the EnergyPlus and ESP-r/TRNSYS results are presented in Figure III-4.

The agreement demonstrated by EnergyPlus, ESP-r and TRNSYS suggest the three implementations comparably compute the heating value of the fuel.

Table III-6: Series 100 test case results — reported fuel lower heating value

	Reported fuel lower heating value (J/kg)		
Test case	EnergyPlus	ESP-r	TRNSYS
101	50 010 226	50 010 164	50 010 164
102	43 948 429	43 948 372	43 948 372
103	44 047 606	44 038 752	44 038 752
104	41 424 478	41 427 968	41 427 968
105	41 491 801	41 495 208	41 495 208
106	—	50 000 000	50 000 000

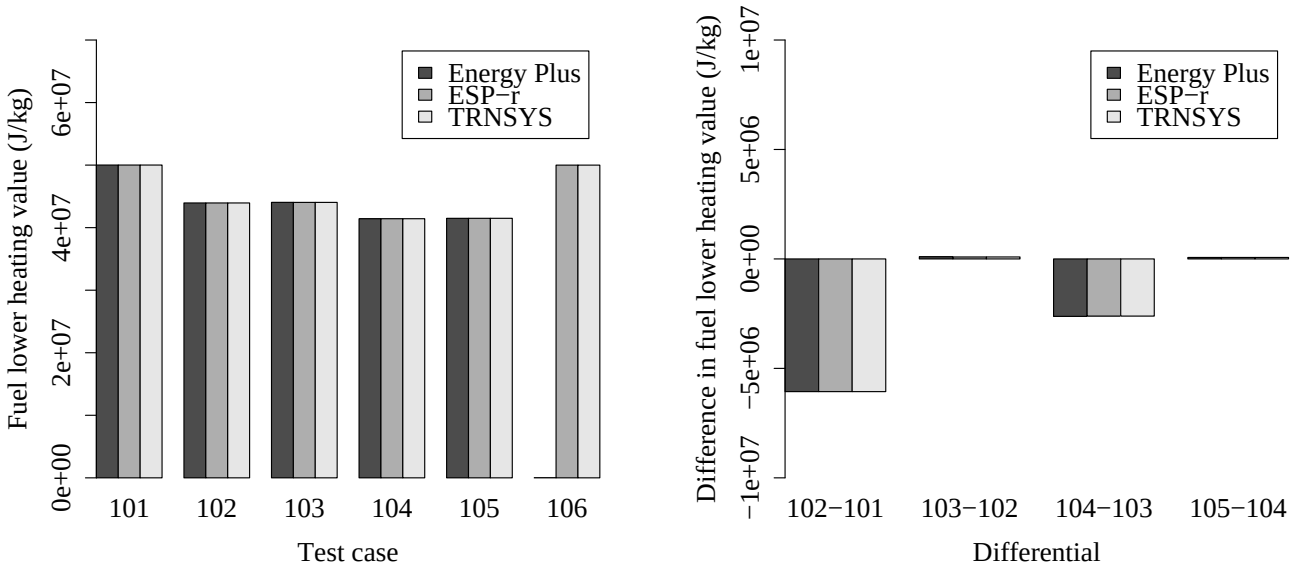

Figure III-3: 100 series test case results: (a) reported fuel lower heating value, and (b) differences between fuel lower heating values reported in successive test cases

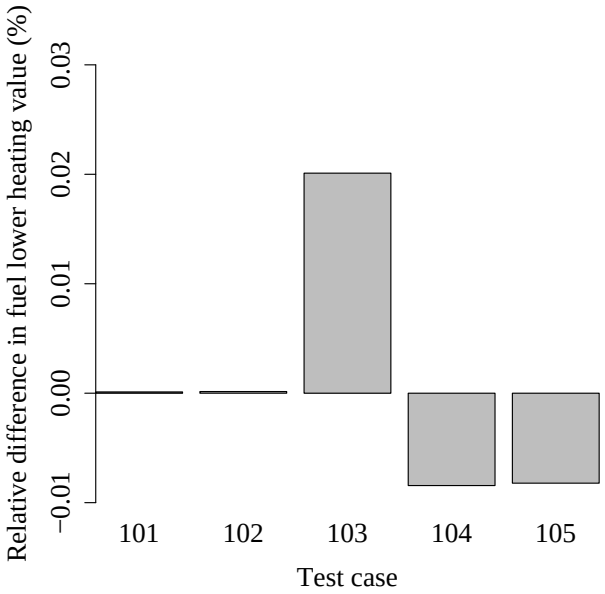

Figure III-4: 100 series test case results: relative differences between fuel lower lower heating values reported by EnergyPlus and ESP-r/TRNSYS

200 Series tests

The 200 series test cases exercise the model's steady-state empirical correlations at different operating points and differing boundary conditions. Test cases 201–203 utilize the external cooling pump configuration, while test cases 204 and 205 utilize the internal cooling pump configuration.

Five 200 series test cases have been devised, and the differences between the model parameters used in these cases and the base case are presented in Table III-7. The boundary conditions used in the 200 series test cases are presented in Table III-8, and the control parameters are presented in Table III-9.

Test cases 204 and 205 specify the internal pump configuration, a feature not yet implemented in EnergyPlus. Therefore, the EnergyPlus implementation could not be exercised over these cases.

Table III-7: Model parameter variations — Series 200 tests

Parameter		Units	Test case		
			Base	201–203	204, 205
Electrical efficiency	a_0	–	0.25	0.25	†
	a_1	W^{-2}	0.0	−4.00 E−07	†
	a_2	W^{-1}	0.0	2.00 E−04	†
	a_3	$(s/kg)^2$	0.0	−2.222	†
	a_4	(s/kg)	0.0	0.667	†
	a_5	$(°C)^{-2}$	0.0	−1.47 E−05	†
	a_6	$(°C)^{-1}$	0.0	2.22 E−03	†
	a_7–a_{26}	–	0.0	0.0	†
Thermal efficiency	b_0	–	0.50	0.50	†
	b_1	W^{-2}	0.0	−4.00 E−07	†
	b_2	W^{-1}	0.0	2.00 E−04	†
	b_3	$(s/kg)^2$	0.0	−2.222	†
	b_4	(s/kg)	0.0	0.667	†
	b_5	$(°C)^{-2}$	0.0	−2.47 E−05	†
	b_6	$(°C)^{-1}$	0.0	2.22 E−03	†
	b_7–b_{26}	–	0.0	0.0	†
Cooling water flow	c_0	kg/s	0.2	‡	0.2
	c_1	kg/W^2s	0.0	‡	−1.00 E−06
	c_2	kg/Ws	0.0	‡	1.00 E−03
	c_3	$kg/(°C)^2s$	0.0	‡	−3.704 E−05
	c_4	kg/(°C)s	0.0	‡	3.333 E−03
	c_5–c_8	–	0.0	‡	0.0
Combustion air flow	d_0	kg/s	0.0	15.0 E−06	†
	d_1	$(s/kg)^2$	0.0	−10.0 E03	†
	d_2	(s/kg)	0.0	2.0	†

Notes:

‡ The cooling water flow correlation is disabled, and the flow rate imposed on the unit by the upstream water source prevails.

† Values are unchanged from test cases 201–203.

Table III-8: Boundary conditions — Series 200 tests

				Test Case				
Condition	Units	Start	End	201	202	203	204	205
Cooling water inlet temperature	°C	00:00	01:00	10.	10.	10.	10.	10.
		01:00	02:00	50.	10.	50.	50.	10.
		02:00	03:00	50.	20.	50.	50.	20.
		03:00	04:00	50.	30.	50.	50.	30.
		04:00	05:00	50.	40.	50.	50.	40.
		05:00	06:00	50.	50.	50.	50.	50.
		06:00	07:00	50.	60.	50.	50.	60.
		07:00	08:00	50.	70.	50.	50.	70.
		08:00	09:00	50.	80.	50.	50.	80.
		09:00	11:00	50.	90.	50.	50.	90.
		11:00	23:59	10.	10.	10.	10.	10.
Cooling water flow rate	kg/s	00:00	01:00	0.20	0.20	0.20	‡	‡
		01:00	02:00	0.20	0.20	0.10	‡	‡
		02:00	03:00	0.20	0.20	0.12	‡	‡
		03:00	04:00	0.20	0.20	0.14	‡	‡
		04:00	05:00	0.20	0.20	0.16	‡	‡
		05:00	06:00	0.20	0.20	0.18	‡	‡
		06:00	07:00	0.20	0.20	0.20	‡	‡
		07:00	08:00	0.20	0.20	0.22	‡	‡
		08:00	09:00	0.20	0.20	0.24	‡	‡
		09:00	10:00	0.20	0.20	0.26	‡	‡
		10:00	11:00	0.20	0.20	0.28	‡	‡
		11:00	23:00	0.20	0.20	0.20	‡	‡
Enclosure temperature	°C	00:00	23:99h	20.0	20.0	20.0	20.0	20.0

Notes:
‡ Cooling water flow rate imposed by model.

Table III-9: Control parameters — Series 200 tests

				Test Case				
Parameter	Units	Start	End	201	202	203	204	205
Control flag	–	00:00	01:00	*off*	*off*	*off*	*off*	*off*
		01:00	11:00	*ECI*	*ECI*	*ECI*	*ECI*	*ECI*
		11:00	23:59	*off*	*off*	*off*	*off*	*off*
Control signal	W	00:00	01:00	0.	0.	0.	0.	0.
		01:00	02:00	100.	500.	500.	100.	500.
		02:00	03:00	200.	500.	500.	200.	500.
		03:00	04:00	300.	500.	500.	300.	500.
		04:00	05:00	400.	500.	500.	400.	500.
		05:00	06:00	500.	500.	500.	500.	500.
		06:00	07:00	600.	500.	500.	600.	500.
		07:00	08:00	700.	500.	500.	700.	500.
		08:00	09:00	800.	500.	500.	800.	500.
		09:00	10:00	900.	500.	500.	900.	500.
		10:00	11:00	1000.	500.	500.	1000.	500.
		11:00	23:59	0.	0.	0.	0.	0.

Notes:
ECI: Electric load following control interface

Test case 201

Test case 201 exercises the model correlations over differing operating points. The model is configured in the external cooling pump configuration, and the cooling water temperature, flow rate and enclosure temperature are held at constant values. The cogeneration device is activated one hour into the test, and its output is varied from 100 W to 1000 W in increments of 100 W.

The model's electrical efficiency correlations are configured using only the first six coefficients in these equations (a_0–a_6 from Equation 14 and b_0–b_6 from Equation 15 in the model specification), while the remainder (a_7–a_{26} and b_7–b_{26}) are set to zero. The model's combustion air flow correlation is configured using the values presented in Table III-7. In this configuration, the flow rate of cooling water though the unit is imposed by the upstream pump, and the model's cooling water flow rate correlation is disabled.

The following parameters should be plotted:

- *The steady-state electrical conversion efficiency (η_e):* These values should be plotted against both time (t) and the net electric output of the device (P_{net}). Disagreement in these values suggests an error in the implementation of the steady-state electrical efficiency correlation (Equation III-14 in the model specification).

- *The steady-state heat generation efficiency (η_q):* These values should be plotted against both time (t) and the net electric output of the device (P_{net}). Disagreement in these values suggests an error in the implementation of the steady-state heat generation efficiency correlation (Equation III-15 in the model specification).

- *The gross heat input to the engine (q_{gross}):* These values should be plotted against both time (t) and the net electric output of the device (P_{net}). Disagreement in these values suggests an error in the solution of Equation III-2 in the model specification.

- *The rate of steady-state heat generation ($q_{gen,ss}$):* These values should be plotted against both time (t) and the net electric output of the device (P_{net}). Disagreement in these values suggests an error in the solution of Equation III-3 in the model specification.

- *The fuel flow rate ($\dot{m}_{fuel}$):* These values should be plotted against both time (t) and the net electric output of the device (P_{net}). Disagreement in these values suggests an error in the solution of Equation III-4 in the model specification.

- *The combustion air flow rate ($\dot{m}_{air}$):* These values should be plotted against both time (t) and the fuel flow rate ($\dot{m}_{fuel}$). Disagreement in these values suggests an error in the evaluation of Equation III-17 in the model specification.

Figure III-5 plots the steady-state electrical efficiency as a function of time and power output, while Figure III-6 plots the steady-state heat generation efficiency. In both cases, the EnergyPlus, ESP-r and TRNSYS results exhibit exact agreement.

Figure III-7 plots the calculated rate of gross heat input as a function of time and power output. Similarly, Figure III-8 plots the calculated rate of heat heat generation inside the engine as a function of both time and power output. Again, the EnergyPlus, ESP-r and TRNSYS results agree exactly.

Finally, Figures III-9 and III-10 plot the predicted rates of fuel flow and air flow as functions of time and power output. The results agree well, although the EnergyPlus predictions differ slightly from the corresponding ESP-r/TRNSYS values when the unit operates at its maximum operating point. The difference between the EnergyPlus and ESP-r/TRNSYS implementations at this point is less than 0.4%, and deemed insignificant.

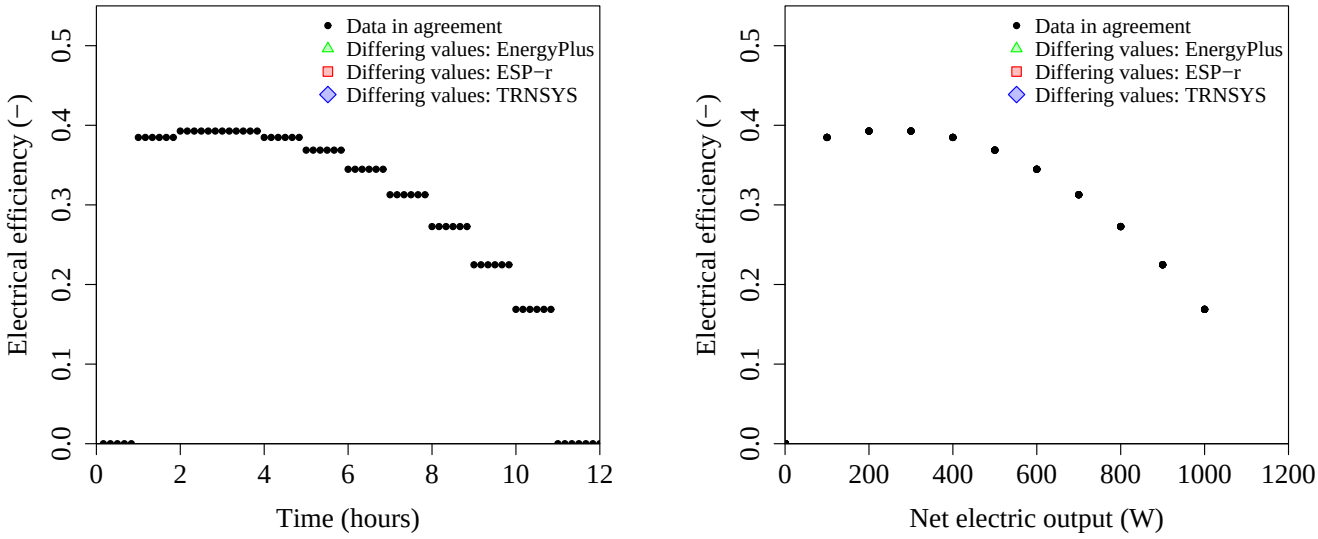

Figure III-5: Test case 201 results — electrical efficiency (η_e) as a function of (a) time, and (b) net electric output (P_{net})

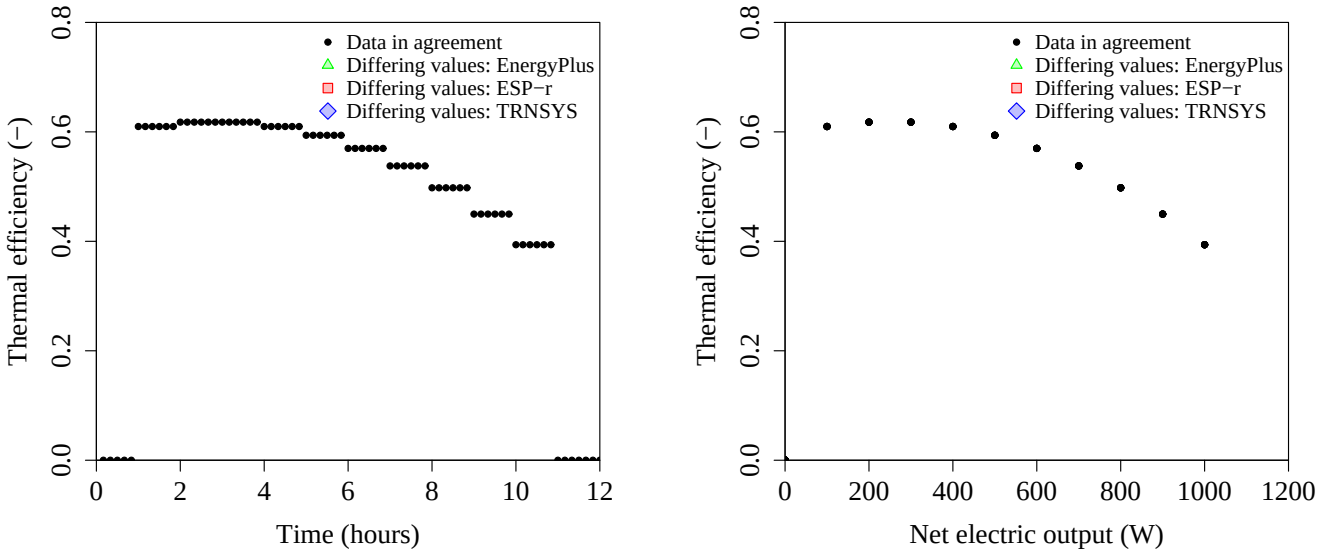

Figure III-6: Test case 201 results — thermal efficiency (η_q) as a function of (a) time, and (b) net electric output (P_{net})

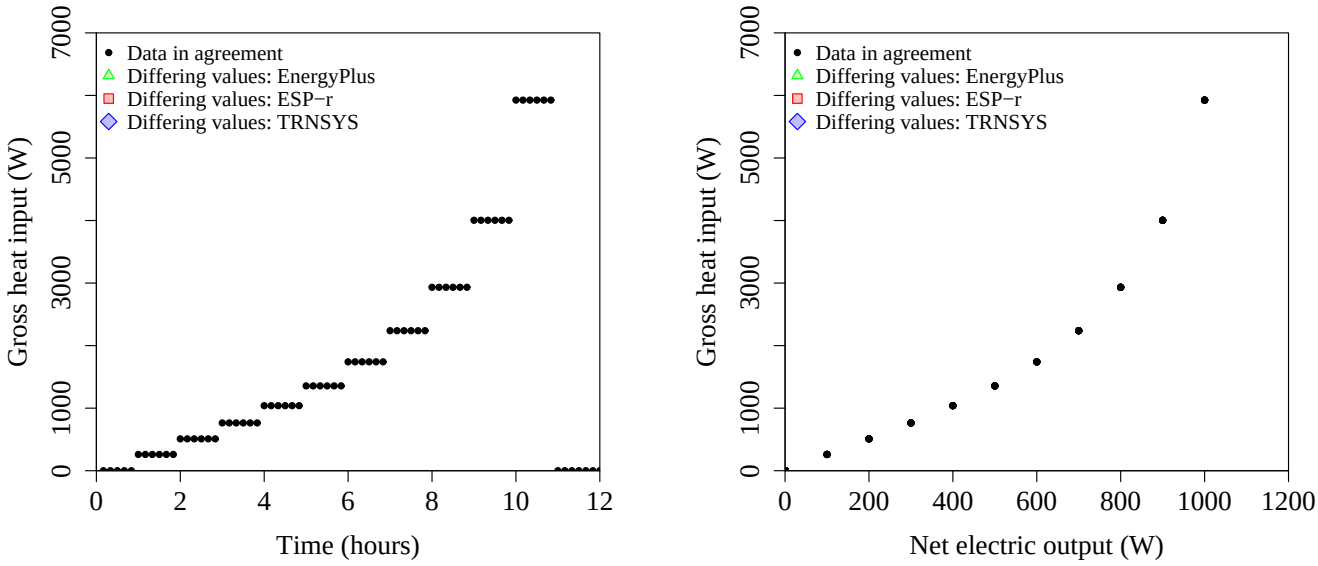

Figure III-7: Test case 201 results — gross heat input (q_{gross}) as a function of time, and (b) net electric output (P_{net})

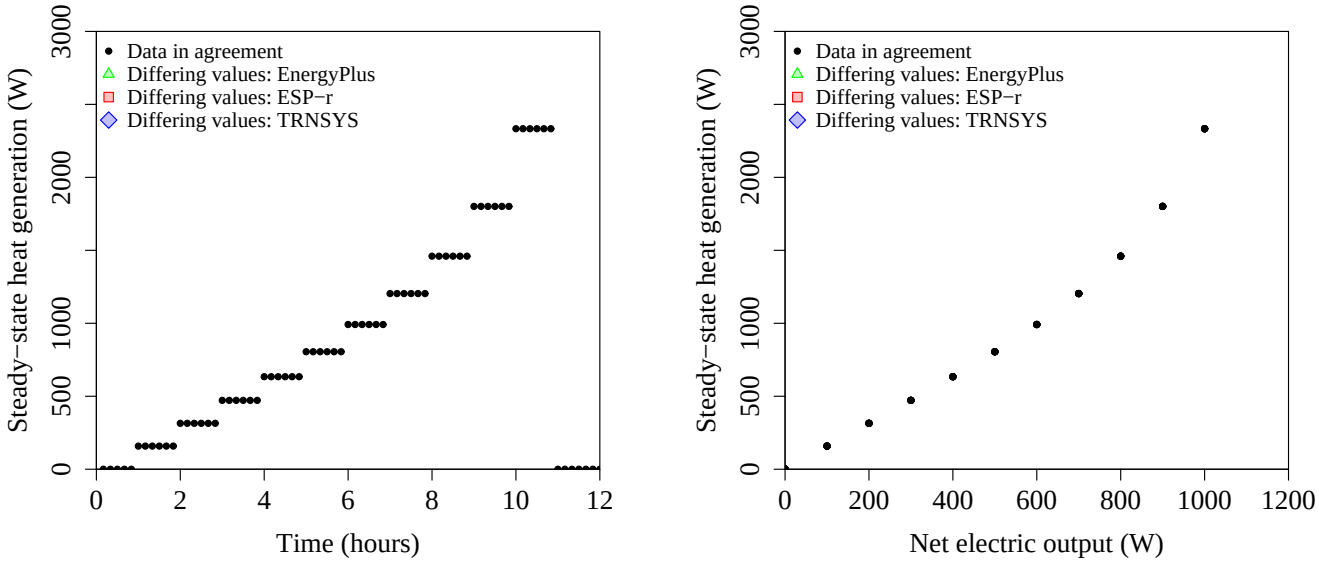

Figure III-8: Test case 201 results — gross heat input ($q_{gen,ss}$) as a function of (a) time, and (b) net electric output (P_{net})

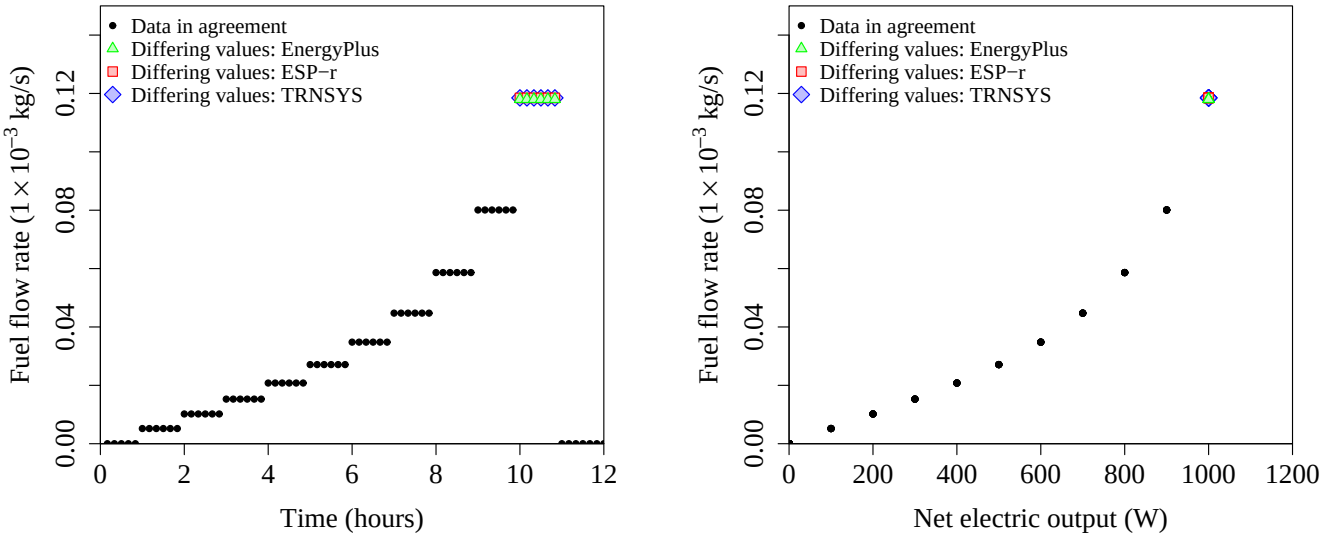

Figure III-9: Test case 201 results — fuel flow rate ($\dot{m}_{fuel}$) as a function of (a) time, and (b) net electric output (P_{net})

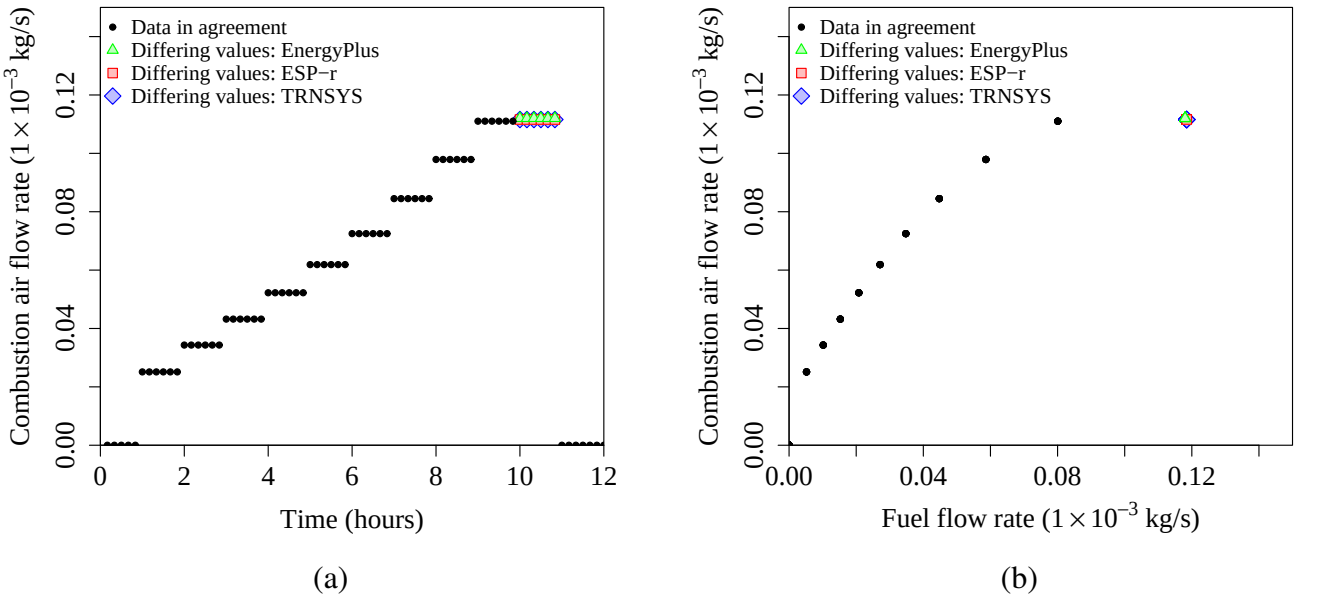

Figure III-10: Test case 201 results — combustion air flow rate ($\dot{m}_{air}$) as a function of (a) time, and (b) fuel flow rate (P_{net})

Test case 202

The model parameters remain unchanged between test cases 201 and 202, and test case 202 also utilizes the external cooling water pump. Instead of varying the cogeneration unit's operating point, test case 202 sets the unit's operating point to a constant value (500 W electric output), and varies the temperature of the cooling water entering the cogeneration unit between 10 °C and 90 °C, in increments of 10 °C. The cooling water flow rate is imposed by the upstream component, and both this flow rate and the unit's operating point are held at constant values.

The following parameters should be plotted against both i) time and ii) the temperature of the incoming cooling water ($T_{cw,i}$):

- *The steady-state electrical conversion efficiency (η_e):* Disagreement in these values suggests an error in the implementation of the steady-state electrical efficiency correlation (Equation 14 in the model specification).
- *The steady-state heat generation efficiency (η_q):* Disagreement in these values suggests an error in the implementation of the steady-state heat generation efficiency correlation (Equation 15 in the model specification).

Figure III-11 plots the steady-state electrical conversion efficiency as a function of time and the cooling water temperature. Similarly, Figure III-12 plots the steady-state heat generation efficiency as a function of time and the cooling water temperature. In both cases, the EnergyPlus, ESP-r and TRNSYS results all exhibit exact agreement.

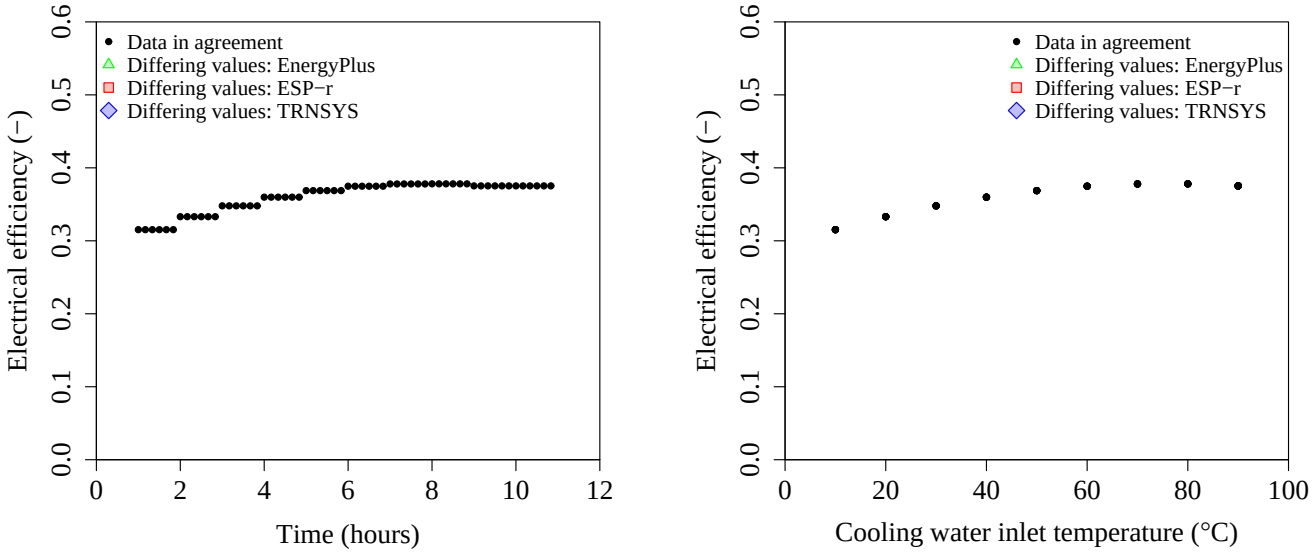

Figure III-11: Test case 202 results — electrical efficiency (η_e) as a function of (a) time, and (b) cooling water temperature ($T_{cw,i}$)

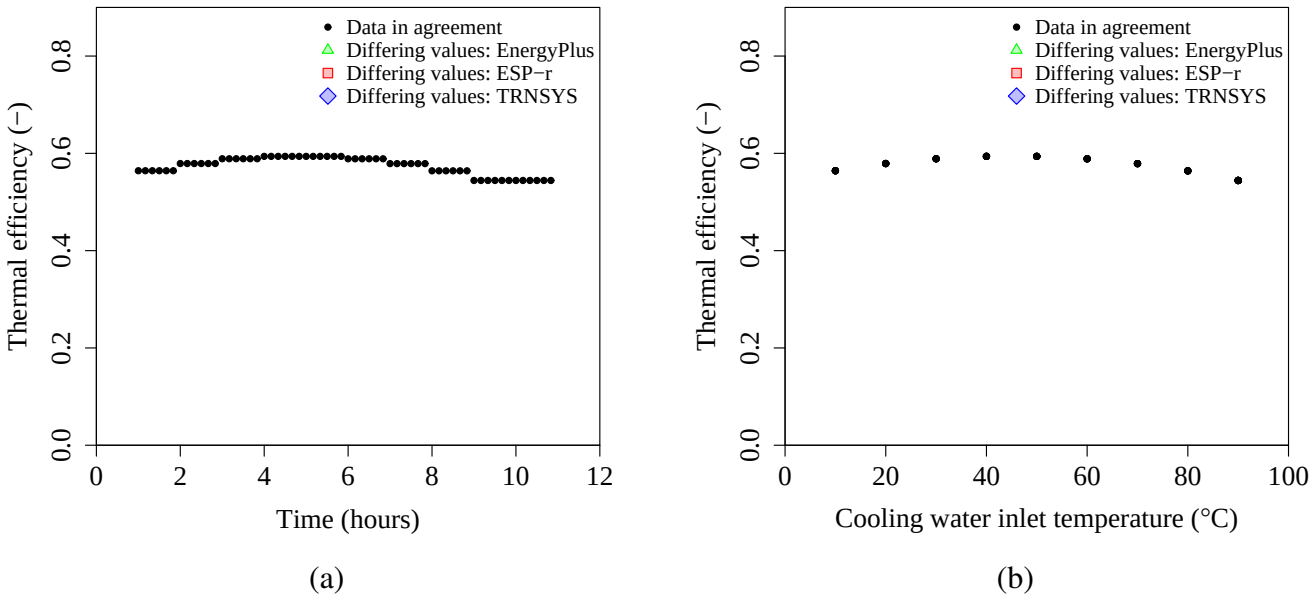

Figure III-12: Test case 202 results — thermal efficiency (η_q) as a function of (a) time, and (b) cooling water temperature ($T_{cw,i}$)

Test case 203

Test case 203 is identical to test case 202, except the flow rate of the cooling water entering the cogeneration unit is varied instead of the temperature. The flow rate is varied between 0.1 kg/s and 0.3 kg/s, in increments of 0.02 kg/s. The cooling water temperature also is imposed by the upstream component, and both this temperature and the unit's operating point are held at constant values.

The following parameters should be plotted against both i) time and ii) the flow rate of the incoming cooling water ($\dot{m}_{cw}$):

- *The steady-state electrical conversion efficiency (η_e):* Disagreement in these values suggests an error in the implementation of the steady-state electrical efficiency correlation (Equation 14 in the model specification).
- *The steady-state heat generation efficiency (η_q):* Disagreement in these values suggests an error in the implementation of the steady-state heat generation efficiency correlation (Equation 15 in the model specification).

Figures III-13 and III-14 compare the EnergyPlus, ESP-r and TRNSYS efficiency predictions for Test case 203. Again, the results agree exactly.

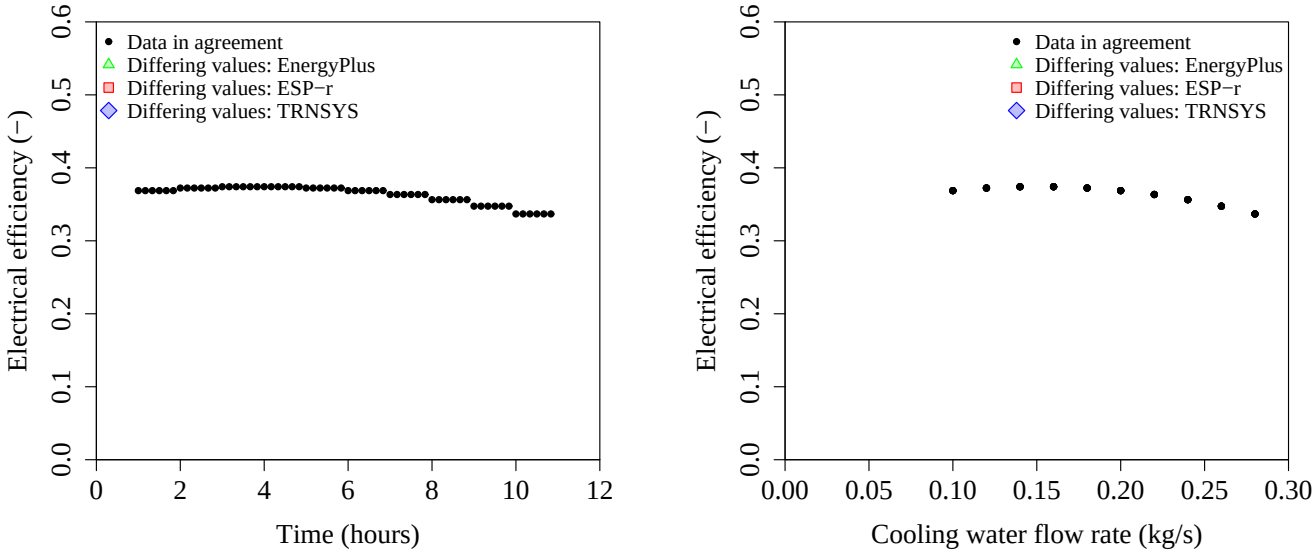

Figure III-13: Test case 203 results — electrical efficiency (η_e) as a function of (a) time, and (b) cooling water flow rate ($\dot{m}_{cw}$)

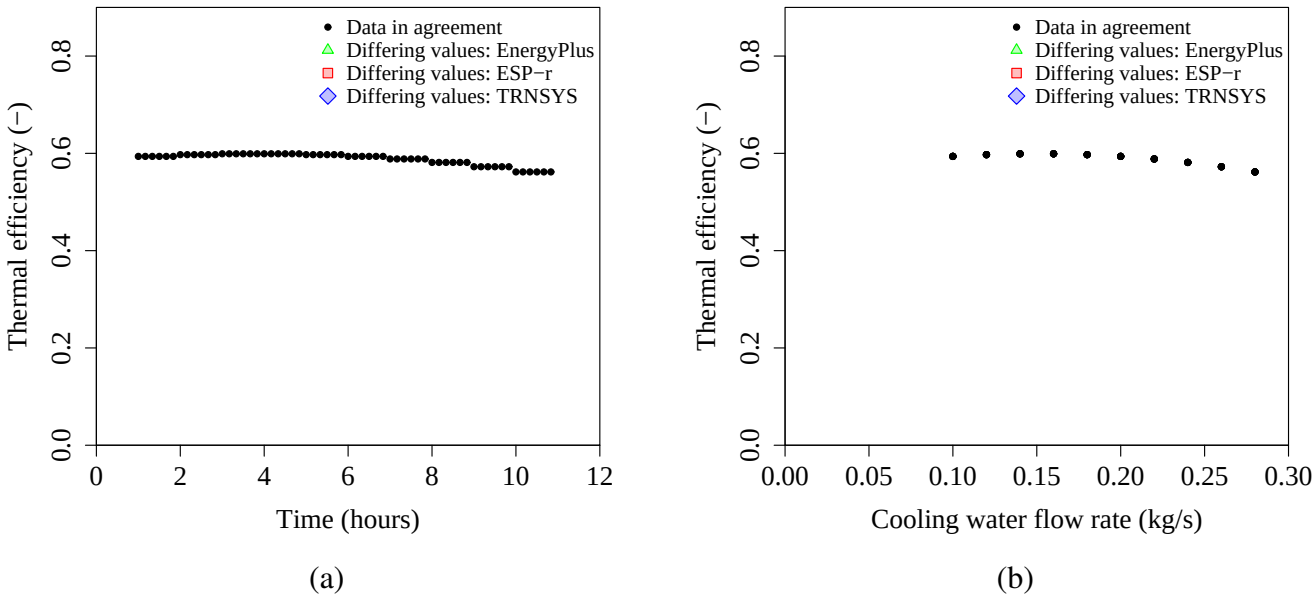

Figure III-14: Test case 203 results — thermal efficiency (η_q) as a function of (a) time, and (b) cooling water flow rate ($\dot{m}_{cw}$))

Test case 204

Test case 204 substitutes the internal cooling pump configuration for the external configuration used in test cases 201–203. In this arrangement, the model imposes the cooling water flow rate based on its current operating point and the temperature of the cooling water.

The boundary conditions used in Test case 204 are identical to those used in test case 201, except the cooling water flow rate is no longer specified. The control parameters are unchanged from case 201, and the model configuration parameters are also identical to test case 201 with the exception of the cooling water flow rate correlation parameters (c_0–c_8 in Equation 16 of the model specification), which are configured as described in Table III-7.

The cooling water mass flow rate though the device should be plotted against both i) time and ii) the electric output of the device (P_{net}). Disagreement in these results suggests an error in the implementation of the cooling water correlation (Equation 16 in the model specification).

Figure III-15 plots the cooling water flow rate imposed by the model as a function of time and the net power output, respectively. The ESP-r and TRNSYS results exhibit exact agreement. Results for test case 204 are not available for EnergyPlus, which does not implement the internal cooling water pump configuration.

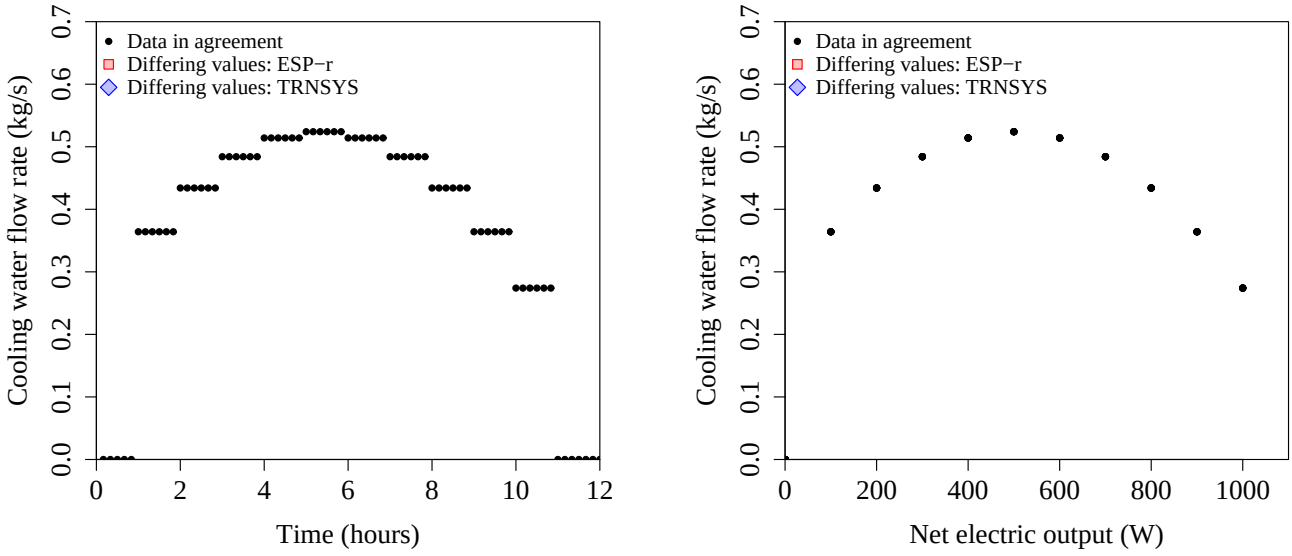

Figure III-15: Test case 204 results — cooling water flow ($\dot{m}_{CW}$) as a function of (a) time and (b) net electric output (P_{net})

Test case 205

Test case 205 is identical to test case 204, except the cogeneration unit is held at a constant operating point while the temperature of the supplied cooling water is varied.

The boundary conditions used in Test case 205 are identical to those used in test case 202, except the cooling water flow rate is no longer specified. The control parameters are unchanged from case 202, and the model configuration parameters are also identical to test case 202 with the exception of the cooling water flow rate correlation parameters (c_0–c_8 in Equation 16 from the model specification), which are configured as described in Table III-7.

The mass flow rate though the device should be plotted against both i) time and ii) the temperature of the supplied cooling water ($T_{cw,i}$). Disagreement in these results suggests an error in the implementation of the cooling water correlation (Equation 16 in the model specification).

Figure III-16 compares the ESP-r and TRNSYS predictions for test case 205. The ESP-r and TRNSYS results exhibit exact agreement. Results for test case 205 are not available for EnergyPlus, which does not implement the internal cooling water pump configuration.

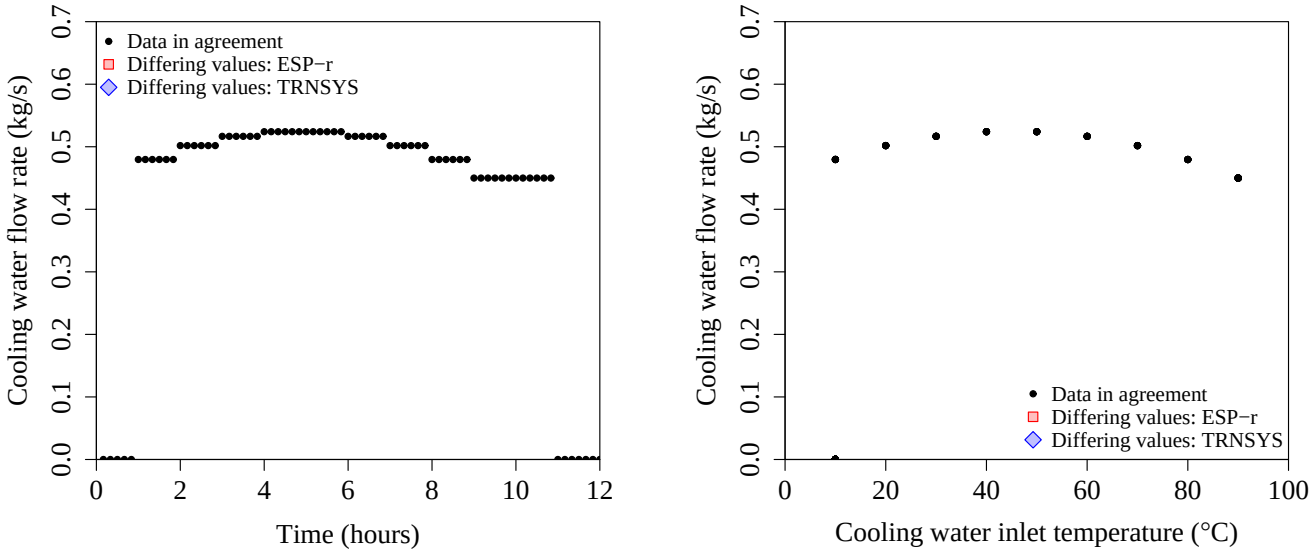

Figure III-16: Test case 205 results — cooling water flow ($\dot{m}_{CW}$) as a function of (a) time and (b) cooling water inlet temperature ($T_{cw,i}$)

300 Series tests

The 300 series tests subject the dynamic thermal model to step changes in operating point and boundary conditions. Eight 300 series test cases have been devised, and the differences between the base model configuration and the inputs used in these test cases are presented in Table III-10. The boundary conditions used in the 300 series test cases are presented in Table III-11, while the control parameters are presented in Table III-12. All of the 300 series test cases utilize the external cooling pump configuration.

Test cases 301–303 characterize the model's response to differing operating points and boundary conditions. Since the dynamic thermal model state equations (Equations III-8–III-11 in the model specification) are highly coupled, these cases serve as general tests for model predictions but offer little insight into the possible sources of disagreement. These tests are complemented by test cases 304–308, which attempt to identify individual errors in the model implementations by perturbing individual inputs.

Table III-10: Model parameter variations — Series 300 tests

		Test case						
Parameter	Units	Base	301–303	304	305	306	307	308
$[MC]_{eng}$	J/K	20.0 E03	†	40.0 E03	†	†	†	†
$[MC]_{HX}$	J/K	20.0 E03	†	†	40.0 E03	†	†	†
$[UA]_{HX}$	W/K	50.	†	†	†	20.	†	†
$[UA]_{loss}$	W/K	0.0	†	†	†	†	10.0	10.0

Notes:
† Value unchanged from base case.

Table III-11: Boundary conditions — Series 300 tests

				Test Case				
Condition	Units	Start	End	301, 304–306	302	303	307	308
Cooling water inlet temperature	°C	00:00	02:00	25.	25.	25.	25.	25.
		02:00	04:00	25.	50.	25.	25.	25.
		04:00	23:59	25.	25.	25.	25.	25.
Cooling water flow rate	kg/s	00:00	02:00	0.15	0.15	0.15	0.15	0.15
		02:00	02:20	0.15	0.15	0.015	0.15	0.15
		02:20	04:00	0.15	0.15	0.015	0.	0.
		04:00	23:59	0.15	0.15	0.15	0.	0.
Enclosure Temperature	°C	00:00	23:99	20.0	20.0	20.0	20.0	40.0

Table III-12: Control parameters — Series 300 tests

				Test Case		
Parameter	Units	Start	End	301, 306	302, 303	307, 308
Control flag	–	00:00	01:00	*off*	*ECI*	*ECI*
		01:00	02:00	*ECI*	*ECI*	*ECI*
		02:00	03:00	*ECI*	*ECI*	*off*
		03:00	23:59	*off*	*ECI*	*off*
Control signal	W	00:00	01:00	0.	500.	1000.
		01:00	02:00	1000.	500.	1000.
		02:00	03:00	1000.	500.	0.
		03:00	23:59	0.	500.	0.

Notes:
ECI: Electric load following control interface

Test case 301

Test case 301 exercises the dynamic thermal model over step changes in operating point. The model's electric output is changed from 0 W to 1000 W one hour into the test, and then returned to 0 W two hours later. An upstream component provides cooling water at constant temperature and flow rate throughout the test, and the enclosure temperature is maintained at a constant value.

The model inputs are unchanged from the base case. In this configuration, heat transfer between the model and the enclosure is eliminated by setting the coefficient of heat loss between the model's engine control volume and the surroundings to zero.

The following test case 301 results should be plotted against time:

- The rate of heat transfer (q_{HX})
- The rate of heat loss (q_{loss})
- The engine control volume temperature (T_{eng})
- The cooling water control volume outlet temperature ($T_{cw,o}$)

Disagreement in the case 301 results may indicate an error in the heat transfer or heat loss equations (Equations III-8 and III-9 in the model specification), or in the general solution of the dynamic thermal model (Equations III-10 and III-11).

The engine and cooling water outlet temperature predictions in test case 301 are depicted in Figure III-17, while the predicted rates of heat transfer and heat loss are plotted in Figure III-18. In all cases, EnergyPlus predicts a transient response that is significantly faster than the ESP-r and TRNSYS predictions. The differences between the predictions are most pronounced immediately following activation of the engine one hour into the test. EnergyPlus predicts an engine temperature (T_{eng}) nearly 8 °C higher than corresponding

ESP-r/TRNSYS predictions, and a cooling water outlet temperature ($T_{cw,o}$) nearly 0.7 °C higher than corresponding ESP-r/TRNSYS predictions.

In this case, disagreement between the EnergyPlus and ESP-r/TRNSYS predictions does not reflect errors in the model implementations, but rather the differing philosophies used to solve the combustion-based cogeneration model's state equations. Consider the state equations describing the temperature of the engine and cooling water control volumes (Equations III-10 and III-11 in the model specification):

$$[MC]_{eng}\frac{dT_{eng}}{dt} = UA_{HX}(T_{cw,o} - T_{eng}) + UA_{loss}(T_{room} - T_{eng}) + q_{gen,ss}$$
$$[MC]_{HX}\frac{dT_{cw,o}}{dt} = [\dot{m}C_p]_{cw}(T_{cw,i} - T_{cw,o}) - UA_{HX}(T_{cw,o} - T_{eng})$$

While the EnergyPlus, ESP-r and TRNSYS environments all implement the same state equations, they solve these equations in fundamentally different ways:

- EnergyPlus evaluates each state equation separately using the equation's analytical solution.
- ESP-r and TRNSYS use a finite-difference approximation to linearize the differential equations.

EnergyPlus solution strategy

On each time step, the EnergyPlus implementation determines the future values of the engine temperature ($T_{eng}^{t+\Delta t}$) and cooling water outlet temperature ($T_{cw,o}^{t+\Delta t}$) using the analytical solutions of the state-space equations:

$$T_{eng}^{t+\Delta t} = \left(T_{eng}^{t} + \frac{a_{eng}}{b_{eng}}\right)e^{b_{eng}t} - \frac{a_{eng}}{b_{eng}} \quad \text{(III-1)}$$
$$T_{cw,o}^{t+\Delta t} = \left(T_{cw,o}^{t} + \frac{a_{cw,o}}{b_{cw,o}}\right)e^{b_{cw,o}t} - \frac{a_{cw,o}}{b_{cw,o}} \quad \text{(III-2)}$$

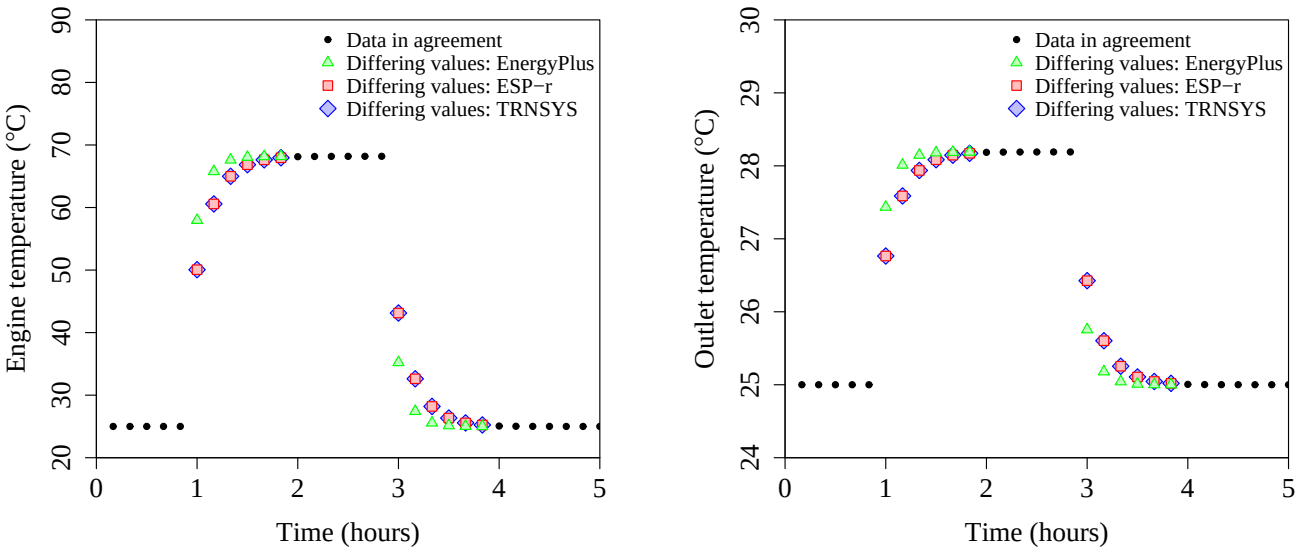

Figure III-17: Test case 301 results — (a) engine temperature (T_{eng}) and (b) cooling water temperature ($T_{cw,o}$) as functions of time

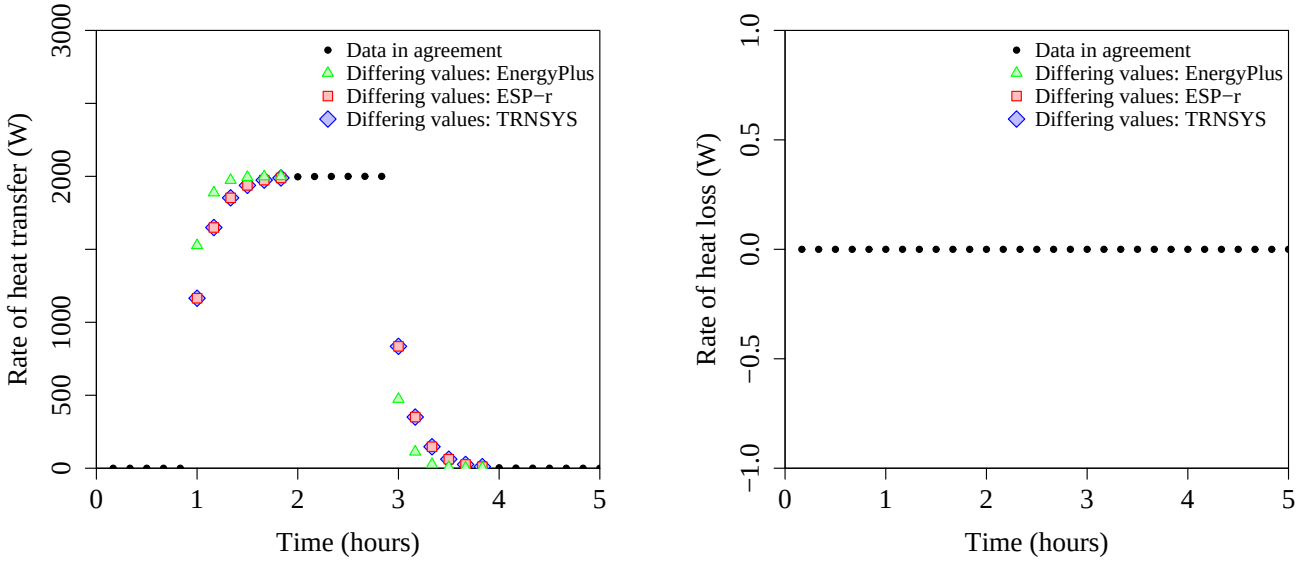

Figure III-18: Test case 301 results — rates of (a) heat transfer (q_{HX}) and (b) heat loss (q_{loss}) as functions of time

where a_{eng} and b_{eng} are given by:

$$a_{eng} = \frac{UA_{HX}T_{cw,o} + UA_{loss}T_{room} + q_{gen,ss}}{[MC]_{eng}} \tag{III-3}$$

$$b_{eng} = -\left(\frac{UA_{HX} + UA_{loss}}{[MC]_{eng}}\right) \tag{III-4}$$

and $a_{cw,o}$ and $b_{cw,o}$ are given by:

$$a_{cw,o} = \frac{[\dot{m}C_p]_{cw}T_{cw,i} + UA_{HX}T_{eng}}{[MC]_{HX}} \tag{III-5}$$

$$b_{cw,o} = -\left(\frac{[\dot{m}C_p]_{cw} + UA_{HX}}{[MC]_{cw}}\right) \tag{III-6}$$

These two analytical solutions are coupled—term a_{eng} used in the solution of the future engine control volume temperature ($T_{eng}^{t+\Delta t}$) references the instantaneous cooling water outlet temperature, which itself is time-variant ($T_{cw,o} = f(t)$). Similarly, term $a_{cw,o}$ used in the solution of the future cooling water outlet temperature ($T_{cw,o}^{t+\Delta t}$) references the instantaneous engine control volume temperature, which is also time variant ($T_{eng} = f(t)$).

The EnergyPlus implementation copes with this coupling by assuming that, for the purpose of evaluating the analytical solutions, the instantaneous engine and cooling water outlet temperatures ($T_{eng}(t)$ and $T_{cw,o}(t)$) referenced in a_{eng} and b_{eng} can be approximated by their future time row values:

$$T_{eng}(t) \approx T_{eng}^{t+\Delta t} \tag{III-7}$$

$$T_{cw,o}(t) \approx T_{cw,o}^{t+\Delta t} \tag{III-8}$$

The EnergyPlus implementation then iterates between the coupled analytical solutions (Equations III-1 and III-2). The iteration loop exits when the predicted values of the future time row engine and cooling water outlet temperatures yield balanced state equations (Equations III-8 and III-9 in the model specification).

Though derived from their analytic solutions, the EnergyPlus implementation is not an exact representation of the model's state equations. The assumption that the instantaneous

engine and cooling water outlet temperatures ($T_{eng}(t)$ and $T_{cw,o}(t)$) can be approximated by their future time row values is only valid as the simulation time step duration approaches zero, and causes the predicted temperatures to diverge from their actual values as the time step duration is increased.

ESP-r and TRNSYS solution strategy

Like EnergyPlus, the ESP-r and TRNSYS implementations only approximate the true solution of the state equations. However ESP-r and TRNSYS use a finite-difference method to solve the equations.

In ESP-r and TRNSYS, these equations are represented using forward- and backward-difference approximations at each time step. The forward-difference of the engine control volume state equation (Equation III-10 in the model specification) taken at time t over interval Δt is:

$$[MC]_{eng}\frac{T_{eng}^{t+\Delta t}-T_{eng}^{t}}{\Delta t} = UA_{HX}(T_{cw,o}^{t}-T_{eng}^{t})+UA_{loss}(T_{room}^{t}-T_{eng}^{t})+q_{gen,ss}^{t} \qquad \text{(III-9)}$$

and the backward-difference approximation for the same equation taken at time $t+\Delta t$ is:

$$[MC]_{eng}\frac{T_{eng}^{t+\Delta t}-T_{eng}^{t}}{\Delta t} = UA_{HX}(T_{cw,o}^{t+\Delta t}-T_{eng}^{t+\Delta t}) + UA_{loss}(T_{room}^{t+\Delta t}-T_{eng}^{t+\Delta t})+q_{gen,ss}^{t+\Delta t} \qquad \text{(III-10)}$$

Similarly, the forward- and backward-difference approximations the cooling water control volume state equation (Equation III-11 in the model specification) are:

$$[MC]_{HX}\frac{T_{cw,o}^{t+\Delta t}-T_{cw,o}^{t}}{\Delta t} = [\dot{m}^{t}C_{p}^{t}]_{cw}(T_{cw,i}^{t}-T_{cw,o}^{t})UA_{HX}(T_{cw,o}^{t}-T_{eng}^{t}) \qquad \text{(III-11)}$$

$$[MC]_{HX}\frac{T_{cw,o}^{t+\Delta t}-T_{cw,o}^{t}}{\Delta t} = [\dot{m}^{t+\Delta t}C_{p}^{t+\Delta t}]_{cw}(T_{cw,i}^{t+\Delta t}-T_{cw,o}^{t+\Delta t}) - UA_{HX}(T_{cw,o}^{t+\Delta t}-T_{eng}^{t+\Delta t}) \qquad \text{(III-12)}$$

The forward- and backward-difference approximations for each of the two state-space equations can be combined by i) multiplying the forward-difference approximation by coefficient α, ii) multiplying the backward-difference approximation by coefficient $(1-\alpha)$, and iii) summing the forward- and backward-difference approximations. The combined forward- and backward-difference approximation of the engine control volume state equation (Equation III-10 in the model specification) is:

$$\begin{aligned}[MC]_{eng}\frac{T_{eng}^{t+\Delta t}-T_{eng}^{t}}{\Delta t} = (1-\alpha)\Big(&UA_{HX}(T_{cw,o}^{t}-T_{eng}^{t}) \\ &UA_{loss}(T_{room}^{t}-T_{eng}^{t})+q_{gen,ss}^{t}\Big) \\ +\alpha\Big(&UA_{HX}(T_{cw,o}^{t+\Delta t}-T_{eng}^{t+\Delta t}) \\ &+UA_{loss}(T_{room}^{t+\Delta t}-T_{eng}^{t+\Delta t})+q_{gen,ss}^{t+\Delta t}\Big)\end{aligned} \tag{III-13}$$

and the combined forward- and backward-difference approximation of the cooling water control volume state equation (Equation III-11 in the model specification) is:

$$\begin{aligned}[MC]_{HX}\frac{T_{cw,o}^{t+\Delta t}-T_{cw,o}^{t}}{\Delta t} = (1-\alpha)\Big(&[\dot{m}^{t}C_{p}^{t}]_{cw}(T_{cw,i}^{t}-T_{cw,o}^{t}) \\ &-UA_{HX}(T_{cw,o}^{t}-T_{eng}^{t})\Big) \\ +\alpha\Big(&[\dot{m}^{t+\Delta t}C_{p}^{t+\Delta t}]_{cw}(T_{cw,i}^{t+\Delta t}-T_{cw,o}^{t+\Delta t}) \\ &-UA_{HX}(T_{cw,o}^{t+\Delta t}-T_{eng}^{t+\Delta t})\Big)\end{aligned} \tag{III-14}$$

Coefficient α allows the respective weight of the forward- and backward-difference terms in Equations III-13 and III-14 to be adjusted. Setting α to 1.0 yields a fully implicit solution based entirely on the backward-difference taken at time $t+\Delta t$, while a value of 0.5 provides the well-known Crank-Nicolson solution scheme.

Equations III-13 and III-14 can be rewritten in matrix form as follows:

$$\begin{vmatrix} a_{11} & a_{12} & a_{13} \\ a_{21} & a_{22} & a_{23} \end{vmatrix} \begin{vmatrix} {T_{eng}}^{t+\Delta t} \\ {T_{cw,o}}^{t+\Delta t} \\ {T_{cw,i}}^{t+\Delta t} \end{vmatrix} = \begin{vmatrix} R_1 \\ R_2 \end{vmatrix} \tag{III-15}$$

Where:

$$a_{11} = \frac{[MC]_{eng}}{\Delta t} + \alpha(UA_{HX} + UA_{loss}) \tag{III-16}$$

$$a_{12} = -\alpha UA_{HX} \tag{III-17}$$

$$a_{13} = 0 \tag{III-18}$$

$$a_{21} = -\alpha UA_{HX} \tag{III-19}$$

$$a_{22} = \frac{[MC]_{HX}}{\Delta t} + \alpha\left(UA_{HX} + [\dot{m}^{t+\Delta t} C_p^{t+\Delta t}]_{cw}\right) \tag{III-20}$$

$$a_{23} = -\alpha[\dot{m}^{t+\Delta t} C_p^{t+\Delta t}]_{cw} \tag{III-21}$$

$$\begin{aligned} R_1 = {} & \frac{[MC]_{eng}}{\Delta t} T_{eng}^t \\ & + (1-\alpha)\left(UA_{HX}(T_{cw,o}^t - T_{eng}^t) + UA_{loss}(T_{room}^t - T_{eng}^t) + q_{gen,ss}^t\right) \\ & + \alpha\left(q_{gen,ss}^{t+\Delta t} + UA_{loss} T_{room}^{t+\Delta t}\right) \end{aligned} \tag{III-22}$$

$$\begin{aligned} R_2 = {} & \frac{[MC]_{HX}}{\Delta t} T_{cw,o}^t \\ & + (1-\alpha)\left([\dot{m}^t C_p^t]_{cw}(T_{cw,i}^t - T_{cw,o}^t) - UA_{HX}(T_{cw,o}^t - T_{eng}^t)\right) \end{aligned} \tag{III-23}$$

The equation set described by Equation III-15 can be incorporated into a global linear state-space matrix describing the behaviour of the entire building mechanical plant and solved to determine the future time row temperatures (including $T_{eng}^{t+\Delta t}$, $T_{cw,o}^{t+\Delta t}$, and $T_{cw,i}^{t+\Delta t}$). Alternatively, the linearized equation set can be solved directly provided future cooling water inlet temperature is known.

Like the EnergyPlus implementation, the ESP-r/TRNSYS implementation predictions approach the actual solution of the state space equations as the time-step duration approaches zero. When configured using a practical time step duration, these implementations only provide approximations to the true solution of the state equations.

Effects of time step duration

To explore the sensitivity of the model predictions of the time step duration, independent

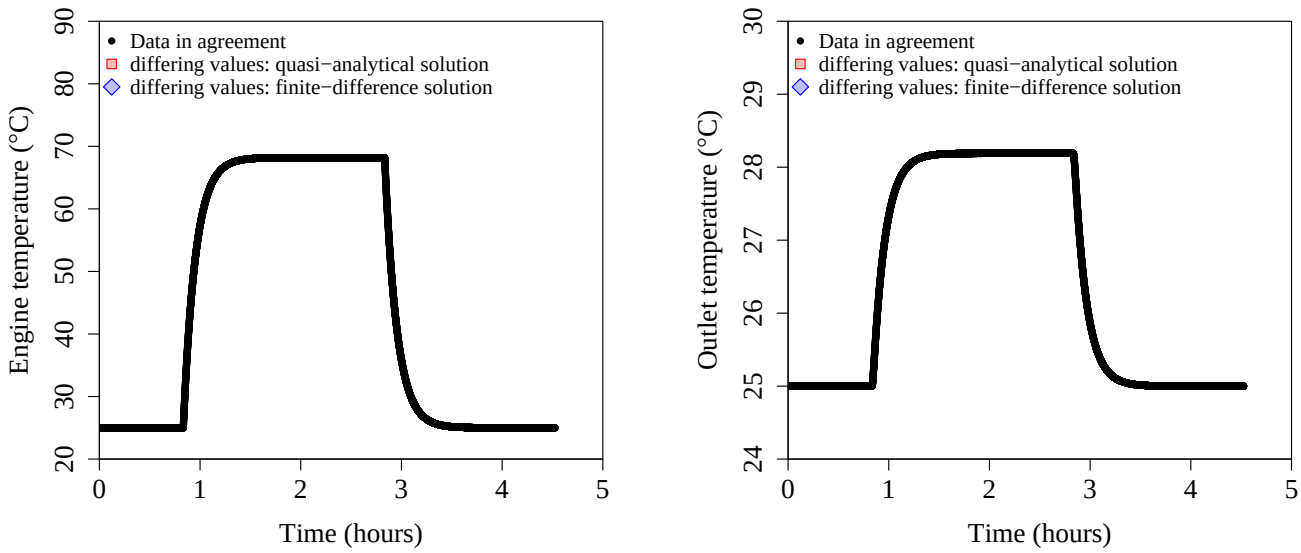

(a) (b)

Figure III-19: Test case 301 results — a) engine temperature (T_{eng}), and b) cooling water outlet temperature ($T_{cw,o}$) predicted by quasi-analytical and forward-difference solutions at one-second time steps

implementations to the quasi-analytical (QA) and finite-difference (FD) solutions used in EnergyPlus and ESP-r/TRNSYS were developed. Whereas the EnergyPlus, ESP-r and TRNSYS implementations are restricted in their minimum time step duration, these independent implementations support arbitrarily small time resolutions.

First, the QA and FD implementations configured to use a ten-minute (or 600-second) time step. At this time resolution, the QA implementation exactly reproduced the EnergyPlus predictions for test case 301, while the FD implementation exactly reproduced the ESP-r and TRNSYS results. Therefore, the independent QA and FD implementations were deemed to faithfully reproduce the EnergyPlus, ESP-r and TRNSYS numerical algorithms.

Next, the time step duration used in the QA and FD implementations was reduced to one-second. Figure III-19 plots the engine and cooling water outlet temperatures predicted by the QA and FD implementations. In both cases, the QA and FD implementations agree ex-

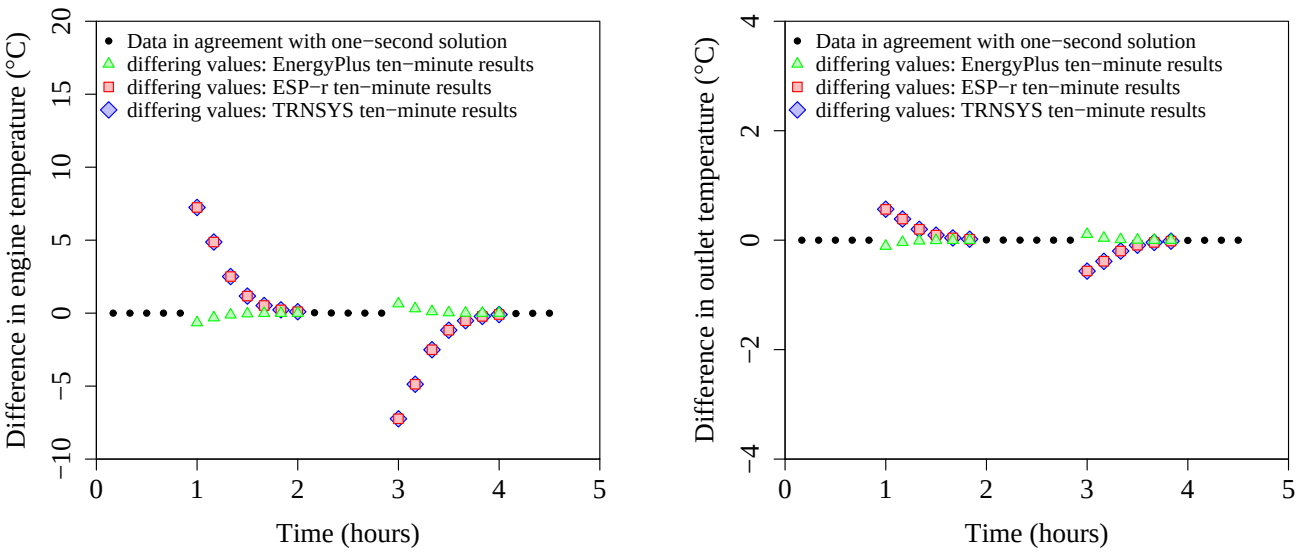

(a) (b)

Figure III-20: Test case 301 results — comparison between one-second and ten-minute results for a) engine temperature (T_{eng}), and b) cooling water outlet temperature ($T_{cw,o}$)

actly. While these algorithms still only approximate the true solution of the state equations, the agreement achieved between the QA and FD approximations suggests the true solution lies very near to the points in Figure III-19.

Finally, the ten-minute EnergyPlus, ESP-r and TRNSYS results were compared to the one-second QA and FD solutions. Differences in the predicted engine and cooling water outlet temperatures are plotted in Figure III-20.

Clearly, increasing the time step duration significantly affects the ESP-r and TRNSYS results. Just after activation of the unit, the engine temperature predicted by ESP-r/TRNSYS differs from the one-second solution by nearly 8 °C, and the predicted cooling water outlet temperature differs by nearly 1 °C. These data suggest a ten-minute time step is really too large to accurately characterize the transient behaviour in the 300-series test cases. Fortunately, both ESP-r and TRNSYS support simulations with time steps as small as one-

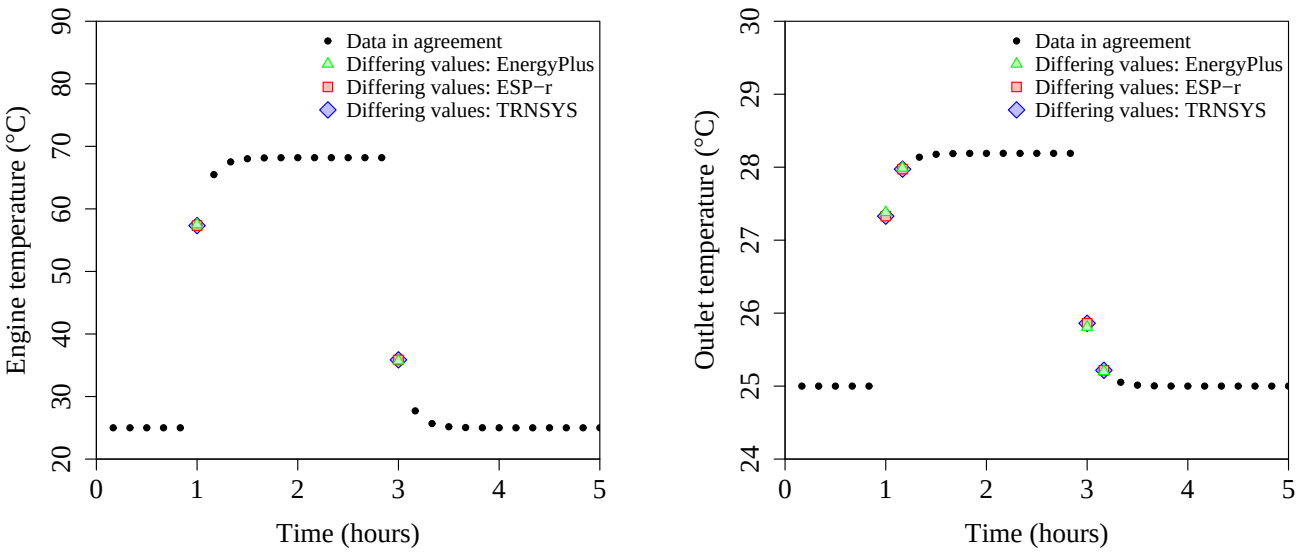

Figure III-21: Test case 301 results — (a) engine temperature (T_{eng}) and (b) cooling water temperature ($T_{cw,o}$) from one-minute EnergyPlus results and one-second ESP-r and TRNSYS results

second.

The EnergyPlus results are significantly less sensitive to the time-step duration, and the EnergyPlus algorithm better approximates the true solution of the state equations at a ten-minute time step. Since this comparative testing study was undertaken, support for one-minute time steps has been added to EnergyPlus, making even more accurate estimates available.

Figure III-21 plots the engine and cooling water outlet temperatures obtained from an one-minute resolution EnergyPlus simulation, and one-second resolution ESP-r and TRNSYS simulations. Similarly, Figure III-22 plots the predicted rates of heat transfer and heat loss from the same simulations. The plots show significantly improved agreement between the implementations.

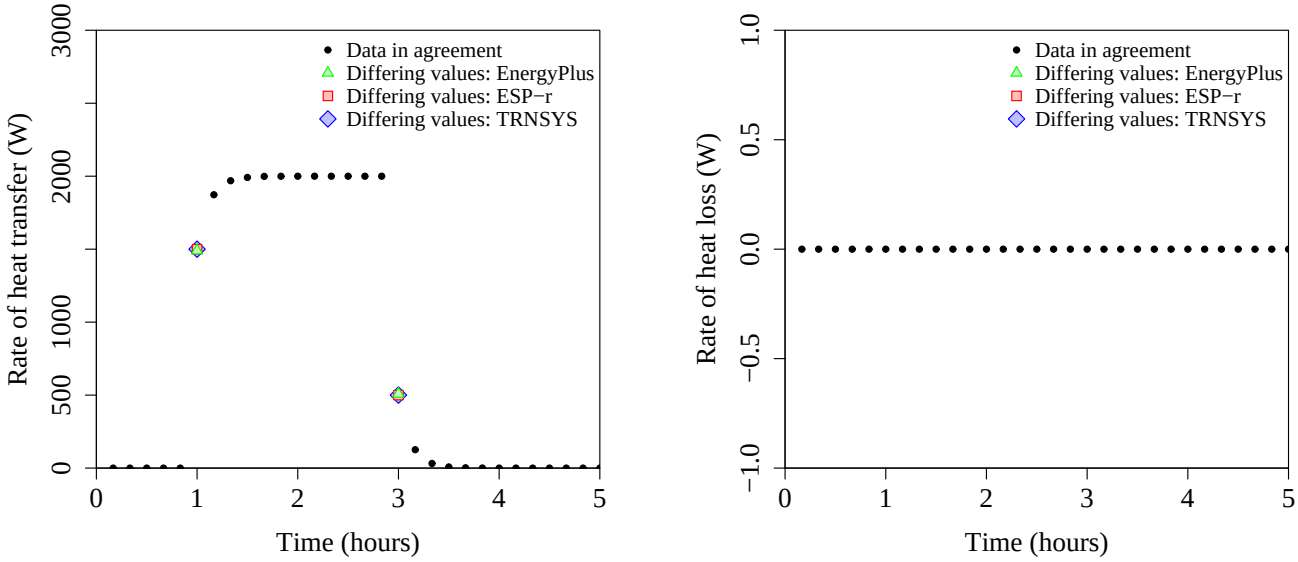

Figure III-22: Test case 301 results — rates of (a) heat transfer (q_{HX}) and (b) heat loss (q_{loss}) from one-minute EnergyPlus results and one-second ESP-r and TRNSYS results

Given the sensitivity of the ESP-r and TRNSYS results to time step duration, these implementations were configured to use a one-second time step for the remainder of the 300 series tests. Although support has recently been added for one-minute simulations in EnergyPlus, time constraints precluded repeating the 300 series tests with a one-minute EnergyPlus time step.

Test case 302

Test case 302 draws upon the same model configuration as test case 301, but subjects the model to a step change in cooling water temperature instead of the change in operating point used in test case 301. In test case 302, the model is configured to operate at a constant 500 W electric output. The cooling water temperature is varied from 25 °C to 50 °C two hours into the test, and then returned to 25 °C two hours later. The flow rate of cooling water provided to the device and the temperature of the enclosure are maintained at constant values. In this configuration, heat transfer between the model and the enclosure is eliminated by setting the coefficient of heat loss between the model's engine control volume and the surroundings to zero.

The following test case 302 results should be plotted against time:

- The rate of heat transfer (q_{HX})
- The rate of heat loss (q_{loss})
- The engine control volume temperature (T_{eng})
- The cooling water control volume outlet temperature ($T_{cw,o}$)

Disagreement in the case 302 results may indicate an error in the heat recovery or heat loss equations (Equations III-8 and III 9 in the model specification), or in the general solution of the dynamic thermal model (Equations III-10 and III-11).

Figure III-24 plots the engine and cooling water outlet temperatures over the course of he test. As in test case 301, the EnergyPlus implementation predicts a faster system response than the ESP-r/TRNSYS implementations. And as in case 301, this disagreement is attributable to the different approaches used to solve the dynamic thermal model's state-space equations.

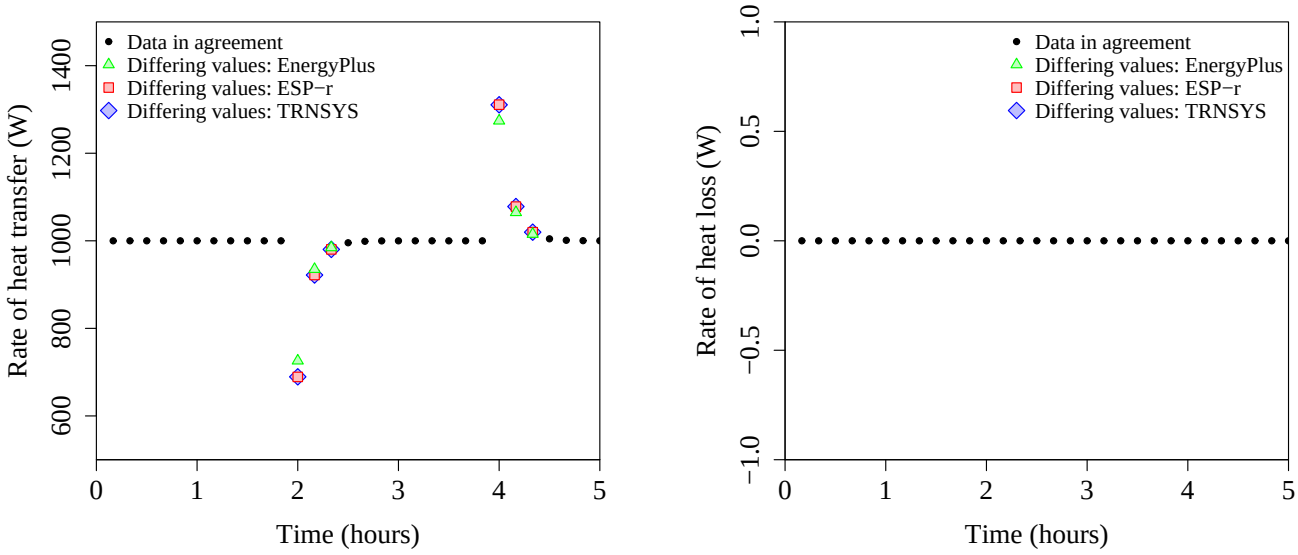

Figure III-23: Test case 302 results — rates of (a) heat transfer (q_{HX}) and (b) heat loss (q_{loss}) as functions of time

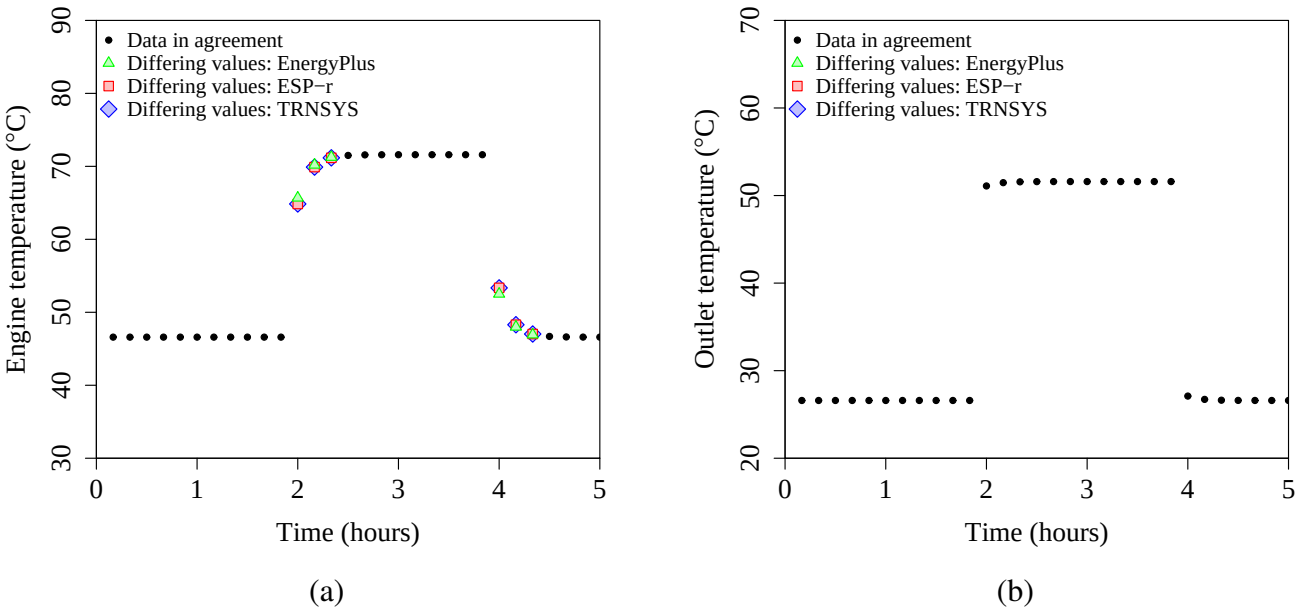

Figure III-24: Test case 302 results — (a) engine temperature (T_{eng}) and (b) cooling water temperature ($T_{cw,o}$) as functions of time

Figure III-23 plots the rates of transfer and heat loss over the course of the simulation. The models predict similar rates of heat transfer, although again the response predicted by the EnergyPlus implementation is again slightly faster. None of the models predict any heat loss from the unit.

Test case 303

Test case 303 draws upon the same model configuration as test case 301, but subjects the model to a step change in cooling flow rate instead of the change in operating point used in test case 301. In test case 303, the model is configured to operate at a constant 500 W electric output. The cooling water flow rate is reduced from 0.15 kg/s to 0.015 kg/s two hours into the test, and then returned to 0.15 kg/s two hours later. The temperature of cooling water provided to the device and the temperature of the enclosure are maintained at constant values. In this configuration, heat transfer between the model and the enclosure is eliminated by setting the coefficient of heat loss between the model's engine control volume and the surroundings to zero.

The following test case 303 results should be plotted against time:

- The rate of heat transfer (q_{HX})
- The rate of heat loss (q_{loss})
- The engine control volume temperature (T_{eng})
- The cooling water control volume outlet temperature ($T_{cw,o}$)

Disagreement in the case 303 results may indicate an error in the heat recovery or heat loss equations (Equations 8 and 9 in the model specification), or in the general solution of the dynamic thermal model (Equations 10 and 11).

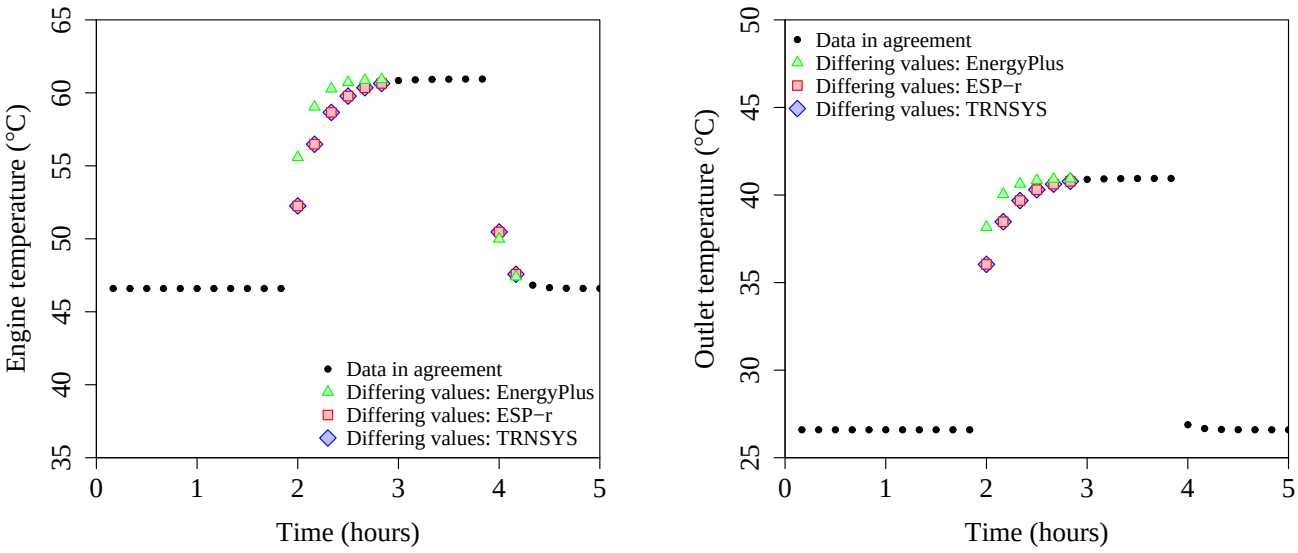

(a) (b)

Figure III-25: Test case 303 results — (a) engine temperature (T_{eng}) and (b) cooling water temperature ($T_{cw,o}$) as functions of time

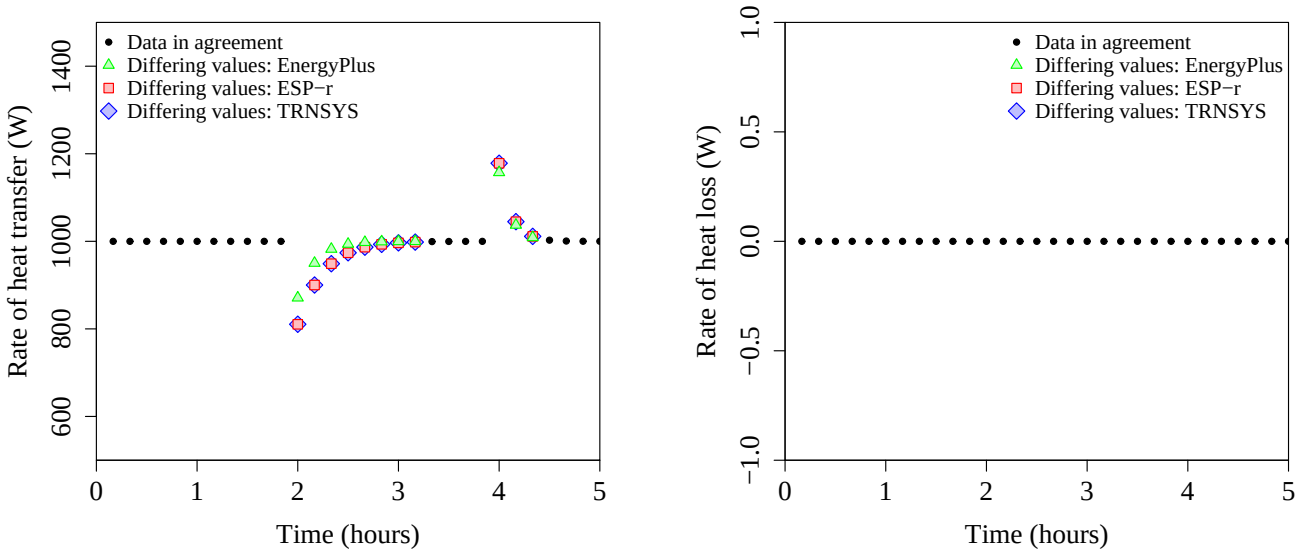

(a) (b)

Figure III-26: Test case 303 results — rates of (a) heat transfer (q_{HX}) and (b) heat loss (q_{loss}) as functions of time

Figure III-25 plots the engine and cooling water outlet temperatures over the duration of the simulation, while Figure III-26 plots the rates of heat transfer and heat loss. The model implementations made similar predictions, although once again, the EnergyPlus predicts a faster response for the reasons discussed in test case 301.

Test case 304

Test case 304 is identical to test case 301, but the thermal mass of the engine control volume is doubled from 20 000 J/K to 40 000 J/K. The following test case 304 results should be plotted against time:

- The difference between the rates of heat transfer calculated in test cases 304 and 301 ($q_{HX,304} - q_{HX,301}$)
- The difference between the rates of heat loss calculated in test cases 304 and 301 ($q_{loss,304} - q_{loss,301}$)
- The difference between the engine control volume temperatures calculated in test cases 304 and 301 ($T_{eng,304} - T_{eng,301}$)
- The difference between the cooling water control volume outlet temperatures calculated in test cases 304 and 301 ($T_{cw,o,304} - T_{cw,o,301}$)

Disagreement in these results suggests an error in the treatment of the engine control volume thermal mass, or the implementation of the engine control volume state equation (Equation III-10 in the model specification).

Figure III-27 plots the engine temperatures (T_{eng}) predicted by EnergyPlus, ESP-r and TRNSYS, while Figure III-28 plots the cooling water outlet temperature predictions. Although differences in the numerical solution of the model state equations produce some

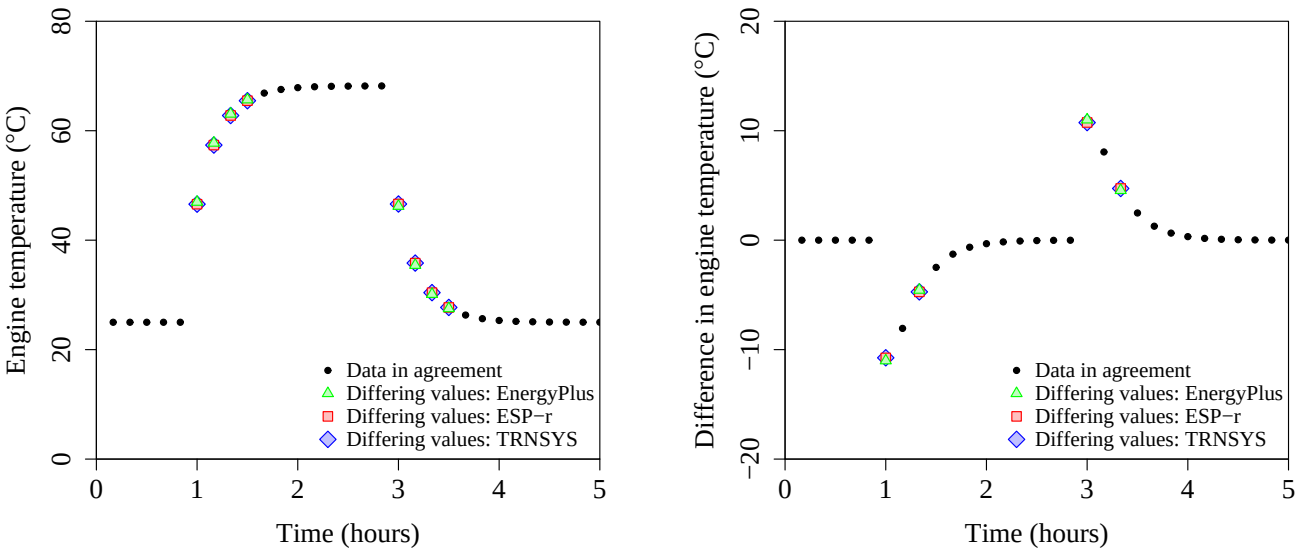

Figure III-27: Test case 304 results — engine temperature (T_{eng}) as a function of time for (a) case 304 and (b) differential between cases 304 and 301 ($T_{eng,304} - T_{eng,301}$)

disparity, the predictions generally agree well. In particular, the differences between case 304 and 301 predictions (ie $T_{eng,304} - T_{eng,301}$ and $T_{cw,o,304} - T_{cw,o,301}$) show similar behaviour, suggesting variations in the engine control volume thermal mass affect all three implementations equally.

Figures III-29 and III-30 compare the predicted rates of heat transfer (q_{HX}) and heat loss (q_{loss}). Again, agreement between the three implementations is excellent.

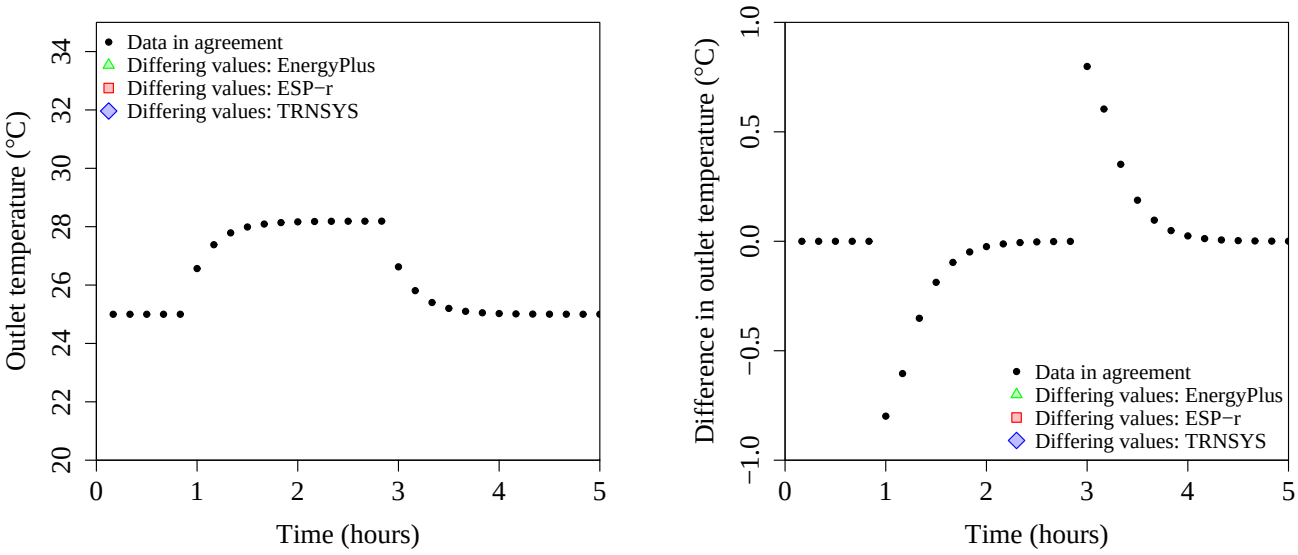

Figure III-28: Test case 304 results — cooling water outlet temperature ($T_{cw,o}$) as a function of time for (a) case 304 and (b) differential between cases 304 and 301 ($T_{cw,o,304} - T_{cw,o,301}$)

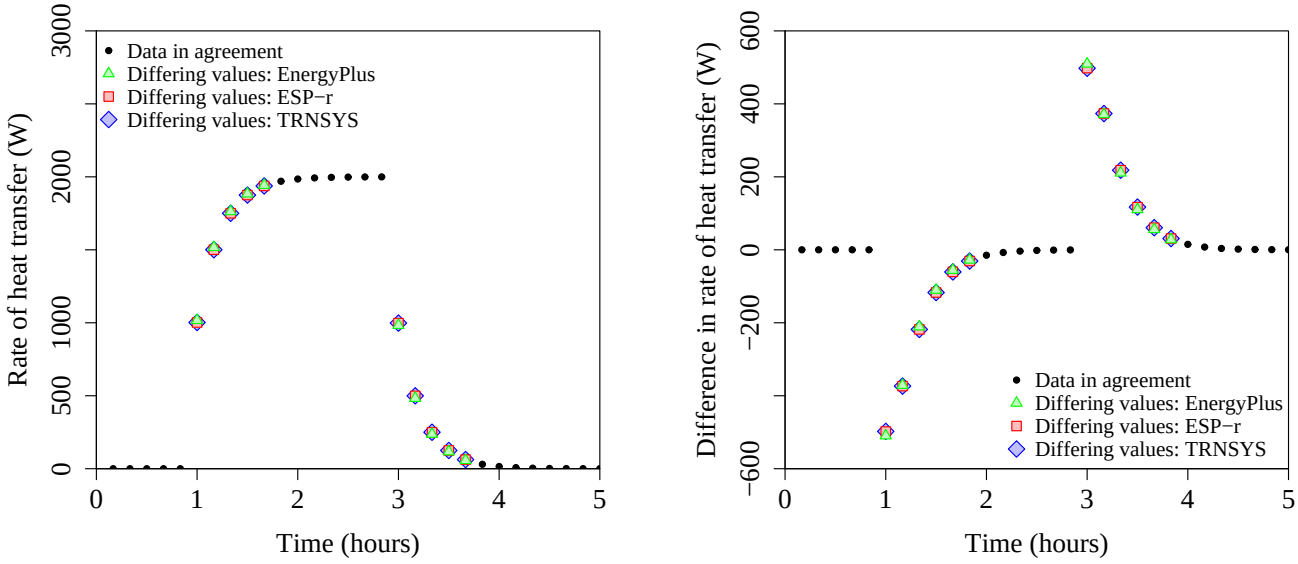

(a) (b)

Figure III-29: Test case 304 results — heat transfer rate (q_{HX}) as a function of time for (a) case 304 and (b) differential between cases 304 and 301 ($q_{HX,304} - q_{HX,301}$)

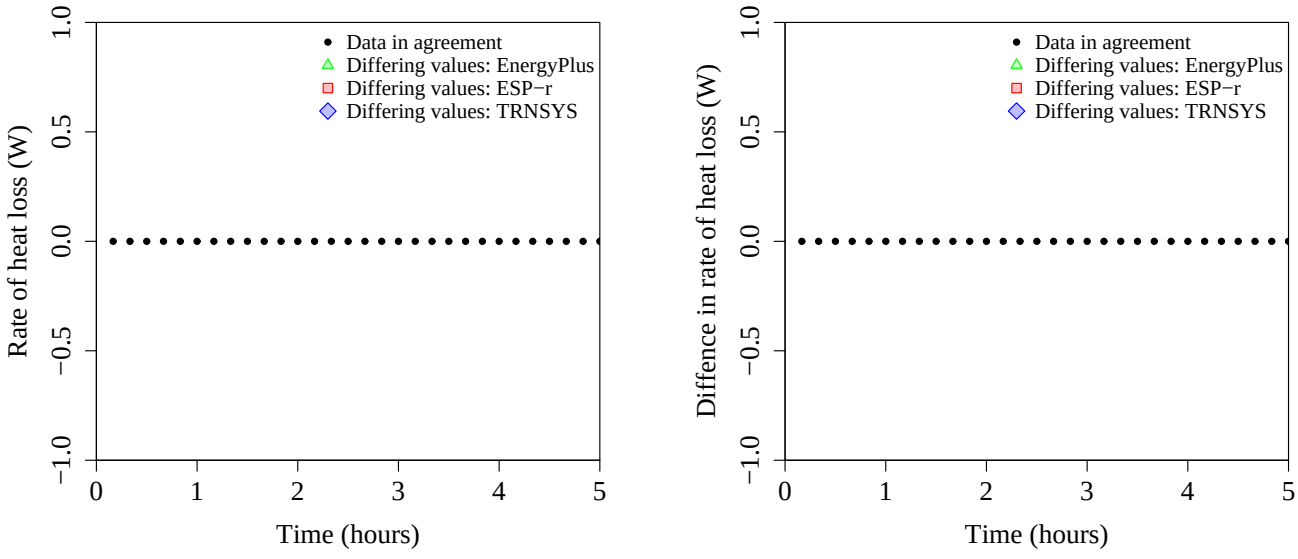

(a) (b)

Figure III-30: Test case 304 results — heat loss rate (q_{loss}) as a function of time for (a) case 304 and (b) differential between cases 304 and 301 ($q_{loss,304} - q_{loss,301}$)

Test case 305

Test case 305 is identical to test case 301, but the thermal mass of the cooling water control volume is doubled from 20 000 J/K to 40 000 J/K. The following test case 305 results should be plotted against time:

- The difference between the rates of heat transfer calculated in test cases 305 and 301 ($q_{HX,305} - q_{HX,301}$)
- The difference between the rates of heat loss calculated in test cases 305 and 301 ($q_{loss,305} - q_{loss,301}$)
- The difference between the engine control volume temperatures calculated in test cases 305 and 301 ($T_{eng,305} - T_{eng,301}$)
- The difference between the cooling water control volume outlet temperatures calculated in test cases 305 and 301 ($T_{cw,o,305} - T_{cw,o,301}$)

Disagreement in these results suggests an error in the treatment of the cooling water control volume thermal mass, or the implementation of the cooling water control volume state equation (Equation III-11 in the model specification).

Figure III-31 plots the predicted engine control volume temperature for test case 305, while Figure III-32 plots the predicted cooling water outlet temperature and Figure III-33 plots the predicted rate of heat transfer. As in the 301–305 test cases, the EnergyPlus implementation predicts a slightly faster response than ESP-r and TRNSYS, and the dissimilar solutions of the model state equations undoubtedly contribute to this difference.

But the differentials between the test case 305 and 301 (that is, $q_{HX,305} - q_{HX,301}$, $q_{loss,305} - q_{loss,301}$, $T_{eng,305} - T_{eng,301}$ and $T_{cw,o,305} - T_{cw,o,301}$) suggest another factor contributes to the disagreement between EnergyPlus and ESP-r/TRNSYS. Increasing the cooling water

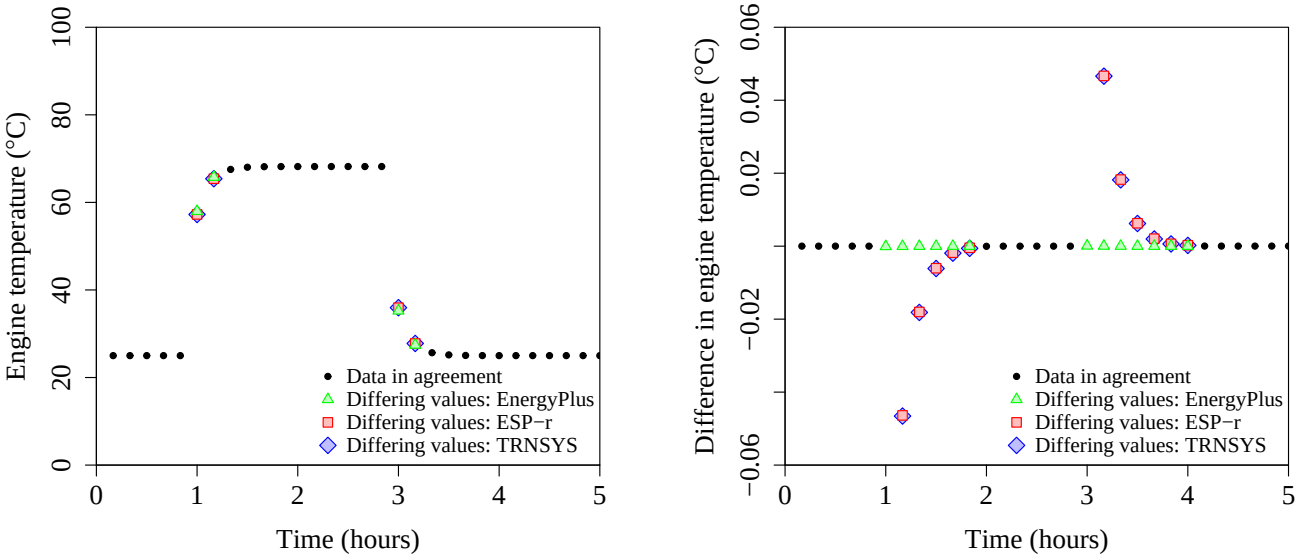

Figure III-31: Test case 305 results — engine temperature (T_{eng}) as a function of time for (a) case 305 and (b) differential between cases 305 and 301 ($T_{eng,305} - T_{eng,301}$)

control volume thermal mass clearly does not affect the EnergyPlus implementation to the same degree as ESP-r/TRNSYS.

The source of this disagreement remains undiagnosed. Ongoing testing efforts hope to identify and remedy the cause of this discrepancy in the near future.

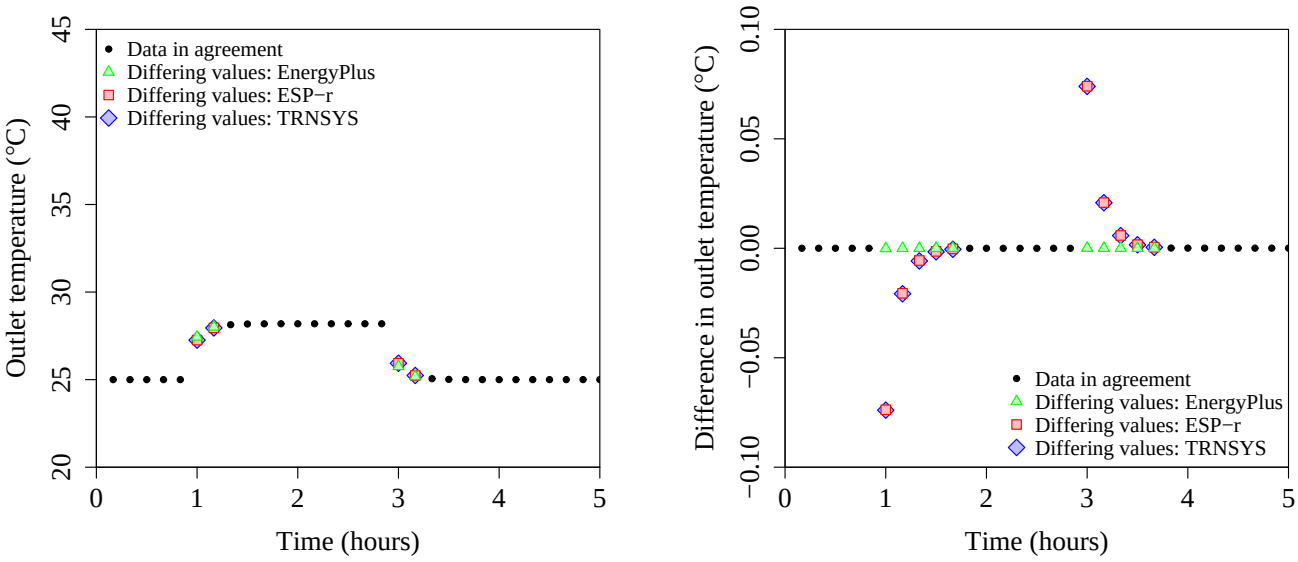

Figure III-32: Test case 305 results — cooling water outlet temperature ($T_{cw,o}$) as a function of time for (a) case 305 and (b) differential between cases 305 and 301 ($T_{cw,o,305} - T_{cw,o,301}$)

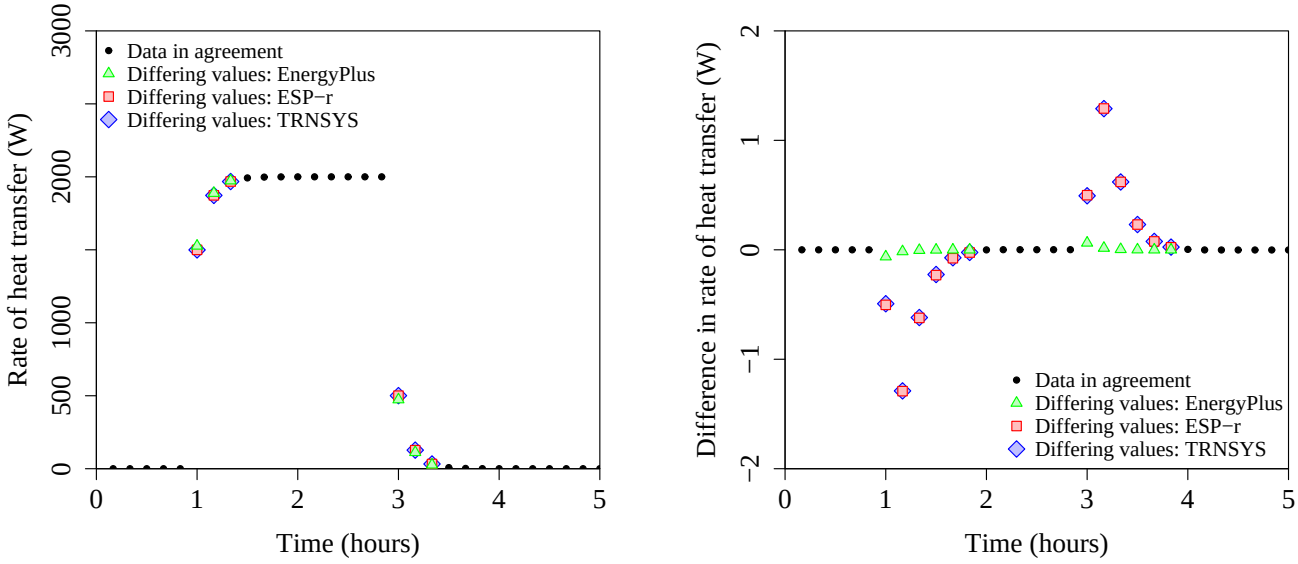

(a) (b)

Figure III-33: Test case 305 results — heat transfer rate (q_{HX}) as a function of time for (a) case 305 and (b) differential between cases 305 and 301 ($q_{HX,305} - q_{HX,301}$)

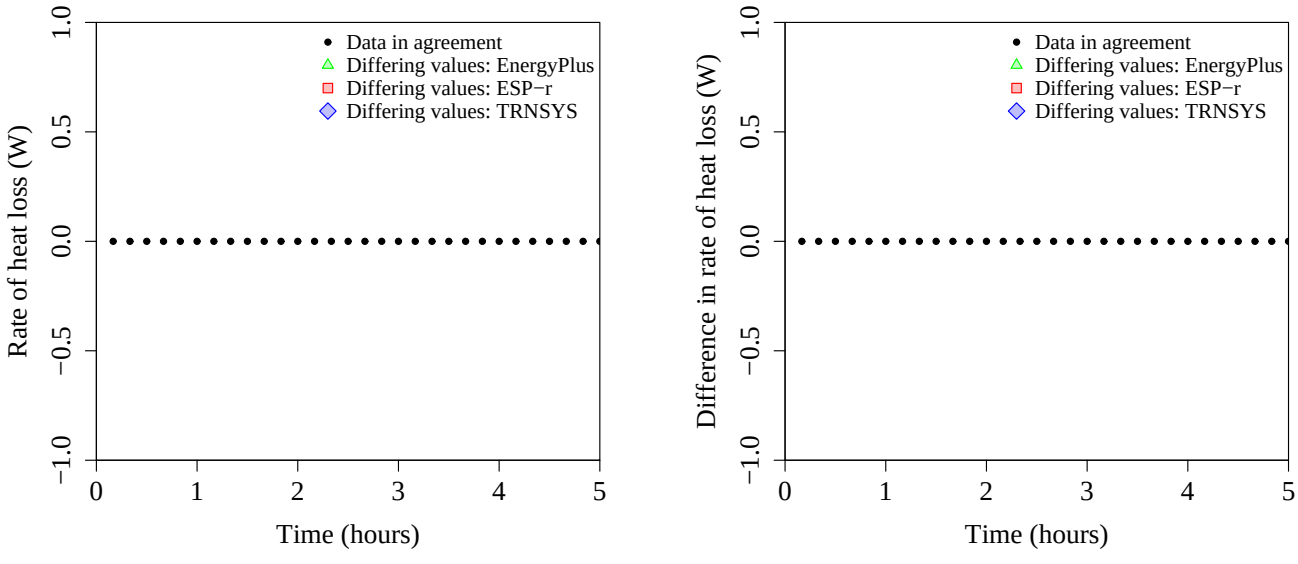

(a) (b)

Figure III-34: Test case 305 results — heat loss rate (q_{loss}) as a function of time for (a) case 305 and (b) differential between cases 305 and 301 ($q_{loss,305} - q_{loss,301}$)

Test case 306

Test case 306 is identical to test case 301, but the coefficient of heat transfer between the engine and cooling water control volumes is doubled from 50 W/K to 100 W/K. The following test case 306 results should be plotted against time:

- The difference between the rates of heat transfer calculated in test cases 306 and 301 ($q_{HX,306} - q_{HX,301}$)
- The difference between the rates of heat loss calculated in test cases 306 and 301 ($q_{loss,306} - q_{loss,301}$)
- The difference between the engine control volume temperatures calculated in test cases 306 and 301 ($T_{eng,306} - T_{eng,301}$)
- The difference between the cooling water control volume outlet temperatures calculated in test cases 306 and 301 ($T_{cw,o,306} - T_{cw,o,301}$)

Disagreement in these results suggests an error in the treatment of the heat transfer coefficient, or the calculation of heat transfer (Equations III-8 and III-9 in the model specification).

Figure III-35 plots the predicted engine control volume temperatures for test case 306, and Figure III-36 plots the predicted cooling water outlet temperatures. The predictions of the three implementations agree well, although the different solution strategies discussed in test case 301 result in some variation between the EnergyPlus and ESP-r/TRNSYS results.

Figures III-37 and III-38 plot the predicted rates of heat transfer and heat loss for test case 306. The agreement between the predicted rates of heat transfer is excellent, and none of the models predict any heat loss from the engine control volume.

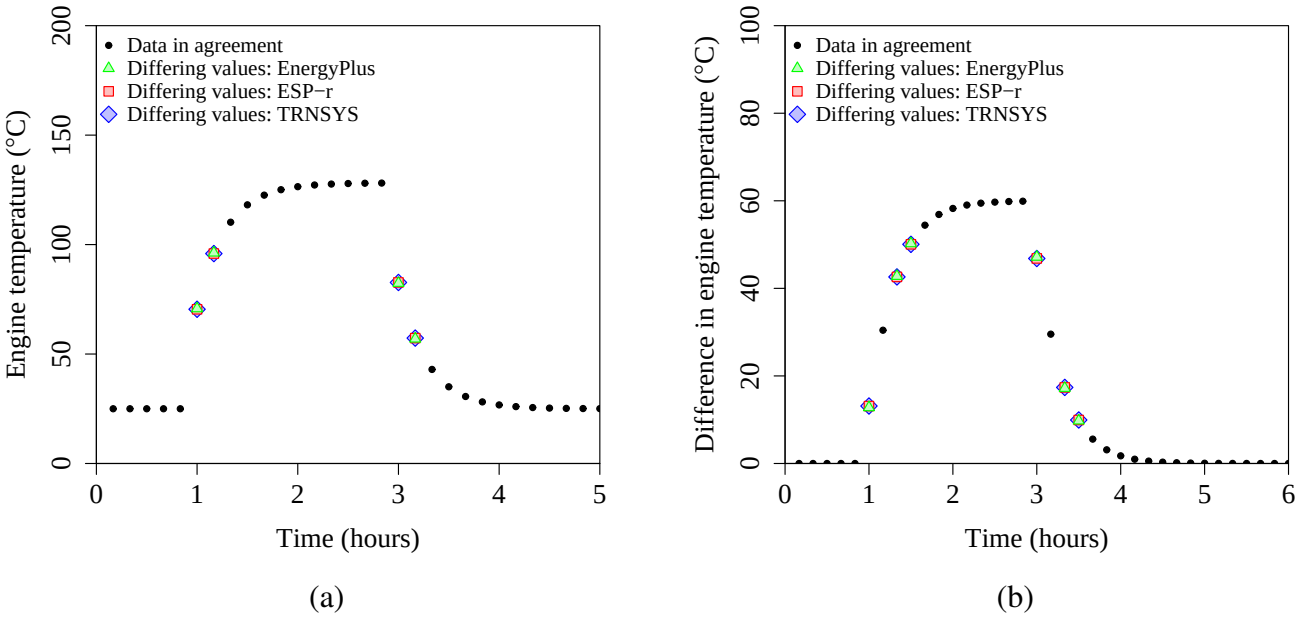

Figure III-35: Test case 306 results — engine temperature (T_{eng}) as a function of time for (a) case 306 and (b) differential between cases 306 and 301 ($T_{eng,306} - T_{eng,301}$)

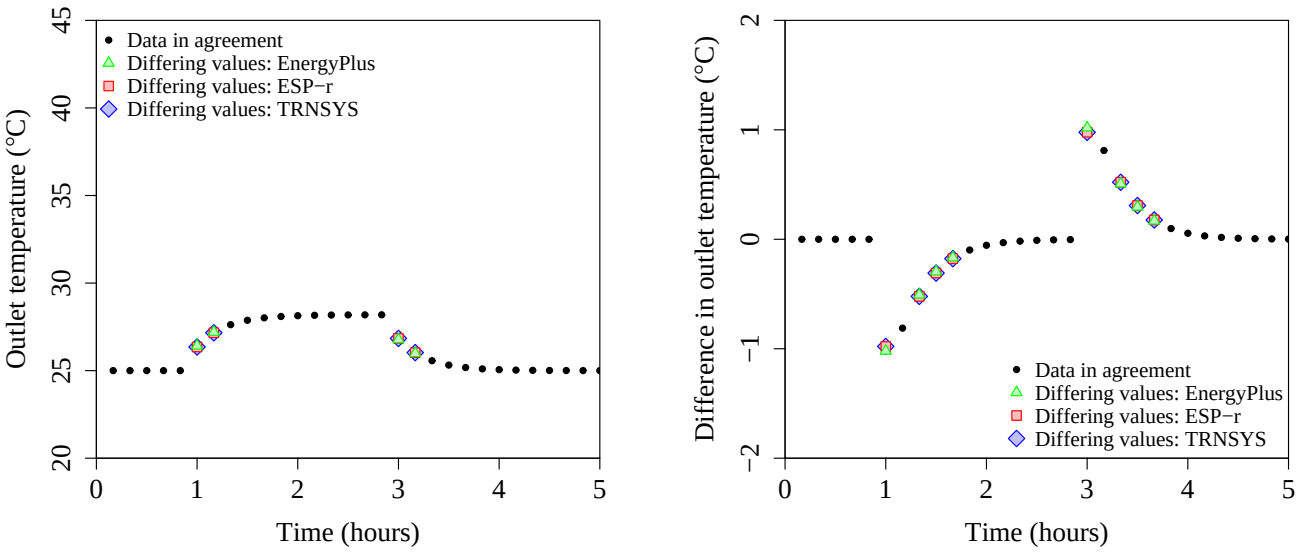

Figure III-36: Test case 306 results — cooling water outlet temperature ($T_{cw,o}$) as a function of time for (a) case 306 and (b) differential between cases 306 and 301 ($T_{cw,o,306} - T_{cw,o,301}$)

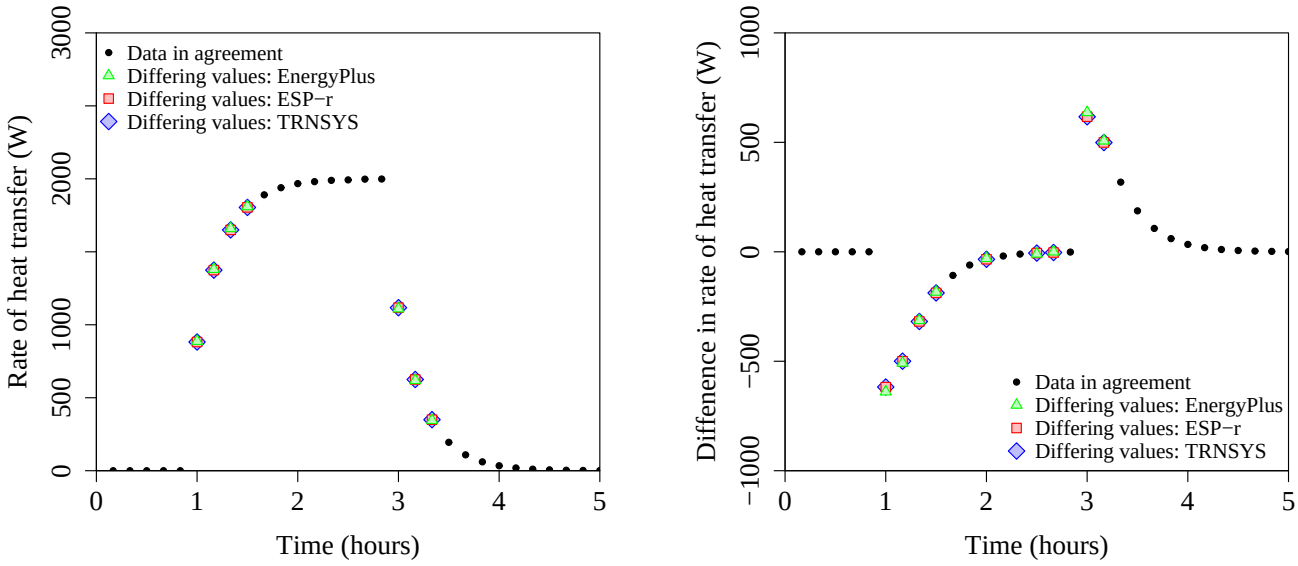

(a) (b)

Figure III-37: Test case 306 results — heat transfer rate (q_{HX}) as a function of time for (a) case 306 and (b) differential between cases 306 and 301 ($q_{HX,306} - q_{HX,301}$)

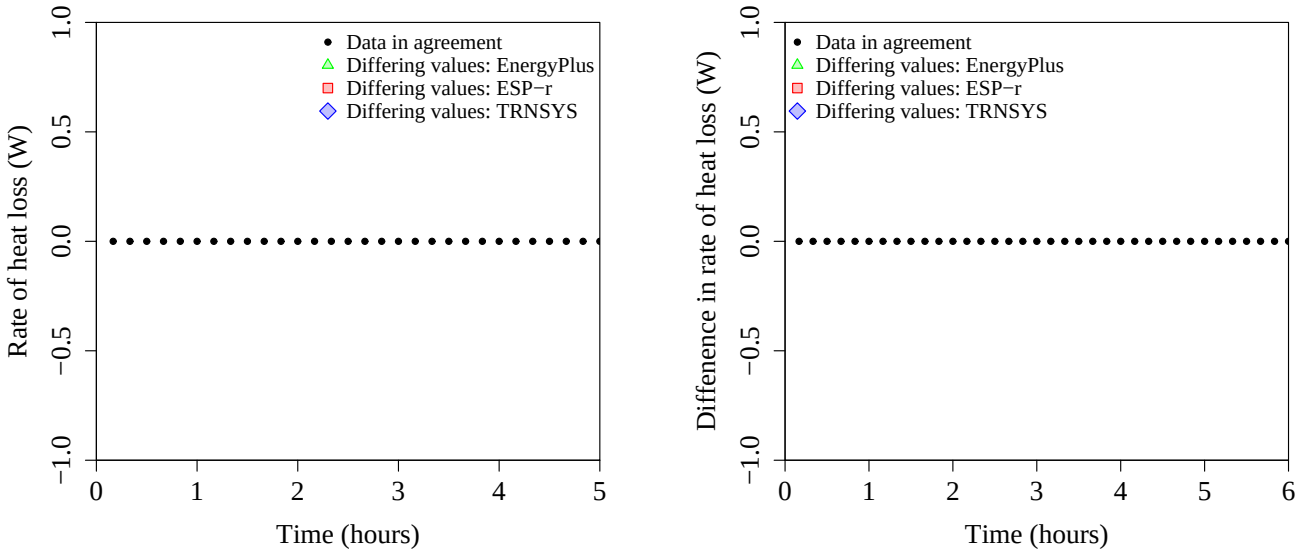

(a) (b)

Figure III-38: Test case 306 results — heat loss rate (q_{loss}) as a function of time for (a) case 306 and (b) differential between cases 306 and 301 ($q_{loss,306} - q_{loss,301}$)

Test case 307

Test case 307 exercises the dynamic thermal model's treatment of heat loss to the surroundings. The model is configured to operate at a constant 1000 W electric output, and is supplied with cooling water at constant temperature and flow rate. The model is deactivated two hours into the test, and the flow of cooling water interrupted 20 minutes later. For the remainder of the test, the model's engine control volume cools as it exchanges heat with the enclosure.

Test case 307 uses the base case model inputs, except the coefficient of heat transfer between the engine and surroundings is increased from 0 W/K to 10 W/K. The enclosure temperature is maintained at a constant 20 °C throughout the simulation.

The following test case 307 results should be plotted against time:

- The rate of heat transfer (q_{HX})
- The rate of heat loss (q_{loss})
- The engine control volume temperature (T_{eng})
- The cooling water control volume outlet temperature ($T_{cw,o}$)

Notwithstanding possible errors identified in test cases 301–306, disagreement in these results suggests an error in the model's treatment of the heat loss coefficient, enclosure temperature or the calculation of heat loss (Equation III-9 in the model specification).

Figure III-39 plots the predicted engine control volume and cooling water outlet temperatures for test case 307. For the same reasons discussed in test case 301, the EnergyPlus implementation predicts a faster response than the ESP-r/TRNSYS implementations. In this case, the numerical differences between the ten-minute EnergyPlus simulation and the

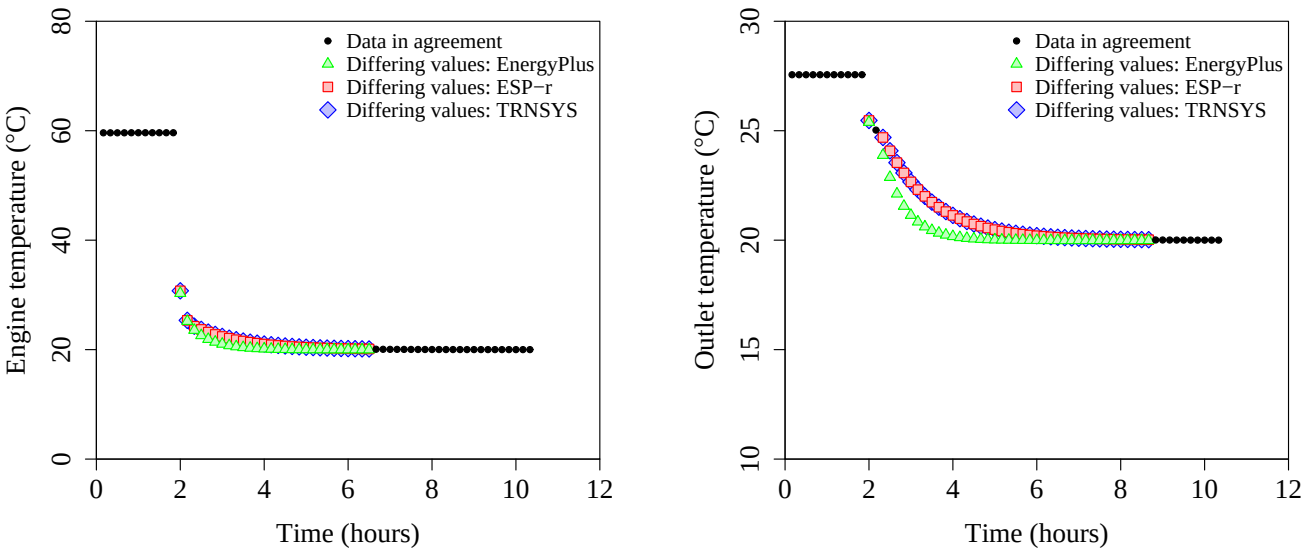

Figure III-39: Test case 307 results — (a) engine temperature (T_{eng}), and (b) cooling water temperature ($T_{cw,o}$) as functions of time

one-second ESP-r/TRNSYS simulations produce more noticeable variation in disagreement. Increasing the EnergyPlus time resolution to one-minute might provide better agreement with the one-second ESP-r and TRNSYS solutions. Unfortunately, insufficient time was available to revisit this test case with EnergyPlus.

Figure III-40 plots the predicted rates of heat transfer and heat loss in test case 307. Again, the EnergyPlus predictions exhibit a slightly faster response. But careful examination of the results indicates that the EnergyPlus results actually lag the ESP-r/TRNSYS results by one time step when the engine is deactivated two hours into the test. Whereas the ESP-r and TRNSYS implementations predict an immediate reduction in the rate of heat loss from the surroundings, EnergyPlus reports that the rate of heat loss will remain unchanged until the following time step.

These results do not indicate an error in EnergyPlus. By design, EnergyPlus models all flux

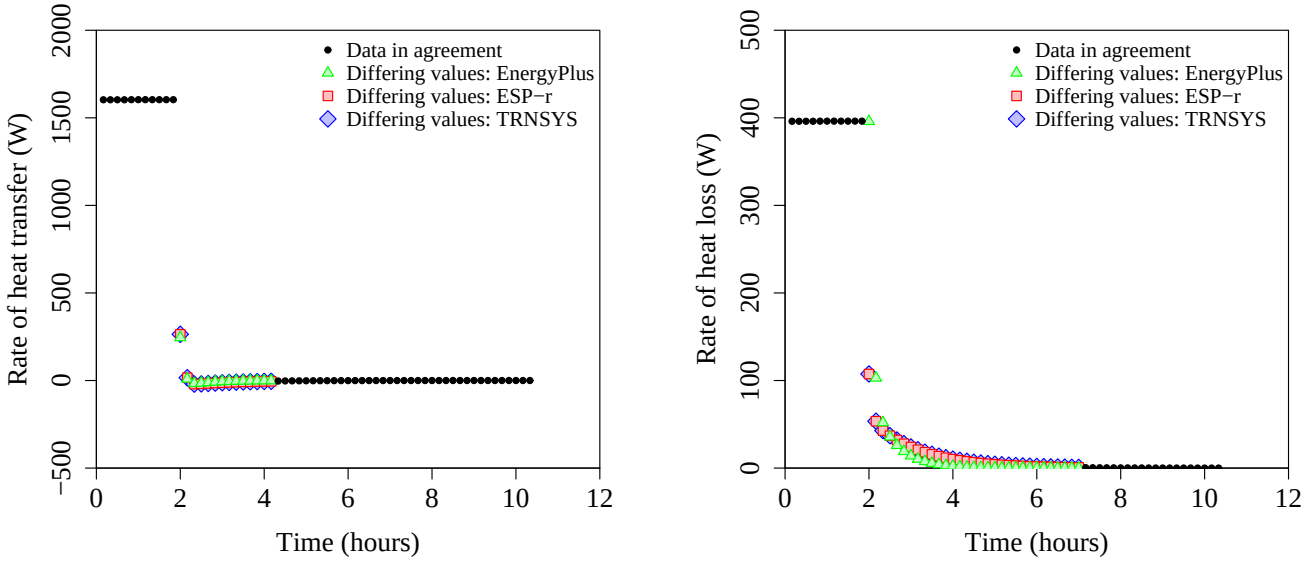

Figure III-40: Test case 307 results — (a) rate of heat transfer (q_{HX}) and (b) rate of heat loss (q_{loss}) as functions of time

interactions between the mechanical plant and zone one time step in arrears of the mechanical plant solution. Thus, even though the EnergyPlus implementation of the Annex 42 combustion cogeneration model predicted a similar rate of heat loss to that reported by ESP-r and TRNSYS upon deactivation of the unit, this change in heat loss was no reflected in the zone energy balance or EnergyPlus output until the following time step.

Test case 308

Test case 308 is identical to test case 307, but the enclosure temperature is increased from 20 °C to 40 °C. The following test case 307 results should be plotted against time:

- The difference between the rates of heat transfer calculated in test cases 308 and 307 ($q_{HX,308} - q_{HX,307}$)

- The difference between the rates of heat loss calculated in test cases 308 and 307 ($q_{loss,308} - q_{loss,307}$)
- The difference between the engine control volume temperatures calculated in test cases 308 and 307 ($T_{eng,308} - T_{eng,307}$)
- The difference between the cooling water control volume outlet temperatures calculated in test cases 308 and 307 ($T_{cw,o,308} - T_{cw,o,307}$)

Disagreement in the test case 308 results may indicate an error in the model's treatment of the enclosure temperature, or the calculation of heat loss (Equation III-9 in the model specification).

Figure III-41 plots the engine temperature predictions for test case 308, while Figure III-42 plots the cooling water outlet temperature predictions. These results show similar characteristics as the test case 307 results—the EnergyPlus implementation consistently predicts a slightly faster response for the reasons discussed earlier. More importantly, increasing the ambient temperature similarly affects all three implementations, suggesting that they implement this aspect of the model specification correctly.

The predicted rates of heat transfer and heat loss are plotted in Figures III-43 and III-44. Again, the EnergyPlus implementation predicts a slightly faster response, but increasing the ambient temperature has the same effect on all implementations. The EnergyPlus heat loss predictions also exhibit the one time step lag discussed in test case 307.

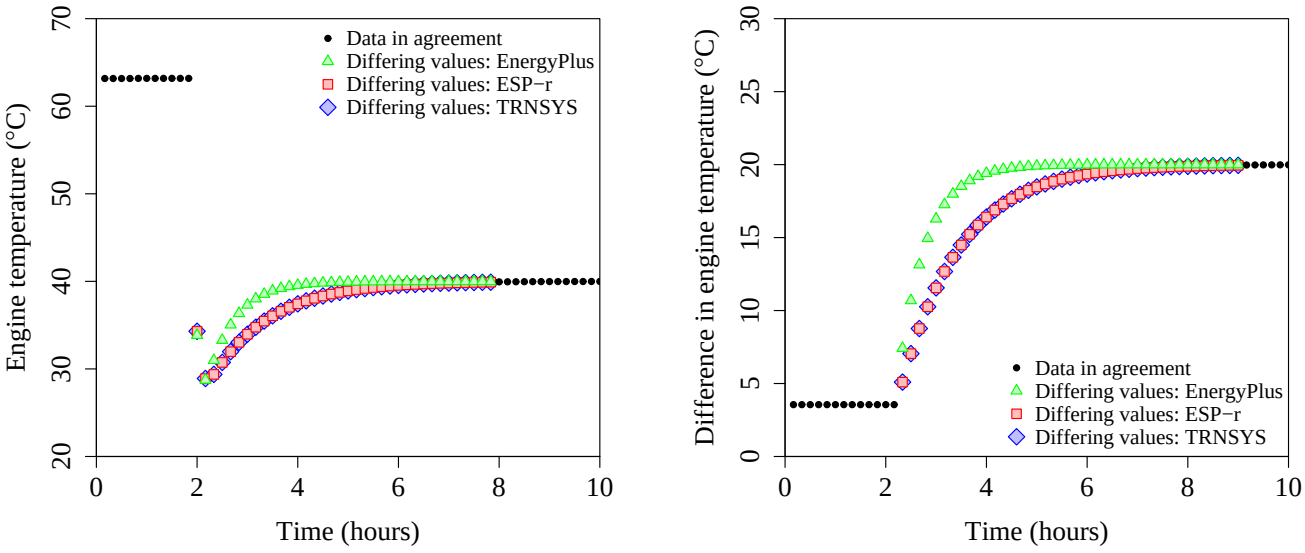

Figure III-41: Test case 308 results — engine temperature (T_{eng}) as a function of time for (a) case 308 and (b) differential between cases 308 and 307 ($T_{eng,308} - T_{eng,307}$)

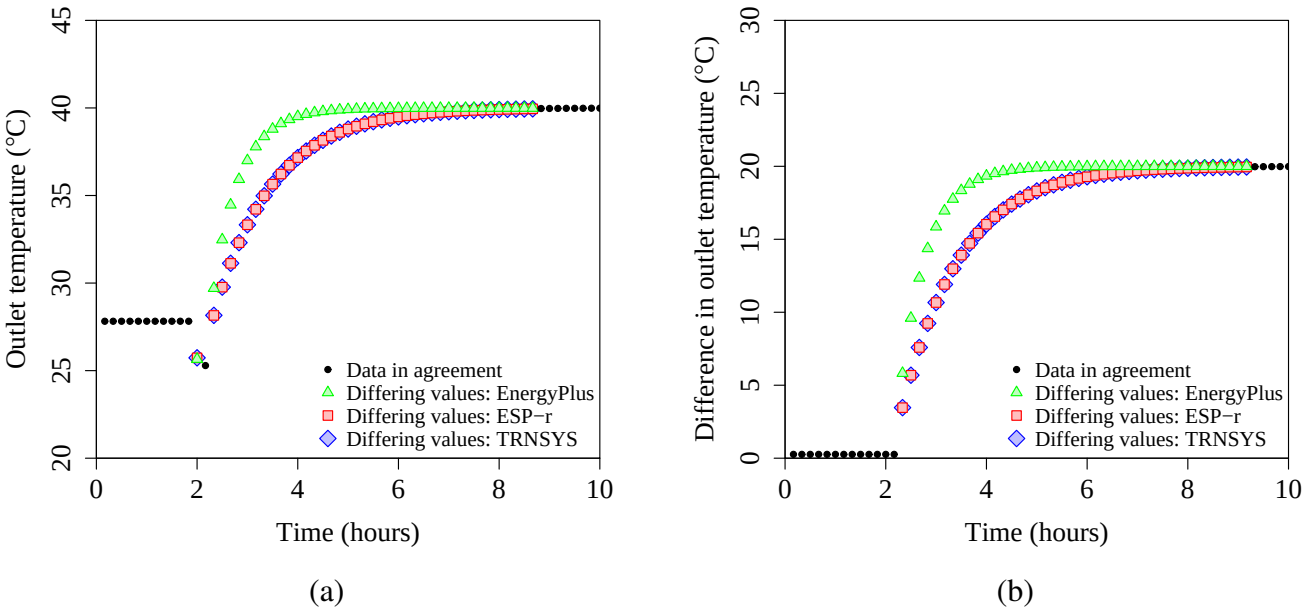

Figure III-42: Test case 308 results — cooling water outlet temperature ($T_{cw,o}$) as a function of time for (a) case 308 and (b) differential between cases 308 and 307 ($T_{cw,o,308} - T_{cw,o,307}$)

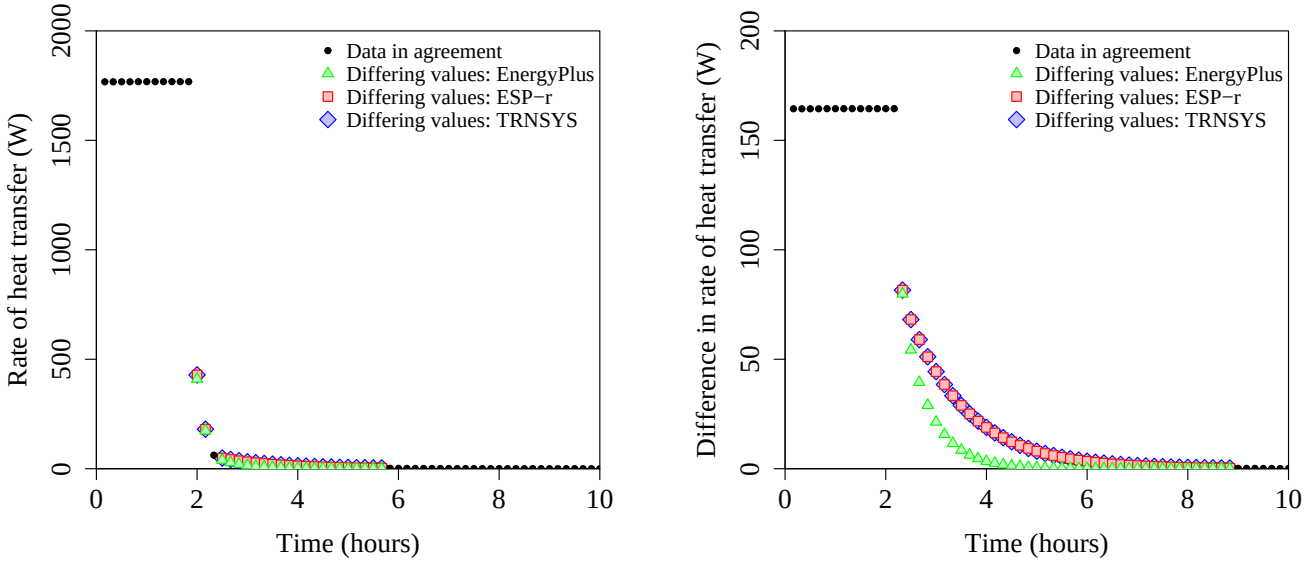

Figure III-43: Test case 308 results — heat transfer rate (q_{HX}) as a function of time for (a) case 308 and (b) differential between cases 308 and 307 ($q_{HX,308} - q_{HX,307}$)

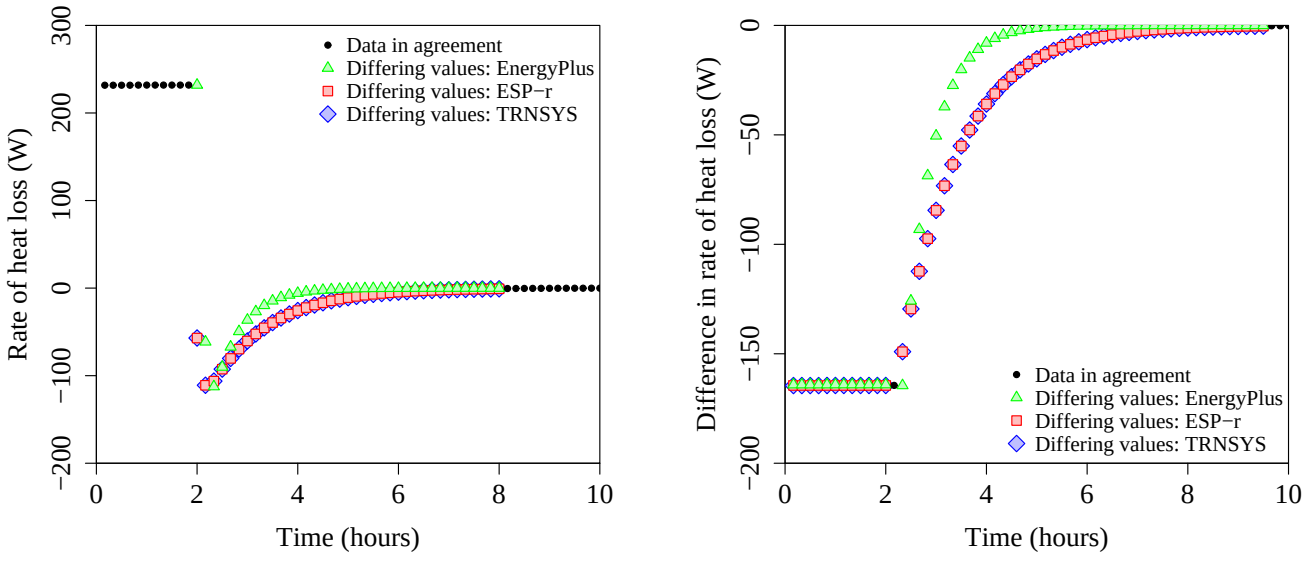

Figure III-44: Test case 308 results — heat loss rate (q_{loss}) as a function of time for (a) case 308 and (b) differential between cases 308 and 307 ($q_{loss,308} - q_{loss,307}$)

400 Series tests

The 400 series tests exercise the cogeneration model's treatment of standby, warm-up and cool-down operation. Eight 400 series test cases have been devised, all of which use the external pump configuration. The differences between the base case configuration and the model inputs used in each of the 400 series test cases are presented in Table III-13.

All eight test cases use the same boundary conditions and control parameters, which are presented in Tables III-14 and III-15, respectively. The cooling water temperature, flow rate and enclosure temperature are held at constant values. The control strategy activates and deactivates the unit three times during the simulation, at intervals of ten, twenty and thirty minutes.

The 400 series test cases are intended for use with a ten-minute time step. Simulations at different time resolutions will not be directly comparable to the 400 series test results published in this report.

Table III-13: Model parameter variations — Series 400 tests

		Test case								
Parameter	Units	Base	401	402	403	404	405	406	407	408
$t_{warm-up}$	s	0.	600.	60.	0.	0.	0.	1200.	900.	900.
$t_{cool-down}$	s	0.	0.	0.	600.	60.	0.	1200.	1500.	1500.
$P_{net,cool-down}$	W	0.	0.	0.	−150.	−150.	0.	−150.	−150.	−150.
Cool-down mode[a]	–	*MC*	*MC*	*MC*	*MC*	*MC*	*MC*	*MC*	*MC*	*OC*
$P_{net,standby}$	W	0.	0.	0.	0.	0.	−50.	−50.	−50.	−50.

Notes:
[a] *MC*: mandatory cool-down period, *OC*: optional cool-down period. See Section III-5.4 in the model specification for more information.

Table III-14: Boundary conditions — Series 400 tests

				Test Case
Condition	Units	Start	End	401–408
Cooling water inlet temperature	°C	00:00	23:59	25.
Cooling water flow rate	kg/s	00:00	23:59	0.15
Enclosure Temperature	°C	00:00	23:99	20.0

Table III-15: Control parameters — Series 400 tests

				Test Case
Parameter	Units	Start	End	401–408
Control flag	–	00:00	01:00	*off*
		01:00	01:30	*ECI*
		01:30	02:00	*off*
		02:00	02:20	*ECI*
		02:20	02:30	*off*
		02:30	02:40	*ECI*
		02:40	23:59	*off*
Control signal	W	00:00	01:00	0.
		01:00	01:30	1000.
		01:30	02:00	0.
		02:00	02:20	1000.
		02:20	02:30	0.
		02:30	02:40	1000.
		02:40	23:59	0.

Test case 401

Test case 401 modifies the base case configuration to reflect a 600 second warm-up period duration for the ICE engine, but leaves the cool-down duration parameters set to zero. Since the specified warm-up period coincides with the duration of the simulation time-step, all model implementations should correctly predict the units transition i) from standby to warm-up at 01:00 h, 02:00 h and 02:30 h, ii) from warm-up to normal operation at 01:10 h, 02:10 h and 02:40 h, and iii) from normal operation to standby at 01:30 h, 02:20 h and 02:40 h (the cogeneration unit will spend no time in normal operation at 02:40 h, as the unit will be deactivated at the same instant the warm-up period is completed).

The following test case 401 results should be plotted against time:

- The fuel flow rate ($\dot{m}_{fuel}$)
- The net power produced (P_{net})
- The rate of steady-state heat generation ($q_{gen,ss}$)

In addition, the intervals spent by the model in each operating mode should be noted.

Disagreement in these results may indicate an error in the model's treatment of the internal combustion engine warm-up period, or the code responsible for switching the model from standby to warm-up and from warm-up to normal operation.

Results from test case 401 are depicted in Figures III-45–III-48. All three implementations show exact agreement.

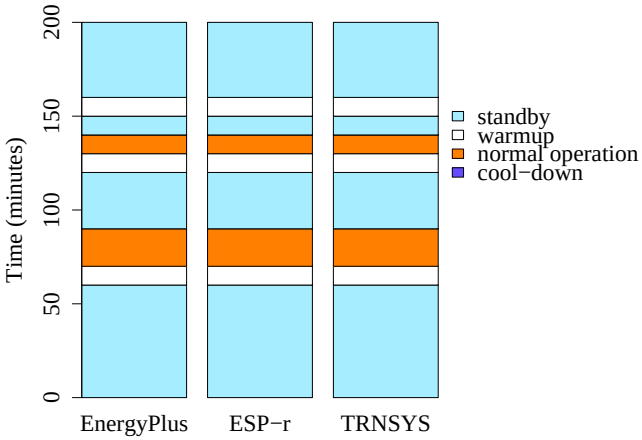

Figure III-45: Test case 401 — time spent in each mode of operation.

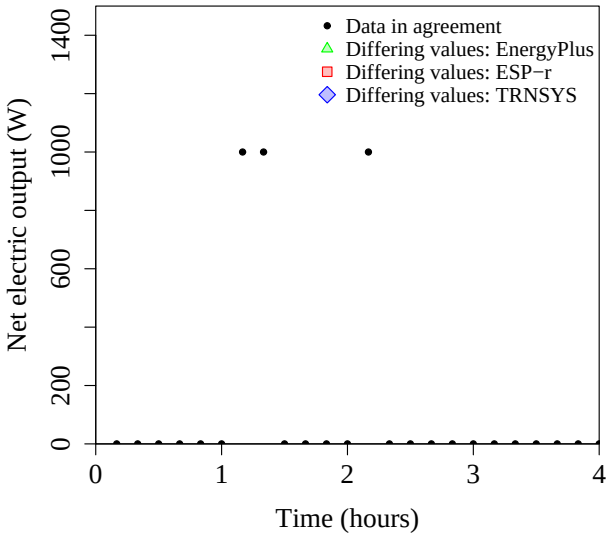

Figure III-46: Test case 401 results — net power (P_{net}) as a function of time

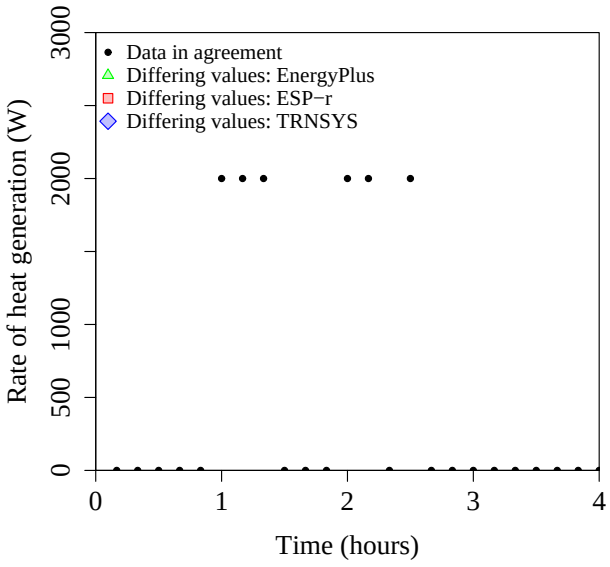

Figure III-47: Test case 401 results — rate of heat generation ($q_{gen,ss}$) as a function of time

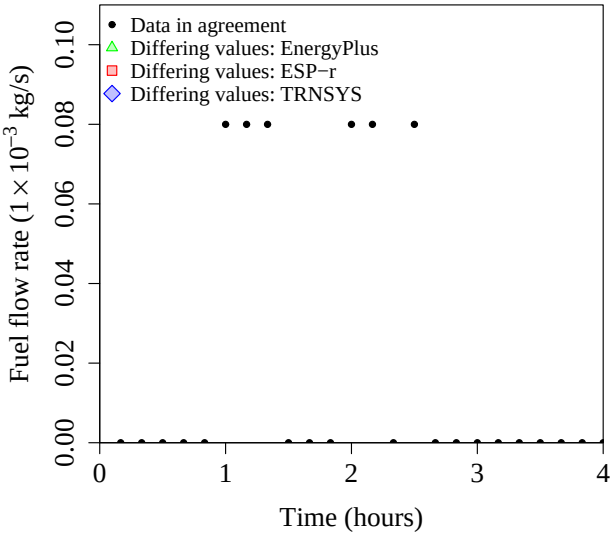

Figure III-48: Test case 401 results — fuel flow rate ($\dot{m}_{fuel}$) as a function of time

Test case 402

Test case 402 is identical to test case 401, but the unit's warm-up period duration parameter is reduced to 60 seconds—a fraction of the length of a single time-step. Given the model specification allows for differing implementations of sub-time step warm-up durations (see Section III-5.4 in he model specification), implementations may exhibit one of two possible behaviours:

- The model may determine that the warm-up period is completed during the 01:00–01:10, 02:00–02:10 and 02:30–02:40 time steps, and calculate the time-step averaged rates of fuel consumption, electricity and heat generation.
- The model may assume the unit remains in warm-up for the duration of these time steps, and report values of fuel consumption, power production and heat generation corresponding to the specified warm-up period parameters.

The following test case 402 results should be plotted against time:

- The fuel flow rate ($\dot{m}_{fuel}$)
- The net power produced (P_{net})
- The rate of steady-state heat generation ($q_{gen,ss}$)

In addition, the intervals spent by the model in each operating mode should be noted. Disagreement in the test case 402 results suggests an error in the treatment of the warm-up period when the period duration is less than the length of a time step.

Results from test case 402 are depicted in Figures III-49–III-52. All three implementations show exact agreement.

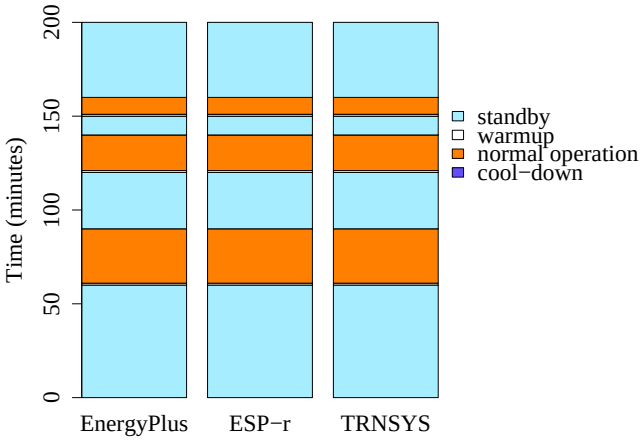

Figure III-49: Test case 402 — time spent in each mode of operation.

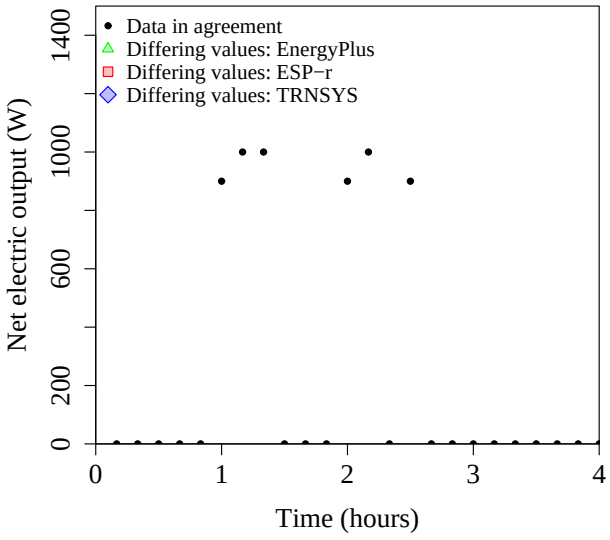

Figure III-50: Test case 402 results — net power (P_{net}) as a function of time

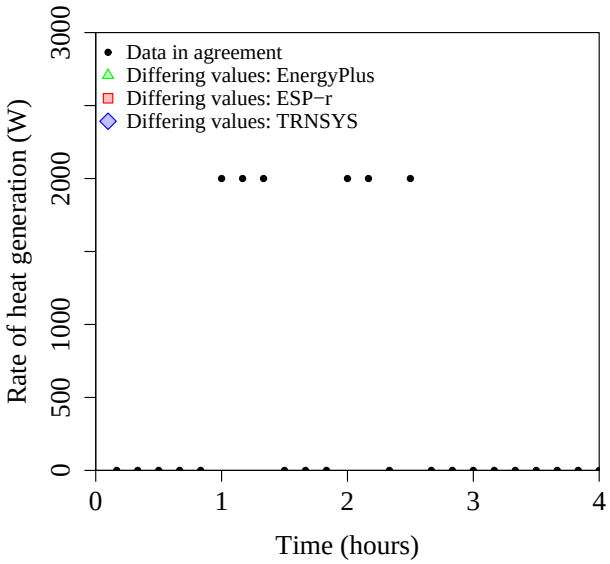

Figure III-51: Test case 402 results — rate of heat generation ($q_{gen,ss}$) as a function of time

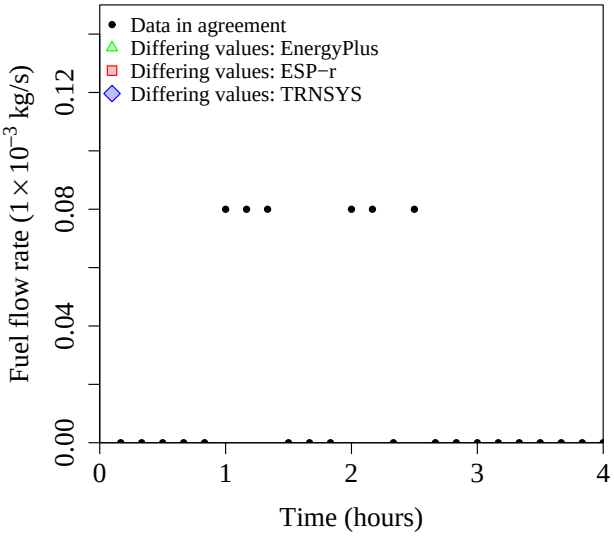

Figure III-52: Test case 402 results — fuel flow rate ($\dot{m}_{fuel}$) as a function of time

Test case 403

Test case 403 modifies the base case configuration to reflect a 600 second cool-down period duration for the ICE engine. During cool-down, the model is also configured draw 150 W of power during cool-down. All model implementations should correctly predict i) the transition from normal operation to cool-down at 01:30 h, 02:20 h and 02:40 h, and the transition from cool-down to standby at 01:40 h, 02:30 h and 02:50 h (the cogeneration unit will spend no time in standby at 02:30 h, as the unit will be reactivated the moment the cool-down period is complete.)

The following test case 403 results should be plotted against time:

- The fuel flow rate ($\dot{m}_{fuel}$)
- The net power produced (P_{net})
- The rate of steady-state heat generation ($q_{gen,ss}$)

In addition, the intervals spent by the model in each operating mode should be noted. Disagreement in the case 403 results may indicate an error in the model's treatment of the cool-down period, or the code responsible for switching from normal operation to cool-down mode and from cool-down to standby mode.

Results from test case 403 are depicted in Figures III-53–III-56. All three implementations show exact agreement.

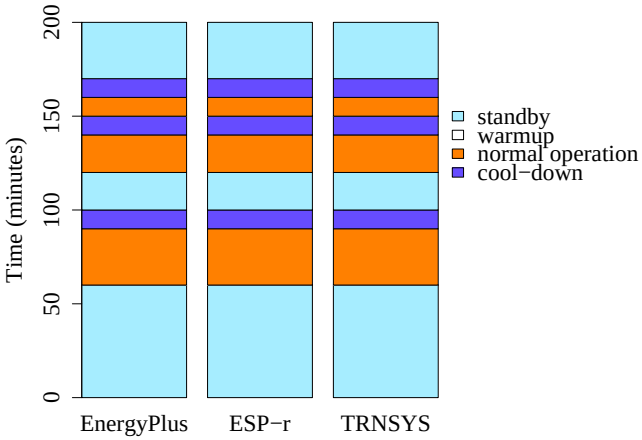

Figure III-53: Test case 403 — time spent in each mode of operation.

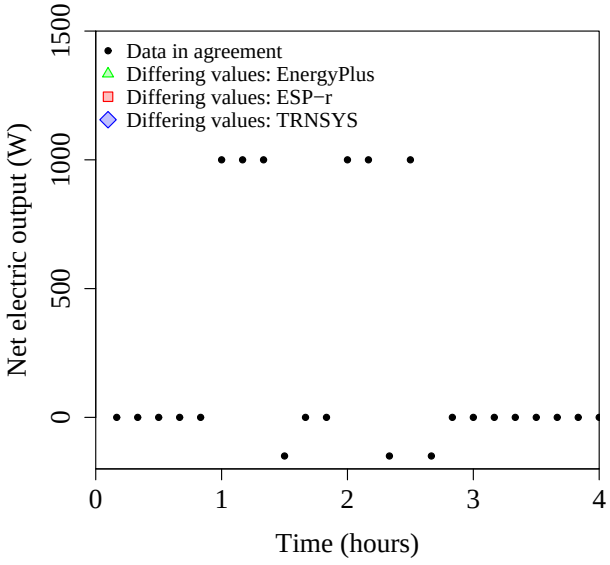

Figure III-54: Test case 403 results — net power (P_{net}) as a function of time

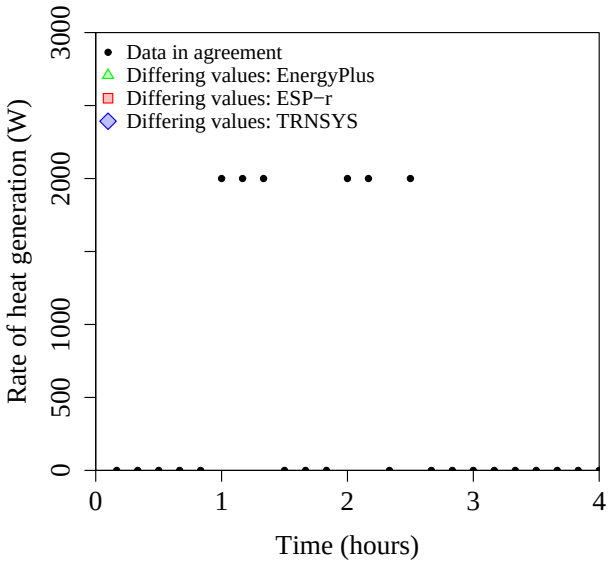

Figure III-55: Test case 403 results — rate of heat generation ($q_{gen,ss}$) as a function of time

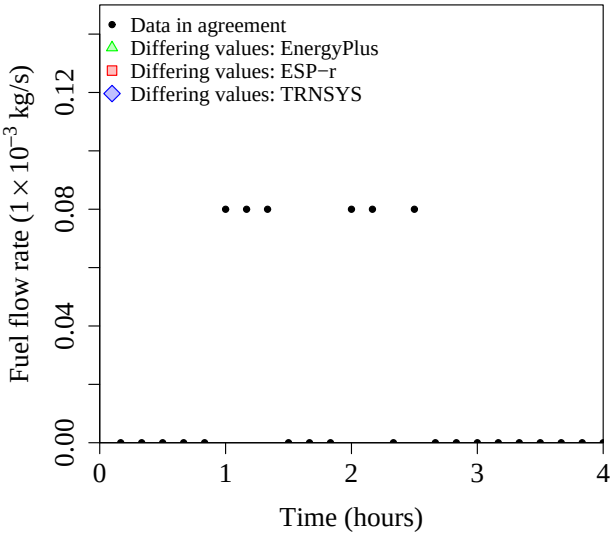

Figure III-56: Test case 403 results — fuel flow rate ($\dot{m}_{fuel}$) as a function of time

Test case 404

Test case 404 is identical to test case 403, but the ICE engine's cool-down period duration is decreased to 60 seconds, a fraction of the length of a single time step. As in test case 402, implementations may exhibit differing behaviour:

- The model may determine the cool-down period is completed during the 01:30–01:40, 02:20–02:30 and 02:40–02:50 time steps, and report period averaged values for power production, fuel flow and heat generation.
- The model may assume the unit remains in cool-down for the duration of these time steps, and report values of fuel consumption, power production and heat generation corresponding to the specified cool-down period parameters.

The following test case 404 results should be plotted against time:

- The fuel flow rate ($\dot{m}_{fuel}$)
- The net power produced (P_{net})
- The rate of steady-state heat generation ($q_{gen,ss}$)

In addition, the intervals spent by the model in each operating mode should be noted. Disagreement in the test case 404 results suggests an error in the treatment of the cool-down period when the period duration is less than the length of a time step.

Results from test case 404 are depicted in Figures III-57–III-60. All three implementations exhibit exact agreement.

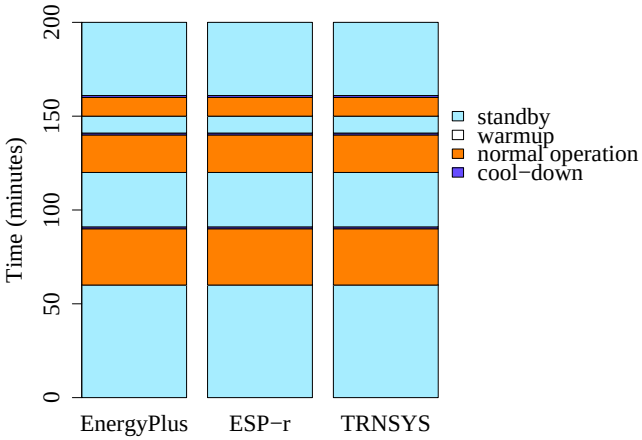

Figure III-57: Test case 404 — time spent in each mode of operation.

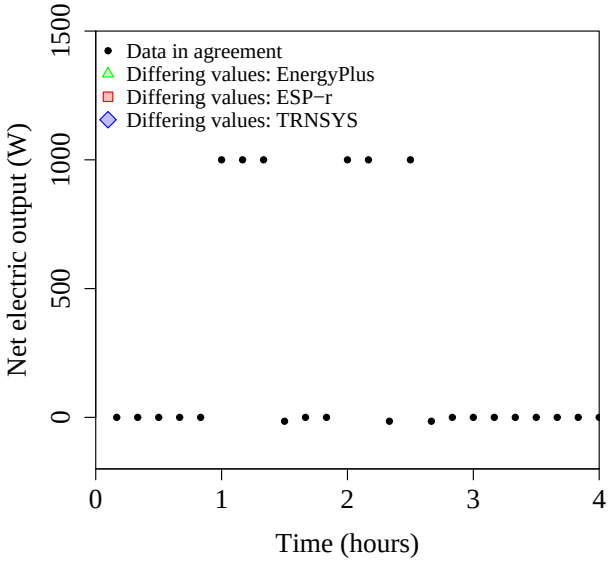

Figure III-58: Test case 404 results — net power (P_{net}) as a function of time

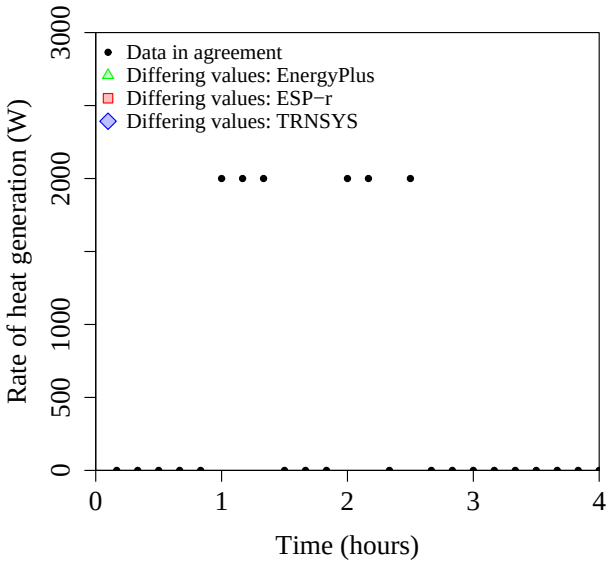

Figure III-59: Test case 404 results — rate of heat generation ($q_{gen,ss}$) as a function of time

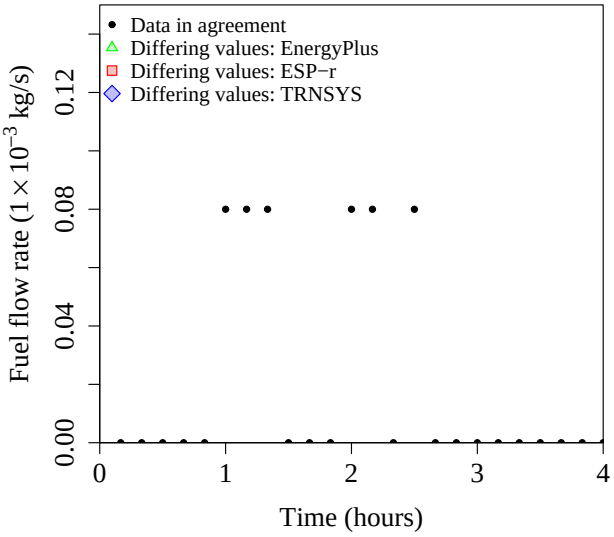

Figure III-60: Test case 404 results — fuel flow rate ($\dot{m}_{fuel}$) as a function of time

Test case 405

Test case 405 modifies the base case configuration to reflect a standby power consumption of 50 W. All implementations should correctly report this value when the unit is in standby.

The following test case 405 results should be plotted against time:

- The fuel flow rate ($\dot{m}_{fuel}$)
- The net power produced (P_{net})
- The rate of steady-state heat generation ($q_{gen,ss}$)

In addition, the intervals spent by the model in each operating mode should be noted. Disagreement in the test case 405 results suggests an error in the treatment of the standby electrical use.

Results from test case 405 are depicted in Figures III-61–III-64. All three implementations exhibit exact agreement.

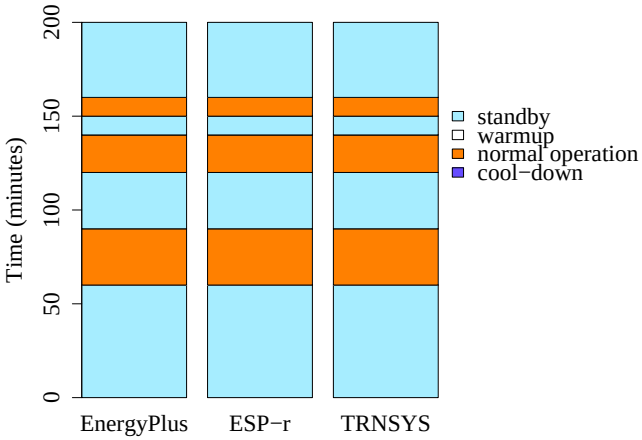

Figure III-61: Test case 405 — time spent in each mode of operation.

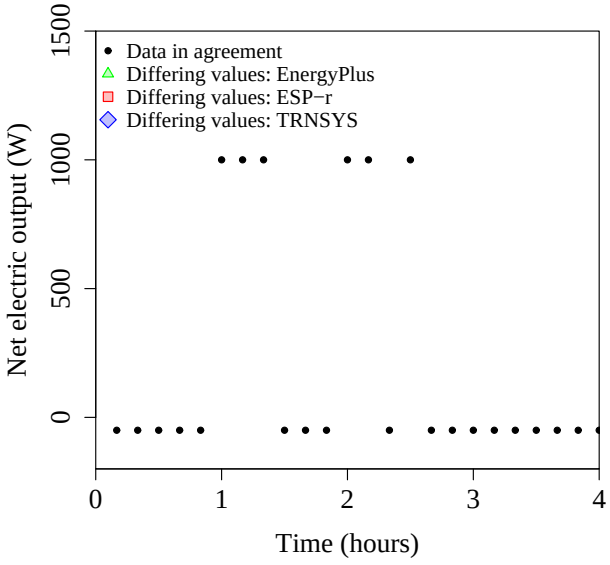

Figure III-62: Test case 405 results — net power (P_{net}) as a function of time

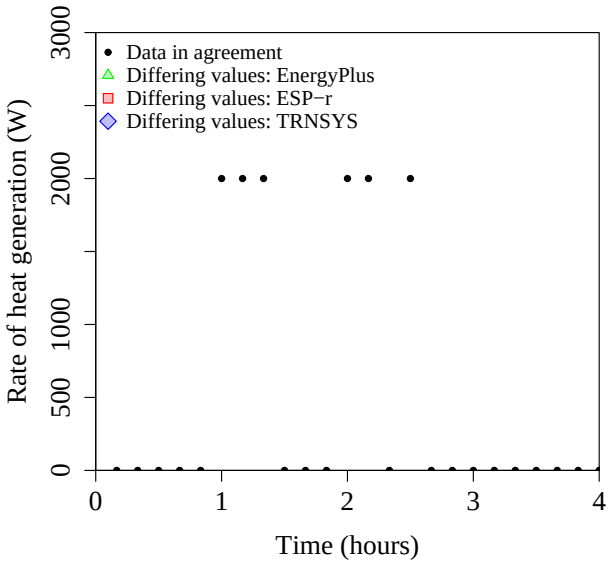

Figure III-63: Test case 405 results — rate of heat generation ($q_{gen,ss}$) as a function of time

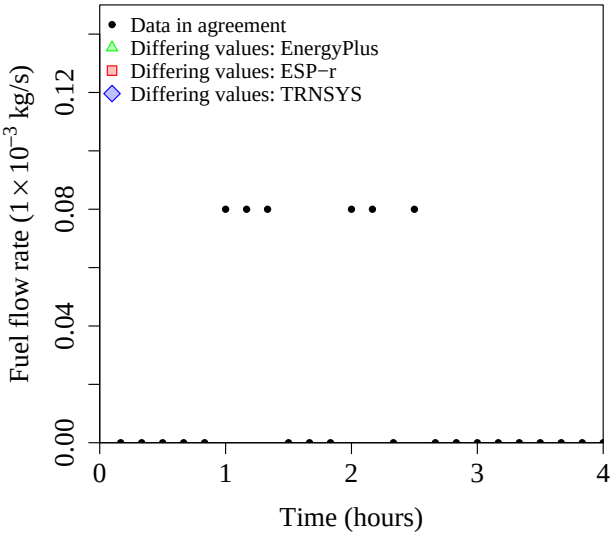

Figure III-64: Test case 405 results — fuel flow rate ($\dot{m}_{fuel}$) as a function of time

Test case 406

Test case 406 combines elements from test cases 401–405. The unit is configured with 600 second warm-up and cool-down periods. The net power generation during standby is set to -50 W, while the net power generation during cool-down is set to -150 W.

In this configuration, the duration of the warm-up and cool-down periods corresponds to two time steps. All model implementations should correctly predict the transition from cool-down to standby at 01:50 h and 02:40 h. Since the mandatory cool-down configuration is specified, the unit should not respond to reactivation at 02:30 h—half way through its cool-down period.

The following test case 406 results should be plotted against time:

- The fuel flow rate ($\dot{m}_{fuel}$)
- The net power produced (P_{net})
- The rate of steady-state heat generation ($q_{gen,ss}$)

In addition, the intervals spent by the model in each operating mode should be noted. Disagreement in the test case 406 results suggests an error in the treatment of the standby electrical use.

Notwithstanding sources of error identified in the 401–405 test cases, disagreement in the test case 406 results suggests an error in the treatment of warm-up and cool-down period durations spanning several time-steps, or in the code controlling the models progression from standby to warm-up, normal operation and finally cool-down modes.

Results from test case 406 are depicted in Figures III-65–III-68. All three implementations show exact agreement.

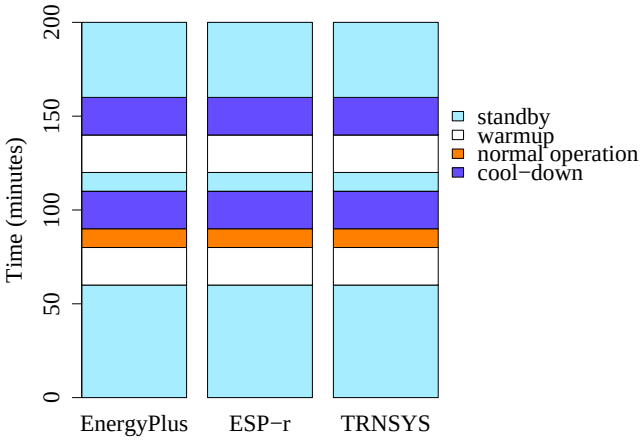

Figure III-65: Test case 406 — time spent in each mode of operation.

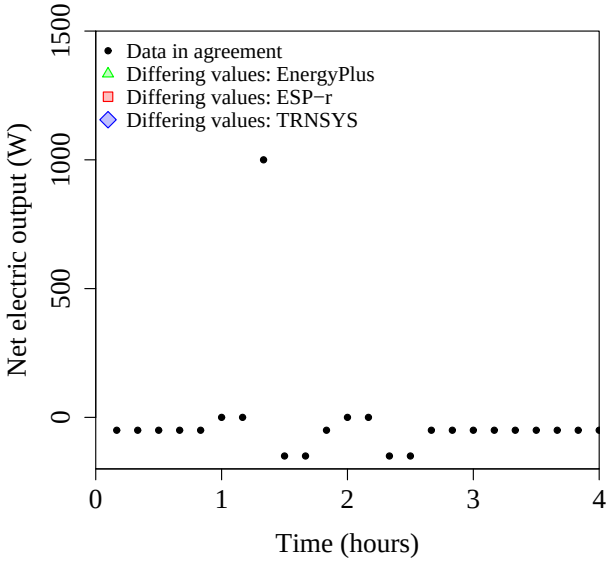

Figure III-66: Test case 406 results — net power (P_{net}) as a function of time

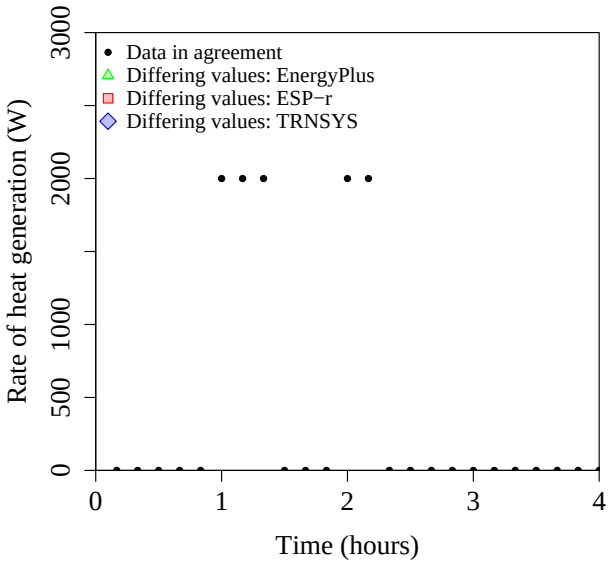

Figure III-67: Test case 406 results — rate of heat generation ($q_{gen,ss}$) as a function of time

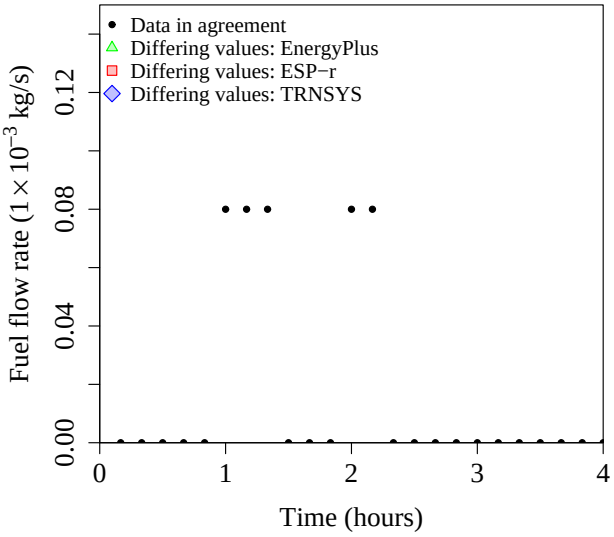

Figure III-68: Test case 406 results — fuel flow rate ($\dot{m}_{fuel}$) as a function of time

Test case 407

Test case 407 further adjusts the warm-up and cool-down period durations used in case 406 such that transitions between modes will occur in the middle of a simulation time step. The cool-down and standby power consumption values remain unchanged.

As in test cases 402 and 404, the model specification allows for two possible behaviours. After activation at 01:00 h, the model may:

- determine that the warm-up period will be completed midway through the 01:10–01:20 time-step, and report period averaged values for power production, fuel flow and heat generation, or
- assume the warm-up period persists until 01:20 h, and report power production, fuel flow and heat generation values based on the specified standby warm-up parameters.

After deactivation at 01:30 h, the model may:

- determine that the cool-down period will be completed midway through the 01:50–02:00 time-step, and report period averaged values for power production, fuel flow and heat generation, or
- assume the cool-down period persists until 02:00 h, and report power production, fuel flow and heat generation values based on the specified standby cool-down parameters.

After reactivation at 02:00 h, the model may:

- determine that the warm-up period will be completed midway through the 02:10–02:20 time-step, and report period averaged values for power production, fuel flow and heat generation, or

- assume the warm-up period persists until 02:20 h, and report power production, fuel flow and heat generation values based on the specified standby warm-up parameters.

After deactivation at 2:20 h, the model may:

- determine that the cool-down period will be completed midway through the 02:40–02:50 time-step, and report period averaged values for power production, fuel flow and heat generation, or
- assume the cool-down period persists until 02:50 h, and report power production, fuel flow and heat generation values based on the specified standby cool-down parameters.

Since the mandatory cool-down period is specified, all model implementations should ignore the reactivation signal received at 02:30 h and the subsequent deactivation signal received at 02:40 h, as the unit is still completing its cool-down cycle at this time.

The following test case 407 results should be plotted against time:

- The fuel flow rate ($\dot{m}_{fuel}$)
- The net power produced (P_{net})
- The rate of steady-state heat generation ($q_{gen,ss}$)

In addition, the intervals spent by the model in each operating mode should be noted. Disagreement in test case 407 results suggests an error in the treatment of warm-up and cool-down periods when i) they persist for longer than a single time-step, and ii) their termination does not coincide with the end of a time step.

Results from test case 407 are depicted in Figures III-69–III-72. All three implementations agree exactly.

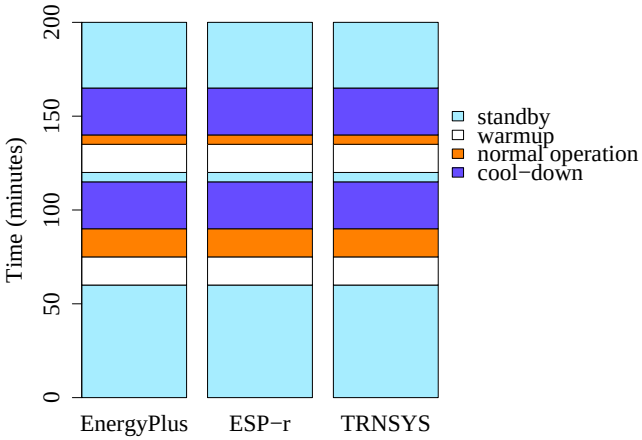

Figure III-69: Test case 407 — time spent in each mode of operation.

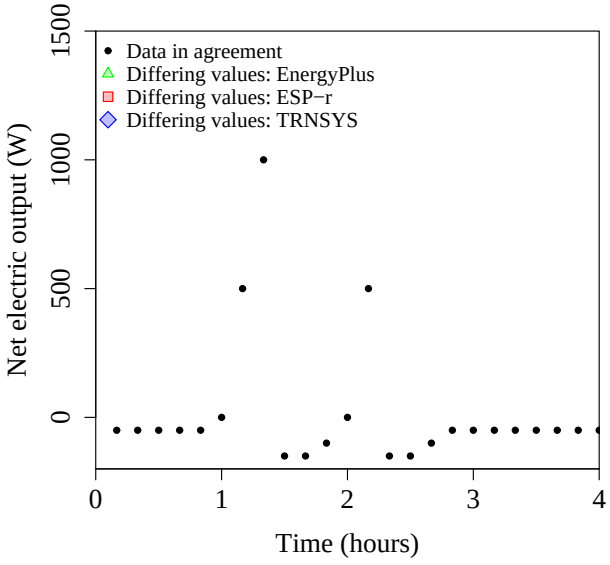

Figure III-70: Test case 407 results — net power (P_{net}) as a function of time

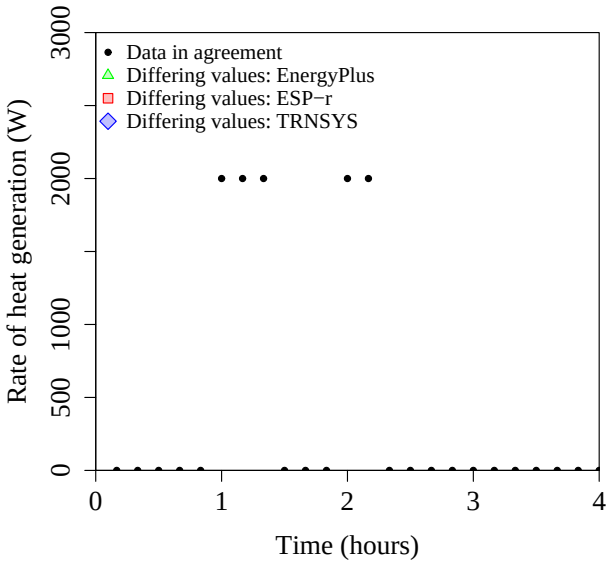

Figure III-71: Test case 407 results — rate of heat generation ($q_{gen,ss}$) as a function of time

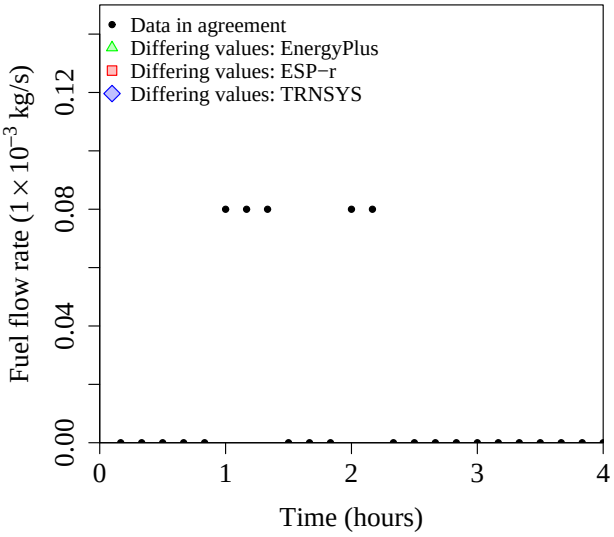

Figure III-72: Test case 407 results — fuel flow rate ($\dot{m}_{fuel}$) as a function of time

Test case 408

Test case 408 is identical to test case 407, but the optional cool-down period configuration is specified. The test case 408 results should be identical to those from test case 407 until 02:20 h, when the unit is reactivated. In test case 407, the model remained in cool-down mode when the reactivation signal is received, but in test case 408 the model should switch from cool-down to warm-up.

The following test case 408 results should be plotted against time:

- The fuel flow rate ($\dot{m}_{fuel}$)
- The net power produced (P_{net})
- The rate of steady-state heat generation ($q_{gen,ss}$)

In addition, the intervals spent by the model in each operating mode should be noted. Disagreement in test case 408 results suggests an error in the implementation of the optional cool-down configuration.

Results from test case 408 are depicted in Figures III-73–III-76. All three implementations show exact agreement.

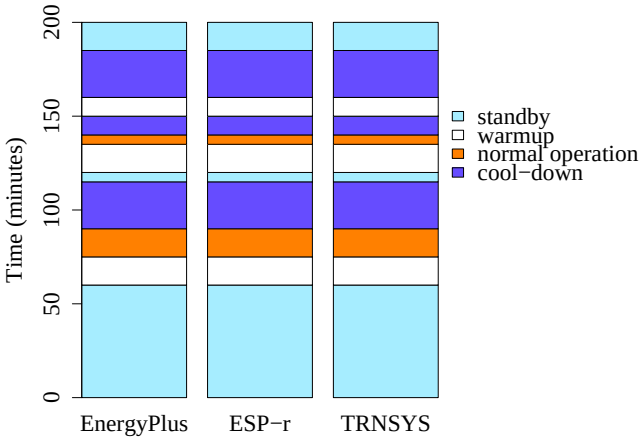

Figure III-73: Test case 408 — time spent in each mode of operation.

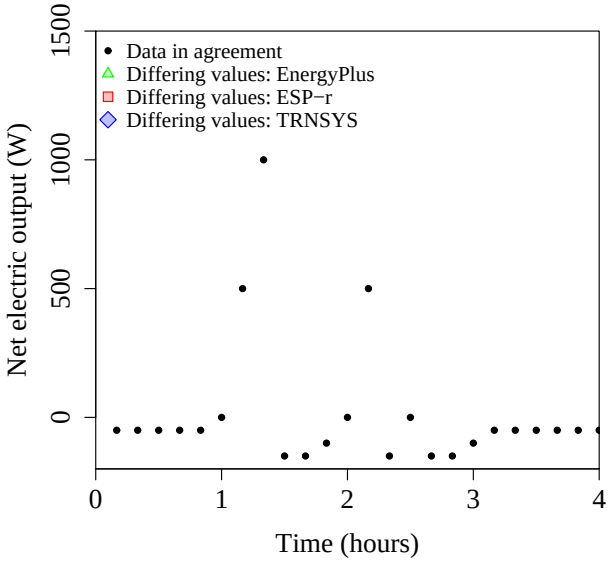

Figure III-74: Test case 408 results — net power (P_{net}) as a function of time

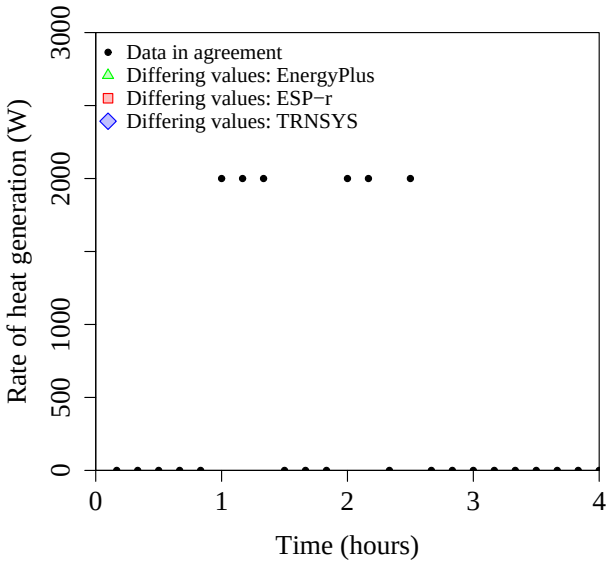

Figure III-75: Test case 408 results — rate of heat generation ($q_{gen,ss}$) as a function of time

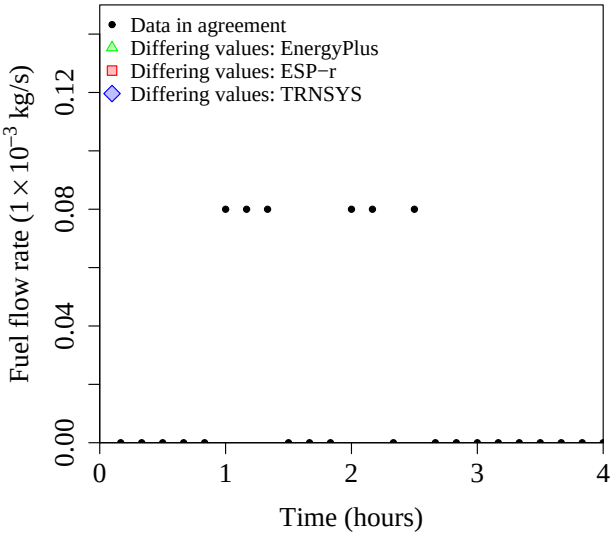

Figure III-76: Test case 408 results — fuel flow rate ($\dot{m}_{fuel}$) as a function of time

500 Series tests

The 500 series test cases exercise the correlations predicting the warm-up behaviour in Stirling engines. While the 100–400 series test cases exercised the model in its internal combustion engine configuration, the 500 series cases specify the model's Stirling engine configuration be used. Thus, the Stirling engine warm-up parameters will affect the model's predictions.

The Stirling engine warm-up correlations (Equations III-23 and III-25 in the model specification) predict the cogeneration unit's fuel and power production in response to the temperature of the engine control volume, and are therefore coupled to the dynamic thermal model. Since the dynamic thermal model was exercised in the 300 series test cases, the effects of the dynamic thermal model parameters on the warm-up period correlations are not explored here. Instead, it is assumed that the model can correctly predict the control volume temperatures, and the effects of these temperatures on the warm-up period fuel flow and power output are scrutinized.

Six series 500 test cases have been defined, and the variations between these cases and the base configuration are presented in Table III-16. All of the 500 series test cases use the same boundary conditions and control parameters, which are presented in Tables III-17 and III-18, respectively.

Table III-16: Model parameter variations — Series 500 tests

		Test case						
Parameter	Units	Base	501	502	503	504	505	506
Engine type	–	*ICE*	*SE*	*SE*	*SE*	*SE*	*SE*	*SE*
$T_{eng,nom}$	°C	150.	70.	50.	70.	70.	70.	70.
k_f	–	1.0	†	†	0.5	†	†	†
k_p	–	1.0	†	†	†	0.5	†	†
$r_{fuel,warm-up,max}$	kg/s	10.	†	†	†	†	2.	†
$[MC]_{eng}$	J/K	20.0 E03	120.0 E03	120.0 E03	120.0 E03	120.0 E03	120.0 E03	60.0 E03

Notes:
† Value unchanged from base case.

Table III-17: Boundary conditions — Series 500 tests

				Test Case
Condition	Units	Start	End	501–506
Cooling water inlet temperature	°C	00:00	23:59	25.
Cooling water flow rate	kg/s	00:00	23:59	0.15
Enclosure temperature	°C	00:00	23:59	20.

Table III-18: Control parameters — Series 500 tests

				Test Case
Parameter	Units	Start	End	501–506
Control flag	–	00:00	01:00	*off*
		01:00	03:00	*ECI*
		03:00	23:59	*off*
Control signal	W	00:00	01:00	0.
		01:00	03:00	1000.
		03:00	23:59	0.

Notes:
ECI: Electric load following control interface

Test case 501

Test case 501, is identical to the base case configuration, except the engine type is specified as a Stirling engine. In this configuration, the model's Stirling engine warm-up period correlations will be exercised. The model should predict higher fuel consumption and lower power production during the warm-up period.

The fuel flow and power production predicted in test case 501 should be plotted against i) time and ii) the temperature of the engine control volume (T_{eng}). Disagreement in these results is indicative of an error in the warm-up period correlations—test cases 502–506 attempt identify the specific sources of error.

Figure III-77 plots the engine temperature (T_{eng}) predictions for test case 501. As in the 300 series tests, EnergyPlus predicts a slightly faster response following the unit's activation and deactivation. These effects are due to the differing philosophies used to solve the dynamic thermal model's state equations, as discussed in the 300 series section.

The 500-series tests also exercise the model's start-up fuel flow and net power correlations. Figure III-78 plots the fuel flow rate ($\dot{m}_{fuel}$) predictions over the duration of the simulation, and Figure III-79 plots the net power (P_{net}) predictions.

Differences in the implementations of the dynamic thermal model affect these results too. Since the EnergyPlus implementation predicts slightly higher temperatures, it also calculates slightly higher power output and lower fuel flow rates during the warm-up period. In fact, the engine temperature and fuel flow rate predictions are coupled during warm-up—an increase in engine temperature causes the model to adjust the fuel flow rate according to the warm-up fuel flow correlation (Equation III-23 in the model specification), which alters the heat flux into the engine control volume and further changes the predicted engine temperature.

Given their coupled nature, the results from the warm-up period correlations can not be

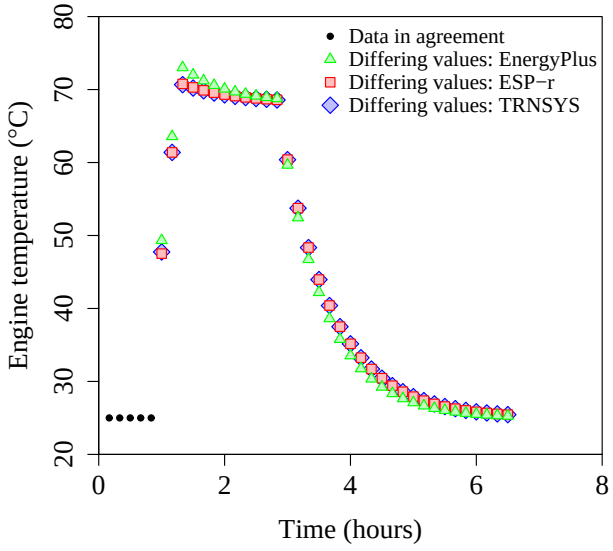

Figure III-77: Test case 501 — engine control volume temperature (T_{eng}) as a function of time

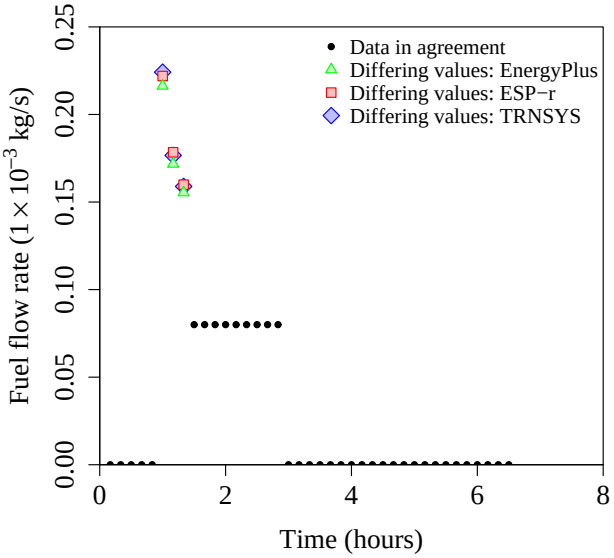

Figure III-78: Test case 501 — fuel flow rate ($\dot{m}_{fuel}$) as a function of time

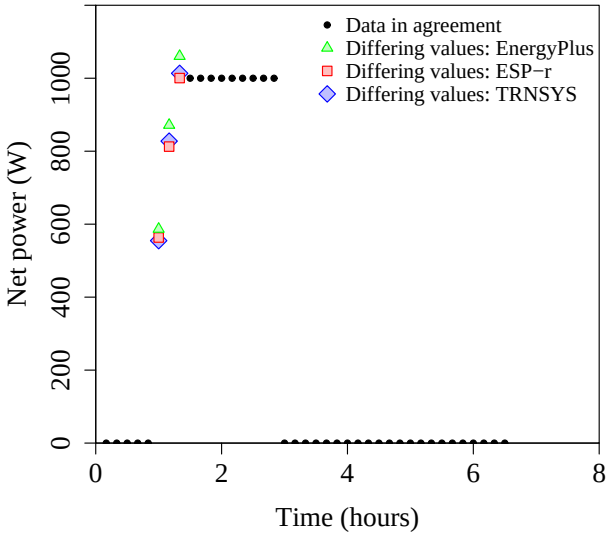

Figure III-79: Test case 501 — net electric output (P_{net}) as a function of time

directly compared without first equivalencing the dynamic thermal model. But as the 300-series tests showed, parity between the EnergyPlus, ESP-r and TRNSYS implementations of the dynamic thermal model is not possible with the current limitations on time step size in these programs.

Instead, the EnergyPlus, ESP-r and TRNSYS predictions were compared to the actual values of the warm-up period correlations. These correlations prescribe a direct relationship between the engine temperature and the fuel flow rate and power output:

$$\dot{m}_{fuel,warmup} = \dot{m}_{fuel,ss-max} + k_f \dot{m}_{fuel,ss-max} \left(\frac{T_{eng,nom} - T_{room}}{T_{eng} - T_{room}} \right)$$

$$P_{net,warm-up} = P_{max} k_p \left(\frac{T_{eng} - T_{room}}{T_{eng,nom} - T_{room}} \right)$$

While the EnergyPlus, ESP-r and TRNSYS implementations may not predict the same engine temperature, fuel flow or power output during start-up period, their estimated fuel flow and power output should agree with these correlations throughout the warm-up period.

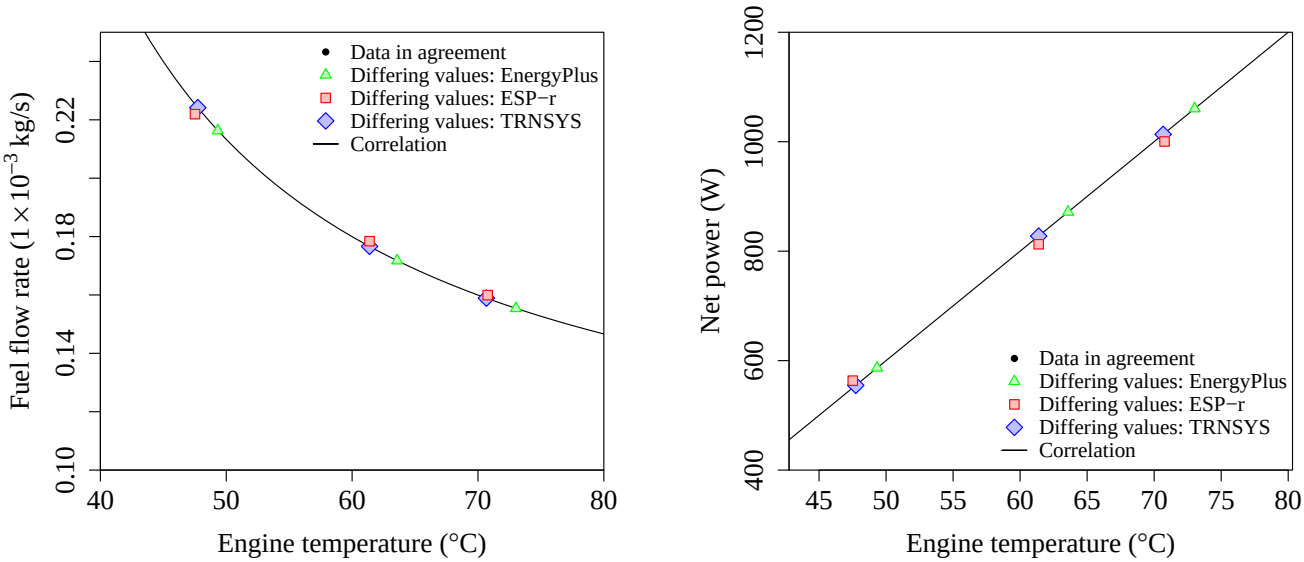

(a) (b)

Figure III-80: Test case 501 — (a) fuel flow rate $\dot{m}_{fuel}$ and (b) net electric output (P_{net}) as functions engine temperature (T_{eng}) during start-up, with ESP-r convergence tolerances set to default values

Figure III-80 plots the predicted fuel flow rate and power output as functions of the predicted engine temperature. These plots also include lines depicting the warm-up period fuel flow and power output correlations. The EnergyPlus and TRNSYS results agree very well with the correlation, while the ESP-r predictions deviate somewhat.

The tolerances used by ESP-r to gauge convergence in the plant network are the culprit. The default temperature tolerance (1 °C) proved too large to ensure convergence in the predicted control volume temperatures between successive iterations. Reducing the tolerance to 0.1 °C caused additional iterations within the network and provided better agreement with the correlation, as shown in Figure III-81. For this reason, ESP-r results for the 502–506 test cases were obtained using the smaller convergence tolerance.

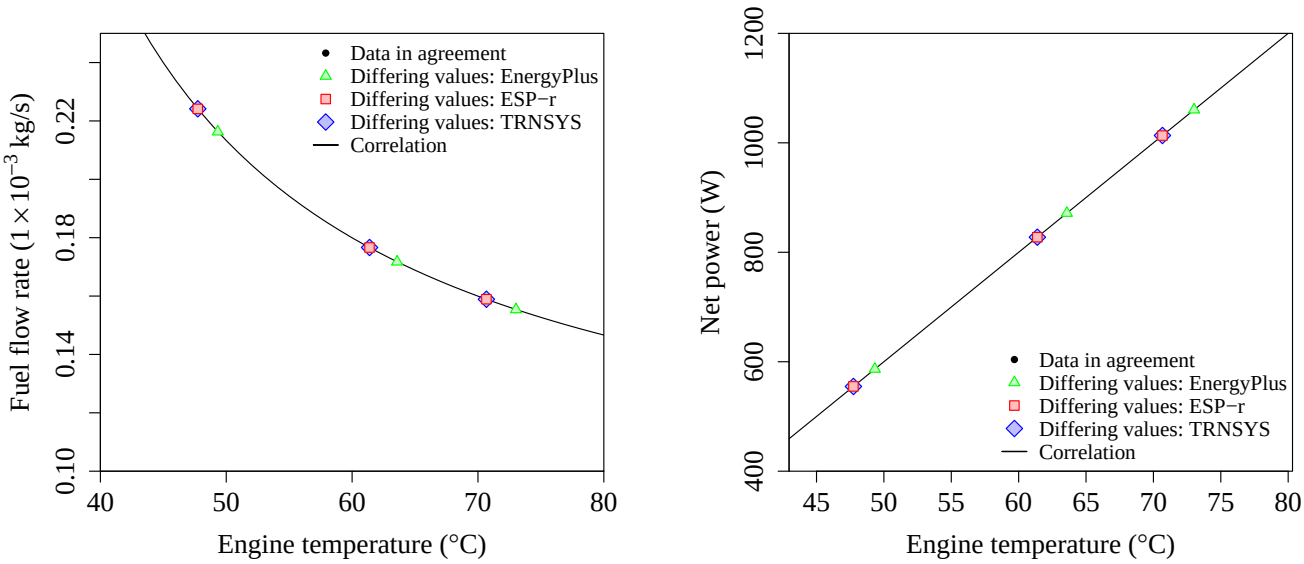

Figure III-81: Test case 501 — (a) fuel flow rate $\dot{m}_{fuel}$ and (b) net electric output (P_{net}) as functions engine temperature (T_{eng}) during start-up, with reduced ESP-r convergence tolerance.

Test case 502

Test case 502 reduces the nominal engine temperature ($T_{eng,nom}$) used in test case 501 from 150 °C to 100 °C. The differences between the fuel flow, power and heat produced in test cases 502 and 501 (ie. $\dot{m}_{fuel,502} - \dot{m}_{fuel,501}$, $P_{net,502} - P_{net,501}$ and $\dot{q}_{gen,ss,502} - \dot{q}_{gen,ss,501}$) should be plotted against i) time and ii) the temperature of the engine control volume (T_{eng}). Disagreement in these results suggests an error in the treatment of the nominal engine temperature. Developers should review the implementation of the warm-up period correlations (Equations III-23 and III-24 in the model specification), and the code that switches the model from warm-up to normal operation when the nominal engine temperature is reached.

Figure III-82 plots the engine control volume temperature predictions. Again, the EnergyPlus model predicts a slightly faster response for the reasons discussed in test case 301. But when the case 502 predictions are compared to case 501, the reduced nominal engine temperature clearly affects all three implementations similarly.

These differences also manifest themselves in the predicted rates of fuel flow (Figure III-83) and electricity generation (Figure III-84), where EnergyPlus again predicts a faster response.

Finally, Figure III-85 plots the predicted rates of electricity generation and fuel consumption as functions of the predicted engine temperature. The black lines on these plots depict the warm-up period fuel flow and power output correlations—clearly, all three implementations agree very well with the correlations.

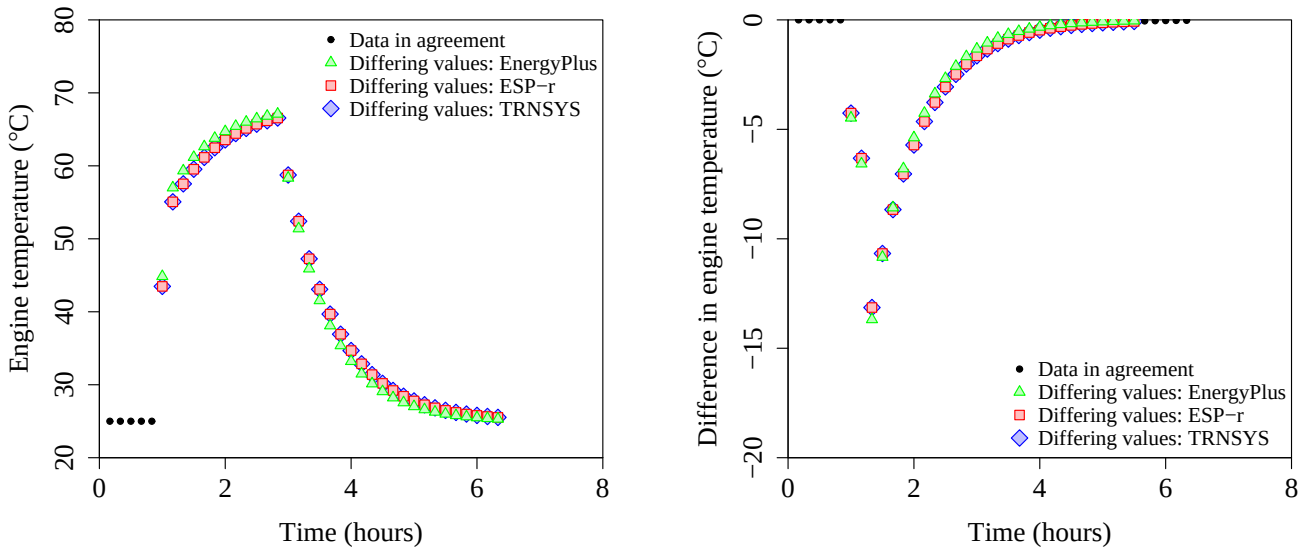

(a) (b)

Figure III-82: Test case 502 — engine temperature (T_{eng}) as a function of time for (a) case 502 and (b) differential between cases 502 and 501 ($T_{eng,502} - T_{eng,501}$)

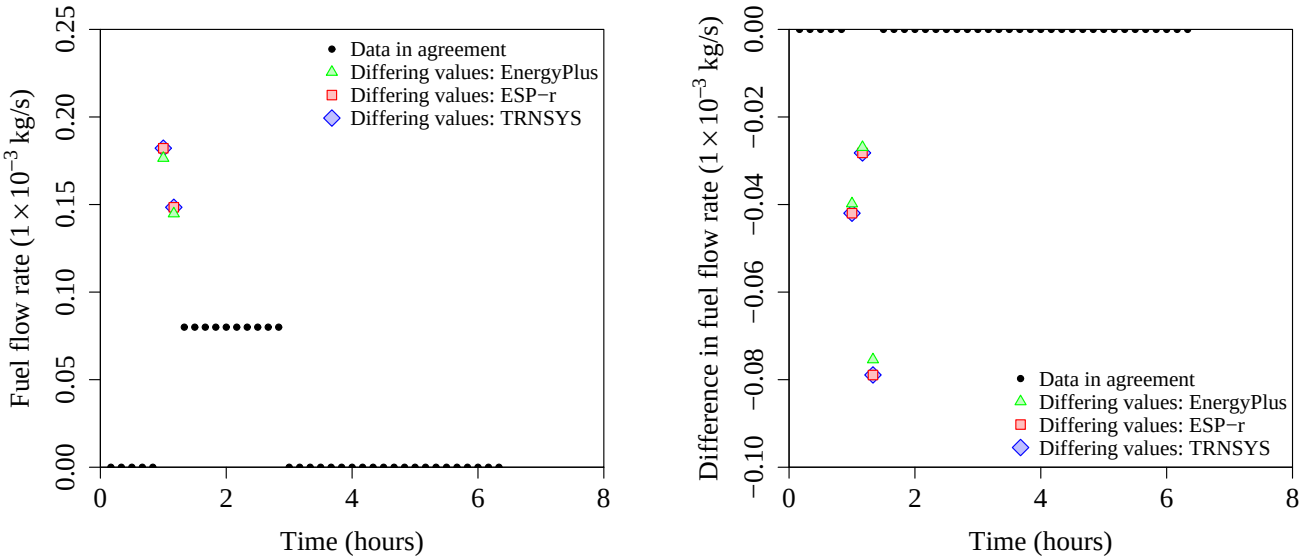

(a) (b)

Figure III-83: Test case 502 — fuel flow rate $\dot{m}_{fuel}$ as a function of time for (a) case 502 and (b) differential between cases 502 and 501 ($\dot{m}_{fuel,502} - \dot{m}_{fuel,501}$)

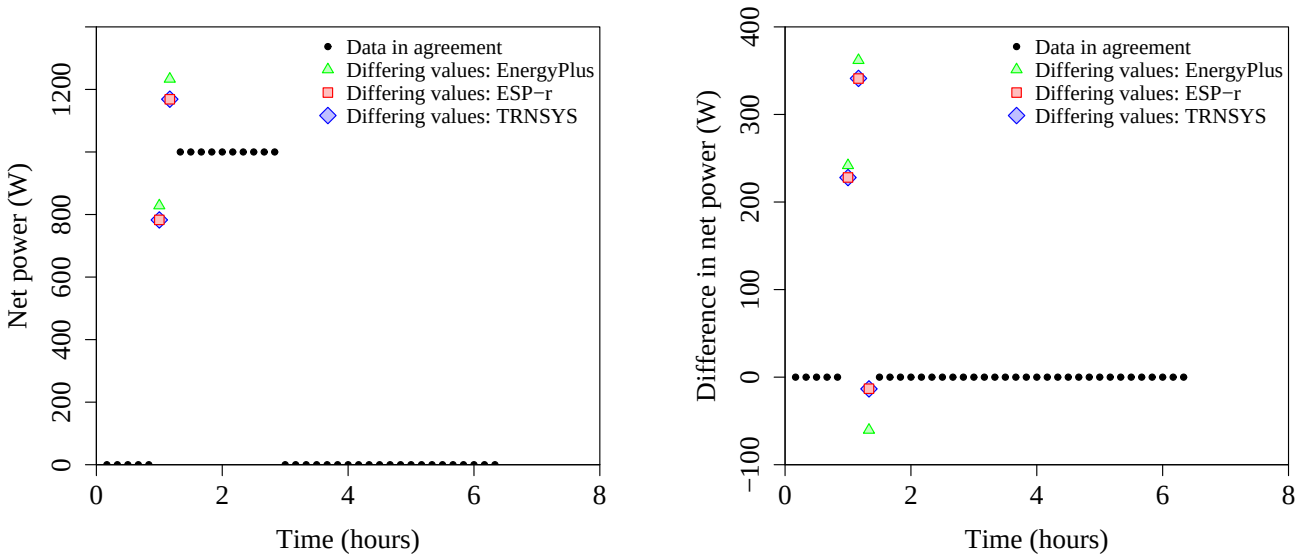

(a) (b)

Figure III-84: Test case 502 — net electric output (P_{net}) as a function of time for (a) case 502 and (b) differential between cases 502 and 501 ($P_{net,502} - P_{net,501}$)

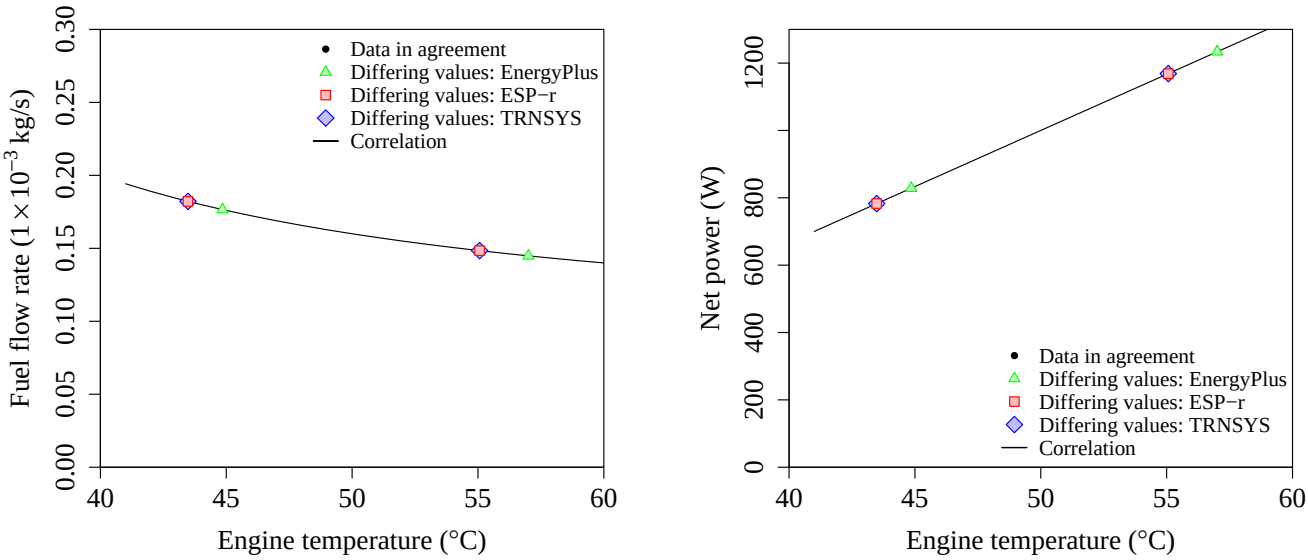

(a) (b)

Figure III-85: Test case 502 — (a) fuel flow rate $\dot{m}_{fuel}$ and (b) net electric output (P_{net}) as functions engine temperature (T_{eng}) during start-up

Test case 503

Test case 503 halves the Stirling engine warm-up fuel flow sensitivity coefficient (k_f) used in test case 501 from 1.0 to 0.5. In this configuration, the predicted fuel flow during warm-up should be lower than that observed in test case 501.

The difference between the fuel flow, power and heat produced in test cases 503 and 501 (ie. $\dot{m}_{fuel,503} - \dot{m}_{fuel,501}$, $P_{net,503} - P_{net,501}$ and $\dot{q}_{gen,ss,503} - \dot{q}_{gen,ss,501}$) should be plotted against i) time and ii) the temperature of the engine control volume (T_{eng}). Disagreement in these results may indicate an error in the warm-up fuel flow correlation—developers should check the implementation of Equation 23 in the model specification .

Figure III-86 plots the engine control volume temperature predictions. Again, the EnergyPlus implementation predicts a slightly faster response for the reasons discussed in test case 301. But when the case 503 predictions are compared to case 501, the reduced nominal engine temperature clearly affects all three implementations similarly. These differences also manifest themselves in the predicted rates of fuel flow (Figure III-87) and electricity generation (Figure III-88), where EnergyPlus again predicts a faster response.

Finally, Figure III-89 plots the predicted rates of electricity generation and fuel consumption as functions of the predicted engine temperature. The black lines on these plots depict the warm-up period fuel flow and power output correlations—clearly, all three implementations agree very well with the correlations.

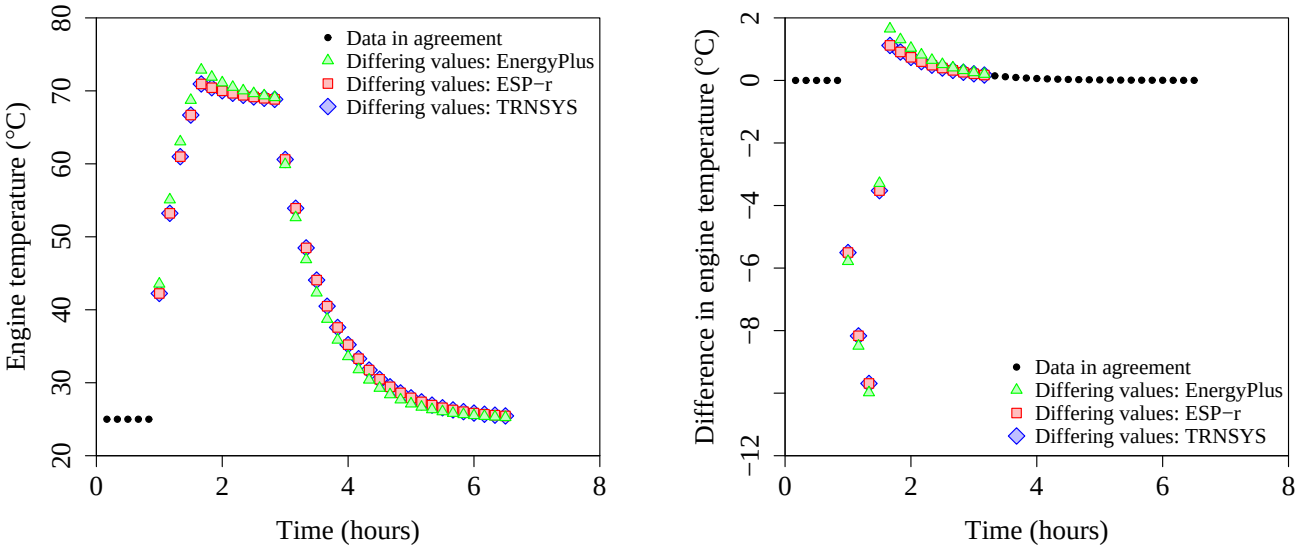

(a) (b)

Figure III-86: Test case 503 — engine temperature (T_{eng}) as a function of time for (a) case 503 and (b) differential between cases 503 and 501 ($T_{eng,503} - T_{eng,501}$)

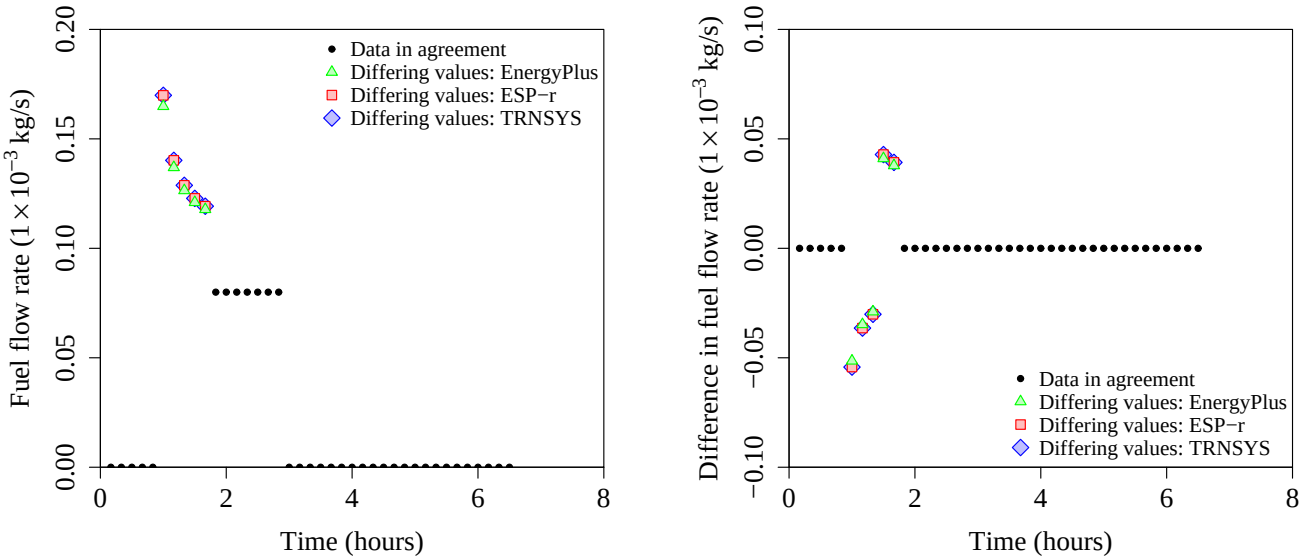

(a) (b)

Figure III-87: Test case 503 — fuel flow rate $\dot{m}_{fuel}$ as a function of time for (a) case 503 and (b) differential between cases 503 and 501 ($\dot{m}_{fuel,503} - \dot{m}_{fuel,501}$)

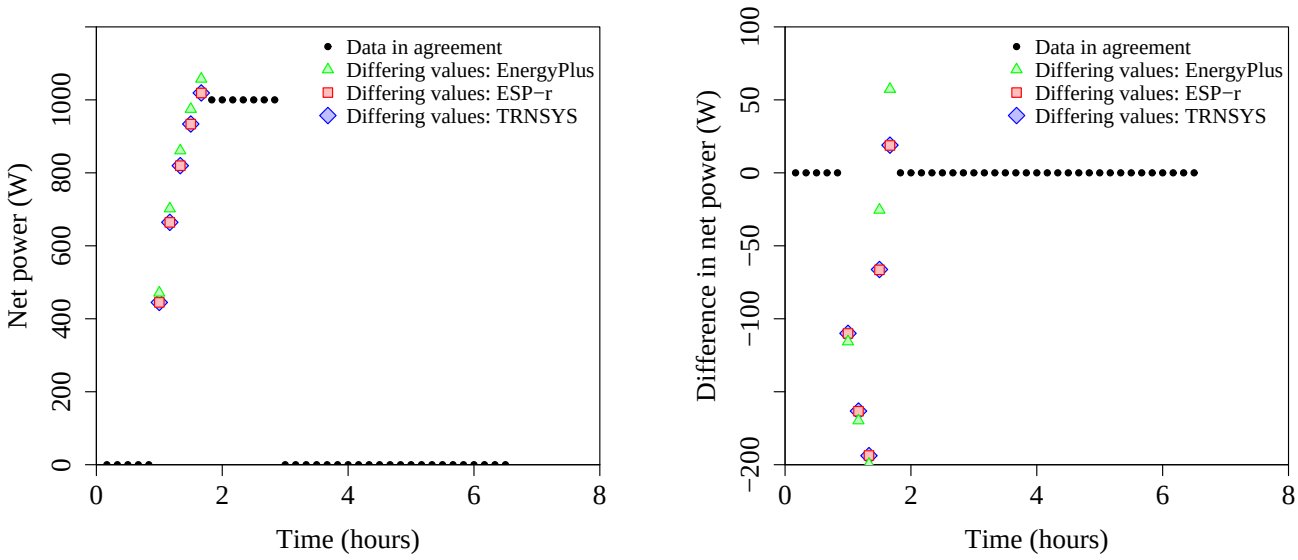

(a) (b)

Figure III-88: Test case 503 — net electric output (P_{net}) as a function of time for (a) case 503 and (b) differential between cases 503 and 501 ($P_{net,503} - P_{net,501}$)

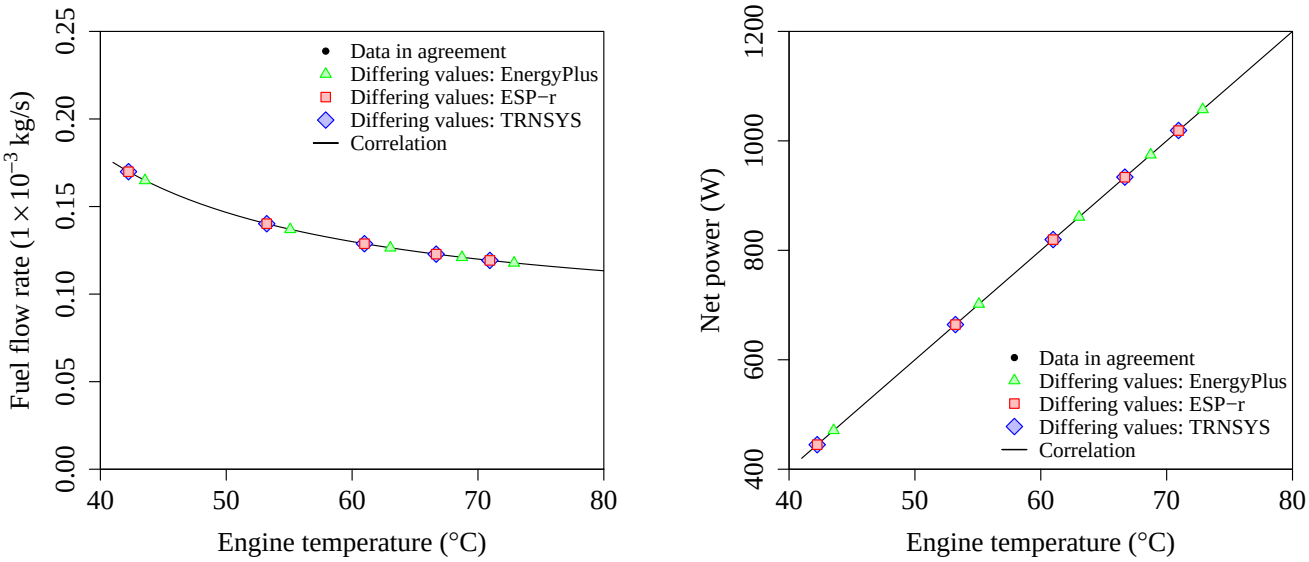

(a) (b)

Figure III-89: Test case 503 — (a) fuel flow rate $\dot{m}_{fuel}$ and (b) net electric output (P_{net}) as functions engine temperature (T_{eng}) during start-up

Test case 504

Test case 503 halves the Stirling engine warm-up power output sensitivity coefficient (k_p) used in test case 501 from 1.0 to 0.5. In this configuration, the predicted power generation during warm-up should be lower than that observed in test case 501.

The difference between the fuel flow, power and heat produced in test cases 504 and 501 (ie. $\dot{m}_{fuel,504} - \dot{m}_{fuel,501}$, $P_{net,504} - P_{net,501}$ and $\dot{q}_{gen,ss,504} - \dot{q}_{gen,ss,501}$) should be plotted against i) time and ii) the temperature of the engine control volume (T_{eng}). Disagreement in these results may indicate an error in the warm-up net power correlation, and developers should check the implementation of Equation 24 in the model specification.

Figure III-90 plots the engine control volume temperature predictions. When the case 504 predictions are compared to case 501, it is clear that the engine temperature predictions are unchanged between the two cases. This is to be expected—neither the warm-up period power sensitivity coefficient nor the calculated rate of electrical generation affect the dynamic thermal model's energy balances.

Similarly, the reported rate of fuel flow (plotted in Figure III-91) is unaffected by variation in the Stirling engine warm-up power output sensitivity coefficient. But Figure III-92 shows that a reduction in the coefficient appreciably reduces the electrical output predicted by all three implementations.

Finally, Figure III-93 plots the predicted rates of electricity generation and fuel consumption as functions of the predicted engine temperature. The black lines on these plots depict the warm-up period fuel flow and power output correlations; clearly, all three implementations agree very well with the correlations.

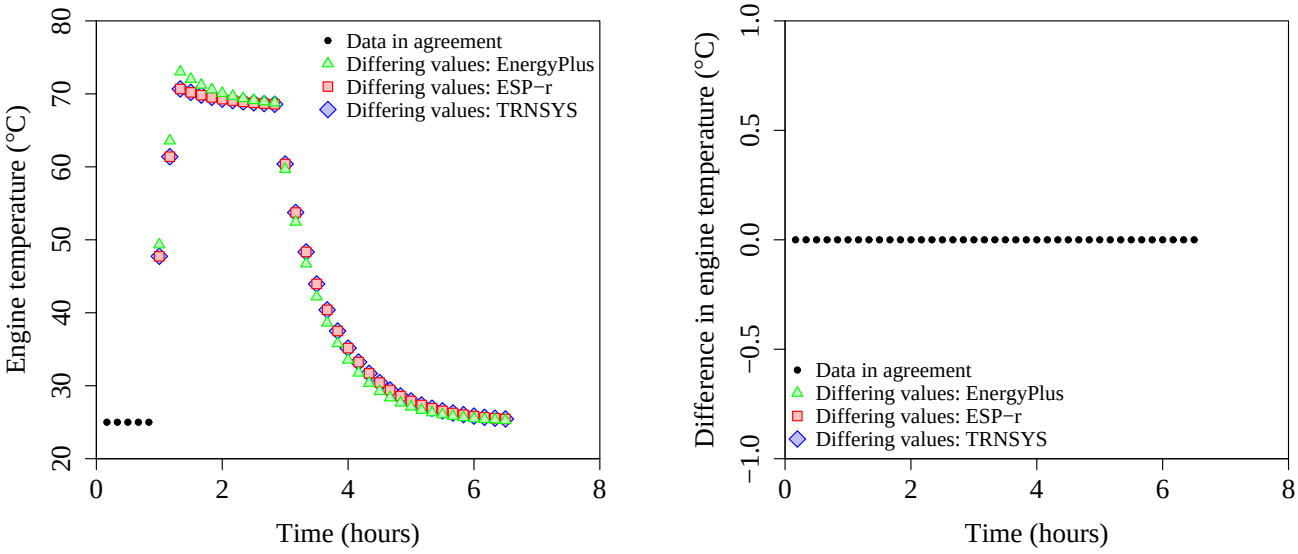

(a) (b)

Figure III-90: Test case 504 — engine temperature (T_{eng}) as a function of time for (a) case 504 and (b) differential between cases 504 and 501 ($T_{eng,504} - T_{eng,501}$)

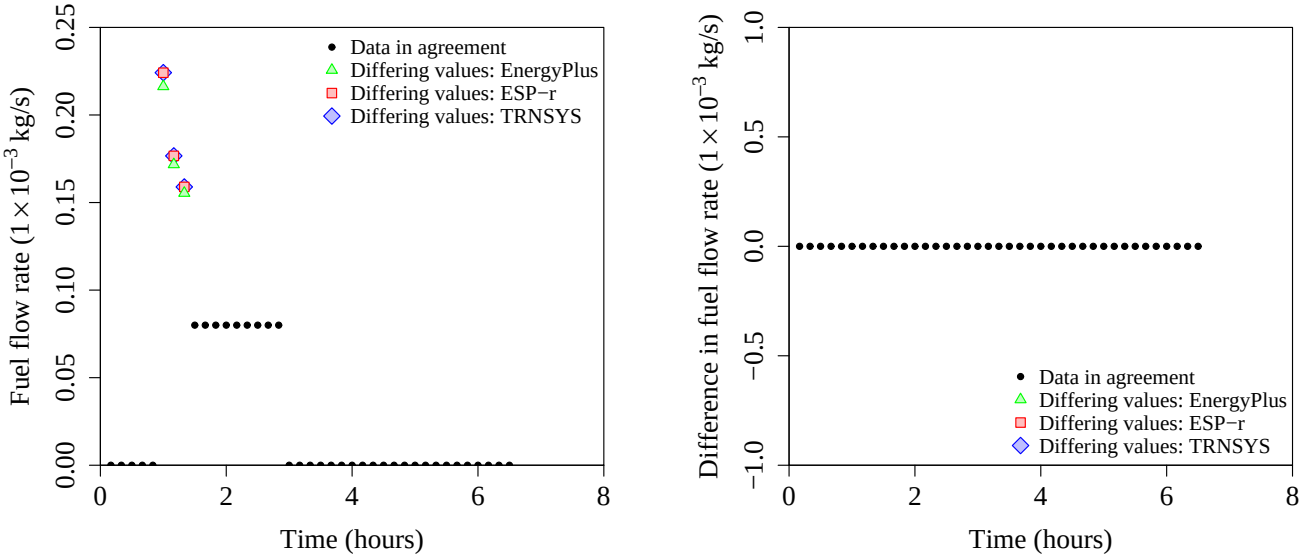

(a) (b)

Figure III-91: Test case 504 — fuel flow rate $\dot{m}_{fuel}$ as a function of time for (a) case 504 and (b) differential between cases 504 and 501 ($\dot{m}_{fuel,504} - \dot{m}_{fuel,501}$)

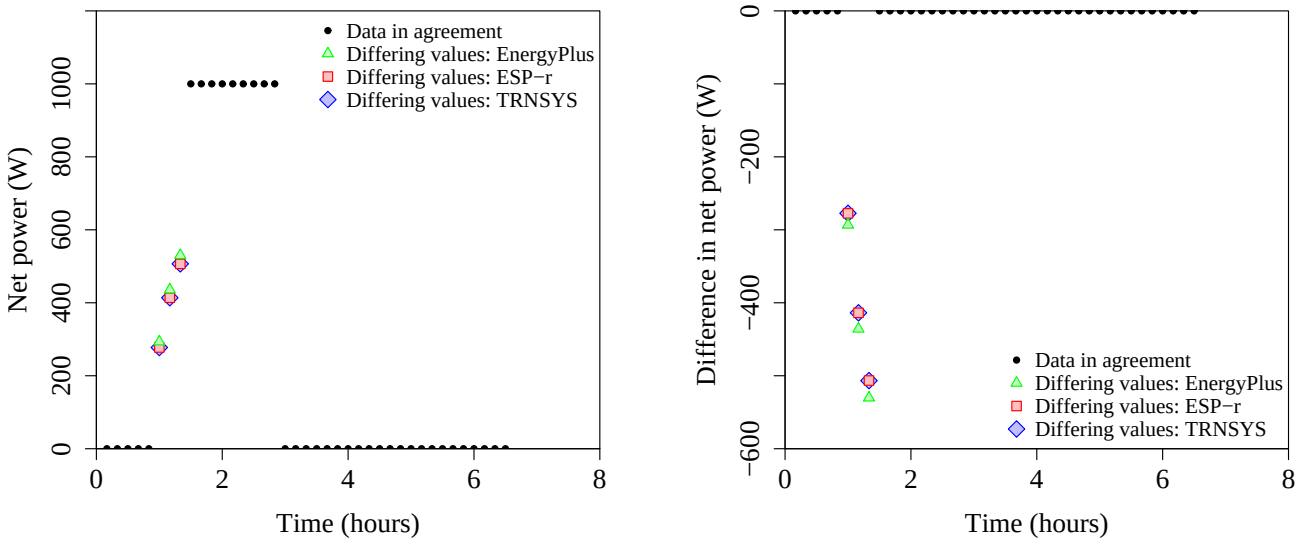

(a) (b)

Figure III-92: Test case 504 — net electric output (P_{net}) as a function of time for (a) case 504 and (b) differential between cases 504 and 501 ($P_{net,504} - P_{net,501}$)

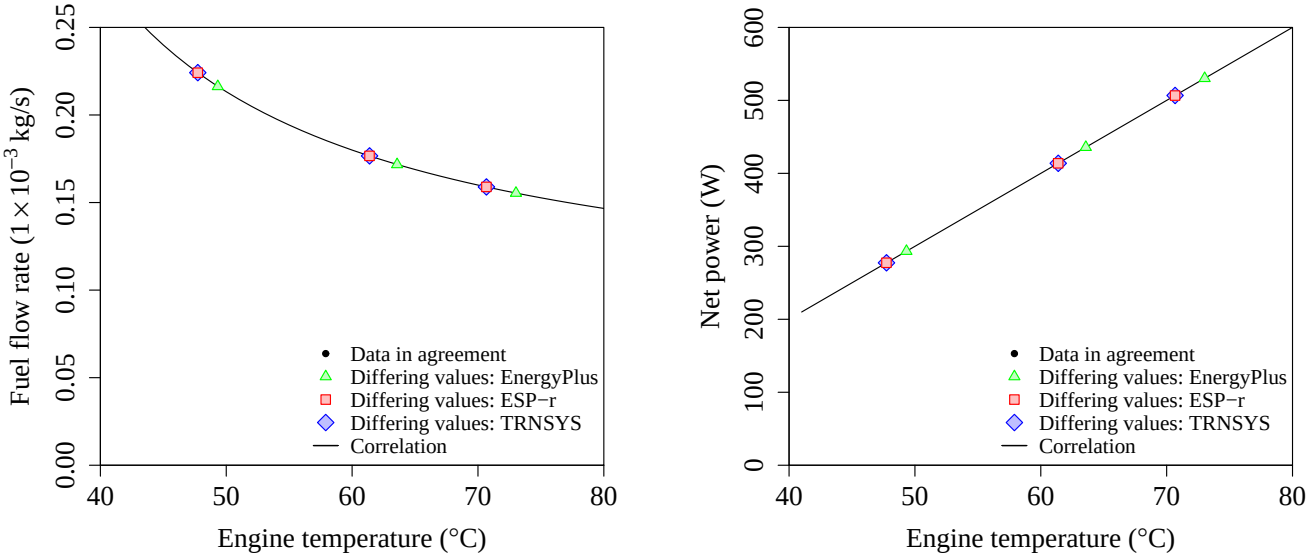

(a) (b)

Figure III-93: Test case 504 — (a) fuel flow rate $\dot{m}_{fuel}$ and (b) net electric output (P_{net}) as functions engine temperature (T_{eng}) during start-up

Test case 505

Test case 505 reduces the ratio between the unit's maximum fuel flow during the warm-up period and normal operation ($r_{fuel,warm-up}$) from 10 to 2. This change should cause the model should predict lower rates of fuel flow during the warm-up period.

The difference between the fuel flow, power and heat produced in test cases 505 and 501 (ie. $\dot{m}_{fuel,505} - \dot{m}_{fuel,501}$, $P_{net,505} - P_{net,501}$ and $\dot{q}_{gen,ss,505} - \dot{q}_{gen,ss,501}$) should be plotted against i) time and ii) the temperature of the engine control volume (T_{eng}). Disagreement in these results may indicate an error in the warm-up fuel flow correlation; developers should check the implementation of Equation III-25 in the model specification.

Figure III-94 plots the predicted engine temperatures for all three implementations. Once again, the EnergyPlus results exhibit a slightly faster response. More importantly, altering the maximum fuel flow ratio produces similar responses across all three models when compared to test case 501.

Similarly, Figure III-95 plots the predicted rate of fuel flow. All three implementations predict the same fuel flow rate for the first 30 minutes of operation, when the warm-up period maximum fuel flow ratio limits the fuel flow rate predicted by the model. The fuel flow rate predictions also exhibit some variation on the forth time step of operation, when the fuel flow rate is no longer limited by the maximum fuel flow ratio, and is instead dependent on the calculated engine control volume temperature.

Variation in the predicted engine control volume temperatures also affects the predicted rates of electric generation, depicted in Figure III-96. EnergyPlus consistently predicts higher values of electric output during the start-up period.

Finally, Figure III-97 plots the predicted rates of fuel flow and power output as functions of the predicted engine temperature. The black lines on the plots predict the warm-up period fuel flow and power output correlations—the fuel flow rate correlation is truncated

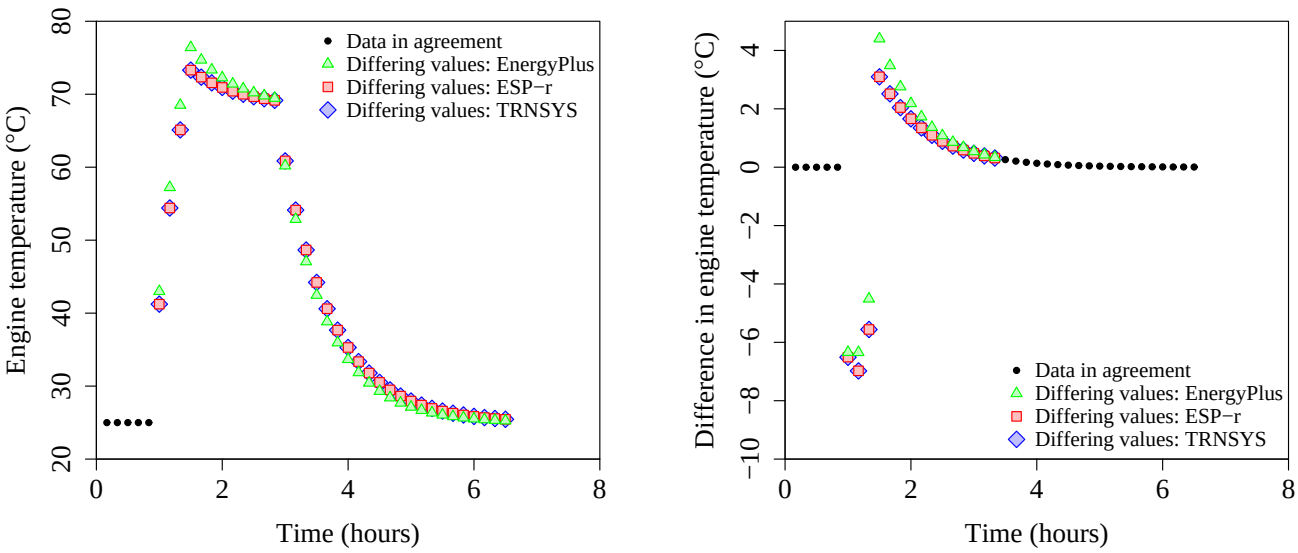

(a) (b)

Figure III-94: Test case 505 — engine temperature (T_{eng}) as a function of time for (a) case 505 and (b) differential between cases 505 and 501 ($T_{eng,505} - T_{eng,501}$)

to reflect the maximum flow permitted by the reduced maximum fuel flow ratio coefficient. Again, all three implementations agree well with the correlations, suggesting this aspect of the model is correctly implemented.

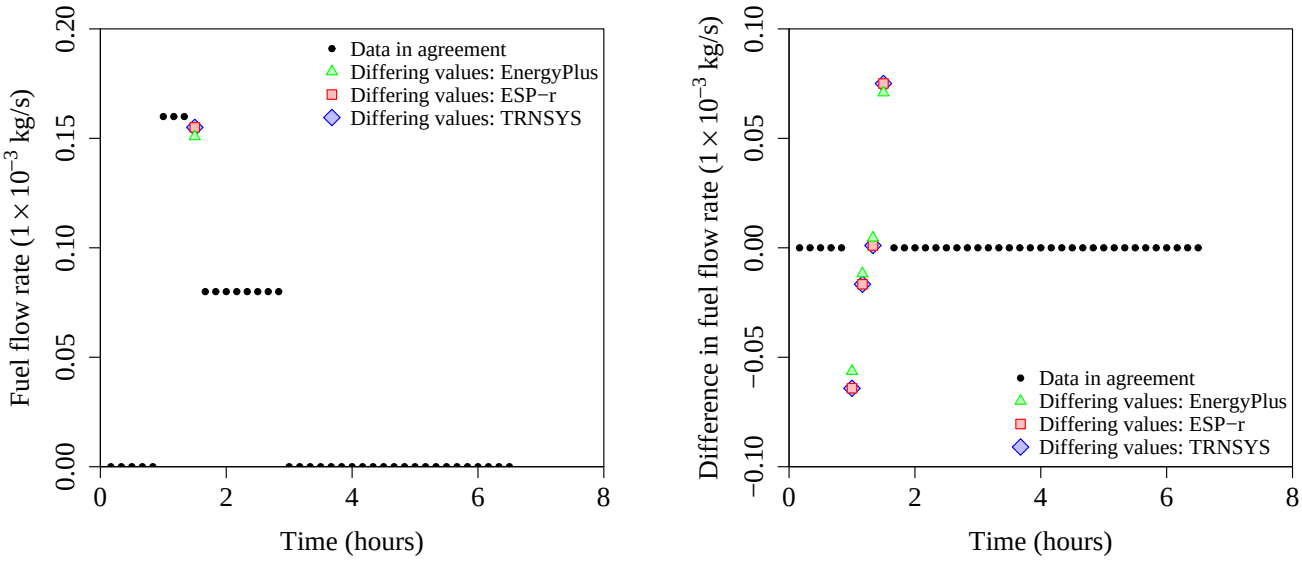

Figure III-95: Test case 505 — fuel flow rate $\dot{m}_{fuel}$ as a function of time for (a) case 505 and (b) differential between cases 505 and 501 ($\dot{m}_{fuel,505} - \dot{m}_{fuel,501}$)

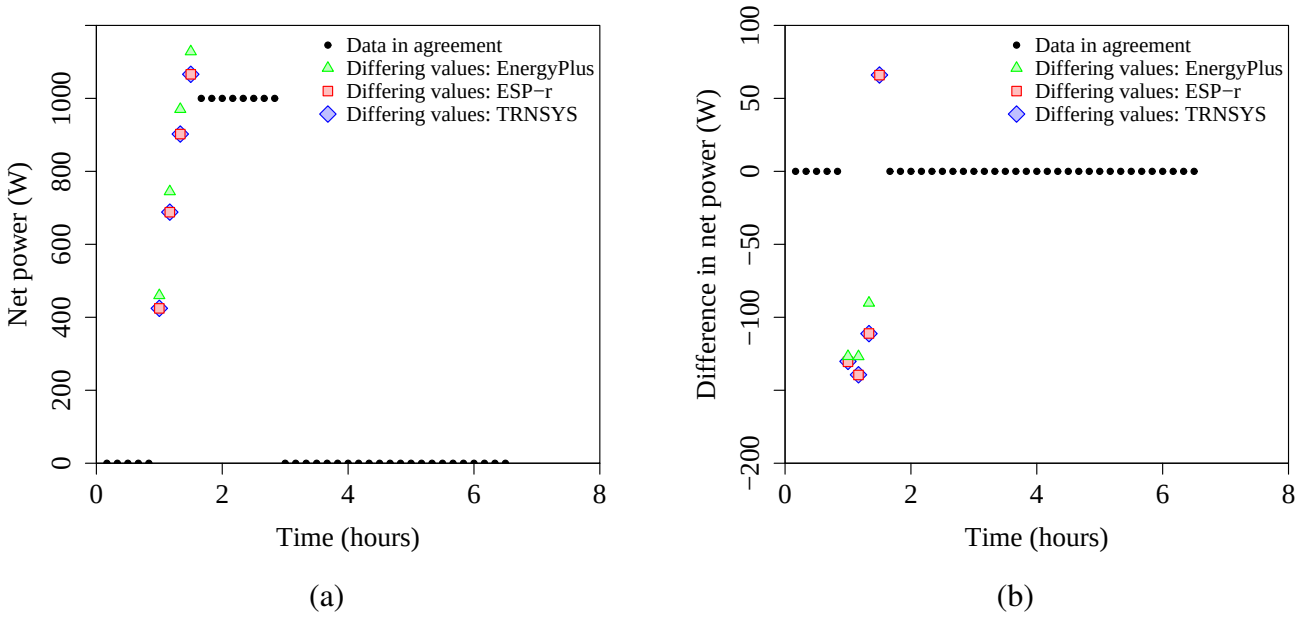

Figure III-96: Test case 505 — net electric output (P_{net}) as a function of time for (a) case 505 and (b) differential between cases 505 and 501 ($P_{net,505} - P_{net,501}$)

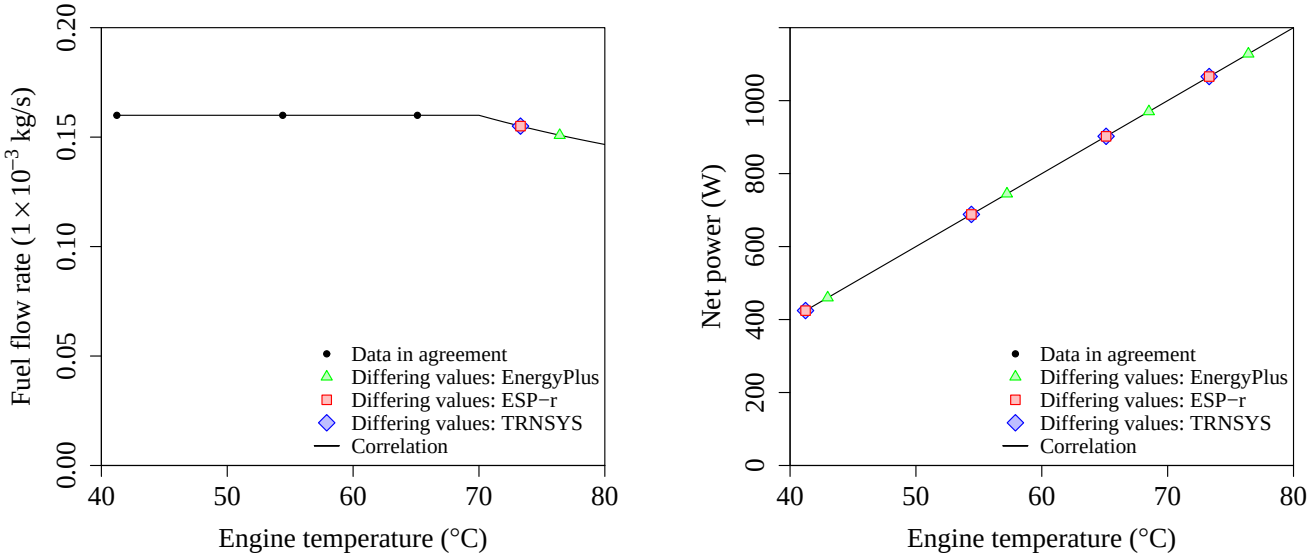

Figure III-97: Test case 505 — (a) fuel flow rate $\dot{m}_{fuel}$ and (b) net electric output (P_{net}) as functions engine temperature (T_{eng}) during start-up

Test case 506

Test case 506 reduces the thermal mass of the engine control volume ($[MC]_{eng}$) from 120000J/K to 60000J/K. With these changes, the engine control volume temperature should reach its nominal value earlier in the simulation.

The difference between the fuel flow, power and heat produced in test cases 506 and 501 (ie. $\dot{m}_{fuel,506} - \dot{m}_{fuel,501}$, $P_{net,506} - P_{net,501}$ and $\dot{q}_{gen,ss,506} - \dot{q}_{gen,ss,501}$) should be plotted against i) time and ii) the temperature of the engine control volume (T_{eng}). Disagreement in these results may indicate an error in the warm-up fuel flow and net power correlations (Equations III-23 and III-24 in the model specification).

Figure III-98 plots the predicted engine temperatures for all three implementations. Once again the EnergyPlus results exhibit a slightly faster response, but altering the engine control volume thermal mass affects all three implementations equally.

Similarly, Figure III-99 plots the predicted rate of fuel flow, and Figure III-100 plots the predicted rate of electricity generation over the course of the test. While EnergyPlus and ESP-r/TRNSYS do not agree exactly, they exhibit similar responses to the reduction in thermal mass when compared to test case 501.

Finally, Figure III-101 plots the predicted rates of fuel flow and power output as functions of the predicted engine temperature. The black lines on the plots predict the warm-up period fuel flow and power output correlations; all three implementations agree well with the correlations, suggesting this aspect of the model is correctly implemented.

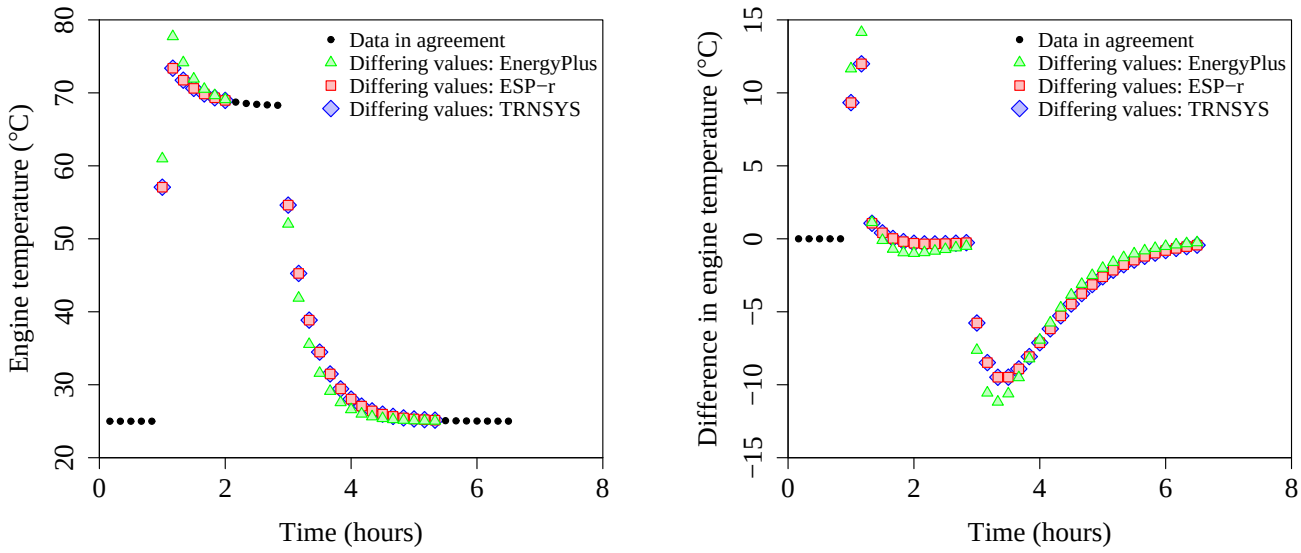

(a) (b)

Figure III-98: Test case 506 — engine temperature (T_{eng}) as a function of time for (a) case 506 and (b) differential between cases 506 and 501 ($T_{eng,506} - T_{eng,501}$)

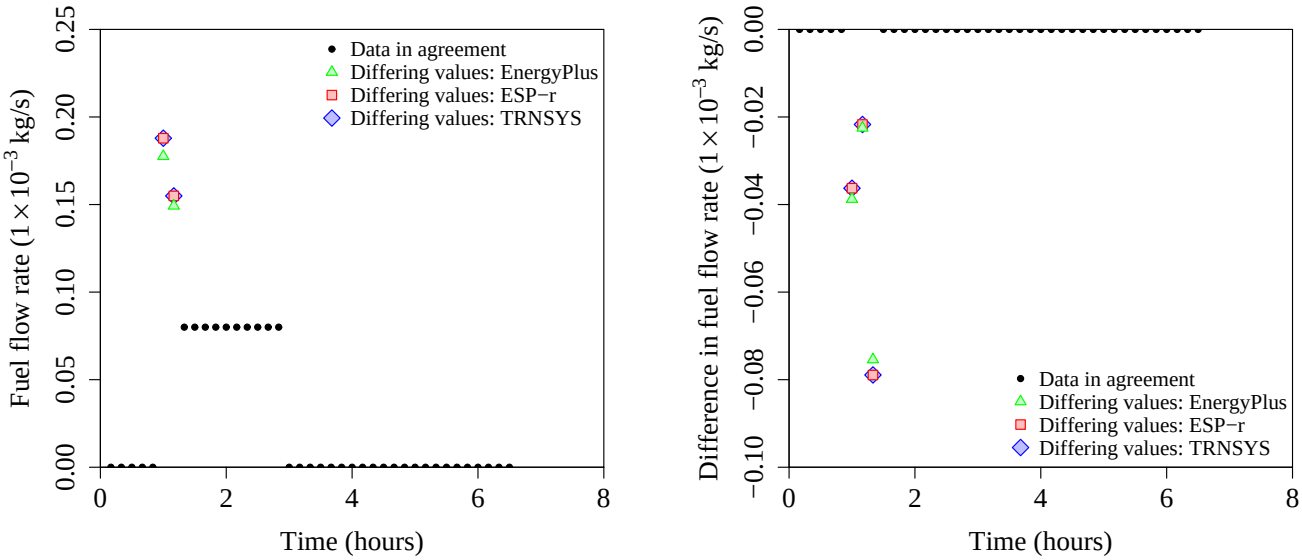

(a) (b)

Figure III-99: Test case 506 — fuel flow rate $\dot{m}_{fuel}$ as a function of time for (a) case 506 and (b) differential between cases 506 and 501 ($\dot{m}_{fuel,506} - \dot{m}_{fuel,501}$)

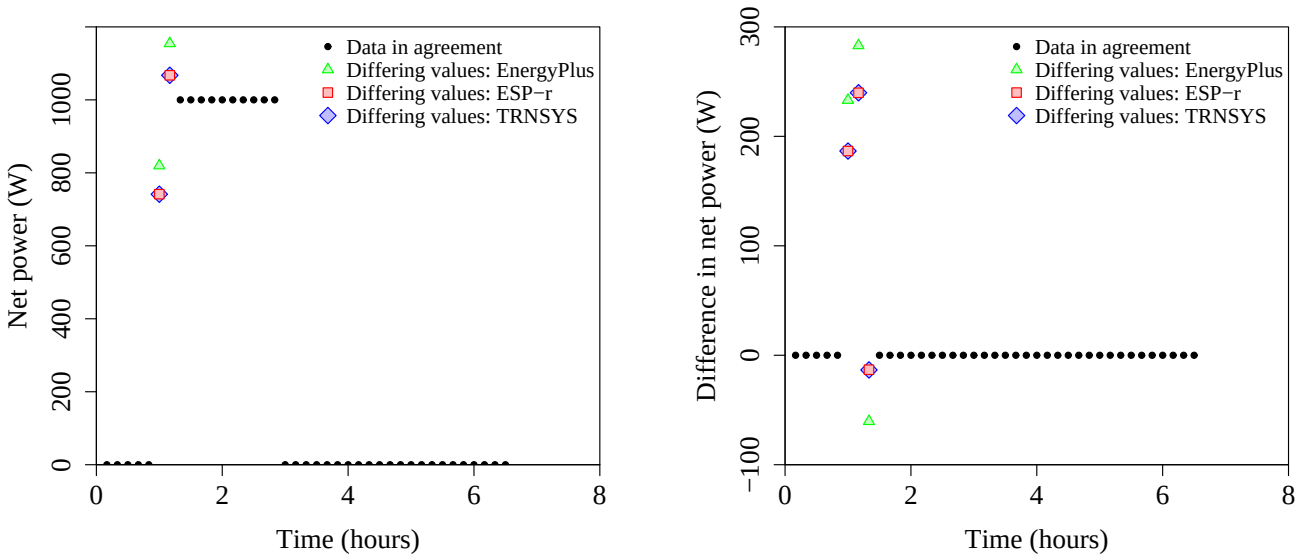

(a) (b)

Figure III-100: Test case 506 — net electric output (P_{net}) as a function of time for (a) case 506 and (b) differential between cases 506 and 501 ($P_{net,506} - P_{net,501}$)

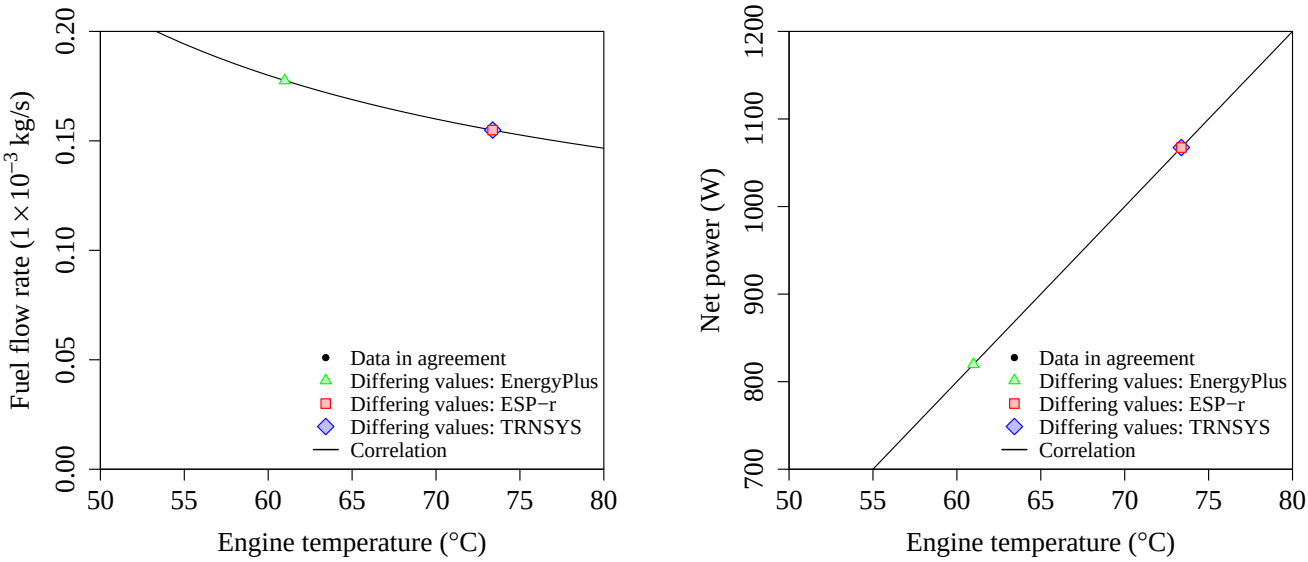

(a) (b)

Figure III-101: Test case 506 — (a) fuel flow rate $\dot{m}_{fuel}$ and (b) net electric output (P_{net}) as functions engine temperature (T_{eng}) during start-up

600 Series tests

The 600 series test cases exercise the rate of change limits that are optionally imposed on the model's predicted fuel flow and power output. These test cases subject the unit to step changes in operating point, and determine if the model correctly predicts the unit's transient response. Only the model's behaviour in normal operation is examined.

Four 600 series test cases have been defined, all of which use the same boundary conditions and control parameters defined in Tables III-19 and III-20, respectively. The differences between the base model configuration and the inputs used in these test cases are summarized in Table III-21.

Table III-19: Boundary conditions — Series 600 tests

				Test Case
Condition	Units	Start	End	601–604
Cooling water inlet temperature	°C	00:00	23:59	25.
Cooling water flow rate	kg/s	00:00	23:59	0.15
Enclosure Temperature	°C	00:00	23:59	20.0

Table III-20: Control parameters — Series 600 tests

				Test Case
Parameter	Units	Start	End	601-604
Control flag	–	00:00	01:00	*off*
		01:00	07:00	*ECI*
		07:00	23:59	*off*
		03:00	23:59	*off*
Control signal	W	00:00	01:00	0.
		01:00	03:00	200.
		03:00	05:00	1000.
		05:00	07:00	200.
		07:00	23:59	0.

Notes:
ECI: Electric load following control interface

Table III-21: Model parameter variations — Series 600 tests

		Test case				
Parameter	Units	Base	601	602	603	604
$(d\dot{m}_{fuel}/dt)_{max}$	kg/s^2	‡	1.0×10^{-8}	‡	1.0×10^{-8}	1.0×10^{-8}
$(dP_{net}/dt)_{max}$	W/s	‡	‡	0.15	0.15	0.04

Notes:
‡ Rate of change limit disabled.

Test case 601

Test case 601 exercises the model's rate limited fuel flow facility. The maximum rate of change in the model's fuel flow is set to $1.0\text{E}\times10^{-8}\,\text{kg/s}^2$, while the rate of change in the unit's electrical output remains unlimited.

The system fuel flow ($\dot{m}_{fuel}$), net electric output (P_{net}), and temperature of the engine control volume (T_{eng}) predicted in test case 601 should be plotted against time. Disagreement in these results suggests an error in the implementation of the rate limited fuel flow facility (Equations III-18 and III-19 in the model specification).

Results from test case 601 are depicted in Figures III-102 and III-103. The ESP-r and TRNSYS results exhibit exact agreement, while the EnergyPlus implementation predicts slightly faster responses in the rates of fuel flow and electricity generation.

This time, the disagreement between the EnergyPlus and ESP-r/TRNSYS results originates from different reporting conventions; EnergyPlus reports the instantaneous rates of fuel flow and electric generation at the end of each time step, while ESP-r and TRNSYS report the time-step averaged values.

Nevertheless, the EnergyPlus, ESP-r and TRNSYS results all exhibit the same slopes during transient operation (that is, dP_{net}/dt and $d\dot{m}_{fuel}/dt$), indicating they implement the fuel-flow rate limiting facility similarly. While test case 601 only prescribed a limit on the rate of change in fuel flow, the resulting power output is also constrained because the unit's fuel flow and electrical output are coupled by the model's steady-state electrical efficiency correlation (Equation III-2 and III-4 in the model specification).

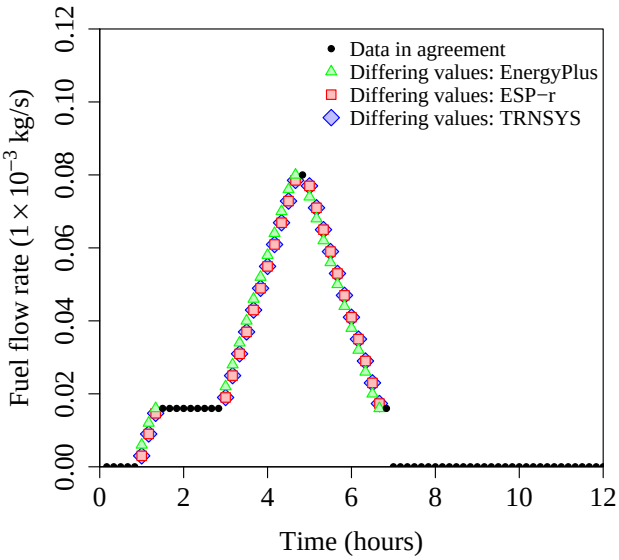

Figure III-102: Test case 601 — fuel flow rate ($\dot{m}_{fuel}$) as a function of time

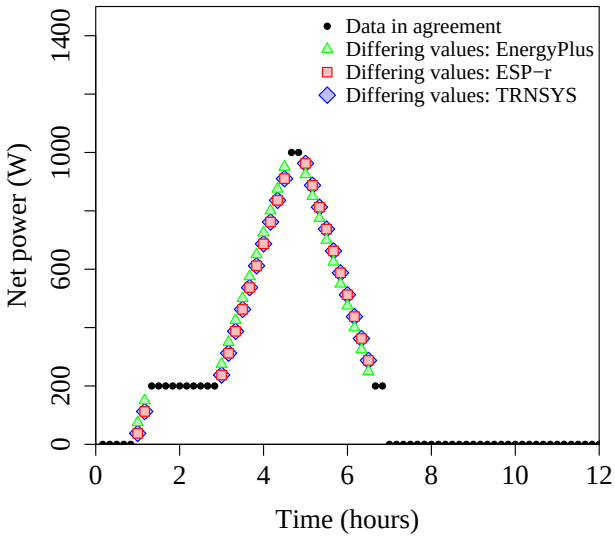

Figure III-103: Test case 601 — net electric output (P_{net}) as a function of time

Test case 602

Test case 602 exercises the model's rate limited electric output facility. The maximum change in the model's electric output is set to 0.15 W/s, while the rate of change in the unit's fuel flow remains unlimited.

The system fuel flow ($\dot{m}_{fuel}$), net electric output (P_{net}), and temperature of the engine control volume (T_{eng}) predicted in test case 602 should be plotted against time. Disagreement in these results suggests an error in the implementation of the rate limited power output facility (Equations III-20 and III-21 in the model specification).

Results from test case 602 are depicted in Figures III-104 and III-105. Again, the results exhibit a slight offset between the EnergyPlus and ESP-r/TRNSYS results; the EnergyPlus results reflect the instantaneous rates of fuel flow and power output at the end of the time step, while ESP-r and TRNSYS report the average value over the time step.

As in test case 601, all three implementations report the same rates of change in both fuel flow and power output (that is, dP_{net}/dt and $d\dot{m}_{fuel}/dt$). Therefore, the three implementations of the power output rate of change limiting facility are comparable.

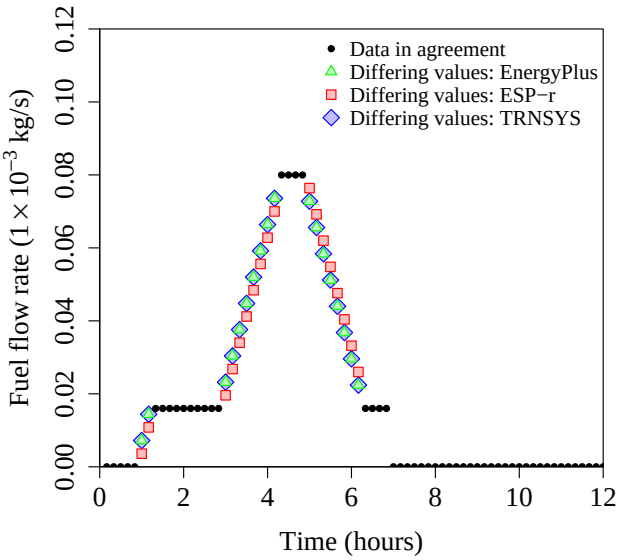

Figure III-104: Test case 602 — fuel flow rate ($\dot{m}_{fuel}$) as a function of time

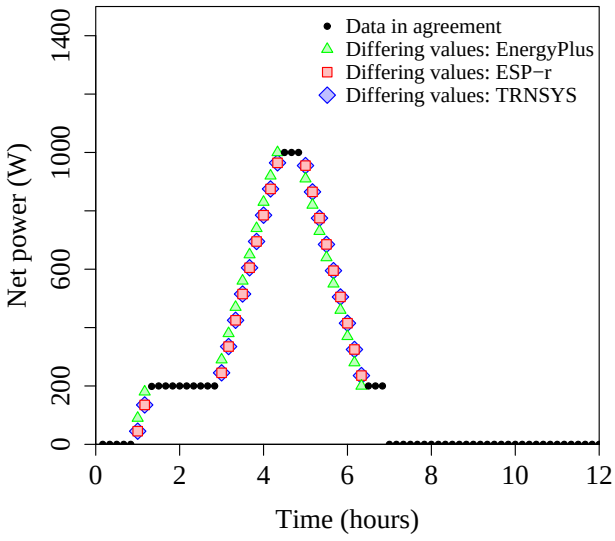

Figure III-105: Test case 602 — net electric output (P_{net}) as a function of time

Test case 603

Test case 603 exercises both the rate limited fuel flow and electric output facilities. The maximum change in the model's electric output is set to 0.15 W/s, while the rate of change in the unit's fuel flow is constrained to $1.0\text{E}\times10^{-8}$ kg/s^2.

The system fuel flow ($\dot{m}_{fuel}$) and net electric output (P_{net}) predicted in test case 603 should be plotted against time. Disagreement in these results suggests an error in either the rate limited fuel flow or net electric output facilities (Equations III-18–III-21 in the model specification).

Results from test case 603 are depicted in Figures III-106 and III-107. Again, the results exhibit a slight offset between the EnergyPlus and ESP-r/TRNSYS results; the EnergyPlus results reflect the instantaneous rates of fuel flow and power output at the end of the time step, while ESP-r and TRNSYS report the average value over the time step. As in test case 601, all three implementations report the same rates of change in both fuel flow and power output (that is, dP_{net}/dt and $d\dot{m}_{fuel}/dt$).

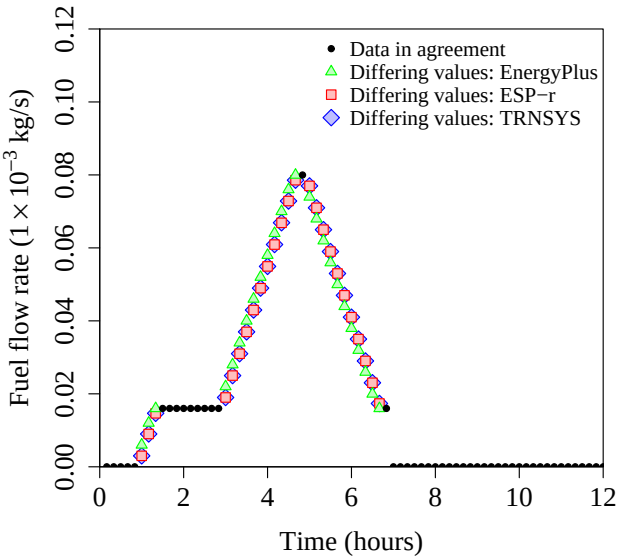

Figure III-106: Test case 603 — fuel flow rate ($\dot{m}_{fuel}$) as a function of time

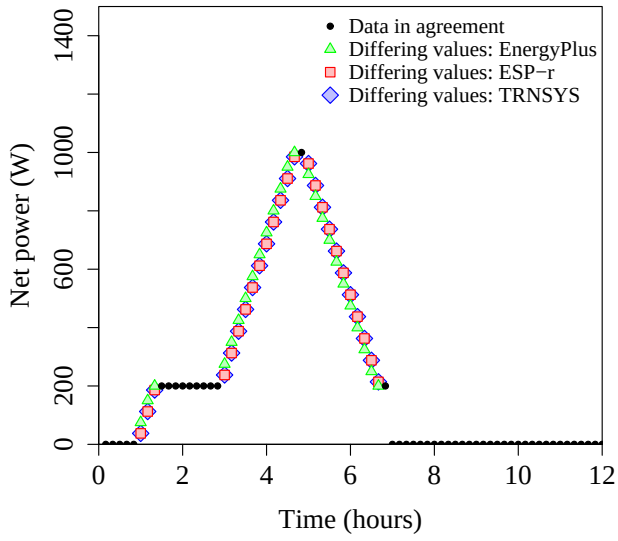

Figure III-107: Test case 603 — net electric output (P_{net}) as a function of time

Test case 604

Test case 604 exercises both the rate limited fuel flow and electric output facilities. The model inputs are identical to test case 603, except the rate limited electric output is reduced from 0.15 W/s to 0.04 W/s.

The system fuel flow ($\dot{m}_{fuel}$), net electric output (P_{net}), and temperature of the engine control volume (T_{eng}) predicted in test case 604 should be plotted against time. Disagreement in these results suggests an error in either the rate limited fuel flow or net electric output facilities (Equations III-18–III-21 in the model specification).

Results from test case 604 are depicted in Figures III-108 and III-109. Again, the results exhibit a slight offset between the EnergyPlus and ESP-r/TRNSYS results; the EnergyPlus results reflect the instantaneous rates of fuel flow and power output at the end of the time step, while ESP-r and TRNSYS report the average value over the time step. As in test case 601, all three implementations report the same rates of change in both fuel flow and power output (that is, dP_{net}/dt and $d\dot{m}_{fuel}/dt$).

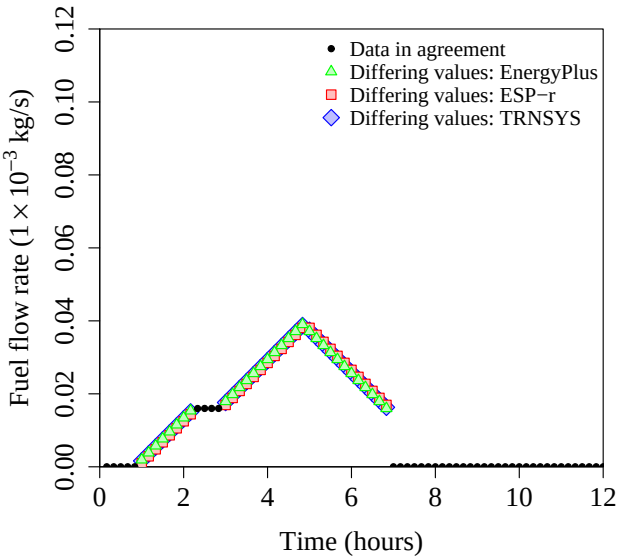

Figure III-108: Test case 604 — fuel flow rate ($\dot{m}_{fuel}$) as a function of time

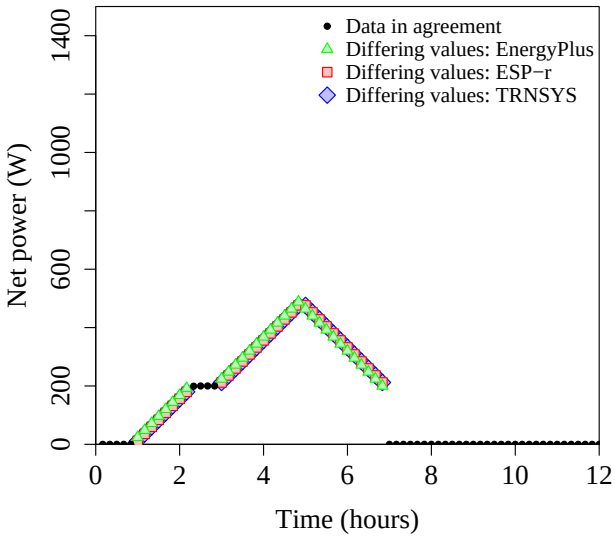

Figure III-109: Test case 604 — net electric output (P_{net}) as a function of time

Table III-22: Model parameter variations — Series 700 tests

		Test case	
Parameter	Units	Base	701, 702
$T_{cw,max}$	°C	100.	70.
$[MC]_{eng}$	J/K	20.0 E03	5.0 E03
$[MC]_{HX}$	J/K	20.0 E03	5.0 E03
UA_{HX}	W/K	50.	100.

700 Series tests

The 700 series tests exercise the model's low-level controls, which protect the unit from overheating when the temperature of the supplied cooling water is too high, or the flow of cooling water is interrupted.

Two 700 series test cases have been defined, and the parameter inputs used in these test cases and the base case are compared in Table III-22. The boundary conditions are described in Tables III-23 and III-24, while the model control parameters are described in Table III-25.

EnergyPlus does not yet implement the cooling water overheating protection aspects of the combustion cogeneration model. For this reason, EnergyPlus 700 series test results are not available.

Table III-23: Boundary conditions — Series 700 tests: enclosure and cooling water inlet temperature

				Test Case	
Condition	Units	Start	End	701	702
Cooling water inlet temperature	°C	00:00	01:00	65.	65.
		01:00	02:00	65.	65.
		02:00	03:00	66.	65.
		03:00	04:00	67.	65.
		04:00	05:00	68.	65.
		05:00	06:00	69.	65.
		06:00	07:00	70.	65.
		07:00	08:00	71.	65.
		08:00	09:00	72.	65.
		09:00	10:00	73.	65.
		10:00	11:00	74.	65.
		11:00	12:00	75.	65.
		12:00	13:00	74.	65.
		13:00	14:00	73.	65.
		14:00	15:00	72.	65.
		15:00	16:00	71.	65.
		16:00	17:00	70.	65.
		17:00	18:00	69.	65.
		18:00	19:00	68.	65.
		19:00	20:00	67.	65.
		20:00	21:00	66.	65.
		21:00	22:00	65.	65.
		22:00	23:00	65.	65.
		23:00	23:59	65.	65.
Enclosure temperature	°C	00:00	23:59	20.	

Table III-24: Boundary conditions — Series 700 tests: cooling water flow rate

				Test Case	
Condition	Units	Start	End	701	702
Cooling water flow rate	kg/s	00:00	01:00	0.2	0.2
		01:00	02:00	0.2	0.2
		02:00	03:00	0.2	0.
		03:00	04:00	0.2	0.
		04:00	05:00	0.2	0.15
		05:00	06:00	0.2	0.14
		06:00	07:00	0.2	0.13
		07:00	08:00	0.2	0.12
		08:00	09:00	0.2	0.11
		09:00	10:00	0.2	0.1
		10:00	11:00	0.2	0.09
		11:00	12:00	0.2	0.08
		12:00	13:00	0.2	0.07
		13:00	14:00	0.2	0.06
		14:00	15:00	0.2	0.05
		15:00	16:00	0.2	0.04
		16:00	17:00	0.2	0.03
		17:00	18:00	0.2	0.02
		18:00	19:00	0.2	0.01
		19:00	20:00	0.2	0.
		20:00	21:00	0.2	0.
		21:00	22:00	0.2	0.
		22:00	23:00	0.2	0.
		23:00	23:59	0.2	0.

Table III-25: Control parameters — Series 700 tests

				Test Case
Parameter	Units	Start	End	701,702
Control flag	–	00:00	01:00	*off*
		01:00	23:00	*ECI*
		23:00	23:59	*off*
Control signal	W	00:00	01:00	0.
		01:00	23:00	1000.
		23:00	23:59	0.

Notes:
ECI: Electric load following control interface

Test case 701

Test case 701 exercises the model's low-level overheating protection control in response increasing cooling water inlet temperatures. The unit is activated at 01:00h, and remains on until 23:00h. Over the course of the test, the cooling water temperature is increased from 65 °C to 75 °C in hourly increments of 1 °C, and then decreased to in decrements of 1 °C. The maximum cooling water outlet temperature ($T_{cw,max}$) is set to 70 °C.

The fuel flow ($\dot{m}_{fuel}$ and net electric output (P_{net}) predicted in test case 701 should be plotted against time. In addition, the cooling water outlet temperature ($T_{cw,o}$), and the difference between outlet and inlet temperatures ($T_{cw,o} - T_{cw,i}$) should be plotted against time.

Figure III-110 plots the predicted system fuel flow rate over the course of the simulation, while Figure III-111 plots the electric output predictions. In both cases the TRNSYS and ESP-r results agree exactly.

Figure III-112 plots the predicted cooling water outlet temperature over the course of the simulation. The outlet temperature increases in 1 °C increments, until it reaches the maximum outlet temperature (70 °C). Once the maximum outlet temperature is exceeded the unit begins to operate intermittently; it shuts down and allows the cooling water control volume to cool below the maximum outlet temperature, at which point it resumes operation. The unit remains off indefinitely once the cooling water inlet temperature rises above 70 °C.

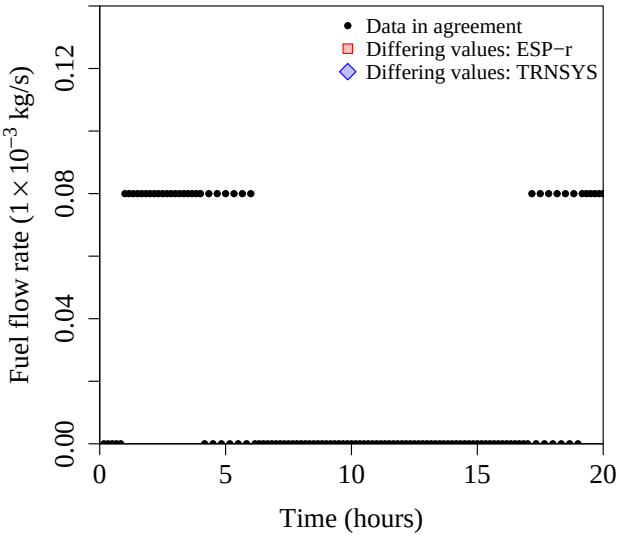

Figure III-110: Test case 701 — fuel flow rate ($\dot{m}_{fuel}$) as a function of time

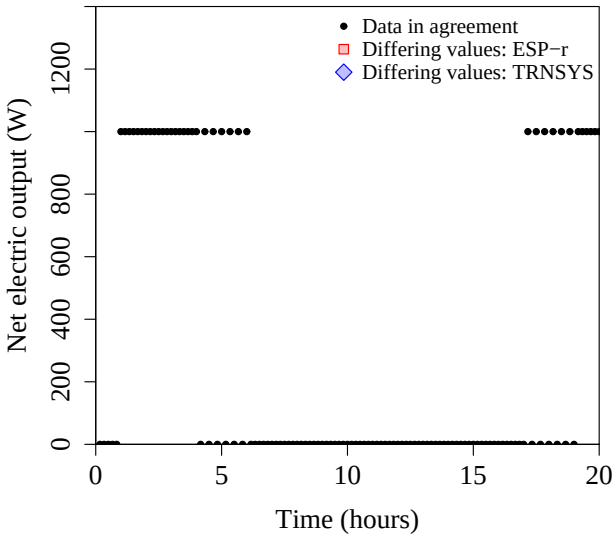

Figure III-111: Test case 701 — net electric output (P_{net}) as a function of time

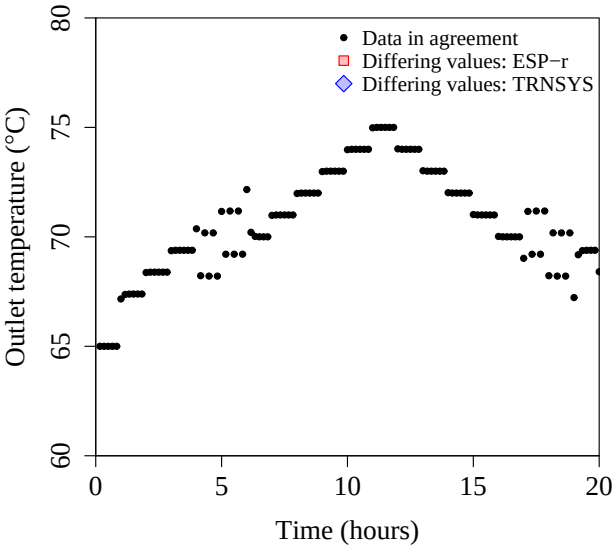

Figure III-112: Test case 701 — Cooling water outlet temperature ($T_{cw,o}$) as a function of time

Test case 702

Test case 702 exercises the model's low-level overheating protection control in response to decreasing cooling water flow rates, and to a complete interruption in cooling water flow. At the start of the test, cooling water is supplied to the unit at a rate of 0.2 kg/s. At 02:00h the flow of cooling water is interrupted for a two-hour period, after which it resumes at 0.15 kg/s. Over the next 15 hours, the cooling water flow rate is reduced in hourly decrements of 0.01 kg/s, until it is again completely interrupted at 19:00 hours.

The fuel flow ($\dot{m}_{fuel}$) and net electric output (P_{net}) predicted in test case 702 should be plotted against time. In addition, the cooling water outlet temperature ($T_{cw,o}$), and the difference between outlet and inlet temperatures ($T_{cw,o} - T_{cw,i}$) should be plotted against time.

The fuel flow predictions for test case 702 are plotted in Figure III-113, while the predicted power output is plotted in Figure III-114. The ESP-r and TRNSYS results agree exactly; both implementations predict deactivation of the unit when the flow of cooling water is interrupted between 02:00 h and 04:00 h. When the cooling water flow rate is gradually reduced between 05:00 h and 18:00 h, both models predict intermittent operation as the cooling water inlet temperature approaches the maximum permitted outlet temperature (70 °C).

Figure III-115 plots the cooling water outlet temperature predictions. Clearly, the outlet temperature increases significantly as the cooling inlet temperature increases, and the unit begins to operate intermittently when the outlet temperature exceeds the specified maximum.

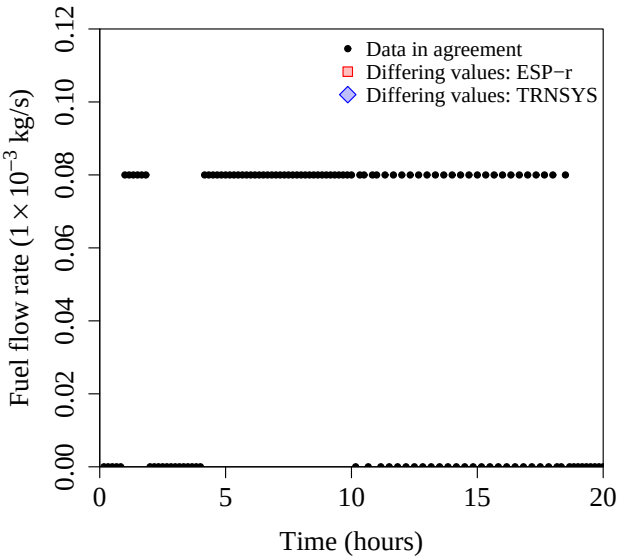

Figure III-113: Test case 702 — fuel flow rate ($\dot{m}_{fuel}$) as a function of time

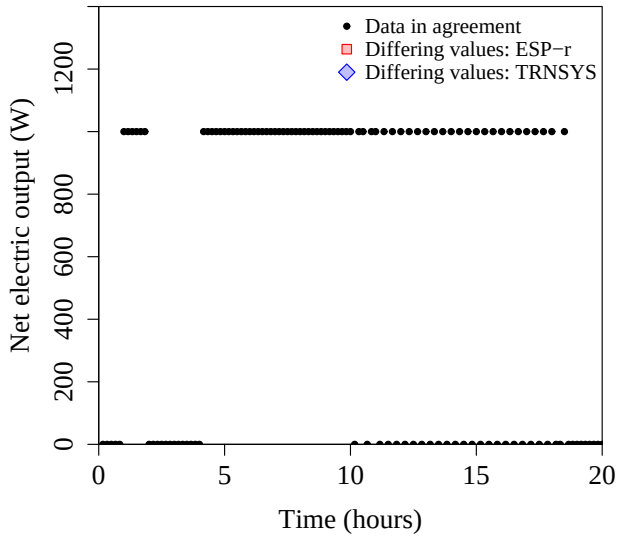

Figure III-114: Test case 702 — net electric output (P_{net}) as a function of time

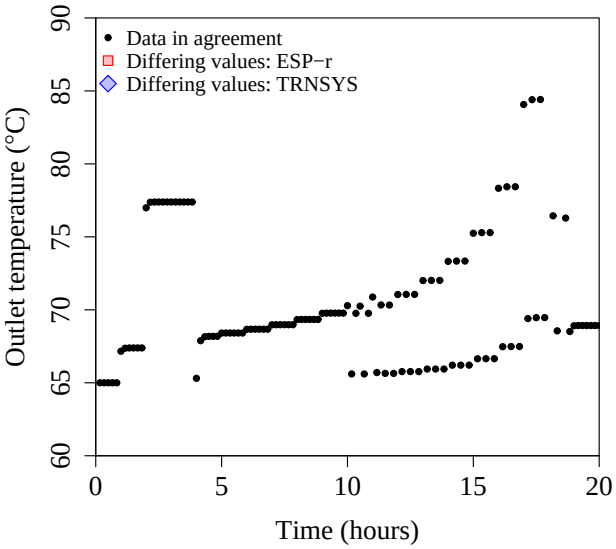

Figure III-115: Test case 702 — Cooling water outlet temperature ($T_{cw,o}$) as a function of time

800 Series tests

The 800 series test cases explicitly exercise various aspects of the model's controls. While the 100–700 series tests have already exercised the model's electrical load following control interface (*ECI*), test case 801 further tests this facility by providing control signals exceeding the unit's specified operating range. Test case 802 focuses on the alternate dimensionless control interface (*DCI*), and exercises it over a range of operation.

The differences between the base configuration and the 800 series test cases are presented in Table III-26, and the boundary conditions and control parameters used in the 800 series test cases are specified in Tables III-27 and III-28, respectively.

Unfortunately, time constraints precluding exercising EnergyPlus over the 800 series tests, and only ESP-r and TRNSYS are compared in these test cases.

Table III-26: Model parameter variations — Series 800 tests

		Test case	
Parameter	Units	Base	801, 802
P_{min}	W	0.	200.

Table III-27: Boundary conditions — Series 800 tests

				Test Case
Condition	Units	Start	End	801, 802
Cooling water inlet temperature	°C	00:00	23:59	25.
Cooling water flow rate	kg/s	00:00	23:59	0.20
Enclosure temperature	°C	00:00	23:59	20.

Table III-28: Control parameters — Series 800 tests

				Test Case	
Parameter	Units	Start	End	801	802
Control flag	–	00:00	01:00	*off*	*off*
		01:00	23:00	*ECI*	*DCI*
		23:00	23:59	*off*	*off*
Control signal	W,–	00:00	01:00	0.	0.
		01:00	02:00	800.	0.2
		02:00	03:00	1100.	0.4
		03:00	04:00	800.	0.6
		04:00	05:00	1010.	0.8
		05:00	06:00	500.	1.0
		06:00	07:00	50.	1.2
		07:00	08:00	500.	0.5
		08:00	09:00	180.	-0.2
		09:00	23:59	0.	0.0

Notes:
DCI: Dimensionless control interface
ECI: Electric load following control interface

Test case 801

Test case 801 explores the model's behaviour when the specified control signal exceeds its maximum and minimum operating points. The test case 801 configuration is identical to the base case configuration, except that the unit's minimum electrical output (P_{min}) is increased to 200 W.

In test case 801, the unit is controlled using the electric load following control interface, and the electrical demand placed on the unit is switched between values alternating inside and outside the unit's operating range on an hourly basis.

The system fuel flow and net power output predicted in test case 801 should be plotted against time. Disagreement in these data may indicate errors in the implementation of the electrical control interface.

The fuel flow rate predictions are plotted in Figure III-116, and the power output predictions are plotted in Figure III-117. In both cases, the ESP-r and TRNSYS implementations agree exactly.

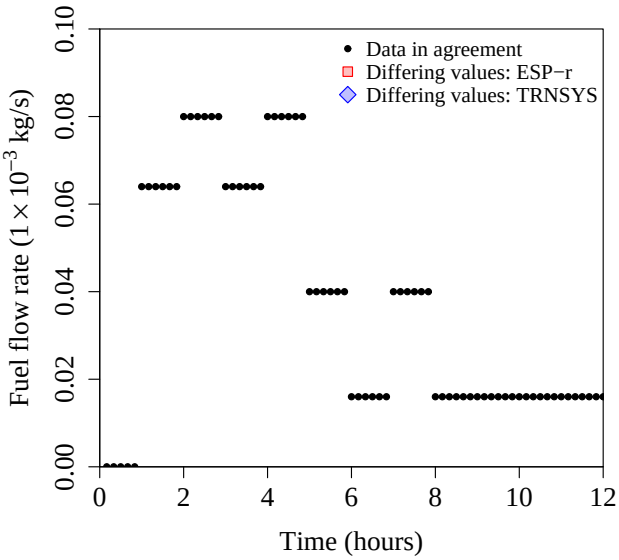

Figure III-116: Test case 801 — fuel flow rate ($\dot{m}_{fuel}$) as a function of time

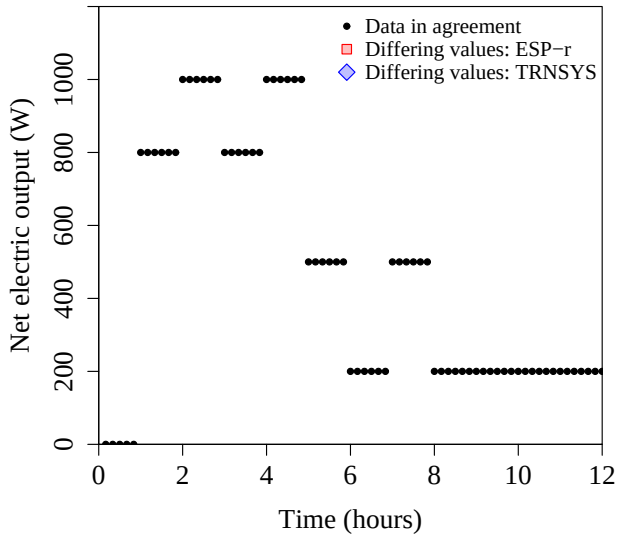

Figure III-117: Test case 801 — net electric output (P_{net}) as a function of time

Test case 802

Test case 802 exercises the model's alternate, dimensionless control interface. In test case 802, the model configuration is unchanged from case 801. The controller activates the unit using the dimensionless control interface and exercises the model at various operating points, some of which lie outside its operating range.

The system fuel flow and net power output predicted in test case 802 should be plotted against time. Disagreement in these data may indicate errors in the implementation of the dimensionless control interface.

The fuel flow rate predictions are plotted in Figure III-118, and the power output predictions are plotted in Figure III-119. In both cases, the ESP-r and TRNSYS implementations agree exactly.

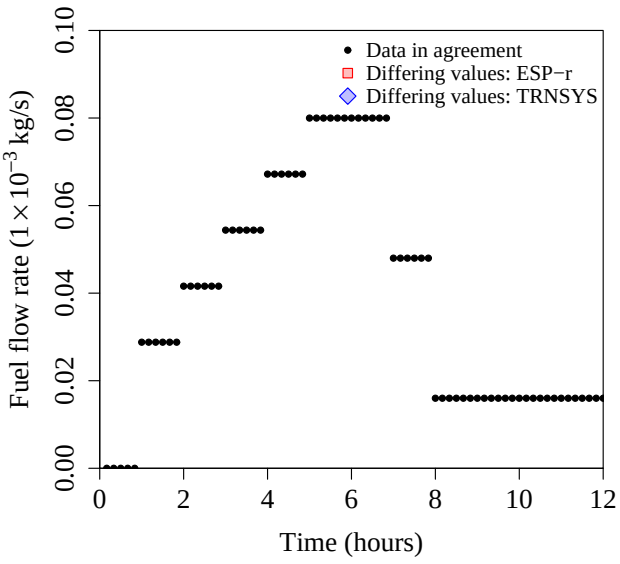

Figure III-118: Test case 802 — fuel flow rate ($\dot{m}_{fuel}$) as a function of time

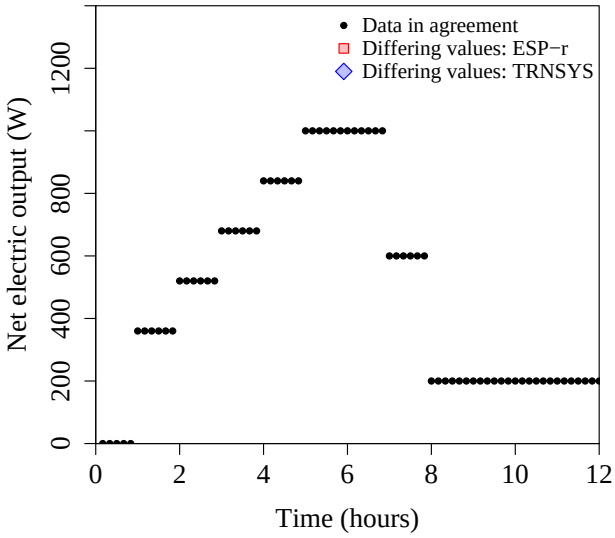

Figure III-119: Test case 802 — net electric output (P_{net}) as a function of time

900 Series tests

The 900 series tests exercise the model's simple carbon-dioxide emission calculation facility, which is described in Section 901 in the model specification. To pass the 900 series tests, the model must correctly predict the mass flow rate of carbon dioxide emissions produced at various operating points.

Three 900 series tests have been devised, and the differences in the input model parameters used in these cases and the base case are presented in Table III-29. All 900 series tests use the same boundary conditions and control parameters, which are described in Tables III-30 and III-31, respectively. The boundary conditions remain constant throughout the test, while the controls vary the unit's electrical output from 0 W to 1000 W in hourly increments of 100 W.

Unfortunately, time constraints precluded exercising EnergyPlus over the 900 series tests, and only ESP-r and TRNSYS are compared in these test cases.

Table III-29: Model parameter variations — Series 900 tests

		Test case			
Parameter	Units	Base	901	902	903
Fuel type	–	*gaseous mixture*	†	†	*liquid fuel*
LHV_{fuel}	J/kg	‡	‡	‡	50.0 E06
e_{CO_2}	kg CO_2/kg fuel	‡	‡	‡	3.50
χ_{H_2}	mol/mol	0.	†	0.1	*
χ_{CH_4}	mol/mol	1.	†	0.34	*
$\chi_{C_2H_6}$	mol/mol	0.	†	0.20	*
$\chi_{C_3H_8}$	mol/mol	0.	†	0.05	*
$\chi_{C_4H_{10}}$	mol/mol	0.	†	0.05	*
$\chi_{C_5H_{12}}$	mol/mol	0.	†	0.05	*
$\chi_{C_6H_{14}}$	mol/mol	0.	†	0.05	*
χ_{CH_3OH}	mol/mol	0.	†	0.05	*
$\chi_{C_2H_5OH}$	mol/mol	0.	†	0.05	*
χ_{CO_2}	mol/mol	0.	†	0.02	*
χ_{N_2}	mol/mol	0.	†	0.02	*
χ_{O_2}	mol/mol	0.	†	0.02	*

Notes:
† Value unchanged from base case.
‡ The fuel lower heating value is calculated by the model when a gaseous fuel mixture is specified
* The fuel composition is inconsequential when the liquid fuel configuration is specified.

Table III-30: Boundary conditions — Series 900 tests

				Test Case
Condition	Units	Start	End	901–903
Cooling water inlet temperature	°C	00:00	23:59	10.
Cooling water flow rate	kg/s	00:00	23:59	0.20
Enclosure temperature	°C	00:00	23:59	20.

Table III-31: Control parameters — Series 900 tests

				Test Case
Parameter	Units	Start	End	901–903
Control flag	–	00:00	01:00	*off*
		01:00	11:00	*ECI*
		11:00	23:59	*off*
Control signal	W	00:00	01:00	0.
		01:00	02:00	100.
		02:00	03:00	200.
		03:00	04:00	300.
		04:00	05:00	400.
		05:00	06:00	500.
		06:00	07:00	600.
		07:00	08:00	700.
		08:00	09:00	800.
		09:00	10:00	900.
		10:00	11:00	1000.
		11:00	23:59	0.

Notes:
ECI: Electric load following control interface

Test case 901

The 901 test case model configuration is identical to the base configuration, in which the cogeneration unit's fuel is specified as 100% methane. To pass test case 901, the model must correctly predict the mass flow rate of carbon dioxide emissions ($\dot{m}_{CO_2}$) for the duration of the test.

The mass flow rate of carbon dioxide emissions should be plotted against time. Disagreement in these values suggests an error in the calculation of carbon dioxide emissions for methane.

Figure III-120 plots the predicted carbon dioxide emissions for test case 901. The ESP-r and TRNSYS results agree exactly.

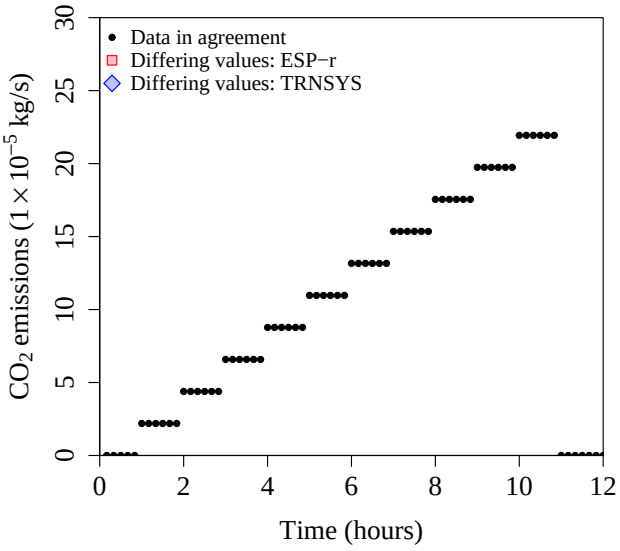

Figure III-120: Test case 901 — carbon dioxide emissions ($\dot{m}_{CO_2}$) as a function of time

Test case 902

Test case 901 uses a model configuration identical to test case 105, in which the cogeneration unit's fuel is specified as a gaseous mixture of hydrocarbons and inert gases. To pass test case 902, the model must correctly predict the mass flow rate of carbon dioxide emissions ($\dot{m}_{CO_2}$) for the duration of the test.

The mass flow rate of carbon dioxide emissions should be plotted against time. Disagreement in these values suggests an error in the calculation of carbon dioxide emissions for mixtures of gaseous fuels.

Figure III-121 plots the predicted carbon dioxide emissions for test case 901. The ESP-r and TRNSYS results agree exactly.

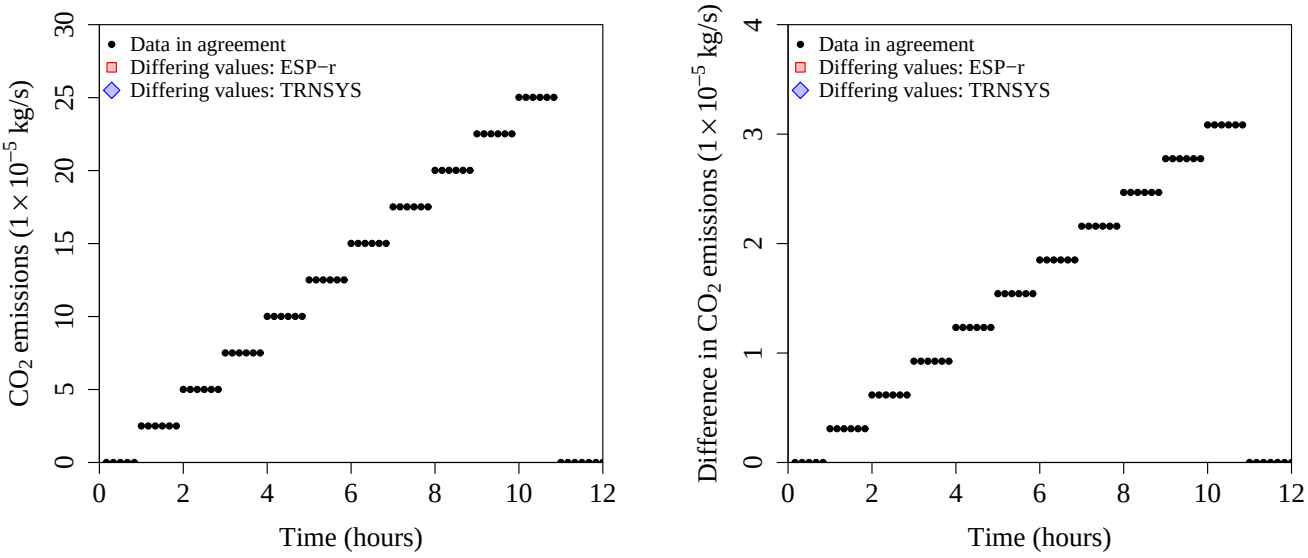

Figure III-121: Test case 902 — carbon dioxide emissions ($\dot{m}_{CO_2}$) as a function of time for (a) case 902 and (b) differential between cases 902 and 901

Test case 903

Test case 903 uses a model configuration identical to test case 106, except that the cogeneration unit's fuel carbon intensity (e_{CO_2}) is set to 3.5 kg CO_2/kg fuel.To pass test case 903, the model must correctly predict the unit's carbon dioxide emissions ($\dot{m}_{CO_2}$) over the duration of the test.

The mass flow rate of carbon dioxide emissions should be plotted against time. Disagreement in these values suggests an error in the treatment of the carbon dioxide intensity factor (e_{CO_2}) and the calculation of carbon dioxide emissions for liquid fuels.

Figure III-122 plots the predicted carbon dioxide emissions for test case 901. The ESP-r and TRNSYS results agree exactly.

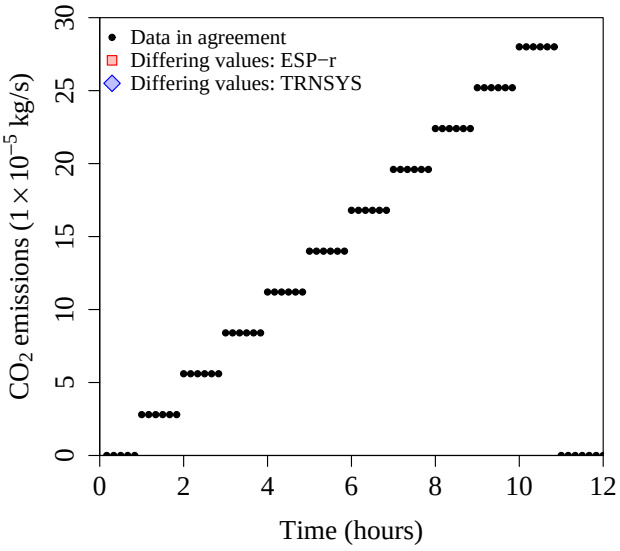

Figure III-122: Test case 903 — carbon dioxide emissions ($\dot{m}_{CO_2}$) as a function of time

Conclusions

A comparative testing suite was derived to aid validating implementations of the Annex 42 combustion cogeneration model. This suite comprises 44 tests in nine groups, each of which exercises a different aspect of the model.

At present, the combustion cogeneration model has been implemented in EnergyPlus, ESP-r and TRNSYS, and these three programs were exercised over the comparative test suite. The EnergyPlus implementation is completely independent, while the ESP-r and TRNSYS implementations share common source code. For this reason, comparisons between EnergyPlus and ESP-r/TRNSYS results provide more insight into coding errors than comparisons between ESP-r and TRNSYS.

The ESP-r and TRNSYS implementations have been exercised over all 44 test cases. The EnergyPlus implementation has been exercised over 34 of the tests in the 100–600 series. In all but one case the results are very good; either exact agreement was achieved between all three implementations, or satisfactory explanations for the differences were proposed. The exception is test case 305.

Test case 305 demonstrated that doubling the cooling water control volume thermal mass differently affects the EnergyPlus and ESP-r/TRNSYS implementations. While all three implementations predicted little variation from the base case (that is, test case 301), the response predicted by ESP-r/TRNSYS is an order-of-magnitude larger than that predicted by EnergyPlus. The cause of this discrepancy remains undiagnosed, but work to identify and remedy it continues.

Over the course of this study, numerous errors were identified and corrected in all three implementations. But the study produced more than just bug-free code—it also qualified the effects that different but equally-valid solution approaches have on simulation results. In particular, the different methodologies used to solve the dynamic thermal model proved

sensitive to the simulation time resolution. The predictions of all three programs were found to be most reliable at their maximum time resolutions (that is, one-second for ESP-r/TRNSYS, and one-minute for EnergyPlus). While EnergyPlus is less sensitive to the time step duration than ESP-r and TRNSYS, the ten-minute time step duration originally proposed for comparative testing work proved too large to accurately characterize the unit's thermal transients in all three programs.

The agreement achieved between the EnergyPlus, ESP-r and TRNSYS implementations bolsters confidence that these programs correctly implement the Annex 42 combustion co-generation model specification. The comparative testing results provide a useful development tool for future researchers implementing the model in other building simulation environments, and confidence in the EnergyPlus, ESP-r and TRNSYS implementations will be even further improved with additional comparisons to results from other programs.

References

Kelly, N. and Beausoleil-Morrison, I., editors (2007). *Specifications for Modelling Fuel cell and Combustion-Based Residential Cogneration devices within Whole-Building Simulation programs*. IEA/ECBCS Annex 42 Report. ISBN No. 978-0-662-47116-5.

Section IV

Empirical Validation of the Annex 42 Fuel Cell Cogeneration Model Using Measured Data from a Solid-Oxide Fuel Cell Device

AUTHORS:

Ian Beausoleil-Morrison (Natural Resources Canada)

WITH INPUT FROM:

Kathleen Siemens (Natural Resources Canada)

Section IV Table of Contents

Introduction to this section

Two companion Annex 42 reports are pertinent to this section:

- Beausoleil-Morrison (2007, sections III-4 and IV-13) documents the series of experiments conducted with a prototype SOFC-cogeneration system developed by Fuel Cell Technologies Ltd. (FCT). Section VII of that report details how data from 45 of these experiments were used to calibrate the Annex 42 FC-cogeneration model (i.e. establish its inputs).
- Kelly and Beausoleil-Morrison (2007, section II) describes the formulation of the Annex 42 FC-cogeneration model. This report is referred to here as the *model specifications*. Equation symbols used here correspond to those used in the model specifications and frequent reference is made its section and equation numbers.

The experimental programme documented in Beausoleil-Morrison (2007, sections III-4 and IV-13) consisted of a series of experiments with varied and controlled boundary conditions. The experiments were segregated into two groups:

- 45 *calibration* experiments which yielded data that were used to calibrate the model to represent the performance of this specific device.
- 16 *empirical validation* experiments.

The current section treats the empirical validation of the Annex 42 FC-cogeneration model. Simulations results produced with the ESP-r implementation of the model using the calibrated inputs are compared with the measurements taken during the *empirical validation* experiments.

Section II of the current document treats the inter-program comparative testing of the five implementations of the Annex 42 FC-cogeneration model. This verified that the implementation of the model into ESP-r is as error-free as possible. Consequently, any discrepancies between ESP-r simulation predictions and the measurements can be attributed to inadequacies in the mathematical model, the calibration of its inputs, or due to measurement errors.

Parameters for comparison

The model's solution procedure is briefly described here to provide context for the selection of the parameters that are contrasted between the measurements and the simulations.

At each time-step of a simulation, ESP-r invokes the FC-cogeneration model and passes it a control signal requesting a given AC power output (P_{AC}). The fuel cell's operating point is established by determining the FCPM's net DC power production (P_{el}) by simulating the behaviour of the DC-AC power conditioning system, specifically by solving equations II-76 and II-77 of the model specifications, subject to the calibrated u_i coefficients. P_{el} is a significant parameter in the model as it appears as an independent variable in the treatment of many of the model's control volumes. Consequently it is a good choice as a parameter for comparison between measurement and simulation.

The FCPM's electrical efficiency (ε_{el}) is calculated with equation II-8 of the model specifications and the required fuel consumption ($\dot{N}_{fuel}$) determined with equation II-10. A polynomial expression is used to estimate the enthalpy of each fuel constituent (CH_4, C_2H_6, N_2, etc.) as a function of its supply temperature (equation II-12 of the model specifications). This along with $\dot{N}_{fuel}$ establishes the first term of the FCPM's energy balance (equation II-1 of the model specifications). Clearly, any errors in the evaluation of these equations or in the calibrated ε_i coefficients used in equation II-8 or the calibrated u_i coefficients used in equation II-77 will lead to errors in the determination of the fuel consumption. As accurately predicting the device's fuel consumption is a key requirement of the model, $\dot{N}_{fuel}$ is selected as a parameter for comparison.

Similar methods are used to establish the other terms of the FCPM energy balance, which is then solved to yield the enthalpy carried out of the control volume by the gas stream ($\dot{H}_{FCPM-cg}$ in equation II-1 of the model specifications). The composition of this gas stream is determined by assuming complete reactions between the fuel constituents and the air's O_2, as given by equation II-15 of the model specifications. When the results of this equation

are added to the flow rates of the non-reacting fuel and air constituents, the composition and flow rate ($\dot{N}_{FCPM-cg}$) of the product gas stream are established. The polynomial function mentioned above is then applied in an iterative manner to establish the temperature ($T_{FCPM-cg}$) corresponding to the value of $\dot{H}_{FCPM-cg}$ solved by equation II-1 of the model specifications. Clearly, any errors in the evaluation of any of the above-mentioned equations (and others not mentioned here) or any errors in their calibration coefficients would lead to errors in the estimate of $T_{FCPM-cg}$.

This temperature is then used in the modelling of the heat exchanger. Firstly, the flow rate of the product gas stream ($\dot{N}_{FCPM-cg}$) is used to establish $(UA)_{eff}$ using equation II-45 of the model specifications. (Note that for the FCT system $T_{FCPM-cg} = T_{aux-mix}$ since there is no auxiliary burner upstream of the heat exchanger.) A re-arrangement of equation II-40 of the model specifications is then solved to determine the cogeneration device's useful thermal output (q_{HX}) and the heat exchanger's exiting gas and water temperatures. Once again, any errors in the evaluation of the many terms that lead to $\dot{N}_{FCPM-cg}$ and $T_{FCPM-cg}$ will propagate into errors in the prediction of q_{HX}. $(UA)_{eff}$ and q_{HX} are selected as parameters for comparison to reflect the importance (and difficulty) of the predicting the device's thermal output.

Boundary condition equivalencing

Four boundary conditions fully define the operational state of the cogeneration device:

- The AC power production, P_{AC} (refer to section II-11 of the model specifications).
- The flow rate of water through the gas-to-water heat exchanger, $\dot{N}_{water}$ (refer to section II-7 of the model specifications).
- The temperature of the cold water at the gas-to-water heat exchanger inlet, $T_{water,in}$ (refer to section II-7 of the model specifications).
- The temperature of the air supplied to the FCPM, $T_{blower-in}$ (refer to sections II-2.6 and II-3 of the model specifications).

These boundary conditions were monitored and maintained as constant as possible during each of the 16 empirical validation experiments. Measurements were taken every 15 seconds and the minutely averages logged.

Figure IV-1 plots the one-minute averages of these four boundary conditions over the 10-minute duration of one of the empirical validation experiments. The error bars in the figure represent the instrumentation bias errors (refer to Beausoleil-Morrison, 2007, section III-4).

An ESP-r simulation was configured to replicate this experiment. The boundary conditions supplied to ESP-r were equivalenced to the measurements and a simulation conducted with a 1-minute time-step. This boundary condition equivalencing is illustrated in Figure IV-1. There is a slight time shift between the measurements and the simulation because the simulation was executed at the top of each minute whereas the experimental data were logged a few seconds past the top of each minute.

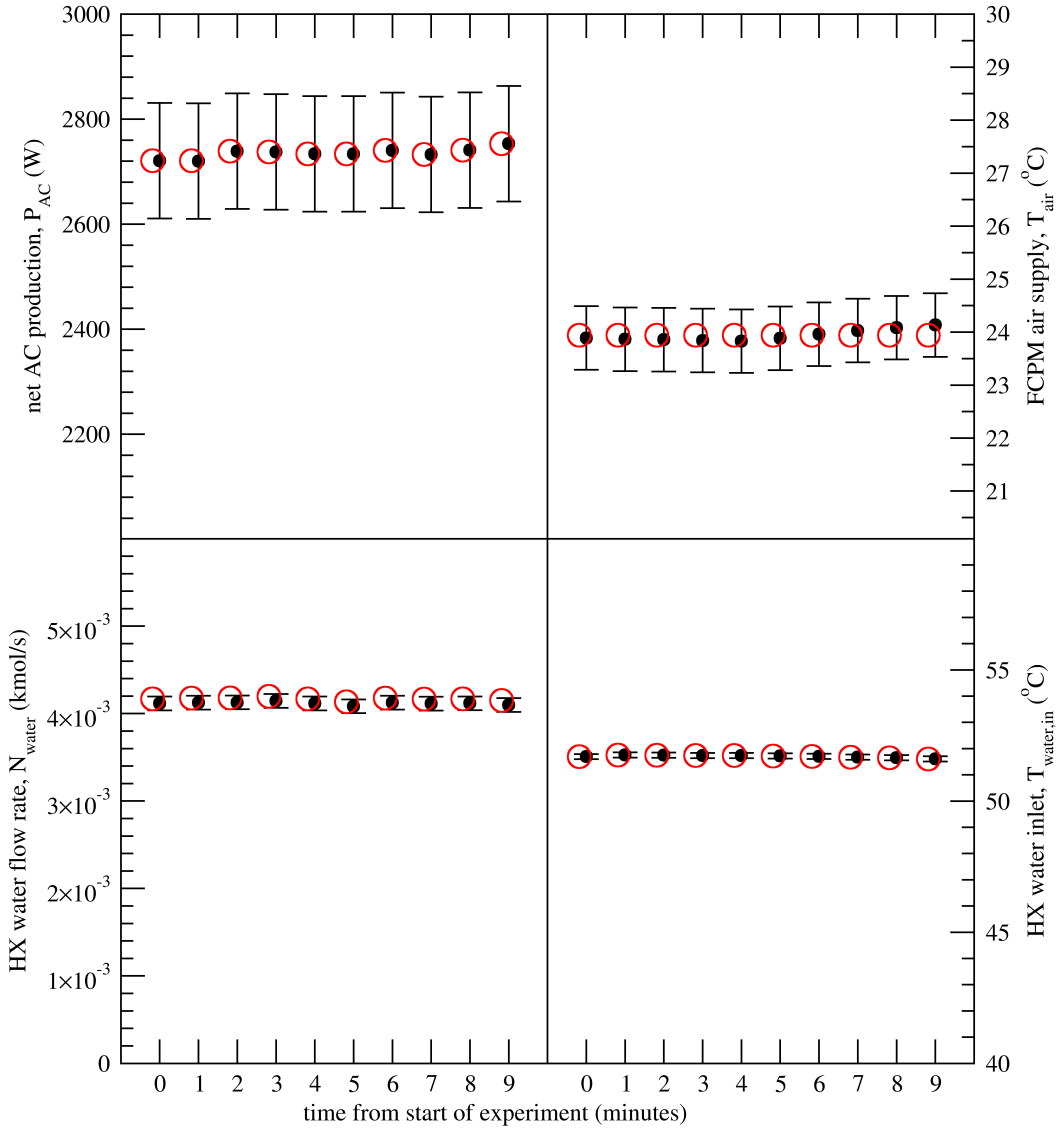

Figure IV-1: Equivalencing simulation boundary conditions to replicate measurements

Time-step comparisons for one experiment

Instantaneous measurements of the FCPM's net DC power production (P_{el}), and the molar flow rates of air ($\dot{N}_{air}$) and fuel ($\dot{N}_{fuel}$) supplied to the FCPM were taken every second and the averages over the minute were logged to file. All other measurements were taken every 15 seconds and the minutely averages logged. By equivalencing the boundary conditions, direct comparisons could then be made between the ESP-r simulation results and these measurements.

In keeping with the accepted validation methodology's tenet of simplicity (refer to section I of this report), the FCPM's net DC power production (P_{el}) is first compared. As previously elaborated, P_{el} is calculated with equations II-76 and II-77 of the model specifications using the calibrated u_i coefficients and subject to the P_{AC} boundary condition. Any disagreement between simulation predictions and measurements would indicate a problem with these aspects of the model and/or the calibration of the u_i coefficients.

The top-left corner of Figure IV-2 compares the simulations to the measurements. As can be seen, the simulation predictions agree with the measurements within the instrumentation bias error at most of the 10 1-minute intervals. The exception occurs at both the beginning and end of the experiment, where the simulation produces a slightly greater variation in P_{el} from one time-step to the next. (Note the scale of the y-axis.) This slight disagreement was determined to be the result of the iterative solution procedure employed in the ESP-r implementation of the model. Notwithstanding, the average, root-mean-square, and maximum deviation between the simulation predictions and measurements indicates excellent agreement overall (see Table IV-1): the maximum deviation is less than 1%.

The comparisons illustrated in Figure IV-2 involve greater interactions between algorithms (i.e. less simplicity) as one moves from left to right and from top to bottom. The top-right corner compares the simulation's predictions of the fuel consumption to the measurements. This examines the same aspects of the model as the preceding P_{el} comparison, in addition

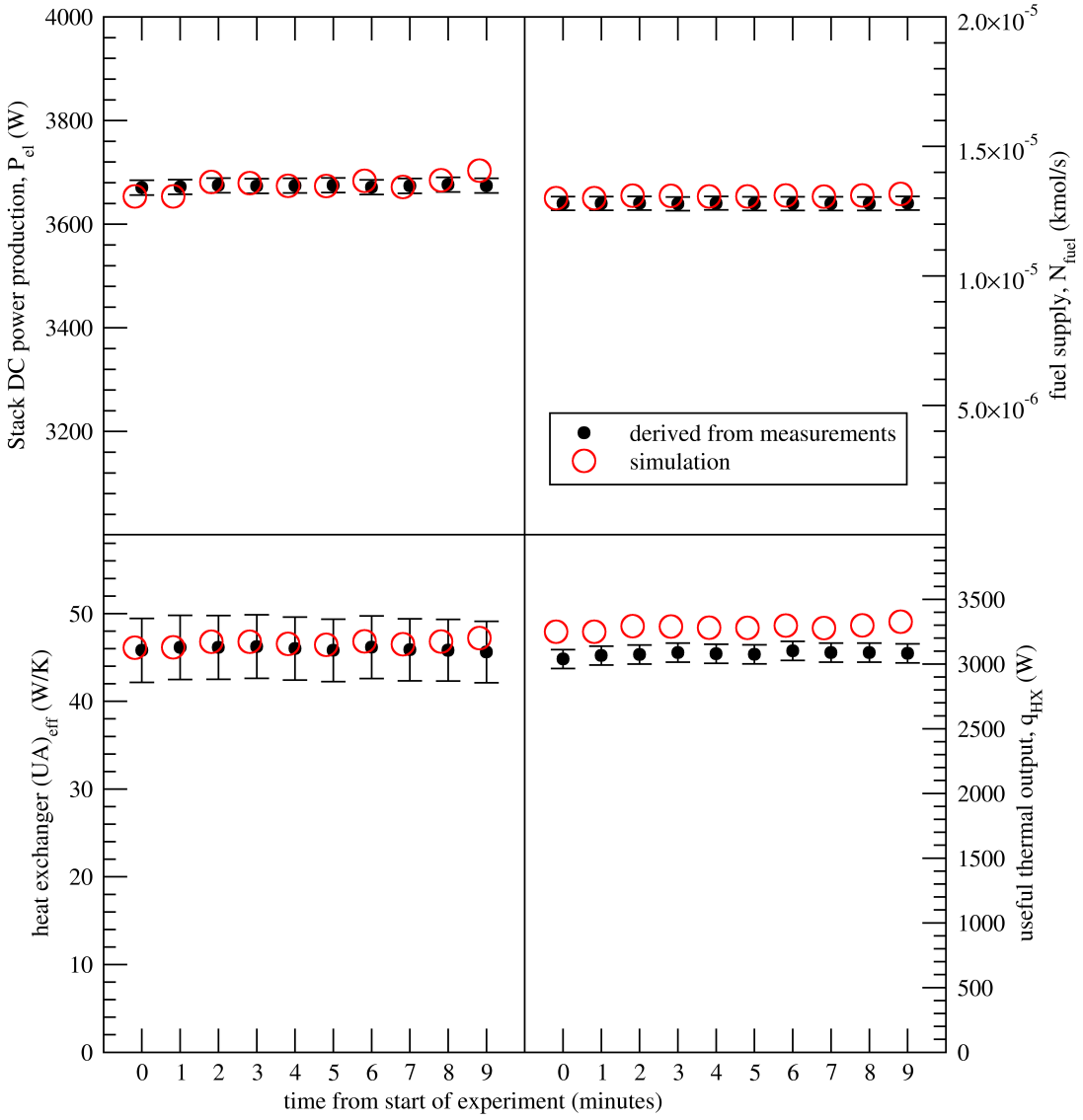

Figure IV-2: Time-step comparisons of the four parameters for one experiment

Table IV-1: Goodness-of-fit metrics for time-step simulation predictions for one empirical validation experiment (refer to Appendix A)

	$\overline{e_{rel}}$	e_{rel}^{RMS}	e_{rel}^{MAX}
P_{el}	0.3%	0.4%	0.8%
$\dot{N}_{fuel}$	2.2%	2.2%	2.9%
$(UA)_{eff}$	1.4%	1.7%	3.5%
q_{HX}	6.7%	6.7%	8.0%

to the model specifications' equations II-8 and II-10 and the accuracy of the calibrated ε_i coefficients (refer to the earlier discussion on *Parameters for comparison*). The simulation predictions agree with the measurements within the instrumentation bias error (only 2% of the measured value for this experiment) at a number of the 10 1-minute intervals and the goodness-of-fit metrics indicate an excellent prediction overall (see Table IV-1).

The bottom-left corner of Figure IV-2 compares the simulation's predictions of the heat exchanger's $(UA)_{eff}$ value to the measurements. This examines the validity of the form of the model specifications' equation II-45 and the calibrated $hx_{s,i}$ coefficients. In addition, it stresses the numerous aspects of the model that establish $\dot{N}_{FCPM-cg}$. The simulation predictions agree with the measurements within the instrumentation bias error at each of the 10 1-minute intervals. The goodness-of-fit metrics are similar in magnitude to those for the calibration of the $hx_{s,i}$ coefficients (see Beausoleil-Morrison, 2007, section VII).

The bottom-right corner of Figure IV-2 compares the simulation's predictions of the useful thermal output (q_{HX}) to the measurements. This examines the combined influence of most aspects of the model. As elaborated in Beausoleil-Morrison (2007, section VII), there is large uncertainty in the calibration of two of the terms that appear in the FCPM energy balance (equation II-1 of the model specifications): the radiant and convective heat transfer to the containing room, $q_{skin-loss}$; and the heat transfer to the air stream which is drawn through the cogeneration device's cabinet to comply with gas venting require-

ments of safety codes, $q_{FCPM-to-dilution}$. The uncertainty of these terms has a significant impact upon the model's ability to predict q_{HX}. As can be seen in the figure, the simulation predictions lie outside the measurement bias uncertainty at all points. However, the goodness-of-fit metrics given in Table IV-1 are reasonable given the uncertainty associated with the calibration of the two aforementioned heat loss terms: the maximum deviation between simulation predictions and the heat flow derived from measurements is 8%. These differences are explored further in the next section.

Table IV-2: Goodness-of-fit metrics for simulation predictions for the 16 empirical validation experiments (refer to Appendix A)

	$\overline{e_{rel}}$	e_{rel}^{RMS}	e_{rel}^{MAX}
P_{el}	0.2%	0.2%	0.5%
$\dot{N}_{fuel}$	1.2%	1.9%	6.1%
$(UA)_{eff}$	5.4%	6.0%	9.5%
q_{HX}	7.9%	8.4%	12.2%
η_{net-AC}	1.2%	1.8%	5.8%
η_{th}	8.5%	8.8%	13%
η_{cogen}	5.3%	5.6%	8.9%

Time-averaged comparisons for 16 experiments

The 16 empirical validation experiments varied in duration from 10 minutes to over 10 hours (long experiments were required when condensation formed in the heat exchanger). The near-constant boundary conditions were time-averaged over each experiment and an ESP-r simulation was configured to equivalence these conditions. This resulted in simulation predictions for 16 sets of time-averaged boundary conditions. The parameters for comparison were derived from the measurements at each time-step. These derived quantities were then time-averaged over each experiment for comparisons with the simulation results.

These comparisons are illustrated in Figure IV-3. The quantities derived from the measurements are plotted along the x-axis while the simulation predictions are plotted on the y-axis. The diagonals represent the line of perfect agreement. The error bars in the x-direction represent the uncertainty at the 95% confidence level of the time-averaged quantities derived from the measurements (see Beausoleil-Morrison, 2007, III-4). The goodness-of-fit metrics are presented in Table IV-2.

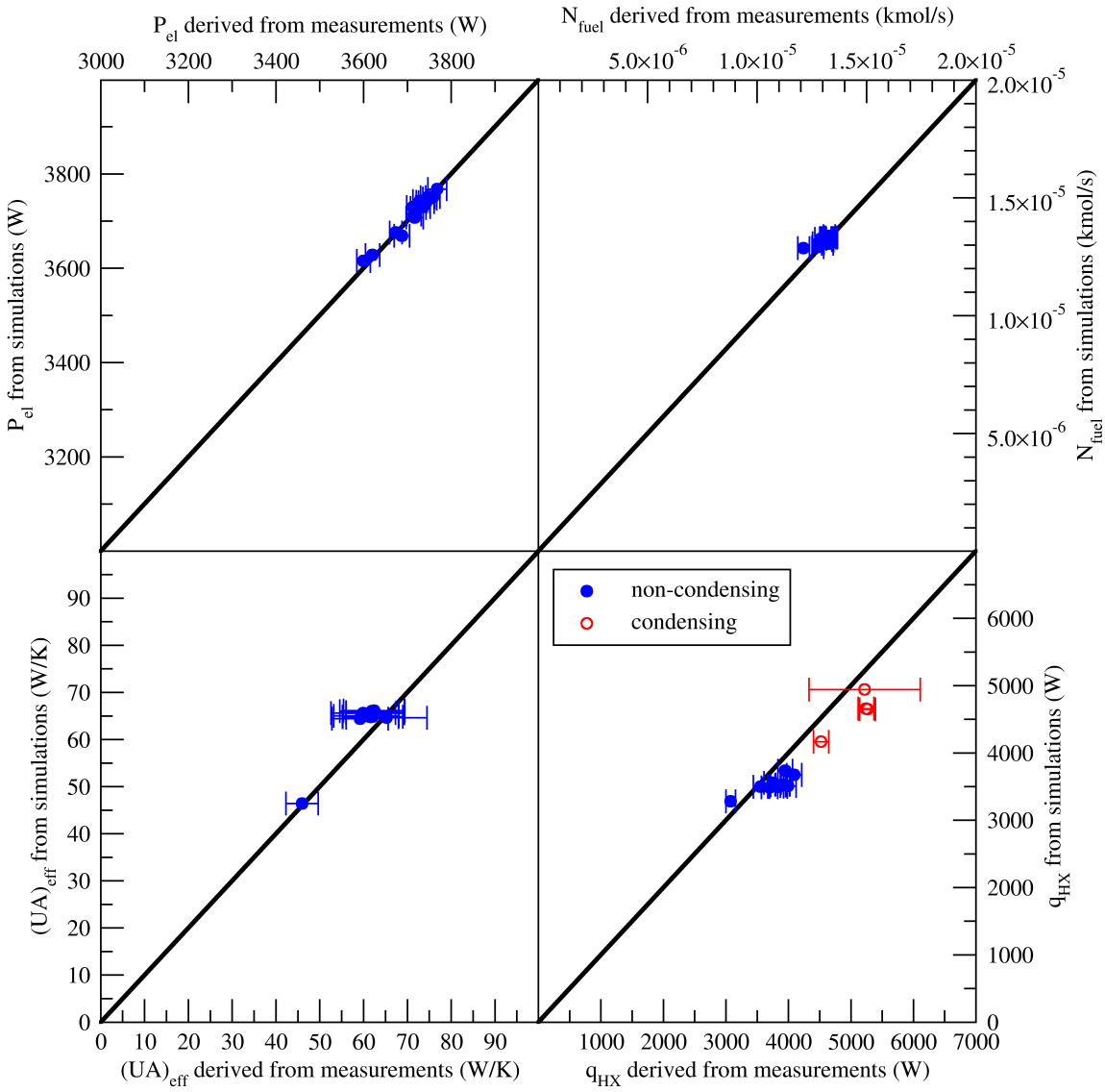

Figure IV-3: Time-averaged comparisons of the four parameters for the 16 empirical validation experiments

In general terms, the simulation predictions deviate further from the measurements as complexity increases. Moving from left to right on the graph and from top to bottom involves greater interaction between algorithms and this affords the possibility of error propagation. It appears from the bottom-right corner of Figure IV-3 that there may be a systematic bias in the q_{HX} predictions. In fact, a number of the predictions lie within or just outside of the uncertainty bars. The four experiments in which water vapour from the gas stream condensed in the heat exchanger produced the greatest values of q_{HX}. These experiments show some of the greatest deviation between simulation results and measurements. As explained in Beausoleil-Morrison (2007, VII) there is considerable uncertainty associated with the calibration of this aspect of the model.

A detailed examination of the measured data was performed to investigate the differences between simulation results and measurements that are illustrated in the bottom-right of Figure IV-3. In this figure, the q_{HX} values were derived from the measurements of the heat exchanger's water stream (refer to the right equality of the model specifications' equation II-41), i.e.,

$$q_{HX} = (\dot{N}\hat{c}_P)_{water} \cdot (T_{water,out} - T_{water,in}) \tag{IV-1}$$

Where $(\hat{c}_P)_{water}$ was derived from the model specifications equation II-12 based upon $T_{water,in}$. (Analysis revealed that it is inconsequential whether $(\hat{c}_P)_{water}$ is evaluated at $T_{water,in}$ or $T_{water,out}$.) The uncertainty at the 95% confidence interval was calculated through the propagation of bias errors and measurement precision indices through a root-sum-square method (Moffat, 1988). The bias errors were established mainly based upon instrumentation specifications (see Beausoleil-Morrison, 2007, sections III-4 and IV-13 for details on the instrumentation bias errors). As such, the uncertainty bars in the figure represent the errors associated with two type-T thermocouples (bias errors of 0.1^oC) that measured $T_{water,in}$ and $T_{water,out}$ and a water flow meter to measure $\dot{N}_{water}$ (bias error of $\sim$2%). In contrast, the simulation predictions are dependent upon the calibration of equation II-45 of the model specifications. This calibration relies upon the aforementioned instruments

as well as two type-K thermocouples (bias errors of 2.2^oC) that measured $T_{FCPM-cg}$ and T_{HX-exh} (refer to equation II-40 of the model specifications).

Furthermore, analysis of the measured data revealed an inconsistency in the measurements of the water and gas streams. This is illustrated in Figure IV-4. The simulation results in this figure are identical to those plotted in Figure IV-3. The results labelled *based upon measurements of water* were derived from the measurements using equation IV-1 and are identical to those plotted in Figure IV-3. The remaining two series in the graph plot the values of q_{HX} that were derived from the measurements of the heat exchanger's gas stream (refer to the left equality of the model specifications' equation II-41), i.e.,

$$q_{HX} = (\dot{N}\hat{c}_P)_{gas} \cdot (T_{FCPM-cg} - T_{HX-exh}) \tag{IV-2}$$

Where $(\hat{c}_P)_{gas}$ was derived from the model specifications equation II-12. This evaluation required the derivation of the composition of the gas stream (e.g. the fractions of CO_2, H_2O, N_2, etc.) from the measured flow rates of the fuel and air supplied to the FCPM with the assumption that these fully reacted and that the heat exchanger's gas stream was composed only of these reactants. In one series in the graph $(\hat{c}_P)_{gas}$ is evaluated at $T_{FCPM-cg}$ whereas in the other it is evaluated at T_{HX-exh}.

Figure IV-4 clearly illustrates the considerable uncertainty in deriving q_{HX} from the measurements. The values derived from the measurements of the gas stream can be 8 to 23% lower than those derived from the measurements of the water stream. This indicates that the instrumentation bias errors may have in fact been greater than the manufacturer specifications. Or, that placement of one or more of the thermocouples may have biased the readings, i.e. it may not have been reading the intended state point. In most cases the simulation results lie between the q_{HX} values derived from the measurements of the water and gas streams[1].

[1]No q_{HX} results are derived from the measurements of the gas stream for the four experiments in which water vapour from the gas stream condensed in the heat exchanger. The measurements of $T_{FCPM-cg}$ were

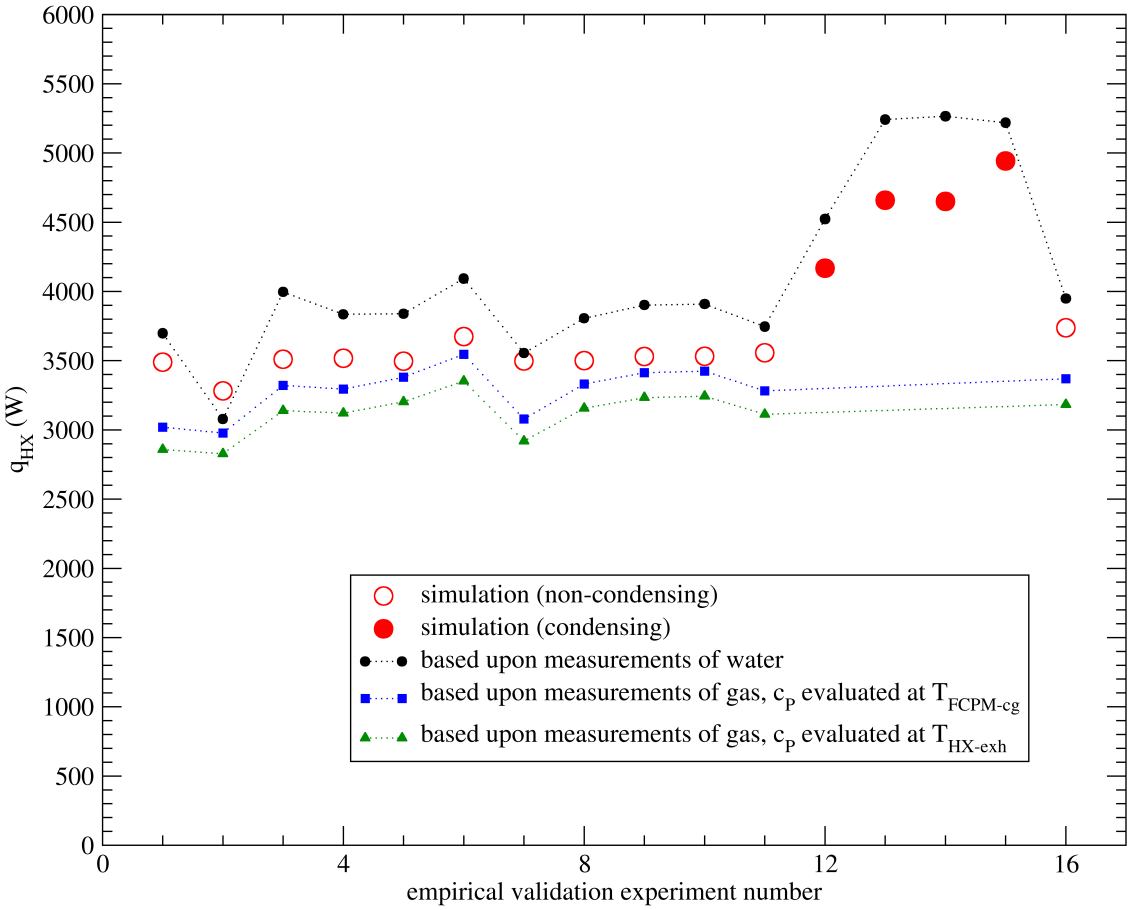

Figure IV-4: Time-averaged comparisons of alternate methods for deriving q_{HX} for the 16 empirical validation experiments

Given the above analysis, it can be concluded that the error bars in the bottom-right of Figure IV-3 likely underestimate the true experimental uncertainty. Taken in this context, it can be stated that the goodness-of-fit metrics given in Table IV-2 indicate reasonable agreement between simulation results and measurements over the 16 empirical validation experiments.

The final check on the model's validity is made through examining the predictions of three key outputs: the net efficiencies for electrical, useful thermal, and total output from the cogeneration device,

$$\eta_{net-AC} = \frac{P_{AC}}{\dot{N}_{fuel} \cdot LHV_{fuel}} \tag{IV-3}$$

$$\eta_{th} = \frac{q_{HX}}{\dot{N}_{fuel} \cdot LHV_{fuel}} \tag{IV-4}$$

$$\eta_{cogen} = \eta_{net-AC} + \eta_{th} \tag{IV-5}$$

These three efficiency values would be of prime importance in a simulation-based assessment of the performance of residential cogeneration systems. Their calculation depends upon the interaction of all aspects of the model. The comparison of the simulation predictions of these quantities with the values derived from the measurements are illustrated in Figure IV-5 and the goodness-of-fit metrics are presented in Table IV-2. The thermal efficiencies plotted in this figure are derived from the measurements of the heat exchanger's water stream. As can be seen, simulation predictions of the electrical efficiency are in better agreement than those for the thermal efficiency. However, for the reasons elaborated above it can be stated that the ability of the model to predict performance is quite reasonable.

unreliable during these experiments for reasons that are detailed in Beausoleil-Morrison (2007, section IV-13).

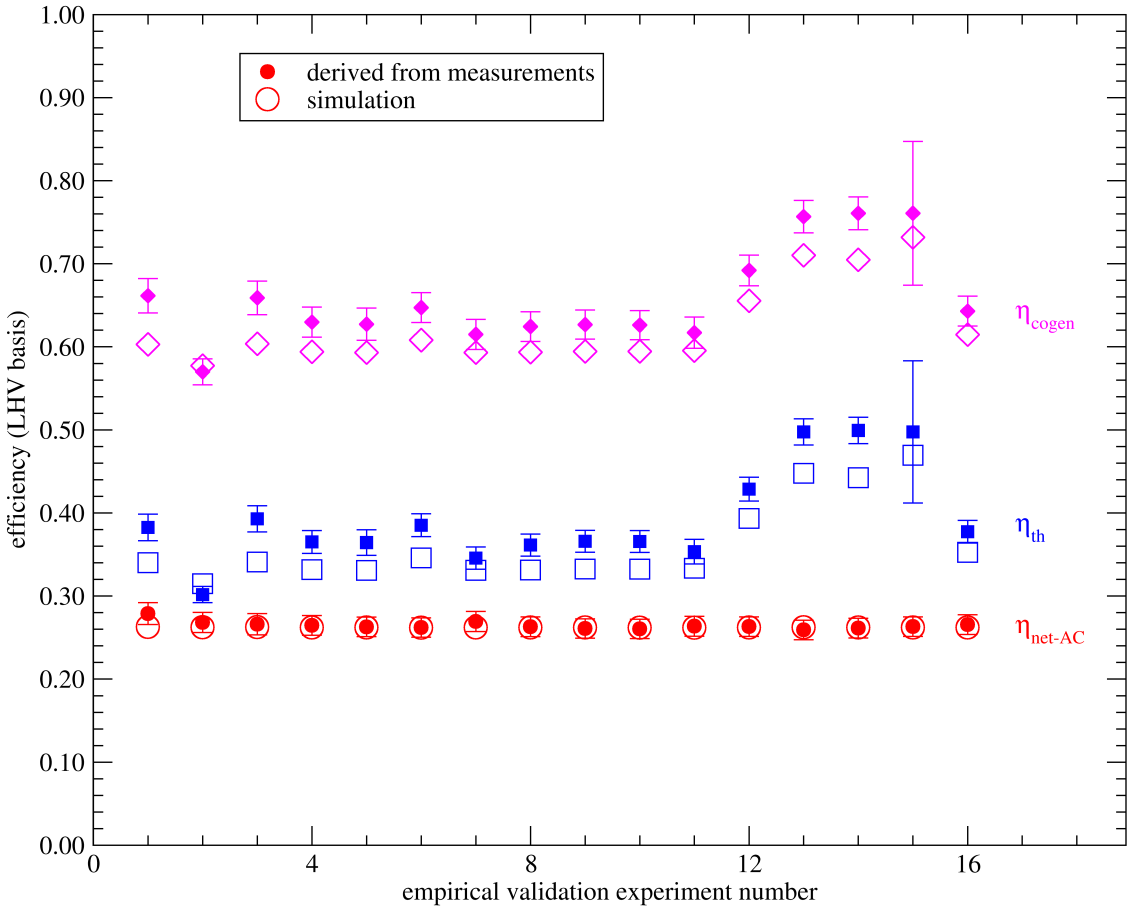

Figure IV-5: Time-averaged comparisons of efficiencies for the 16 empirical validation experiments

Closing remarks for this section

This section has demonstrated the validity of the Annex 42 FC-cogeneration model as well as the accuracy of its calibration to represent the FCT SOFC device. It showed how simulations were equivalenced with experimental conditions and how measured values and quantities derived from the measurements were compared to simulation predictions. These comparisons spanned a range of model parameters, progressing from the simplest case in which only a small subset of the model was exercised, to the complex which involved the concurrent operation and interaction of all aspects of the model.

This section identified the aspects of the model with the greatest uncertainty, that is the calculation of parasitic thermal losses and the condensation of the exhaust gas' water vapour within the heat recovery device. It then explained how this uncertainty could propagate errors into the simulation predictions of the useful thermal output. In addition, an inconsistency in the measurements related to the heat recovery device were revealed and examined in detail. This observation exacerbated comparisons between simulation predictions of the useful thermal output and the values derived from measurements. Notwithstanding, acceptable to excellent agreement between simulation predictions and measurements was found for numerous key parameters and over the range of the 16 experiments.

The conclusion is drawn that the model fairly represents the performance of fuel cell cogeneration devices and their sub-systems and that the calibrated model produces valid predictions of the performance of the prototype SOFC system.

References

Beausoleil-Morrison, I., editor (2007). *Experimental Investigations of Residential Cogeneration Devices and Model Calibration*. IEA/ECBCS Annex 42 Report. ISBN No. 978-0-662-47523-1.

Kelly, N. and Beausoleil-Morrison, I., editors (2007). *Specifications for Modelling Fuel Cell and Combustion-Based Residential Cogeneration Devices within Whole-Building Simulation Programs*. IEA/ECBCS Annex 42 Report. ISBN No. 978-0-662-47116-5.

Moffat, R. (1988). Describing the uncertainties in experimental results. *J Experimental Thermal and Fluid Science*, 1:3–17.

Appendix A : Goodness of fit metrics

Three metrics were chosen to assess the goodness of fit between simulation predictions and measurements:

- The average of the relative errors, $\overline{e_{rel}}$
- The root-mean-square of the relative errors, e_{rel}^{RMS}
- The maximum of the relative errors, e_{rel}^{MAX}

These metrics are calculated as follows:

$$\overline{e_{rel}} = \frac{1}{n}\sum_{i=1}^{n}\frac{\left|\hat{\theta}_i - \theta_i\right|}{\hat{\theta}_i} \tag{IV-6}$$

$$e_{rel}^{RMS} = \sqrt{\frac{1}{n}\sum_{i=1}^{n}\left(\frac{\hat{\theta}_i - \theta_i}{\hat{\theta}_i}\right)^2} \tag{IV-7}$$

$$e_{rel}^{MAX} = \max\left\{\frac{\left|\hat{\theta}_i - \theta_i\right|}{\hat{\theta}_i}\right\}_{i=1}^{n} \tag{IV-8}$$

Where $\hat{\theta}_i$ is the value derived from measurements at time-step i, θ_i is the simulation prediction, and n is the number of measurement points.

Section V

Empirical Validation of the Annex 42 Combustion Cogeneration Model Using Measured Data from a Stirling Engine Device

AUTHORS:

Alex Ferguson (Natural Resources Canada)

WITH INPUT FROM:

Ian Beausoleil-Morrison (Natural Resources Canada)

Kathleen Siemens (Natural Resources Canada)

Section V Table of Contents

Introduction to this Section

Collection of experimental data suitable for calibrating and validating cogeneration models is a principle objective of Annex 42. To support this goal, three agencies contributed data describing the operation of Stirling engines in cogeneration applications:

- The Canadian Centre for Housing Technology (CCHT)
- Forschungsstelle für Energiewirtschaft (FfE)
- The University of Leuven (U.Leuven)

Both CCHT and U.Leuven undertook their Stirling engine experiments prior to their involvement with Annex 42. For this reason, these studies did not adhere to the Annex 42 experimental protocol described in Beausoleil-Morrison (2007, Section II).

In the CCHT experiments, Entchev and Swinton installed a Stirling cogeneration unit into a test house and subjected it to electrical and thermal loads over several months. All of the CCHT data describe the engine's dynamic response to changing conditions inside the house. Without any steady-state measurements, the CCHT data are not optimally suited for calibration and validation of the Annex 42 combustion cogeneration model. Nevertheless, the experiments characterized the engine's performance over a wide range of conditions.

The U.Leuven testing program comprised numerous "runs" in which data was collected over a single operational cycle of the Stirling cogeneration unit. During each cycle, the unit was activated, allowed to operate for several hours and then deactivated. Because the U.Leuven experiments were not designed with the Annex 42 objectives in mind, data collection did not continue during the engine's cool down phase. Absence of these results precluded use of the U.Leuven data for validation of the Annex 42 Combustion cogeneration model.

The FfE experiments were undertaken by connecting a Stirling cogeneration device to a dedicated test bench capable of re-creating conditions inside a residential heating plant. FfE followed the Annex 42 experimental protocol as closely as the physical constraints of the test bench permitted, and produced a rich description of the performance of the Stirling cogeneration unit. Unfortunately, delays in FfE's testing program prevented release of the data until after completion of the Annex's calibration and validation phases. It is expected the results from the FfE experiments will be available in the near future, and calibration and validation of the combustion cogeneration model will proceed as a follow-on activity to Annex 42.

During Annex 42's working phase, the combustion cogeneration model was calibrated and validated using the CCHT data. Empirical validation of the model using the CCHT data is presented in this section.

Related reports

Three companion Annex 42 reports are pertinent to this section:

- A complete description of the Annex 42 combustion cogeneration model's theoretical basis is available in Kelly and Beausoleil-Morrison (2007, Section III).
- The experimental characterization of Stirling engine cogeneration technologies within Annex 42 is discussed in Beausoleil-Morrison (2007, Section IV). Section IV-2 discusses the CCHT experimental tests, while Section IV-1 describes the activities at U.Leuven and Section IV-3 describes the FfE experiments.
- Section V in the same report describes calibration of the Annex 42 combustion cogeneration model using data collected from a Whisper Tech Stirling cogeneration unit.

Assumptions and sources of uncertainty

The CCHT experiments were completed in 2003, prior to Annex 42's working-phase. Thus, the experiments were not designed with Annex 42's goals in mind, and there was no opportunity to modify the testing program to support Annex 42's experimental objectives. As a result, the data collected in the CCHT study are not optimally-suited for Annex 42 validation work.

Principle sources of uncertainty associated with validation of the Annex 42 combustion cogeneration model using the data collected during the CCHT tests include:

Fuel calorific value: The CCHT facility was not equipped to measure the composition or calorific heating value of the natural gas used to fuel the WhisperGen unit. Previous studies at the CCHT facility have assumed a higher heating value of Natural Gas of 37.5 MJ/m^3 under standard temperature and pressure conditions, and this value is deemed representative of the gas available inside the CCHT houses. (Gusdorf, 2006)

The gas meters used at CCHT automatically corrected the reported volumes to standard temperature conditions, but did not account for the gas line pressure. The line pressure at which natural gas is delivered gas also affects its volumetric energy content. Line pressures of 3.45 kPa gauge (0.5 psi) are typical in residential gas delivery in North America. (Gusdorf, 2006)

For the Annex 42 validation work, the natural gas composition presented in Table V-1 was assumed, which provides a higher heating value of 37.5 MJ/m^3 at standard temperature and pressure conditions. The gas line pressure was also assumed to be 3.45 kPa. Under these conditions, the gas has a lower heating value of 35.16 MJ/m^3 and a higher heating value of 38.98 MJ/m^3.

Air flow measurements: The experiments conducted at CCHT did not include measurement of supply air or exhaust flow rates, which were of limited importance to the

CCHT study. Without these data, validation of the model's air flow correlations is not possible.

Casing temperature measurement: The experiments conducted at CCHT did not characterize the casing temperature of the Stirling cogeneration unit. Without these data, the model's heat loss correlation cannot be validated.

Differing time resolutions: While the fuel flow rate, cooling water flow rate, and inlet and outlet temperatures were measured in one-minute intervals, measurements of the cogeneration unit's electrical output were taken at fifteen-minute intervals. Although comparison with these measurements indicates whether the cogeneration model is accurately predicting the unit's aggregate electrical generation, the data provide no opportunity to explore the cogeneration system's transient response on shorter (ie one-minute) time scales. Therefore, model predictions cannot be validated at these time scales.

Standby behaviour: Without invasive instrumentation, the temperature of the encapsulated cooling water inside the unit's heat exchanger must be measured using a thermocouple outside the cogeneration unit near the cooling water outlet. The temperature measured at this outlet closely approximates the temperature inside the unit when cooling water flows through the device. When the flow of cooling water ceases, the temperature measured by the thermocouple does not indicate the actual temperature inside the unit. Therefore, the unit's thermal behaviour during stand-by operation cannot be directly determined.

Instrumentation noise: The rate of fuel consumption was measured using a pulse meter, which notified the logging equipment each time the integrated volume of gas flowing through the meter reached a discrete multiple of the meter's pulse resolution. The logging equipment then recorded the number of pulses sent by the meter during each minute of operation.

The resulting data approximate unit's true fuel consumption in discrete steps. During each one-minute interval, the measurements truncate the actual volume of fuel consumed to the nearest multiple of the pulse resolution, and add the remainder to the volume reported during the next minute.

The instrumentation noise introduced by pulse meters is manageable provided the pulse resolution is much smaller than the volume of fuel flowing through the meter during each measurement interval. But the pulse resolution used in the CCHT WhisperGen tests ($1.42\times10^{3}\,m^{3}$/pulse) proved too coarse to provide meaningful results over one minute intervals. The rates of fuel consumption reported in the CCHT tests varied from $8.50\times10^{-3}\,m^{3}$/min (6 pulses per minute) to $1.84\times10^{-3}\,m^{3}$/min (13 pulses per minute), and the noise introduced by the meter amounted to 7.7%–16.7% of the of the reported reading.

To reduce the uncertainty associated with this instrumentation noise, the fuel consumption data was averaged over ten-minute intervals. Figure V-1 compares the one- and ten-minute average values for the system fuel flow over a two-hour period. While the one-minute data exhibit significant variation from one measurement to the next, the ten-minute integrated values quickly converge towards a constant value, suggesting much of the minute-to-minute variation can be attributed to noise introduced by the pulse meter.

Calibration Strategy: A final source of uncertainty arises from methodology used to calibrate the Annex 42 combustion cogeneration model. Because the CCHT experiments did not include sufficient measurements to directly calibrate all of the inputs required by the model, an iterative parameter identification approach was adopted. This approach used an optimization tool to determine the set of input parameters providing the closest agreement to the experimental data.

While this approach improved the accuracy of the model predictions, the optimization tool picked inputs providing the best fit with experimental data, as opposed to

Table V-1: Assumed composition and pressure of natural gas

Constituent	Value	
H_2	0.0	% mol/mol
CH_4	94.76	% mol/mol
C_2H_6	2.70	% mol/mol
C_3H_8	0.23	% mol/mol
N_2	1.76	% mol/mol
CO_2	0.55	% mol/mol
Pressure	3.446	kPa gauge
Lower heating value (LHV)	35.16	MJ/m^3
Higher heating value (HHV)	38.98	MJ/m^3

inputs physically representative of the system being modelled. Thus, the parameter identification procedure may inadvertently adjust the model inputs to compensate for inherent differences between the model and the physical system it represents, as well as errors in the model's mathematical description and its implementation in computer code.

These uncertainties diminish the confidence with which the Annex 42 Combustion cogeneration model can be validated using the CCHT data. Moreover, the calibration procedure may have inadvertently adjusted the model inputs to compensate for differences between the model and the WhisperGen cogeneration unit. Therefore, validation efforts undertaken with these inputs can only ascertain the accuracy of the calibrated model—they cannot directly validate the underlying relationships used in the model, or their implementation in computer code.

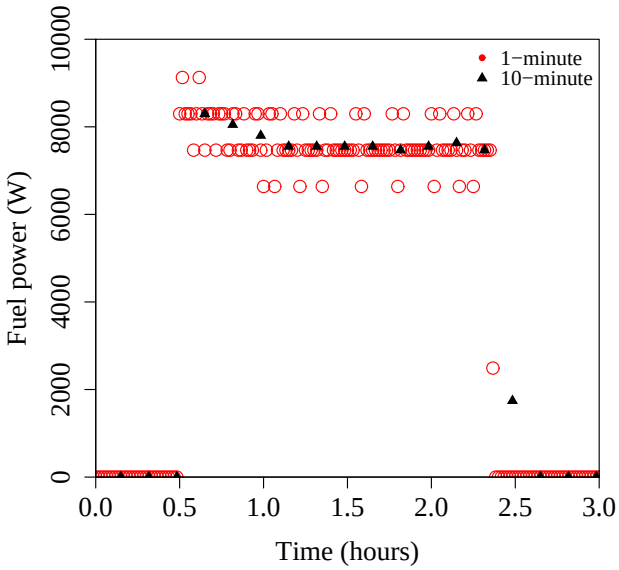

Figure V-1: Comparison of one-minute and 10-minute integrated fuel power.

Validation strategy

Within the CCHT Whisper Gen dataset, three contiguous periods of data were identified as suitable for model calibration and validation work. These subsets are summarized in Table V-2.

Table V-2: Summary of CCHT data subsets

Subset	Data points	Cycles	Duration (hours)
A	1 734	19	67.2
B	2 395	20	63.4
C	1 013	8	23.4

CCHT data subset A was used to calibrate the model, as described in Beausoleil-Morrison (2007, Section V). The accuracy of the calibrated Annex 42 combustion cogeneration model was quantified using the remaining data subsets B and C. The model was configured

with the same plant component network used during the calibration study and simulations were run with the boundary conditions described in subsets B and C.

Comparison metrics

The accuracy of the model was evaluating using metrics quantifying both the instantaneous and cumulative difference in the model predictions. These are:

- the *average absolute error*,
- the *maximum absolute error*,
- the *root mean square error*,
- *Pearson's product-moment correlation coefficient*, and
- the *cumulative error*.

The average absolute error is determined as follows:

$$\bar{e}_{abs} = \frac{1}{n}\sum_{i=1}^{n} |\hat{\theta}_i - \theta_i| \tag{V-1}$$

where:

$\bar{e}_{abs}$ is the average absolute error,

n is the number of measurements, and

$\hat{\theta}_i$ is the measured value at time step i, and θ_i is the predicted value.

The maximum absolute error, $e_{abs,max}$, describes the maximum difference between model and predicted values over the course of the simulation:

$$e_{abs,max} = \max\left(\{|\hat{\theta}_i - \theta_i|\}_{i=1}^{n}\right) \tag{V-2}$$

The root mean square error (e_{RMS}) is:

$$e_{RMS} = \sqrt{\frac{1}{n}\sum_{i=1}^{n}(\hat{\theta}_i - \theta_i)^2} \tag{V-3}$$

and Pearson's product-moment correlation coefficient is calculated as follows:

$$r^2 = \frac{\sum_{i=1}^{n}\left[\left(\hat{\theta}_i - \bar{\hat{\theta}}\right)\left(\theta_i - \bar{\theta}\right)\right]}{\sqrt{\sum_{i=1}^{n}\left[\left(\hat{\theta}_i - \bar{\hat{\theta}}\right)^2\left(\theta_i - \bar{\theta}\right)^2\right]}} \tag{V-4}$$

$$\bar{\hat{\theta}} = \frac{1}{n}\sum_{i=1}^{n}\hat{\theta}_i \tag{V-5}$$

$$\bar{\theta} = \frac{1}{n}\sum_{i=1}^{n}\theta_i \tag{V-6}$$

Finally, the cumulative error in the fuel consumption, electric output and heat recovery estimates were evaluated at the end of the simulation:

$$E_{fuel\ use} = \frac{\sum_{i=1}^{n}(\dot{m}_{fuel,measured} - \dot{m}_{fuel,model})\Delta t}{\sum_{i=1}^{n}\dot{m}_{fuel,measured}\Delta t} \tag{V-7}$$

$$E_{electric\ output} = \frac{\sum_{i=1}^{n}(P_{net,measured} - P_{net,model})\Delta t}{\sum_{i=1}^{n}P_{net,measured}\Delta t} \tag{V-8}$$

$$E_{heat\ recovery} = \frac{\sum_{i=1}^{n}(q_{recovered,measured} - q_{recovered,model})\Delta t}{\sum_{i=1}^{n}q_{recovered,measured}\Delta t} \tag{V-9}$$

where:

$E_{fuel\ use}$ is the cumulative error in the fuel consumption prediction,

$E_{electrical\ output}$ is the cumulative error in power output prediction,

$E_{heat\ recovery}$ is the cumulative error in heat recovery, and

Δt is the time step duration.

Validation results

The differences between the measured and predicted values of fuel flow, power output, heat generation and outlet temperature for both data subsets B and C are presented in Table V-3. The model's predictions agree well with both subsets—over the period described by subset B, the model's cumulative fuel use estimate differed by 0.4%, the heat recovery estimate by 1.5% and the net power estimate by 3.4%. Over the period described by subset C, the model's cumulative fuel use estimate differed by 0.2%, the heat recovery estimate by 2.4% and the net power estimate by 2.4%.

Figure V-2 plots the correlation between the predicted and measured fuel flow rate for both Subsets A and B. Each point represents the average fuel flow rate over a ten-minute interval—the x-axis value represents the experimental observation and the y-axis value represents the model's prediction. If perfect agreement were achieved between the model and measurements, every point in the plot would lie on the black diagonal line.

Clearly, the ten-minute averaged fuel flow estimates agree well. All of the points are in the vicinity of the diagonal, suggesting the model accurately predicts the unit's fuel flow rate at this time resolution.

Figure V-3 plots the correlation between predicted and measured net power output for Subsets B and C. In both subsets, the model predictions agree well in stand-by, normal operation and cool-down, during which time the unit's net electrical output is either near its maximum, or below zero.

In Subset B, the model consistently over-predicts electrical output when starting-up, during

Table V-3: Comparison of Annex 42 combustion cogeneration model predictions with CCHT data (subsets B and C)

			Subset B	Subset C
Absolute error, outlet temperature	Average ($\bar{e}_{abs}$)	°C	0.28	0.28
	Maximum ($e_{abs,max}$)	°C	3.62	2.68
	RMS (e_{RMS})	°C	0.479	0.451
	Correlation coeff. (r)	–	0.995	0.996
Absolute error, heat recovery	Average ($\bar{e}_{abs}$)	W	82.4	34.6
	Maximum ($e_{abs,max}$)	W	3159	2343
	RMS (e_{RMS})	W	244	149
	Correlation coeff. (r)	–	0.996	0.997
Absolute error, fuel flow	Average ($\bar{e}_{abs}$)	kg/s	0.737×10^{-6}	0.243×10^{-6}
	Maximum ($e_{abs,max}$)	kg/s	14.6×10^{-6}	10.5×10^{-6}
	RMS (e_{RMS})	kg/s	2.14×10^{-6}	097×10^{-6}
	Correlation coeff. (r)	–	1.000	1.000
Absolute error, power generation	Average ($\bar{e}_{abs}$)	W	16.3	17.0
	Maximum ($e_{abs,max}$)	W	128	112
	RMS (e_{RMS})	W	29.1	30.8
	Correlation coeff. (r)	–	0.997	0.996
Cumulative heat recovery	Recovered heat	MJ	713	317
	% error (E)	—	-1.45	-2.39
Cumulative power production	Power output	MJ	71.0	31.9
	% error (E)	—	3.35	2.44
Cumulative fuel use	Fuel use	kg	18.4	8.05
	% error (E)	—	0.441	-0.246

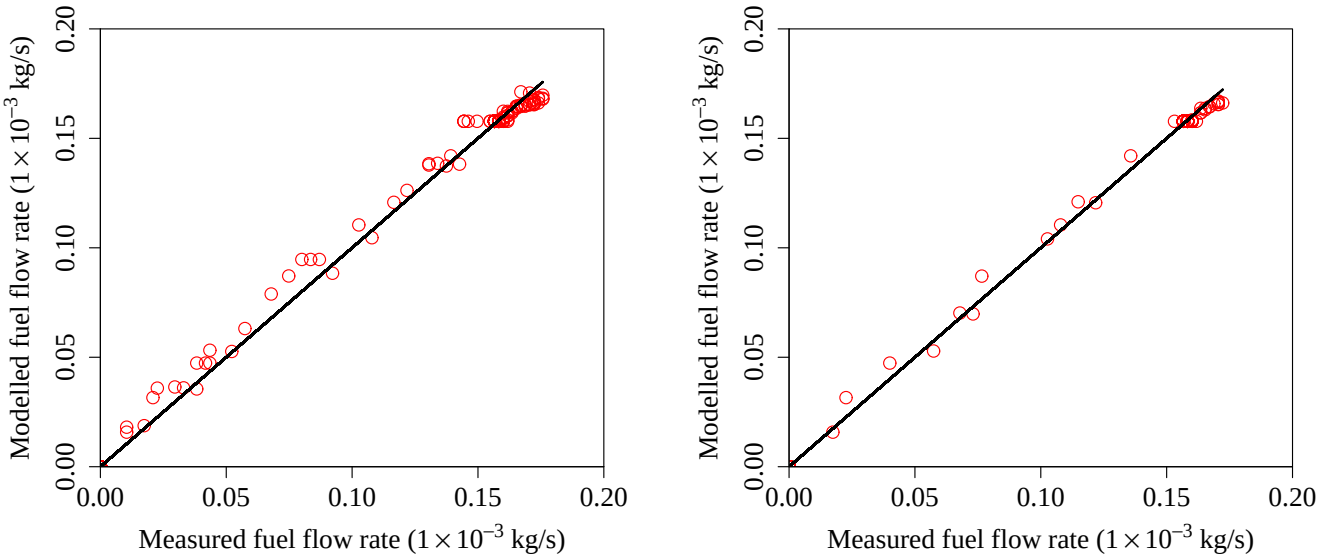

Figure V-2: Comparison of predicted and measured rates of fuel flow for a) Subset B and b) Subset C

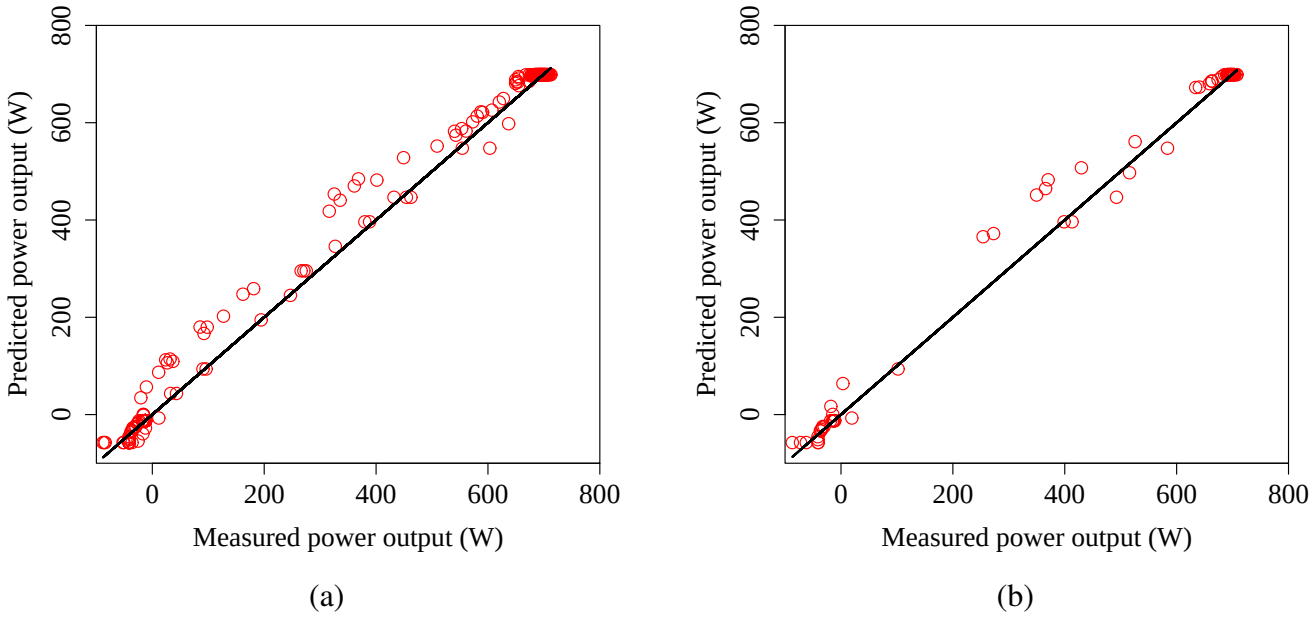

Figure V-3: Comparison of predicted and measured rates of power generation for a) Subset B and b) Subset C

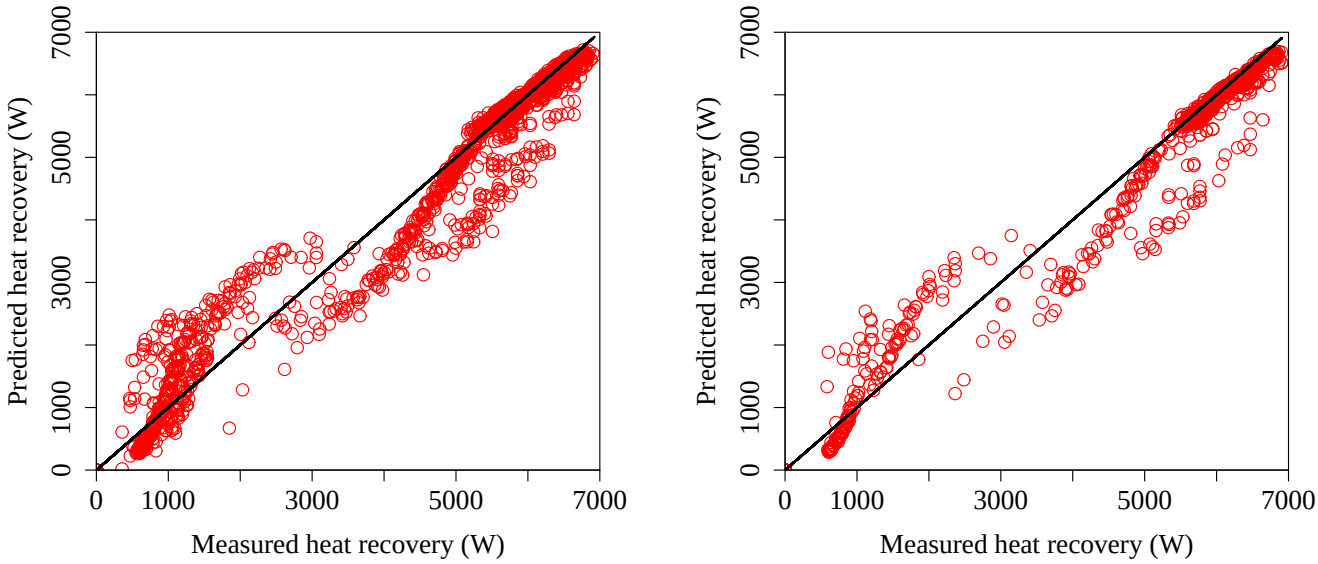

Figure V-4: Comparison of predicted and measured values of heat recovery for a) Subset B and b) Subset C

which time the unit's electrical production varies between zero and its maximum value. This effect is less pronounced in Subset C, which is shorter and describes fewer cycles.

In both subsets, the correlations exhibit a horizontal plateau near the unit's maximum power. This plateau reflects variations in the WhisperGen's electric output while in normal operation; changing conditions in the plant—such as the cooling water inlet temperature—are likely affecting the net power produced from one moment to the next. But as calibrated, the Annex 42 combustion cogeneration model is insensitive to these changes, and always predicts 698 W of power generation in normal operation.

Figure V-4 plots the correlation between the predicted and measured rates of heat recovery for Subsets B and C. Both subsets exhibit considerably more variation between the predicted and measured data.

The superior agreement achieved in the fuel flow and power output predictions with respect

to the heat recovery predictions can be attributed in part to the disparate time frequencies used to collect these data. While the thermal data was collected at one-minute intervals, the electrical data was collected over fifteen-minute intervals, and the one-minute fuel flow data was averaged over ten-minute intervals. Comparing ten- and fifteen-minute averaged data reduces the effects of differences observed between the model's and WhisperGen unit's behaviour over short time scales.

The greater variance between predicted and observed rates of heat recovery may also reflect the WhisperGen unit's sensitivity to cooling water inlet temperature. While coefficients correlating the models heat generation efficiency (η_q) to the cooling water inlet temperature were set to zero in this calibration study, the WhisperGen cogeneration system's electrical and thermal output likely decrease at elevated cooling water inlet temperatures.

Finally, Figures V-5 through V-8 plot the combustion cogeneration model's predicted fuel flow, power output, heat generation and outlet temperature along side observed values for a representative five-hour period extracted from Subset B. In this particular period, the unit was activated and allowed to operate for nearly two hours, deactivated, and then reactivated one hour later. Again, the model's predictions exhibit acceptable agreement with the measured data.

While better agreement may have been achieved between the model if the uncertainties in the CCHT data sets could have been further reduced, these results suggest the calibrated Annex 42 combustion cogeneration model provides a reasonable representation of the WhisperGen cogeneration unit over the range of conditions explored in the CCHT tests. The calibrated model approximates the WhisperGen cogeneration unit's behaviour on a time-step-by-time-step basis, and is accurate when simulation results are aggregated over extended periods.

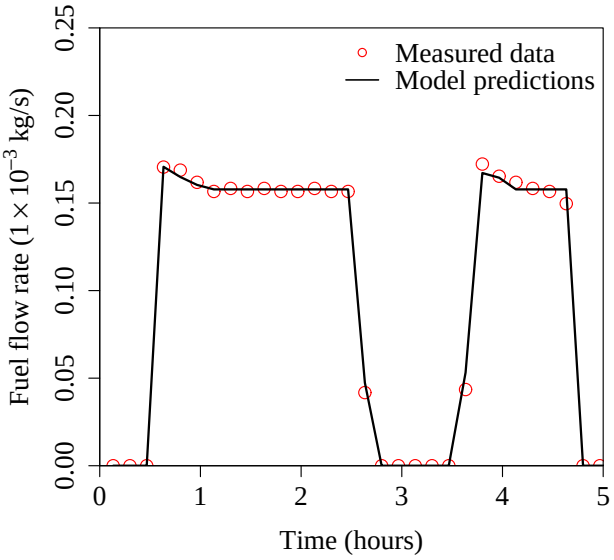

Figure V-5: Comparison between predicted and measured 10-minute averaged fuel flow rate for a five-hour period (CCHT subset B)

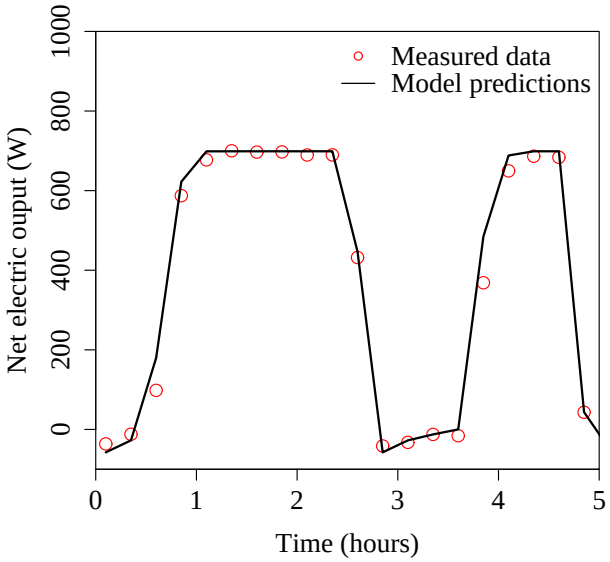

Figure V-6: Comparison between predicted and measured 15-minute averaged net electrical generation for a five-hour period (CCHT subset B)

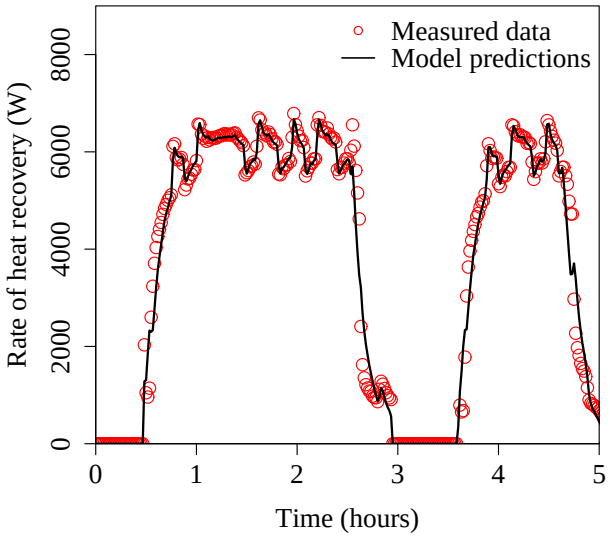

Figure V-7: Comparison between predicted and measured rates of heat recovery for a five-hour period (CCHT subset B)

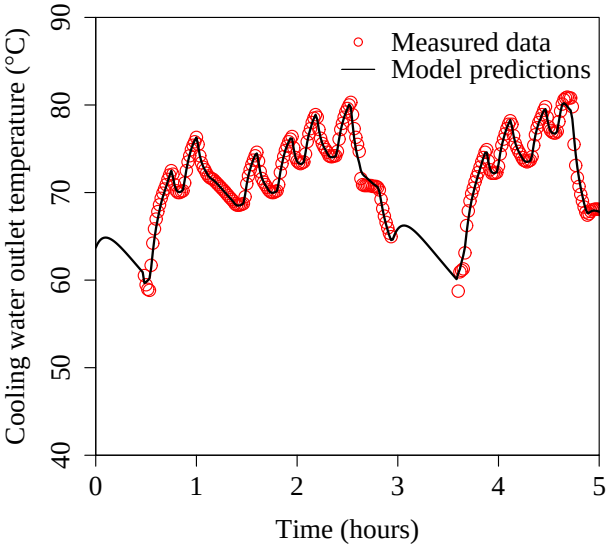

Figure V-8: Comparison between predicted and measured outlet temperatures for a five-hour period (CCHT subset B)

Conclusions

In this study, the calibrated Annex 42 combustion cogeneration model was exercised over CCHT datasets B and C, and its predictions agree well with the experimental measurements.

Uncertainty associated with the CCHT data and the calibration of the model using these data diminish the confidence with which the combustion cogeneration model can be validated—in particular, the calibration procedure may have inadvertently selected input values that compensate for logical or coding errors in the model. Therefore, the model's underlying principles and its implementation in computer code cannot be rigorously validated using the CCHT data set.

Nevertheless, the combustion cogeneration model provides an accurate representation of the WhisperGen cogeneration unit when used with the inputs derived during the calibration study. Although the model might be further validated in the future if data collected according to the Annex 42 experimental protocol becomes available, it may be used with confidence to study the WhisperGen cogeneration system in the meantime.

This study also illustrates the importance of carefully designing experiments to collect data for calibration and validation exercises. Because the CCHT experiments began prior to Annex 42's working phase, they were not designed with Annex 42's experimental objectives in mind. As the result, tests and measurements that would have been highly useful to Annex 42 were not performed.

References

Beausoleil-Morrison, I., editor (2007). *Experimental Investigation of Residential Cogeneration Devices and Calibration of Annex 42 Models*. IEA/ECBCS Annex 42 Report. ISBN No. 978-0-662-47523-1.

Gusdorf, J. (2006). Natural Resources Canada, private communication.

Kelly, N. and Beausoleil-Morrison, I., editors (2007). *Specifications for Modelling Fuel cell and Combustion-Based Residential Cogneration devices within Whole-Building Simulation programs*. IEA/ECBCS Annex 42 Report. ISBN No. 978-0-662-47116-5.